"Federico II" University of Naples

DOCTORATE IN BIOLOGY
(XXXI Cycle)

"Bacterial Spore: analysis of surface proteins and biotechnological applications"

Tutor
Prof. Rachele Isticato

PhD student
Mariamichela Lanzilli

Index

Outline of the Thesis

This PhD Thesis reports the results of my research work in the laboratory of Prof. Racheal Isticato at the Department of Biology of the Federico II University of Naples, Italy. This Thesis is organized in four parts as follows:

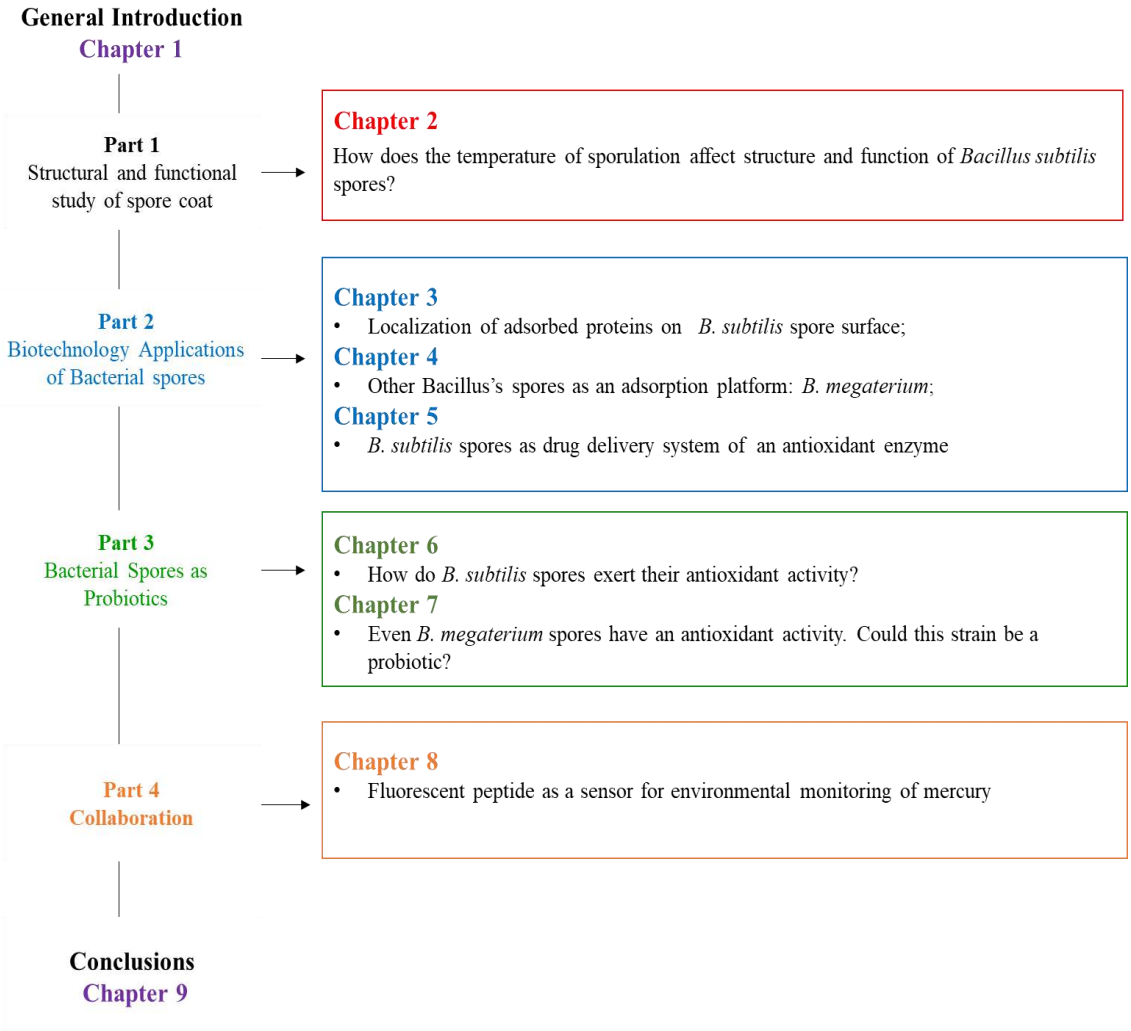

During these three years, I focused on two bacteria of the same genus, *Bacillus subtilis* and *Bacillus megaterium*. These organisms are Gram-positive, aerobic, spore formers and, therefore, share the ability to undergo a complex developmental cell differentiation process and produce highly resistant spores [Tan IS and Ramamurthi KS, 2014]. As reported in the Introduction, the process is induced by unfavorable environmental conditions and starts with an asymmetric cell division that produces a large mother cell and a small forespore. The mother cell contributes to forespore maturation and undergoes autolysis at the end of the process, allowing the release of the mature spore into the environment. The peculiar structure of the spore, characterized by a dehydrated cytoplasm surrounded by various protective layers, is responsible for the resistance of the spore to extremes of heat and pH, to UV radiations, and to the

presence of solvents, hydrogen peroxide and lytic enzymes. In the presence of water, nutrients and favorable environmental conditions the mature spore can germinate generating a cell able to grow and, eventually, to re-sporulate [Setlow P., 2003].

Spore resistance is in part due to the presence of the spore coat, a multi-layered structure composed of more than 70 proteins that surrounds the spore [McKenney *et al*. 2013]. The biogenesis of the spore coat is finely regulated at multiple levels as reported in chapter 1 (paragraph 1.6 of the *Introduction*) and represents an interesting model system to study mechanisms of gene expression and of protein-protein interaction in bacteria.

The spore surface of the two bacterial species I used for my PhD work, substantially differs from each other for the presence around the spore of *B.megaterium* of an exosporium, a poorly characterized outermost spore layer not present around the *B. subtilis* spore. The large dimension of *B.megaterium* spores that are 2.5- fold larger than that of *B. subtilis* is another difference between the two bacteria.

The **Part I** focuses on the investigation of the sporulation temperature consequences on the ultrastructure and the protein composition of the spore surface layers and on the functional properties of spores produced at growth temperature (25 and 42°C), in comparison to an optimal growth temperature (37°C). The changes in resistance properties, ultrastructure and protein composition, were greater in spores formed at 25°C than at 37 and 42°C. Moreover, I observed that CotH and a series of CotH-dependent coat proteins were more abundantly present in the coat of 25°C than 37 and 42°C spores, suggesting that CotH played a more relevant role at low temperature. To gain further insight into the role of CotH, I have analyzed the protein stability and activity and then the transcriptional levels of *cotH* at the three temperatures.

Understanding the spore assembly mechanisms under different environmental conditions may help to assess the structure and properties of spores existing in the natural environment and the development of optimized industrial treatments, particularly in the food chain, to limit the survival and germination of contaminating spores.

The **Part II** (**chapter 3-4-5**) includes studies about the use of bacterial spores as Drug Delivery system. The bacterial spore has been proposed as a platform to display heterologous proteins, with potential applications ranging from the development of mucosal vaccine to re-usable biocatalysts, diagnostic tools and bioremediation devices for field use [Cutting *et al*., 2009; Knecht *et al*., 2011; Hinc *et al*., 2010; Isticato R, Ricca E. 2014]. Furthermore, various reasons support the use of the spore as a display system: (i) the remarkable and well documented resistance of the spore [McKenney et al., 2013] that ensures high stability of the display system; (ii) the availability of genetic tools [Harwood C, Cutting S.1990] that allows an easy manipulation; (iii) the safety record of several endospore-forming species [Cutting SM. 2011, Baccigalupi *et al*., 2015], that makes spores of those species ideal candidates also to deliver displayed molecules to mucosal surfaces [Cutting et al., 2009;Isticato R, Ricca E. 2014]. Two strategies have been developed to display heterologous proteins on the spore surface. A recombinant strategy based on the construction of gene fusions between the gene coding for a selected spore surface protein (carrier) and the heterologous DNA coding for the protein to be displayed. Instead, the non-recombinant approach is based on the spontaneous adsorption between purified spores and purified proteins. The molecular details controlling spore adsorption have not been fully elucidated but hydrophobic and electrostatic

interactions seem to be involved. An interesting challenge for future work will be to establish the mechanism or route of infiltration in the spore surface of adsorbed heterologous proteins. These challenges are partially addressed in this part of thesis.

In the **CHAPTER 3**, I used the monomeric Red Fluorescent Protein (mRFP) of the coral *Discosoma* sp. and *B. subtilis* spores of a wild type and an isogenic mutant strain (with a strongly altered coat) lacking the CotH protein to clarify the adsorption process. For this purpose, I constructed some isogenic strains carrying GFP fused to proteins restricted in different compartments of the *B. subtilis* spore. This system allowed me to localize adsorbed mRFP molecules and demonstrate that in wild type spores mRFP infiltrated through crust and outer coat, localized in the inner coat and was not surface exposed. Instead, in the mutant spores mRFP was present in all surface layers, inner, outer coat and crust and was exposed on the spore surface. These findings shed light on the mechanism of spore adsorption and indicate that different spores, wild type or mutant, can potentially have different applications. As a carrier of enzymes to be re-used several times a surface display of the enzyme may be not strictly required while a tight adhesion to the carrier could desirable making wild type spores preferable over the mutant spores. On the contrary, as a drug/vaccine delivery vehicle a surface display could be essential and the release of the drug/antigen in some cases an useful property, making mutant spores preferable over the wild type. Data reported in Chapter 3 have been published in 2016:

Giuliana Donadio,[#] **Mariamichela Lanzilli,**[#] Teja Sirec Ezio Ricca, and Rachele Isticato. *Localization of a red fluorescence protein adsorbed on wild type and mutant spores of Bacillus subtilis*. Microb Cell Fact 15(1): 153.

In the **CHAPTER 4,** I shifted my attention on spores of *B.megaterium* display system. The spores of *B.megaterium* (strain QMB1551) have aroused this interest at least for two reasons: the large dimensions of its spore (2.5 larger than that *B.subtilis* spore) that allow to adsorb a greater amount of heterologous proteins , and the presence of the exosporium, a poorly characterized structure composed of proteins and carbohydrates [Di Luccia *et al.* 2016] lacking in *B. subtilis* spores. Since so far only spores of species that lack an exosporium have been considered as adsorption platforms, no data are available on the impact of the exosporium in the interaction with heterologous proteins. Therefore, I verified whether spores surrounded by an exosporium were able to display heterologous proteins like spores that do not have such additional surface layer (*B. subtilis* spores). To this focus, I followed the non-recombinant display approach and used the monomeric form of the Red Fluorescent Protein (mRFP) of the coral *Discosoma sp.* [Campbell et al., 2002] as a model heterologous protein. Non-recombinant adsorption of mRFP to spores was monitored by western- and dot-blotting and by fluorescence microscopy. My results showed that *B.megaterium* spores were more efficient than *B. subtilis* spores in tightly adsorbing mRFP with over 100 µg of mRFP adsorbed. I found that the exosporium of *B.megaterium* is permeable to mRFP molecules that infiltrates through it and fill up the space between the outercoat and the exosporium. Furthermore, the *B.megaterium* spore could be an ideal vehicle to bind and deliver heterologous proteins. Data reported in Chapter 4 have been published in 2016:

Lanzilli M., Donadio G., Addevico R., Saggese A., Cangiano G., Baccigalupi L., Christie G., Ricca E. and Isticato R. 2016. *The exosporium of Bacillus megaterium QM B1551 is permeable to the red fluorescence protein of the coral Discosoma sp*. Front. Microbiol. 7:1752.

In the **CHAPTER 5**, I used *B.megaterium* spores as delivery system to bind Bcp1 (bacterioferritin comigratory protein 1), a peroxiredoxin of the archaeon *Sulfolobus solfataricus*, known to have an antioxidant activity. Here, the idea is to use *B.megaterium* spores for the delivery of therapeutic molecules to the gastrointestinal mucosa. The delivery of drugs and antigens by the oral or nasal routes offers several advantages over parenteral administration and is gaining increasing relevance for the treatment of human and animal diseases. For instance, the high vascularization of the mucosal surfaces allows the direct transfer of molecules into the systemic circulation, making the mucosal routes a promising alternative to delivery by injection [Zhang et al., 2002]. However, the successful development of mucosal therapeutic molecules relies on efficient delivery systems, able to stabilize and protect the molecules from degradation and to reduce or avoid completely the loss of biological activity. First of all, I verified that the spores were highly efficient in adsorbing Bcp1 and that the adsorbed enzyme localized beneath the exosporium, filling the space between the outer coat and the exosporium.
Then, I checked the stability and the protection of the adsorbed enzyme to the gastro-intestinal conditions demonstrating that the enzyme retained its activity in all conditions. In addition, I observed by this report that *B.megaterium* spores have an endogenous antioxidant activity. Data reported in Chapter 5 have been published in 2018:

Mariamichela Lanzilli, Giuliana Donadio, Francesca Anna Fusco, Carmen Sarcinelli, Danila Limauro, Ezio Ricca, Rachele Isticato. *Display of the peroxiredoxin Bcp1 of Sulfolobus solfataricus on probiotic spores of Bacillus megaterium. New BIOTECHNOLOGY 46 (2018) 38–44.*

The antioxidant activity, the safety and resistence of spores encouraged the topics covered in the **Part III** (chapter 6-7) of this Thesis. The oxidative stress is defined as a disturbance in the balance between the production of reactive oxygen species (ROS-free radicals) and antioxidant defences. [Betteridge DJ, 2000]. These ROS are common products of the cells' metabolism, in fact low and moderate amounts of ROS have beneficial effects on several physiological processes [Ames *et al*., 1993]. On the other hand, an excessive production of ROS, due to stress factors, damages DNA, protein, and lipids, leading to a variety of chronic diseases such as atherosclerosis, cardiovascular problems, inflammatory bowel diseases and so on [Eftekharzadeh *et al*., 2010; Harrison *et al*., 2003; Ostrakhovitch *et al*., 2001; Griendling *et al*., 2003; Ceriello *et al*., 2004]. Our cells are normally equipped with an array of antioxidant systems (catalase, superoxide dismutase, glutathione peroxidase and glutathione reductase) and there are a lot of natural antioxidants; however, these systems are not enough for complete scavenging of ROS. For this reason, a continuous search for new products able to prevent or retard stress induced damages is still needed. Here, I proposed the use of bacterial spores to counteract the damage due to oxidative stress. In particular, in the **CHAPTER 6,** I analysed the effects of *B. subtilis* spores, widely studied and used ,on human normal keratinocytes (*in vitro*) in presence of an oxidative stress. I found that the spores exert

their protective effect against stress injury, as oxidative stress markers (ROS, GSH and lipid peroxidation) were reported to physiological levels both when cells were stressed before incubating them with spores and when cells were pre- treated with spores. Interestingly, I also found that spores exert their protective effect by the nuclear translocation of Nrf-2, involved in the activation of stress response genes. Therefore, the activation of the antioxidant system, through the up-regulation of Nrf-2, is critical for the protection of cells from oxidative stress-induced damage. These findings suggest that spores can be an effective component in the treatment of cell damage. Data reported in Chapter 6 have been published in 2018:

Ganna Petruk, Giuliana Donadio, **Mariamichela Lanzilli**, Rachele Isticato, and Daria Maria Monti. *Alternative use of Bacillus subtilis spores: protection against environmental oxidative stress in human normal keratinocytes.* Sci Rep. 2018; 8: 1745.

In the **CHAPTER 7,** I focused on the antioxidant activity *in vitro* and *in vivo* of both *B.megaterium* spores wild type strain, QMB 1551 and a human isolate of *B.megaterium,* SF185. Both strains were characterized by similar antioxidant activities *in vitro.* Based on this and on human origin of strain, I decided to perform all further experiments using only spores of the strain SF185. Then , the antioxidant effects of SF185 spores were tested *in vitro* on Caco-2 cells measuring the ability of spores to reduce the toxicity of hydrogen peroxide and *in vivo* in a murine model of dextran sodium sulfate (DSS) -induced oxidative stress. The human origin of SF185, its strong antioxidant activity, and its protective effects both *in vitro* and *in vivo* led to propose the spore of this strain as a new probiotic for gut health.
A manuscript reporting these results is in preparation.

The results of chapters 6 and 7 allowed me to conclude that the consumption of spores-based products could prevent or reduce the damages caused by oxidative stress.

In the last part, **Part IV**, I have dealt with a different topic (Collaboration).In particular in the **CHAPTER 8,** I developed a fluorescent peptide as a sensor for environmental monitoring of mercury.
Heavy metal ions when present in excess are toxic for all organisms [De Silva *et al*., 2002]. They are difficult to remove from the environment and unlike many other pollutants cannot be chemically or biologically degraded, therefore, heavy metals constitute a global environmental hazard [Tchounwou *et al*., 2003]. Mercury and its compounds, in particular, are regarded as "priority hazardous substances" by the Agency for Toxic Substances and Disease Registry (ATSDR) because of its toxicity, mobility, long residence time, and biomagnification in food chains [Singh *et al*., 2004]. For examples, Hg^{2+} is highly toxic even at low levels [Talanova *et al*., 1999] and in humans it can affect liver, kidneys and the cardiovascular, gastro-intestinal and neurological systems [Rasheed *et al*.,2018]. It has been previously developed a fluorescent peptidyl sensor, dH3w, for monitoring Zn^{2+} in living cells. This probe, designed on the base on the internal repeats of the human histidine rich glycoprotein, shows a turn on response to Zn^{2+} and a turn off response to Cu^{2+}. Other heavy metals (Mn^{2+}, Fe^{2+}, Ni^{2+}, Co^{2+}, Pb^{2+} and Cd^{2+}) do not interfere with the detection of Zn^{2+} and Cu^{2+}. Here, I demonstrated that dH3w has an affinity for Hg^{2+} considerably higher than that for Zn^{2+} or Cu^{2+}, therefore the strong fluorescence of the Zn^{2+}/dH3w

complex is quenched when it is exposed to aqueous solutions of Hg^{2+}, allowing the detection of sub-micromolar levels of Hg^{2+}. Fluorescence of the Zn^{2+}/dH3w complex is also quenched by Cu^{2+} whereas other heavy metals (Mn^{2+}, Fe^{2+}, Ni^{2+}, Co^{2+}, Cd^{2+}, Pb^{2+}, Sn^{2+} and Cr^{3+}) have no effect. The high affinity and selectivity suggest that dH3w and the Zn^{2+}/dH3w complex are suited as fluorescent sensor for the detection of Hg^{2+} and Cu^{2+} in environmental as well as biological samples. Data reported in Chapter 9 have been published in 2018:

Marialuisa Siepi, Rosario Oliva, Luigi Petraccone, Pompea Del Vecchio, Ezio Ricca, Rachele Isticato, **Mariamichela Lanzilli**, Ornella Maglio, Angela Lombardi, Linda Leone , Eugenio Notomista and Giuliana Donadio . *Fluorescent peptide dH3w: a sensor for environmental monitoring of mercury (II).* PLoS One. 2018 Oct 10;13(10):e0204164.

In addition, a collaboration with Dott. Angelo Fontana's group of CNR of Pozzuoli allowed me to work with a hyperthermophilic marine bacterium: *Thermotoga neapolitana*. It is having a significant achievement in the field of bioenergy development with the production of H_2 which is due to its particular metabolic pathway. The process is named capnophilic (CO_2-requiring) lactic fermentation (CLF) and is mostly based on CO_2- induced recycling of acetate deriving from glycolysis [d'Ippolito *et al.*, 2014] by coupling with H_2 production. Furthermore, the process offers the potential advantage of combining carbon capture with the production of energy from a renewable source and the synthesis of highly added value products such as lactic acid. The mechanism behind the high H_2 and lactic acid yields achieved by *T. neapolitana* are likely related to the unique characteristic of the heterotrimeric [FeFe]-hydrogenase (H_2ase) and the reversible activity of the Pyruvate ferredoxin oxido-reductase (PFOR) that are present in the bacterium [Prahdan *et al*., 2015].
In order to promote the production of H_2 or lactic acid, I have analyzed the localization of the CLF pathway's key enzymes at different times in cells grown on different carbon sources (glucose or starch). By different methods of protein extraction and by immunofluorescence technique, I found a cytoplasmic PFOR at the beginning of fermentation and then a periplasmic PFOR suggesting a reversible activity of the enzyme in cells grown on glucose. Instead, in cells grown on starch, I found a predominantly cytoplasmic PFOR. In both cases, PFOR is coupled with a cytoplasmic membrane-associated H_2ase.
This study could explain the different H_2 yield and lactic acid production reported in literature [Pradhan *et al*., 2016a].

During these three years, I visited for three months the "Laboratoire de Chemie Bacterienne" of Dott.ssa Emilia Mauriello of CNRS in Marseille, France. In particular, I worked with *Myxococcus xanthus*, a soil bacterium capable of saprophytic feeding on products derived from predation of other bacteria. An important part of *M. xanthus* behavior is its ability to move on soft and solid surfaces by two forms of motility [Faure *et al*., 2016; Islam *et al*., 2018; Islam and Mignot, 2015].
Upon local nutrient depletion, cells initiate a developmental cycle resulting in aggregation and fruiting body formation within 72h, generating three differentiated cell subpopulations: (i) cells that form desiccation-resistant myxospores in the centre of the fruiting body, (ii) those that remain at the base of the

fruiting body, termed “peripheral rods”, and (iii) forager cells that continue their outward motility away from the fruiting body. Moreover, *M. xanthus* produces a specific secreted exopolysaccharide (EPS) that is crucial for biofilm formation [Berleman *et al*., 2016; Li *et al*., 2003; Palsdottir *et al*., 2009; Smaldone *et al*., 2014].

The secreted bacterial polysaccharides are produced by three biosynthesis schemes in which many proteins are involved. The *M. xanthus* genome encodes proteins, yet incompletely annotated, associated with the polysaccharide assembly pathways [Lu *et al*., 2005; Holkenbrink *et al*., 2014; Müller *et al*., 2012]. In this context, I monitored the spatial and temporal distribution of EPS pathway gene expression by construction of various transcriptional fusions between a selected promoter and a gene reporter (gfp, mcherry), then followed within the biofilm via fluorescence microscopy. The differential spatial modulation of EPS production within *M. xanthus* communities was found to be important for migration, development, and predation. Moreover, I have used an innovative approach to spatiotemporally resolve protein interactions in living cells [Braden T. *et al*., 2017]. A manuscript reporting these results is in preparation.

References

Ames BN, Shigenaga MK, Hagen TM (1993) Oxidants, antioxidants, and the degenerative diseases of aging. Proc Natl Acad Sci USA 90:7915–7922.

Baccigalupi L, Ricca E, Ghelardi E. Non-LAB probiotics: spore formers. In: Probiotics and prebiotics: current research and future trends, Norfolk: Caister Academic Press; 2015. p. 93–103.

Berleman, J.E., Zemla, M., Remis, J.P., Liu, H., Davis, A.E., Worth, A.N., West, Z., Zhang, A., Park, H., Bosneaga, E., et al. (2016). Exopolysaccharide microchannels direct bacterial motility and organize multicellular behavior. ISME J.

Betteridge DJ1. What is oxidative stress? Metabolism. 2000 Feb;49(2 Suppl 1):3-8.

Braden T. Lobingier, Ruth Hüttenhain, Kelsie Eichel, Kenneth B. Miller, Alice Y. Ting, Mark von Zastrow, and Nevan J. Krogan. An Approach to Spatiotemporally Resolve Protein Interaction Networks in Living Cells. Cell. 2017 Apr 6; 169(2): 350–360.e12.

Campbell, R.E., Tour, O., Palmer, A.E., Steinbach, P.A., Baird, G.S., Zacharias, D.A., and Tsien R.Y. 2002. A monomeric red fluorescent protein. Proc. Natl. Acad. Sci. 99, 7877-7882.

Ceriello A, Motz E (2004) Is oxidative stress the pathogenic mechanism underlying insulin resistance, diabetes, and cardiovascular disease? The common soil hypothesis revisited. Arterioscler Thromb Vasc Biol 24:816–823.

Cutting SM, Hong HA, Baccigalupi L, Ricca E. Oral vaccine delivery by recombinant spore probiotics. Int Rev Immunol. 2009; 28(6):487-505.

Cutting SM. Bacillus Probiotics. Food Microbiol. 2011 Apr; 28(2):214-20

DeSilva TM, Veglia G, Porcelli F, Prantner AM, Opella SJ. Selectivity in heavy metal- binding to peptides and proteins. Biopolymers. 2002;64: 189–197. doi:10.1002/bip.10149

Di Luccia B., Varriale F., Baccigalupi L., Ricca E. and Pollice A. 2016. Bacillus megaterium SF185 induces stress pathways and affects the cell cycle distribution of human intestinal epithelial cells. Benef Microbes. 7(4):609-20.

D’Ippolito G, Dipasquale L, Fontana A (2014) Recycling of carbon dioxide and acetate as lactic acid by the hydrogen-producing bacterium Thermotoga neapolitana. ChemSusChem 7:2678–2683.

Eftekharzadeh B, Maghsoudi N, Khodagholi F (2010) Stabilization of transcription factor Nrf2 by tBHQ prevents oxidative stress-induced amyloid β formation in NT2N neurons. Biochimie 92:245–253.

Fakhry S., Sorrentini I., Ricca E., De Felice M., Baccigalupi L. 2008. Characterization of spore forming Bacilli isolated from the human gastrointestinal tract. J Appl Microbiol, 105(6):2178-86.

Faure, L.M., Fiche, J.-B., Espinosa, L., Ducret, A., Anantharaman, V., Luciano, J., Lhospice, S., Islam, S.T., Tréguier, J., Sotes, M., et al. (2016). The mechanism of force transmission at bacterial focal adhesion complexes. Nature 539, 530-535.

Giglio R, Fani R, Isticato R, De Felice M, Ricca E, Baccigalupi L. 2011. Organization and evolution of the cotG and cotH genes of Bacillus subtilis. J Bacteriol. 193(23):6664-73.

Griendling KK, FitzGerald GA (2003) Oxidative stress and cardiovascular injury part I: Basic mechanisms and in vivo monitoring of ROS. Circulation 108:1912–1916.

Harwood C, Cutting S. Molecular biological methods for Bacillus. Chichester: Wiley; 1990.

Harrison D, Griendling KK, Landmesser U, Hornig B, Drexler H (2003) Role of oxidative stress in atherosclerosis. Am J Cardiol 91:7–11.

Hinc K, Ghandili S, Karbalaee G, Shali A, Noghabi K, Ricca E, Ahmadian G. Efficient binding of nickel ions to recombinant Bacillus subtilis spores. Res Microbiol. 2010;161:757–764

Holkenbrink, C., Hoiczyk, E., Kahnt, J., and Higgs, P.I. (2014). Synthesis and assembly of a novel glycan layer in *Myxococcus xanthus* spores. J. Biol. Chem.

Islam, S.T., Belgrave, A.M., Fleuchot, B., Jolivet, N.Y., My, L., Faure, L.M., Sharma, G., Lemon, D.J., Fiche, J.-B., Bratton, B.T., et al. (2018). Integrin-like tethering of motility complexes at bacterial focal adhesions. Cell (under review).

Islam, S.T., and Mignot, T. (2015). The mysterious nature of bacterial surface (gliding) motility: a focal adhesion-based mechanism in *Myxococcus xanthus*. Semin. Cell Dev. Biol. 46, 143-154.

Isticato R, Ricca E. 2014. Spore Surface Display. Microbiol Spectr. 2(5) doi: 10.1128/microbiolspec.

Knecht LD, Pasini P, Daunert S. Bacterial spores as platforms for bioanalytical and biomedical applications.Anal Bioanal Chem. 2011 May; 400(4):977-89.

Li, Y., Sun, H., Ma, X., Lu, A., Lux, R., Zusman, D., and Shi, W. (2003). Extracellular polysaccharides mediate pilus retraction during social motility of *Myxococcus xanthus*. Proc. Natl. Acad. Sci. USA. 100, 5443-5448.

Lu, A., Cho, K., Black, W.P., Duan, X.-y., Lux, R., Yang, Z., Kaplan, H.B., Zusman, D.R., and Shi, W. (2005). Exopolysaccharide biosynthesis genes required for social motility in *Myxococcus xanthus*. Mol. Microbiol. 55, 206-220.

McKenney PT, Driks A., Eichemberger P. 2013. The Bacillus subtilis endospore: assembly and functions of the multilayered coat. Nat Rev Microbiol. 11(1):33-44.

Müller, F.D., Schink, C.W., Hoiczyk, E., Cserti, E., and Higgs, P.I. (2012). Spore formation in *Myxococcus xanthus* is tied to cytoskeleton functions and polysaccharide spore coat deposition. Mol. Microbiol. 83, 486-505.

Naclerio G, Baccigalupi L, Zilhao R, De Felice M and Ricca E. 1996. Bacillus subtilis spore coat assembly requires cotH gene expression. J Bacteriol. 178:4375-4380.

Ostrakhovitch EA, Afanas'ev IB (2001) Oxidative stress in rheumatoid arthritis leukocytes: Suppression by rutin and other antioxidants and chelators. Biochem Pharmacol 62:743–746.

Palsdottir, H., Remis, J.P., Schaudinn, C., O'Toole, E., Lux, R., Shi, W., McDonald, K.L., Costerton, J.W., and Auer, M. (2009). Three-dimensional macromolecular organization of cryofixed *Myxococcus xanthus* biofilms as revealed by electron microscopic tomography. J. Bacteriol. 191, 2077-2082.

Pradhan N., Dipasquale L., d'Ippolito G., Panico A., Lens PN, Esposito G., Fontana A. Hydrogen production by the thermophilic bacterium, Thermotoga neapolitana. Int J Mol Sci. 2015 Jun 4;16(6):12578-600.

Pradhan N., Dipasquale l., d'Ippolito G., Fontana A., Panico A., Pirozzi F., Lens Piet N.L., Esposito G. Model development and experimental validation of capnophilic lactic fermentation and hydrogen synthesis by Thermotoga neapolitana. Water Research 99 (2016) 225e234

Rasheed T, Bilal M, Nabeel F, Iqbal HMN, Li C, Zhou Y. Fluorescent sensor based models for the detection of environmentally-related toxic heavy metals. Sci Total Environ. 2018;617: 476–487.

Ricca E, Baccigalupi L, Cangiano G, De Felice M, Isticato R. 2014. Mucosal vaccine delivery by non-recombinant spores of Bacillus subtilis. Microb Cell Fact. 13:115.

Setlow P. 2003. Spore germination. Curr Opin Microbiol. 6(6):550-6.

Singh AK, Bhattacharjee G, Singh R. Mercury(II)-selective membrane electrode using tetrathia-

diazacyclotetradeca-2,9-diene as neutral carrier. Sens Actuators B Chem. 2004;99: 36–41.

Smaldone, G.T., Jin, Y., Whitfield, D.L., Mu, A.Y., Wong, E.C., Wuertz, S., and Singer, M. (2014). Growth of *Myxococcus xanthus* in continuous-flow-cell bioreactors as a method for studying development. Appl. Environ. Microbiol. 80, 2461-2467.

Talanova GG, Elkarim NSA, Talanov VS, Bartsch RA. A Calixarene-Based Fluorogenic Reagent for Selective Mercury(II) Recognition. Anal Chem. 1999;71: 3106–3109.

Tan IS and Ramamurthi KS. (2014). Spore formation in Bacillus subtilis. Environ Microbiol Rep. 6(3):212-25.

Tchounwou PB, Ayensu WK, Ninashvili N, Sutton D. Environmental exposure to mercury and its toxicopathologic implications for public health. Environ Toxicol. 2003;18: 149–177.

Zhang H, Zhang J, Streisand JB. Oral mucosal drug delivery: clinical pharmacokinetics and therapeutic applications. Clin Pharmacokinet 2002;41:661–80.

Zheng L., Donovan W.P., Fitz-James P.C., Losick R. 1988. Gene encoding a morphogenic protein required in the assembly of the outer coat of the Bacillus subtilis endospore. Genes Develop. 2:1047-1054.

Zilhao R, Naclerio G, Baccigalupi L, Henriques A, Moran C and Ricca E. 1999. Assembly requirements and role of CotH during spore coat formation in Bacillus subtilis. J. Bacteriol. 181(8):2631-2633.

Chapter 1

Introduction

1 Introduction

1.1 Bacterial spore

The bacterial spore is a dormant, highly resistant cell type, which allows spore-forming organisms to survive adverse conditions, such as starvation, high temperatures, ionizing radiations, mechanical abrasion, chemical solvents, detergents, hydrolytic enzymes, desiccation, pH extremes and antibiotics [Nicholson *et al.*, 2000]. Spore formers mainly belong to the *Bacillus* and *Clostridium* genera. The most studied species of these two genera is *B. subtilis*, a model system for gram-positive bacteria. In both cases the process of spore formation (sporulation) is induced by a variety of environmental conditions that limit cell growth and/or block DNA replication and occurs through a series of generally similar morphological changes. However, substantial differences in the regulation of the process and in the structure of the protective layers of the mature spore have been observed between various species [Onyenwoke *et al*., 2004; Paredes *et al*., 2005; De Hoon *et al.*, 2010; Galperin *et al*., 2012]. Genomic analysis have shown that a common set of 56 key sporulation genes are present in the genomes of all spore formers while an approximately additional 60 genes are found in all *Bacilli* but are absent in all *Clostridia* [Galperin *et al*., 2012].

1.2 Sporulation

The mechanism of spore formation has been finely characterized in the model species *Bacillus subtilis*. In response to nutritional starvation or a variety of environmental conditions that limit cell growth and/or block DNA replication, the intracellular levels of the master regulator Spo0A-P increase and the sporulation pathway is activated. The first morphological evidence of the induction of sporulation is the formation of an asymmetrically cell division septum that produces a large mother cell and a small forespore (Fig. 1). The mother cell contributes to the spore development and at the end of sporulation process will lyse releasing the spore in the environment. Soon after the asymmetric cell division, the septum membrane migrates around the forespore, that results surrounded by a double membrane as result of the engulfment process (Fig. 1). A series of protective layers (cortex, coat, crust and in some species, exosporium) are then synthesized in the mother cell cytoplasm and assembled around the forming spore. The cortex is a peptidoglycan layer chemically different from that of the vegetative cells that is deposited between the two membranes and is essential for the attainment and maintenance of the dehydrated state of the spore core, for spore mineralization and for dormancy [Henriques and Moran, 2007]. Concomitantly with cortex formation, the proteinaceous coat is deposited around the outer surface of the outer membrane. Two major coat layers can be observed by electron microscope analysis: a darkly stained outer coat and a more lightly stained lamellar inner coat. At the end of the development process the mature spore is characterized by a dehydrated cytoplasm containing a condensed and inactive chromosome and surrounded by various protective layers. The final step is the lysis of the mother cell and the release of the formed spore. Because of such a peculiar structure, the spore can survive in the absence of water and nutrients and in the presence of unfavorable conditions (extremes of heat and pH, UV radiations, solvents, hydrogen peroxide and lytic enzymes) for very long

periods. When environmental conditions are suitable, the spore can germinate and there by convert back into a growing cell. When this occurs, first the spore core rehydrates and swells and then cortex and coat crack, releasing the nascent cell that can eventually, re-sporulate (Fig. 1). The processes of sporulation and germination have been recently reviewed [Higgins and Dworkin, 2012; Dworkin and Shah, 2010].

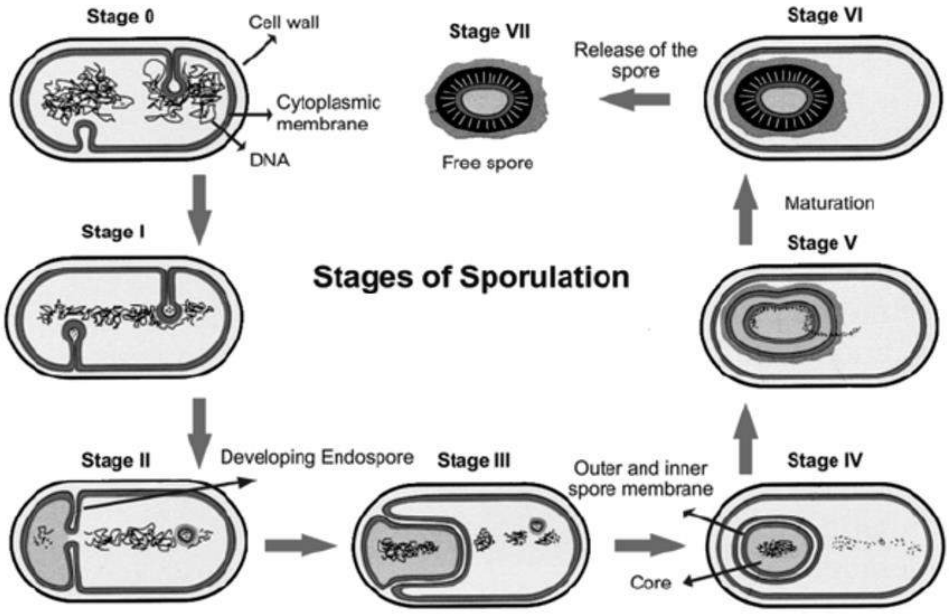

Figure 1: Schematic representation of sporulation and germination in *Bacillus subtilis*.

1.3 Genetic control of sporulation

The sporulation represents an example of cell differentiation in bacteria because two cells with an identical chromosome, the forespore and the mother cell, follow different gene expression programmes. The main mechanisms responsible for the establishment of cell-specific and time specific gene is due to sequential appearance of four transcription factors, called sigma factors, alternate to σ^A factor active during vegetative life (σ^F, σ^E, σ^G, σ^K), which bind to core of RNA polymerase and direct it to transcribe only from promoters of sporulation genes (spo genes), [Losick and Stragier, 1992].
Two of these sigma factors (σ^F and σ^G) are specifically expressed in the forespore and two (σ^E and σ^K) are only expressed in the mother cell determining a differentiated gene expression in the two cell compartments. Anyway, the gene expression in one cell is coordinated with the gene expression in the other one. According to the *criss-cross* model (Fig. 2), σ^F in the prespore is responsible of the activation of the gene coding for σ^G in the same compartment but also of σ^E in the mother cell. Similarly σ^E in the mother cell, is responsible of the expression of σk but also activates σ^G in the prespore that in turn activates the last sigma factor, σ^k in the mother cell. This model, confirmed by several experimental data, ensures the spatially and temporary controlled activation of the four sigma factors that causes the formation of a cascade of gene expression that guides the spore development.

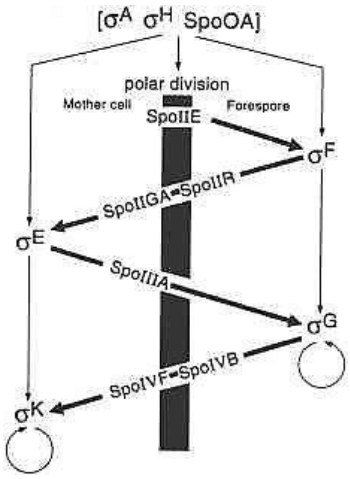

Figure 2: C*riss-cross regulation*. The thin arrows indicate the transcriptional control in the two different cells, while the thick arrows indicate the three checkpoints that coordinate the gene expression of one cell with the morphological changes of the other.

1.4 Germination and outgrowth

The spore is a metabolically inactive cell but remains able to sense the presence of nutrient thanks to the presence of specific sensors recognizing mainly amino acids and sugars, located in the inner membrane [Hornstra *et al*., 2005].

When the environmental conditions became favorable to the vegetative growth, the spore is able to germinate, returning to active growth. The process is called germination and is an irreversible process [Parker *et al*., 1996] that involves a series of morphological and biochemical changes that lead to degradation of the spore layers, cytoplasm rehydration and loss of spore dormancy and resistance. The germination takes few min. to complete and is followed by the cell enlargement process termed outgrowth. The amino acids necessary for the protein synthesis during the outgrowth are provided by the degradation of the coat components and of the SASP (Small Acid Soluble Proteins, DNA binding proteins responsible for UV resistance). In laboratory conditions, the germination is efficiently induced by L-alanine or L-asparagine and a mixture of molecules known as GFK (glucose, fructose and KCl). The correct assembly of the coat is important to guarantee proper germination efficiency.

1.5 Spore Structure

The bacterial spore is characterized by a core surrounded by several layer that in sequence are: the inner membrane, the cortex, the outer membrane, the spore coat and the spore crust (Fig. 3). The core is the innermost part of the spore. It contains the spore cytoplasm with all cellular components, such as cytoplasmic proteins, ribosomes and DNA associated to a large amount of Small Acid Soluble Proteins (SASPs) which protects the DNA against many types of damage. The core cytoplasm has a water content of only 30 – 50 % instead of the 70 – 88 % of the vegetative cytoplasm [Setlow, 1994]. This dehydrated state plays an important role in spore longevity, dormancy and resistance. The core is surrounded by the inner membrane, containing the germination receptors, that in turn is surrounded by

the cortex, a modified peptidoglycan layer. The cortex is important for the maintenance of spore core dehydration, resistance and dormancy. The outer membrane, the second membrane layer that derives from the engulfment process and that has opposite polarity with respect to the inner membrane. The most external structure of the spore is the coat, a complex multilayered structure composed of more than 70 proteins, which plays roles in spore resistance, germination, and apparently possesses enzymatic functions that may possibly permit interactions with other organisms in the environment. It consists of two main layers (Fig. 3): the inner layer (IC, thick 20 - 40 nm) is formed by the juxtaposition of three to six lamellae aligned along the periphery of the spore, and the outer layer (OC, thick 40 - 90 nm) that appears more electrons dense. Another recently characterized layer is the crust (Cr) mainly composed by glycoproteins [McKenney *et al*., 2010].

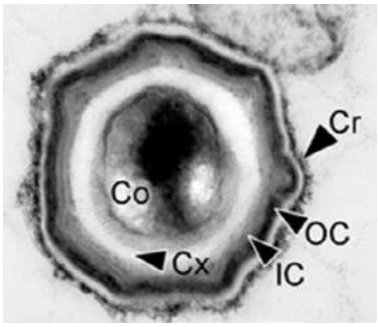

Figure 3: *Bacillus subtilis* spore ultrastructure. The figure shows the spore core (Co), the cortex peptidoglycan layer (Cx), the inner coat (IC) and the outer coat (OC) and the crust (Cr) [McKenney *et al*, 2010].

It has been proposed that the crust could represent a rudimentary exosporium, a layer found in other *Bacillus* species such as *B.antracis* and *B.megaterium*. This glycosylated layer is intimately connected to the rest of the coat and both coat layers are packed closely together and appear thicker at the spore poles and thinner along its sides [Driks, 1999]. Till date it was shown that CgeA, CotZ and CotY are major structural components of the crust [Imamura *et al*., 2011].

About the exosporium, some features have been elucidated in the species of the *Bacillus cereus* group, *B.cereus, B. anthracis*, and *B. thuringiensis* [Terry *et al*, 2017; Maes *et al*, 2016]. It is composed of an external hair-like nap and a paracrystalline basal layer and it contains approximately 20 different proteins [Steichen *et al*, 2003; Steichen *et al* 2005*;* Redmond *et al*., 2004), which are deposited around the spore in a progressive encasement process [Qi Peng *et al.* 2016] . The exosporium acts as the outer permeability barrier of the spore and contributes to spore survival and virulence.

1.6 Regulation of coat assembly

Analysis of localization of various coat proteins and their timing of appearance, suggest that the assembly of the layers does not occur from inner to outer, but that it is under a complex control mechanism acting at two levels: the transcriptional level, controlling the temporal synthesis of the various proteins; and at the post-translational level, with the involvement of a series of morphogenetic proteins controlling the assembly of other coat components. Moreover a series of post-translational

modifications, including phosphorylation and glycosylation, have been reported to occur [Driks *et al*., 1994; Ricca *et al*., 1997].

1.6.1 Transcriptional regulation of cot genes

Coat assembly is mainly a function of the mother cell and covers a period of about 6 hours, beginning with asymmetric division of the sporangial cell. Thus, the expression of genes coding for coat components (*cot* genes) is under the control of the two sigma factors that regulate the mother cell gene expression: σ^E and σ^K; in addiction, three DNA binding proteins, SpoIIID, GerR and GerE, act as transcriptional regulators, activating and/or repressing the gene expression in the mother cell. Due to the action of these transcriptional factors it is possible to identify four classes of *cot* genes (Fig. 4). The gene expression program in the mother cell compartment involves the activation of 383 genes that represent about 9% of *Bacillus subtilis* genome. The first transcription factor acting in the mother cell is σ^E that is responsible of the expression of genes coding for the coat morphogenetic proteins SpoIVA and SpoVID, and for the transcriptional factors SpoIIID and GerR. SpoIIID acts together with σ^E to repress or to activate the gene expression while GerR, seems to work only as a repressor of σ^E – activated genes [Eichenberger *et al*., 2004]. After engulfment, σ^K is activated and directs the expression of a large group genes coding for the other coat proteins (Fig. 4). The σ^K –controlled regulon is composed of *cotA, cotD, cotF, cotH, cotM, cotP, cotT, cotV, cotW, cotY,* and *cotZ.* The transcription factor gene *gerE* is also part of this regulon. GerE works in conjunction with σ^K to activate a final regulon comprising the genes *cotB, cotC, cotG, cotV, cotW, cotX, cotY,* and *cotZ.* GerE can act as repressor or activator of the expression some σ^K –controlled genes. It down regulates *cotA* and *cotM* and activates *cotD,cotG, cotV, cotW, cotX, cotY,* and *cotZ.* A further level of complexity in the control of mother cell gene expression comes from a feedback-like regulation in which late regulatory events modulate ones that were initiated earlier.

For example, σ^K down regulates transcription of the gene encoding σ^E, thereby helping to terminate expression of σ^E–directed genes. GerE is also able to down regulate the activity of σ^K [Zhang *et al.* 1999].

The production of the spore coat proteins in the correct cellular compartment and at the proper time is critical to the formation of the coat. Mutants in which the timing of σ^K activation is altered and the coat components of classes III and IV, are synthesized one hour earlier than in the wild type cells, produce spores impaired in their germination efficiency [Cutting *et al*., 1991; Ricca *et al*., 1992].

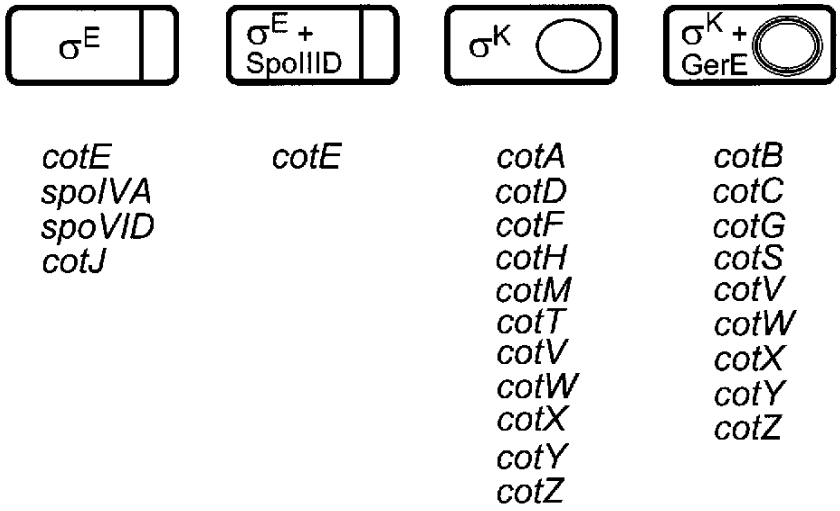

Figure 4: Program of mother cell gene expression

1.6.2 Post-translational regulation of Cot proteins assembly

The coat assembly is also regulated by the action of proteins with morphogenetic activity, i.e. structural coat components that control the assembly of other coat components within the coat layers without influencing their structural gene expression. The most important morphogenetic proteins are: SpoIVA, SpoVID, CotE and CotH and are all produced in the mother cell compartment [Driks *et al*., 1994; Ricca *et al*., 1997]. SpoIVA is produced in the mother cell early in sporulation, under the control of σ^E and is essential for the assembly of both the spore cortex and the coat layers. SpoIVA localizes at near to the mother cell surface of the septum and at later stages, following engulfment of the forespore by the mother cell, the protein forms a shell that surrounds the forespore. Studies from *Ramamurthi and Losick* [2008] have demonstrated that SpoIVA is an ATPase and that this activity allows itself assembly. It has been proposed that two interaction sites are involved in SpoIVA assembly: one is used for ATP-dependent polymerization, and the second for lateral interactions between the polymers. Localization of SpoIVA marks the forespore outer membrane for its use both in the synthesis of the cortex (below) and as the site of coat attachment (above). Mutants carrying a *spoIVA null* allele, show a coat correctly formed with inner and outer parts but dispersed in the mother cell cytoplasm and not assembled around the forespore [Roels *et al*., 1992; Stevens *et al*., 1992]. So its role is probably to attach the coat to the forespore surface from the mother cell side [Driks *et al.*, 1994]. SpoIVA is also required for the proper localization of another key morphogenetic protein, SpoVID [Beall *et al*., 1993], to the surface of the developing spore. SpoVID governs a morphogenetic transition, called spore encasement, using a N-terminal that seems to be essential to form multimeric structures [Wang *et al*., 2009]. *spoVID* mutants like *spoIVA* mutants, have a spore coat dispersed in the cytoplasm. The proper localization of SpoIVA to the forespore outer membrane is a prerequisite also for the localization of another morphogenetic protein, CotE [Zheng *et al*., 1990]. CotE is a 24 kDa protein found in several *Bacillus* species and also in a *Geobacillus* and an *Oceanobacillus* [Henriques and Moran, 2007]. Expression of *cotE* relies on two promoters, designed P1 and P2. Transcription from P1 initiates soon after the asymmetric division and is turned off by the repressive action of SpoIIID. Transcription from

P2 appears to be under the joined control of σ^E and SpoIIID, but remains active also after the activation of σ^K, to be repressed in the final stages of sporulation by GerE [Costa, *et al.*, 2006].. CotE localizes about 75 nm from the forespore outer membrane and then encircles the engulfed forespore. Electron microscope analysis has shown that *cotE* mutants totally lack the outer coat layer [Zheng *et al.*, 1990]. The region delimited by the SpoIVA and the CotE rings is referred as *matrix* or *precoat*. The precoat is of unknown composition, but it most likely contains proteins that are synthesized early and recruited under SpoIVA control. Probably the inner coat proteins assemble in the space between CotE and the forespore surface, forming the inner lamellar layer [Driks, *et al.*, 1994]. Instead, the outer coat proteins assemble simultaneously around the CotE layer to form the electron dense outer layer (Fig. 5). Assembly of the outer coat involves the cooperation between CotE and an additional morphogenetic protein CotH [Naclerio *et al.*, 1996]. A mutagenesis study has revealed that CotE has a modular structure with a C-terminal domain involved in directing the assembly of various coat proteins, an internal domain involved in the targeting of CotE to the forespore, and the N-terminal domain that, together with the internal domain, directs the formation of CotE homo-multimers [Little and Driks, 2001]. Also Krajcikova *et al.* [2009] confirmed CotE multimerization, moreover it was demonstrated that CotE physically interacts with many other spore coat components [Kim *et al*., 2006, Fig. 6] and is essential for formation of CotC-CotU hetero-oligomers [Isticato *et al*., 2010].

CotH is a 42.8-kDa protein found in several *Bacillus* and also in some *Clostridium* species [Henriques and Moran, 2007]. CotH plays a morphogenetic role in the assembly of at least 9 other coat components: CotB, CotC, CotG, CotS, CotSA, CotQ, CotU, CotZ and YusA [Kim *et al*., 2006, Zilhao *et al.*, 2004] and in the development of the lysozyme resistance and the germination efficiency of the mature spore [Naclerio *et al.*, 1996, Zilhao *et al*., 1999]. Moreover, CotH directs deposition of a subset of the CotE-dependent coat proteins and is itself, at least partially CotE dependent [Naclerio *et al*., 1996; Zilhao *et al*., 1999; Little and Driks, 2001]. CotH may function in part in the mother cell cytoplasm, perhaps as a protease inhibitor or as a chaperone [Baccigalupi *et al*., 2004; Isticato *et al.*, 2004], as far as it is required for the stabilization of CotG and CotC. Its important role in protein assembly during late stages of sporulation was observed also in TEM images, which reveal that absence of CotH severely affects spore surface (Fig. 6).

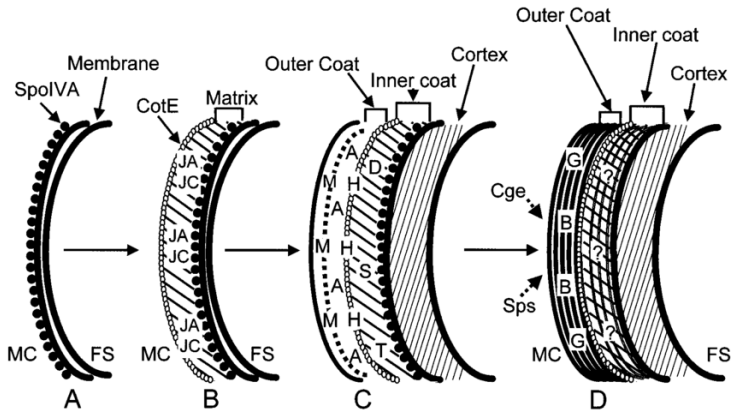

Figure 5: spore coat assembly model

The structural gene coding for CotH is clustered together with *cotG* on the *Bacillus subtilis* chromosome that is divergently transcribed [Naclerio *et al.*, 1996, Giglio *et al*, 2011]. CotG is another morphogenetic protein important in late stages of sporulation. It is a 24 kDa protein produced in the mother cell compartment of the sporangium around hour 8 of sporulation under the control of the mother cell specific factor σ^K and of transcriptional regulator GerE.

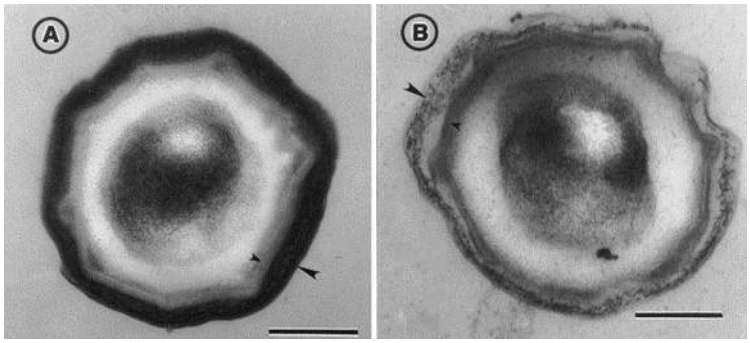

Figure 6: EM analysis of spores purified from wild-type strain (**A**) and congenic *cotH* deletion mutant (**B**)

The *cotG* expression is indirectly controlled by another transcriptional regulator GerR, through the activation of SpoVIF, which positively acts on GerE and on GerE-dependent genes [Cangiano *et al.*, 2010]. CotG is assembled around the forming spore as two main forms of about 32 and 36 kDa. The 32-kDa form most likely represents the unmodified product of the *cotG* gene (24 kDa) whose abnormal migration may be attributed to its unusual primary structure characterized by the presence of 7 tandem repeats of 7 and 6 amino acids followed by 5 repeats of 7 amino acids [Giglio *et al.*, 2011]. It has been proposed that the modular structure of *cotG* is the outcome of several rounds of gene elongation events of an ancestral module [Giglio *et al*., 2011]. It is interesting to note that in all CotG-containing *Bacilli* CotG has a modular structure although the number and the length of the repeats differ in the various microorganisms [Giglio *et al*., 2011]. The other CotG form of 36-kDa could be due to extensive cross-linking of the protein as it is assembled into the spore coat. That CotG is able to form cross-linked forms has been suggested based on the analysis of the coat structure in *sodA* mutant cells [Henriques *et al.*, 1998]. Spores produced by *cotG* mutants are not affected in their resistance to lysozyme or germination properties [Sacco *et al*., 1995]. CotG strictly requires *cotH* expression for its assembly and none of the CotG forms is assembled in the coat of *cotH* spores [Naclerio *et al*., 1996). CotG has also a morphogenetic role on the assembly of CotB and controls the conversion of the CotB-46 form into the mature form of 66 kDa (CotB-66) extracted from wild type spores [Zilhao *et al*., 2004]. The interactions between various coat components, inferred only on the base of by genetic dependence, form a complex network and are schematically reported in Fig. 7 [Kim *et al.*, 2006].

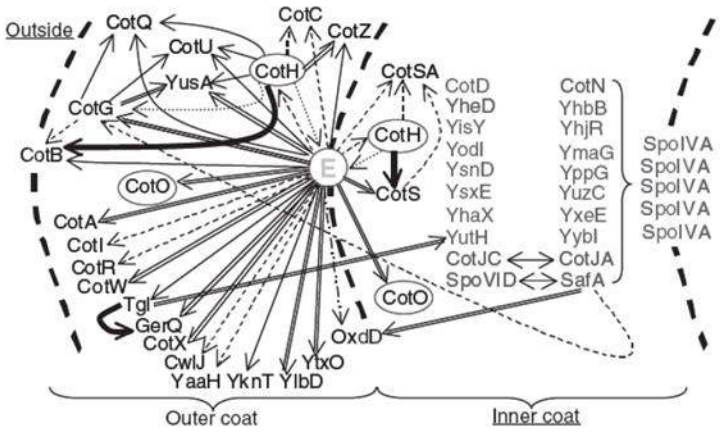

Figure 7: Model of the coat protein interaction network. An arc of the spore coat is indicated; E is CotE. The interior of the spore is to the right of the diagram. The inner and outer coat layers are indicated, as well as the outside of the spore (on the left). Directions of the arrows indicate the assembly dependencies. In some cases, the dependencies are partial. A double line indicates that the dependency was detected by fluorescence microscopy. A thicker line indicates that the dependency was detected by SDS-PAGE, but not by fluorescence microscopy. A dashed line indicates that the dependency was detected by SDS-PAGE. [Kim, *et al.*, 2006].

1.7 New applications of spores as display system

The bacterial spore has been proposed as a platform to display heterologous proteins, with potential applications ranging from the development of mucosal vaccines to re-usable biocatalysts, diagnostic tools, and bioremediation devices [Knecht *et al*., 2011; Isticato and Ricca, 2014; Ricca *et al.*, 2014]. The remarkable and well documented resistance of the spore [McKenney *et al*., 2012], the amenability of several spore-forming species to the genetic manipulation [Harwood and Cutting, 1990] and the safety record of several species [Cutting, 2011] support the use of the spore as a display and delivery system.

Two strategies (recombinant and non-recombinant) have been developed to display heterologous proteins on the spore surface and *Bacillus subtilis* has been used as model.

Both the recombinant and non-recombinant spore display systems have a number of advantages over cell- or phage-based systems. The stability, safety and amenability to laboratory manipulations of spores of several bacterial species, together with the lack of some constrains limiting the use of other systems, make the spore a highly efficient platform to display heterologous proteins.

1.7.1 Surface display on *B. subtilis* spores on recombinant approach

The rigidity and compactness of the spore coat immediately suggest the possibility of using its structural components as anchoring motifs for the expression of heterologous polypeptides on the spore surface. A genetic system to engineer the coat of *B. subtilis* spores has been developed (Fig. 8) and a model passenger efficiently displayed [Isticato *et al*., 2001]. The spore-based approach provides several advantages over other display systems, such as a high stability even after a prolonged storage, the possibility to display large multimeric proteins and the safety for a human use (Table 1). Attempts

to expose heterologous proteins on the spore surface were focused mainly on *CotB* protein selected for the surface location [Isticato *et al*., 2001], CotC and CotG, for their high relative abundance in spore coat [Mauriello *et al*., 2004].

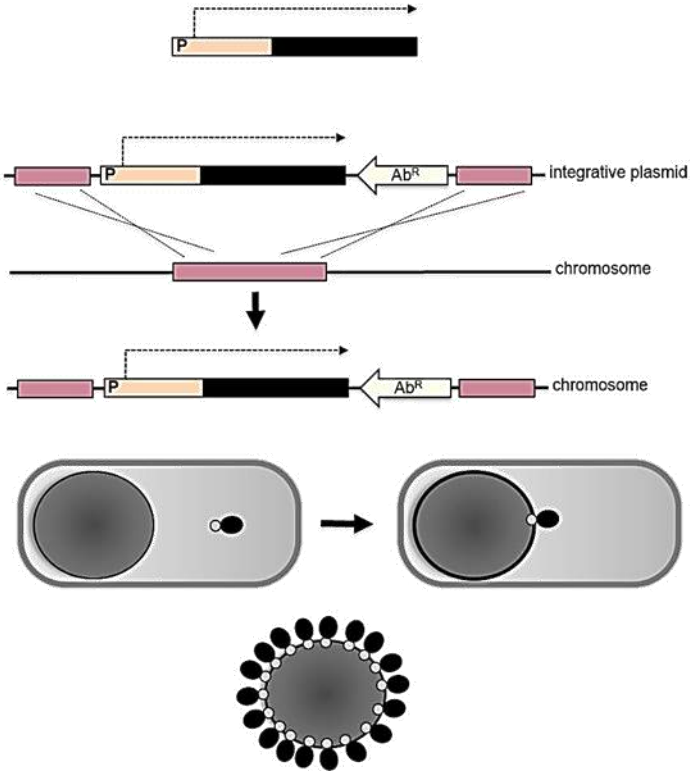

Figure 8: The image shows the way of expression of heterologous protein through genetic manipulation.

Bacterium	Carrier	Passenger	Potential application
B. subtilis	**CotB**	TTFC of *C. tetani*	**Vaccine**
		LTB of *E. coli*	**Vaccine**
		PA of *B. anthracis*	**Vaccine**
		CPA of *C. perfringens*	**Vaccine**
		UreA of *H. acinonychis*	**Vaccine**
		18xHis	**Bioremediation**
	CotC	TTFC of *C. tetani*	**Vaccine**
		LTB of *E. coli*	**Vaccine**
		PA of *B. anthracis*	**Vaccine**
		Pep23 of HIV	**Vaccine**
		GP64 of *B. mori*	**Anti-viral**
		TcdA-TcdB of *C. difficile*	**Vaccine**
		HAS	**Clinical use**
		ADH of *B. mori*	**Biocatalysis**
	CotG	Streptavidin	**Diagnostic tool**
		GFPUV	**Display system**
		α-Transaminase	**Biocatalysis**
		β-Galactosidase	**Biocatalysis**
		Phytase	**Animal probiotic**
		UreA of *H. acinonychis*	**Vaccine**
	OxdD	Phytase	**Animal probiotic**
	SpsC	pIII coat protein of M13	**Display system**
	CotA		**Autodisplay**
B.thuringensis	**Cry1Ac**	GFP	**Display system**
		Anti-PhOxscFv	**Diagnostic tool**
	InhA	β-Gal	**Display system**
B. anthracis	**BlcA/B**	GFP	**Display system**

Table 1: List of carriers, passenger proteins and potential applications described for spore surface display systems.

1.7.2 Surface display on non-recombinant spores

Spore-based display systems summarized above rely on the genetic engineering of the host. This is a major drawback when the application of the display system involves the release into nature of the recombinant host (field applications) and, in particular, when the display system is thought for human or animal use (delivery of antigens or enzymes to mucosal surfaces). Serious concerns over the use of live genetically modified microorganisms, their release into nature and their clearance from the host following oral delivery have been raised [Detmer *et al*., 2006]. To overcome this obstacle, a non-recombinant approaches to display heterologous proteins on the spore surface have been recently proposed (Fig. 9). A different approach for spore adsorption was followed by Huang et al. [2010]. A collections of antigens (the TTFC of *C. tetani*, PA of *B. anthracis*, Cpa of *C. perfringens* and glutathione S transferase (Sj26GST) from *Shistosomas japonica)* [Dryden *et al*., 2007] were expressed in *E. coli* and purified by affinity chromatography. Adsorbed spores were shown able to induce specific and protective immune responses in mice immunized mucosally [Huang *et al*., 2010]. Spore adsorption resulted more efficient when the pH of the binding buffer was acidic (pH 4) and less efficient or totally

inhibited at pH values of 7 or 10 [Huang *et al*., 2010]. A combination of electrostatic and hydrophobic interactions between spores and antigen were suggested to drive the adsorption that was shown to be not dependent on specific spore coat components but rather due to the negatively charged and hydrophobic surface of the spore [Huang *et al*., 2010].

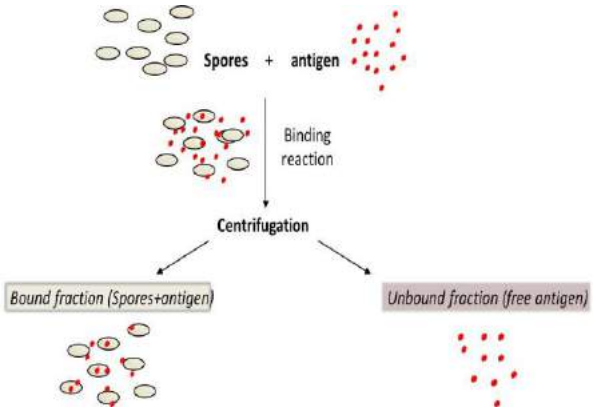

Figure 9: Schematic representation of a typical adsorption experiment. Purified spores were mixed to the purified antigen in PBS buffer (pH 4.0) and incubated one hour at25°C. The reaction was fractionated by centrifugation and fractions assayed independently.

In addition, the same study showed that killed or inactivated spores were equally effective as live spores in adsorbing the various antigens [Huang *et al*., 2010].

1.7.3 Physicochemical properties of spores important for protein adhesion

The physicochemical properties of the spore surface have been addressed in different studies with different approaches. A first study showed that spores of *B. subtilis* are negatively charged by time-resolved micropotentiometry [Kazakov *et al*., 2008]. In an aqueous environment, the spore behaves like an almost infinite ionic reservoir and is able of accumulating billions of protons (approximately 2 x 10^{10} per spore) [Kazakov *et al*., 2008]. The carboxyl groups were identified as the major ionizable groups in the spore and on the basis of the diffusion time analysis, it was found that proton diffusion is much lower in the spore core than within the coats and cortex [Kazakov *et al*., 2008]. This, then, suggested that the inner membrane, separating core from cortex and coats in a dormant spore, is probably a major permeability barrier for protons [Kazakov *et al*., 2008]. The role of electrostatic forces in spore adhesion to a planar surface has been also addressed studying spores of *B. thuringiensis* [Chung *et al*., 2010]. The surface potentials of a spore and a mica surface were experimentally obtained using a combined atomic force microscopy (AFM)-scanning surface potential microscopy technique [Chung *et al*., 2010]. By these techniques, the surface charge density of the spores was estimated at 0.03 μC/cm2 at 20% relative humidity and decreased with increasing humidity. The electrostatic force can be an important component in the adhesion between the spore and a planar surface [Chung *et al*., 2010].

1.7.4 Advantages of the spore surface display systems

Spore-based surface display systems provide several advantages with respect to other display approaches using microbial cells or bacteriophages. A first advantage comes from the well documented robustness of the *Bacillus* spore which grants high stability to the display system even after a prolonged storage. This aspect has been tested with spores displaying CotB 107-TTFC. Aliquots of purified recombinant spores were stored at -80°C, -20°C, +4°C and at room temperatures and assayed for the amount of heterologous protein present on the spore after different storage times. The stability of the display system is an extremely useful property for a variety of biotechnological applications. Heat-stability is, for example, a stringent requirement in the development of new mucosal vaccine delivery systems, mainly for those intended for use in developing countries, where poor distribution and storage conditions are main limitations. High stability of the display system is an extremely useful property also for industrial and environmental applications, in which cell-based systems have found so far limited use in the field because of the inability of bacterial cells to survive long term, especially under extreme conditions [Knecht *et al*., 2011]. The safety record of several *Bacillus* species [Cutting *et al*., 2011] is another important advantage of spores over other systems. Several *Bacillus* species, including *B. subtilis*, are widely used as probiotics and have been on the market for human or animal use for decades in many countries [Cutting *et al*., 2011]. Although most of the study so far performed has been carried out with laboratory strains of *B. subtilis*, in some cases intestinal isolates and strains with probiotic properties have been also used to display heterologous proteins [Cutting *et al*., 2009]. The safety of the live host is obviously an essential requirement if the display system is intended for human or animal use, such as delivery of vaccines or therapeutic molecules to mucosal surfaces. A limitation of cell- and phage-based display systems is the size of the heterologous protein to be exposed, since it may affect the structure of a cell membrane-anchoring protein or of a viral capsid. In addition, cell-based systems need a membrane translocation step in order to externally expose a protein produced in their cytoplasm [Knecht *et al*., 2011]. Spore-based systems do not have such limitations. A first reason for the successful display of those large proteins is that the coat components used as carriers are dispensable for the formation of an apparently normal spore as well as for its germination [Henriques *et al*., 2007]. Therefore, if the coat component-carrier does not behave as a wild type protein because of the presence of the heterologous part fused to it, this is unlikely to affect coat structure and function. Moreover, all known coat proteins are expressed in the mother cell compartment of the sporulating cell and, as a consequence, coat-based chimera do not need to undergo a cell wall translocation step, thus eliminating a severe limitation often encountered with cell-based display systems. Identical arguments apply for display systems based on spore adsorption. Independently purified proteins or proteins synthesized in the mother cell during sporulation can be attached to spores and the immobilization has been shown to provide increased stability to the protein without interfering with the spore structure or the need to translocate across a cell membrane.

1.8 References

Baccigalupi, L., Castaldo, G., Cangiano, G., Isticato, R., Marasco, M., De Felice, M., and Ricca, E. 2004. GerE independent expression CotH leads to CotC accumulation in the mother cell

compartment during *Bacillus subtilis* sporulation. Microbiology 150: 3441-3449.2.

Beall, B., Driks, R., and C. P. Moran. Jr. 1993. Cloning and characterization of a gene required for assembly of the *Bacillus subtilis* spore coat. J. Bacteriol. 175:1705-1716.

Cangiano, G., Mazzone, A., Baccigalupi, L., Isticato, R., Eichenberger, P., De Felice, M., Ricca, E. 2010. Direct and indirect control of late sporulation genes by GerR of *Bacillus subtilis*. J. Bacteriol. 192:3406-3413.

Costa, T., M., Serrano, L., Steil, U., Völker, C. P., Moran, Jr., Henriques, A.O. 2006. The timing of cotE expression affects *Bacillus subtilis* spore coat morphology but not lysozyme resistance. J. of Bacteriol. 189 (6):2401-2410.

Chen, G., Driks, A., Tawfiq, K., Mallozzi, M., Patil, S. 2010. *Bacillus anthracis* and *Bacillus subtilis* spores surface properties and transport. Colloid and Surfaces B: Biointerfaces 76:512-518.

Cho, E. A., Kim, E. J., Pan, J. G. 2011. Adsorption immobilization of *Escherichia coli* phytase on probiotic *Bacillus polyfermenticus* spores. Enzyme Microb Technol. 49: 66-71.

Cutting, S., Driks, A., Shimdt, R., Kunkel, B., and Losick, R. 1991. Forespore specific transcription of a gene in the signal transduction pathway that governs pro-σK processing in *Bacillus subtilis.* Genes & Dev. 5:456-466.

Chung, E. A., Iacoumi, S., Lee, I., Tsouris, C. 2010. The role of the electrostatic force in spore adhesion. Environ. Sci. Technol. 44:6209–6214.

Cutting, S. M., Hong, H. A., Baccigalupi, L., Ricca, E. 2009. Oral vaccine delivery by recombinant spore probiotics. Intern. Rev. Immunol. 28:487-505.

Cutting, S. M., 2011. Bacillus probiotics. Food Microbiology. 28:214-220.

De Hoon MJ, Eichenberger P, Vitkup D. 2010. Hierarchical evolution of the bacterial sporulation network. Curr Biol.20(17):R735-45.

Detmer, A., Glenting, J. Live bacterial vaccines a review and identification of potential hazards. Microb Cell Fact 2006, 5:23.

Driks, A., Roels, S., Beall, B., Moran, C. P., Jr, Losick, R. 1994. Subcellular localization of proteins involved in the assembly of the spore coat of *Bacillus subtilis*. Genes Dev. 8 (2): 234-44.

Driks, A. 1999. Bacillus subtilis spore coat. Microbiol Mol Biol Rev; 63:1–20.

Dryden GW Jr, Deaciuc I, Arteel G, McClain CJ. Clinical implications of oxidative stress and antioxidant therapy. Curr Gastroenterol Rep. 2005 Aug;7(4):308-16.

Dworkin J, Shah IM. 2010. Exit from dormancy in microbial organisms. Nat Rev Microbiol. 8(12):890-6.

Eichenberger, P., Fujita, M., Jensen, S. T., Conlon, E. M., Rudner, D. Z., Wang S. T., Ferguson, C., Haga, K., Sato, T., Liu, J. S., Losick, R. 2004. The program of gene transcription for a single differentiating cell type during sporulation in *Bacillus subtilis*. PLOS Biology 2(10):1664-1683

Galperin MY, Mekhedov SL, Puigbo P, Smirnov S, Wolf YI, Rigden DJ. 2012. Genomic determinants of sporulation in Bacilli and Clostridia: towards the minimal set of sporulation-specific genes. IEnviron Microbiol. 14(11): 2870-90.

Giglio R. , Fani R., Isticato R., De Felice, M., Ricca E., Baccigalupi L. 2011. Organization and Evolution of the cotG and cotH Genes of *Bacillus subtilis.* Journal of Bacteriol., 193(23):6664–6673.

Henriques AO, Melsen LR, Moran CP Jr. 1998. Involvement of superoxide dismutase in spore coat assembly in *Bacillus subtilis.* J Bacteriol.; 180(9):2285-91.

Harwood and S. Cutting. 1990. Molecular Biological Methods for Bacillus. John Wiley and Sons, Chichester, UK. pp. 27-74.

Henriques, A. O., Moran, C. P. Jr. 2007. Structure, assembly and function of the spore surface layers. Annu. Rev. Microbiol. 61: 555-88.

Higgins D, Dworkin J. 2012. Recent progress in *Bacillus subtilis* sporulation. FEMS Microbiol Rev.36(1):131-48.

Hinc K, Ghandili S, Karbalaee G, Shali A, Noghabi K, Ricca E, Ahmadian G. Efficient binding of nickel ions to recombinant *Bacillus subtilis* spores. Res. Microbiol. 2010, 161:757-764.

Hornstra LM, de Vries YP, de Vos WM, Abee T, Wells-Bennik MH. 2005. gerR, a novel ger operon involved in L-alanine- and inosine-initiated germination of *Bacillus cereus* ATCC 14579. Appl Environ Microbiol. 71(2):774

Huang JM, Hong HA, Van Tong H, Hoang TH, Brisson A, Cutting SM. 2010. Mucosal delivery of antigens using adsorption to bacterial spores. Vaccine. 28(4):1021-30.

Imamura D, Kuwana R, Takamatsu H, Watabe K. Proteins involved in formation of the outermost layer of *Bacillus subtilis* spores. J. Bacteriol. 2011, 193:4075-4080.

Isticato, R., Cangiano, G., Tran, H.,T., Ciabattini, A., Medaglini, D., Oggioni, M.,R., De Felice, M., Pozzi, G., Ricca, E. Surface display of recombinant proteins on *Bacillus subtilis* spores. J. Bacteriol. 2001, 183: 6294-6301.

Isticato R, Esposito G, Zilhão R, Nolasco S, Cangiano G, De Felice M, Henriques AO, Ricca E. 2004. Assembly of multiple CotC forms into the *Bacillus subtilis* spore coat. J Bacteriol.186(4):1129-35.

Isticato, R., Pelosi, A., De Felice, M., Ricca, E. 2010. CotE binds to CotC and CotU and mediates their interaction during spore coat formation in *Bacillus subtilis.* Journal of Bacteriol.,192(4):949–954.

Isticato R, Ricca E. 2014. Spore Surface Display. Microbiol Spectr. 2(5): doi: 10.1128/microbiolspec.

Kazakov S, Bonvouloir E, Gazaryan I. Physicochemical characterization of natural ionic microreservoirs: Bacillus subtilis dormant spores. 2008. J. Phys. Chem. 112:2233- 2244

Kim, H., Hahn, M., Grabowski, P., McPherson, D.C., Otte, M.M., Wang, R., Ferguson, C.C., Eichenberger, P. and Driks, A. 2006. The *Bacillus subtilis* spore coat protein interaction network. Mol. Microbiol. 59:487-502.

Klobutcher, L.A, Ragkousi, K., Setlow, P. 2006. The *Bacillus subtilis* spore coat provides "eat resistance" during phagocytic predation by the protozoan Tetrahymenathermophila. ProcNatl. Acad. Sci USA 103:165–170.

Knecht LD, Pasini P, Daunert S. 2011. Bacterial spores as platforms for bioanalytical and biomedical applications. Anal Bioanal Chem. 400(4):977-89.

Krajcíkova D., Lukacova M., Mullerova D., Cutting S. M., and Barak I.2009. Searching for protein-protein interactions within the *Bacillus subtilis* spore coat. J. Bacteriol. 191:3212–321.

Kwon, S.J., Jung, H.C., Pan, J.G. 2007. Transgalactosylation in a water solvent biphasic reaction system with β-Galactosidase displayed on the surfaces of *Bacillus subtilis* spores. Appl. Environ. Microbiol. 73:2251-2256.

Little, S., Driks, A. 2001. Functional analysis of the *B. subtilis* morphogenetic spore coat proteins. Molecular Microbiology.42(4): 1107-1120.

Losick, R., and P. Stragier. 1992. Crisscross regulation of cell-type-specific gene expression during development in *Bacillus subtilis*. Nature 355:601-604.

Maes E, Krzewinski F, Garenaux E, Lequette Y, Coddeville B, Trivelli X, Ronse A, Faille C, Guerardel Y. 2016. Glycosylation of BclA Glycoprotein from *Bacillus cereus* and *Bacillus anthracis* Exosporium is domain-specific. Biol Chem. 291(18):9666-77

Mauriello EMF, Duc LH, Isticato R, Cangiano G, Hong HA, De Felice M, Ricca E, Cutting SM. Display of heterologous antigens on the *Bacillus subtilis* spore coat using CotC as a fusion partner. Vaccine 2004, 22:1177-1187.

McKenney, P. T., Driks, A., Eskandarian, H. A., Grabowski, P., Guberman, J., Wang, K. H., Gitai, Z., Eichenberger, P. 2010. A Distance-Weighted Interaction Map Reveals a Previously Uncharacterized Layer of the *Bacillus subtilis* Spore Coat. Current Biology 20: 934–938

McKenney PT, Eichenberger P. 2012. Dynamics of spore coat morphogenesis in *Bacillus subtilis*. Mol Microbiol. Jan;83(2):245-60. doi: 10.1111/j.1365-2958.2011.07936.x.

Naclerio, G., Baccigalupi, L., Zilhao, R., De Felice, M. and Ricca, E. 1996. *Bacillus subtilis* spore coat assembly requires cotH gene expression. J. Bacteriol. 178: 4375-4380.

Nicholson, W. L., Munakata, N., Horneck, G., Melosh, H. J., and Setlow, P. 2000. Resistance of Bacillus endospores to extreme terrestrial and extraterrestrial environments. Microbiol. Mol. Biol. Rev. 64: 548-572.

Onyenwoke RU, Brill JA, Farahi K, Wiegel J. 2004. Sporulation genes in members of the low G+C Gram-type-positive phylogenetic branch (Firmicutes). Arch Microbiol. 182(2-3):182-92.

Ozin, A.J., Samford, C.S., Henriques, A.O., Moran, C.P. 2001. SpoVID guides SafA to the spore coat in *Bacillus subtilis*. J. Bacteriol. 183:3041–3049.

Paredes CJ, Alsaker KV, Papoutsakis ET. 2005. A comparative genomic view of clostridial sporulation

and physiology. Nat Rev Microbiol. 3(12): 969-78.

Parker, G. F., Daniel, R. A., and Errington, J. 1996. Timing and genetic regulation of commitment to sporulation in *Bacillus subtilis*. Microbiology 142:3445-3452.

Potot S, Serra CR, Henriques AO, Schyns G. Display of recombinant proteins on *Bacillus subtilis* spores, using a coat-associated enzyme as the carrier. Appl Environ Microbiol. 2010, 76:5926-5933.

Qi Peng, Guiwei Kao, Ning Qu, Jie Zhang, Jie Li, and Fuping Song. 2016. The Regulation of Exosporium-Related Genes in *Bacillus thuringiensis*. Sci Rep. 6: 19005.

Ramamuthi, K.S. and Losick, R. 2008. ATP-driven self-assembly of morphogenetic protein in *Bacillus subtilis.* Mol. Cell. 31(3): 406-414.

Redmond C, Baillie LW, Hibbs S, Moir AJ, Moir A. 2004. Identification of proteins in the exosporium of *Bacillus anthracis*. Microbiology. 150(Pt 2):355-63

Ricca, E., Cutting, S., and Losick, R. 1992. Characterization of bofA, a gene involved in intercompartimental regulation of pro-σK processing during sporulation in *Bacillus subtilis*. J. Bacteriol. 174:3177-31.

Ricca, E., Baccigalupi, L., Naclerio, G. and Cutting, S. 1997. Spore coat differentiation. Res. Microbiol. 148: 5-9.

Ricca E, Baccigalupi L, Cangiano G, De Felice M, Isticato R. 2014. Mucosal vaccine delivery by non-recombinant spores of *Bacillus subtilis*. Microb Cell Fact. 13:115.

Roels, S., Driks, A. and Losick, R. 1992. Characterization of spoIVA, a sporulation gene involved in coat morphogenesis in *Bacillus subtilis.* J. Bacteriol. 174: 575-585.

Sacco, M., Ricca, E., Losick, R. and Cutting, S. 1995. An additional GerE controlled gene encoding an abundant spore coat protein from *Bacillus subtilis.* J. Bacteriol. 177:372–377.

Setlow, P. 1994. Mechanisms which contribute to the long-term survival of spores of Bacillus species. J. Appl. Bacteriol. Symp. Suppl. 76:49S–60S.

Sirec T, Strazzulli A, Isticato R, De Felice M, Moracci M, Ricca E. 2012. Adsorption of β-galactosidase of Alicyclobacillus acidocaldarius on wild type and mutants spores of *Bacillus subtilis*. Microb Cell Fact. 11:100

Steichen C, Chen P, Kearney JF, Turnbough CL Jr. 2003. Identification of the immunodominant protein and other proteins of the *Bacillus anthracis* exosporium. J Bacteriol. 185(6):1903-10.

Steichen CT, Kearney JF, Turnbough CL Jr . 2005. Characterization of the exosporium basal layer protein BxpB of *Bacillus anthracis*. J Bacteriol. 187(17):5868-76

Stevens, C. M., Daniel, R., Illing, N. and Errington, J. 1992. Characterization of a sporulation gene spoIVA involved in spore coat morphogenesis in *Bacillus subtilis.* J. Bacteriol. 174: 586-594.

Terry C, Jiang S, Radford DS, Qiang W, Tzokov S, Moir A, Bullough PA 2017. Molecular tiling on the surface of a bacterial spore- the exosporium of the *Bacillus anthracis/cereus/thuringiensis* group. Mol Microbiol.

Wang Katherine, H., Isidro, A. L., Domingues, L., Eskandarian, H. A., McKenney, P. T., Drew, K., Grabowski, P., Chua, M. H., Barry, S. N., Guan, M., Bonneau, R., Henriques, A. O. Eichenberger P. 2009. The coat morphogenetic protein SpoVID is necessary forespore encasement in *Bacillus subtilis.* Molecular Microbiol. 74: 634-649.

Yim SK, Jung HC, Yun CH, Pan JG. 2009. Functional expression in *Bacillus subtilis* of mammalian NADPH-cytochrome P450 oxidoreductase and its spore-display. Protein Expr Purif. 63(1):5-11

Zhang B., Struffi P. and Kroos L. 1999. σK can negatively regulate sigE expression by two different mechanisms during sporulation of *Bacillus subtilis.* J. Bacteriol. p. 4081–4088

Zheng, L., and Losick, R. 1990. Cascade regulation of spore coat gene expression in *Bacillus subtilis.* J. Mol. Biol. 212:645- 660

Zilhao, R., Serrano, M., Isticato, R., Ricca, E., Moran, P. M., Henriques, A. O. 2004. Interactions among CotB, CotG and CotH during assembly of the *Bacillus subtilis* spore coat. J. Bacteriol. 186(4):1110-1119.

Zilhao, R., Naclerio, G., Henriques, A.O., Baccigalupi, L., Moran, C.P., Jr, and Ricca, E. 1999. Assembly requirements and role of CotH during spore coat formation in *Bacillus subtilis.* J Bacteriol 181: 2631–2633.

Part I:

Structural and functional study of spore coat

Chapter 2

The temperature of sporulation affects structure and function of *Bacillus subtilis* spores

2.1 Abstract

Bacterial spore formers are commonly and abundantly isolated from soil, water and air samples and are also found in large numbers associated to other organisms. Such diverse habitats are characterized by extremely different chemical and physical conditions, raising the question of whether spores produced at different conditions are identical or differ in terms of structure and function. We used *Bacillus subtilis* spores produced at 25°C, 37°C and 42°C but of similar age to analyze and compare their coat structure, their resistance properties and germination efficiency. Wild type spores produced at the 25°C were more hydrophobic than those produced at 37°C but contained less DPA and were less heat-resistant. We observed that CotH and a series of CotH-dependent coat proteins were more abundantly present in the coat of 25°C than 37 and 42°C spores, suggesting that CotH played a more relevant role at low temperature. Consistently, spores of a *cotH* null mutant were more damaged when produced at 25°C than at 37°C or 42°C.

2.2 Introduction

Bacterial endospores are formed in a wide range of ecological niches in soil, as well as in the gastrointestinal tract of invertebrate and vertebrate animals, and in both natural and anthropized environments [Nicholson *et al*., 2000]. Physical and chemical conditions prevailing in such niches play a major role in triggering sporulation and in determining the final properties of the resulting spores [Carlin F. 2011]. Laboratory experiments demonstrate the major influence of environment, in particular of temperature, on the efficiency and yield of sporulation, and in spore resistance to wet heat, UV, high hydrostatic pressure, and preservatives or spore response to germinants [Melly *et al*., 2002; Nicholson *et al*., 2000, Setlow P. 2006]. Spore resistance and functional properties result from the assembly of several protective structures: cortex, coat, and exosporium. The spore peptidoglycan cortex, a structure common to all endospores, is a major factor in the resistance of spores to heat [Nicholson *et al*., 2000, Setlow P. 2006]. The cortex is surrounded by a proteinaceous coat, and in organisms such as *Bacillus anthracis* or *Bacillus cereus* the coat is further enveloped by an exosporium, a "balloon-like" structure consisting of a paracrystalline basal layer and an external hair-like nap formed mainly by the collagen-like glycoprotein BclA [Ball DA *et al*., 2008; Boydston JA *et al*., 2005; Sylvestre P *et al*., 2009; Daubenspeck *et al*., 2004; Kailas *et al*., 2011; McKenney *et al*., 2013; Henriques *et al*., 2007] . While the coat contributes to protection against peptidoglycan-breaking enzymes, UV light, and oxidative agents, it is also central to the proper interaction of spores with compounds that trigger germination [Kailas *et al*., 2011]. The exosporium also contributes to spore resistance and germination and is additionally a key determinant in the adhesion of spores to cells and abiotic surfaces [Henriques *et al*., 2007; Terry C *et al*., 2011; Lequette Y *et al*., 2011]. A number of studies have shown that the temperature of sporulation affects some properties of spores, including resistance to heat and chemicals in *B. subtilis* [Melly *et al*., 2002] as well as in other Bacillus species [El-Bisi & Ordal, 1956; Warth,1978]. In *B.cereus* the temperature of sporulation also causes significant alterations in the composition of the spore coat and of the exosporium [Bressuire-Isoard *et al*., 2016]. The morphogenetic coat protein CotE of *B. cereus* is more represented in extracts from spores formed at

20°C than at 37°C, indicating that higher amounts of the protein is required to maintain proper assembly of spore surface layers at the former temperature suggesting a complex relationship between the function of a spore regulatory protein and environmental factors such as the temperature during spore formation [Bressuire-Isoard *et al*., 2016].

It has been previously reported that "early spores" (i.e. the first 10% of spores released from sporangia during sporulation) have resistance property that significantly differ from older spores [Sanchez-Salas *et al*., 2011] and that entering dormancy requires a few days, during which spores are affected by the environment and undergo corresponding molecular changes influencing their emergence from quiescence (germination) [Segev *et al*., 2012].

Here we have first analyzed cells sporulating at 25, 37 and 42°C and determined that the former are 2.5-fold slower while the latter are faster than 37°C in producing spores. Based on this, we have collected spores of similar age bit grown at the three different temperatures and have compared the functional properties of spores produced at 25 and 42°C with those formed at the optimal growth temperature (37°C). Then, we studied the effects of the sporulation temperature on the structure of the spore surface layers and we found that the morphogenetic coat protein CotH was more abundant in spores produced at 25°C than at the other two temperatures. The different amount of CotH and so the different organization of the spore surface-layers could be responsible for different properties of the spore formed at 25, 27 and 42°C.

Our analysis highlights the strict relationship between the environmental factors and the spore coat morphogenetic proteins, able to influence the spore structure.

2.3 Results and Discussion

2.3.1 Production of spores of similar age at 25°C, 37°C and 42°C

It has been previously reported that spores of different age have significantly different resistance properties and germination efficiency [Sanchez-Salas et al., 2011; Segev et al., 2012]. Based on this, to analyze the structure and function of spores grown at 25, 37 and 42°C we developed a method to identify, collect and then compare spores of similar age but produced at different temperatures. To this aim, we used isogenic strains of *B. subtilis* carrying the gene coding for the green fluorescent protein (*gfp*) posed under the control of sporulation-specific promoters recognized by the RNA polymerase sigma factors σ^F (*spoIIQ* gene [Donadio *et al*., 2016]), σ^K (*gerE* gene [Donadio *et al*., 2016]) or σ^K in conjunction with GerE (*cotC* gene [Donadio *et a*l., 2016]) (Fig. 1). Cells were induced to sporulate in Difco Sporulation Medium (DSM) at 25, 37 and 42°C, aliquots were collected at various times after the onset of sporulation and analyzed by flow cytometry and fluorescent microscopy to assess the percentage of fluorescent cells in each sample. Inducing the sporulation at 37°C, fluorescent forespore appeared after 2 hours when the gfp expression was controlled by the σ^F-dependent promoter, while fluorescent sporangium compared after 5 or 7 hours when the gfp expression was controlled by σ^K or σ^K-GerE, respectively (Fig.1; Table 1). These results are in agreement with literature data [Fujita and Losick, 2003]. In all three strains, the production of fluorescent cells was delayed at 25°C with respect to 37 and 42°C (Table 1). We calculated the delay factor of sporulation caused by the low temperature as the ratio between the hours needed to observe the appearing of fluorescent cells at 25°C vs 37-42°C

and we obtained a value of 2.5 as the average of the results obtained with the three strains (Table 1)

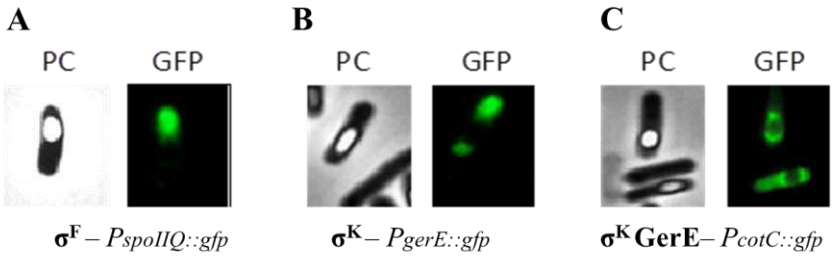

Figure 1: Fluorescence microscopy images of sporulating cells expressing gfp under the control of sporulation-specific sigma and transcriptional factors. Images were taken at 2 hours (A- P_{spoIIQ}*::gfp*), 5,5 hours (B - P_{gerE}*::gfp*) and 7 hours (C - P_{cotC}*::gfp*) from the onset of sporulation. . PC: phase contrast image, GFP: Green fluorescent microscopy image

		25 °C	37 °C	42°C	Delay factor respect to 37°C sporulation (hours)	
		Hours after onset of sporulation			25 °C	42°C
$P_{spoIIQ::gfp}$	σ^F	5	2	1	2,5	2
$P_{gerE::gfp}$	σ^k	15	5,5	5	2,7	1,1
$P_{cotC::gfp}$	σ^k GerE	19	7	6	2,7	1,1

Table 1: Time of gfp expression during sporulation at 25, 37 and 42°C. The analyzed gfp fusions, the relative sigma and transcriptional factors and the delay factors respect the 37°C samples are reported.

We then used the *B. subtilis* strain PY79, isogenic to the strains used for the experiment of Fig. 1, to produce spores in DSM at 25, 37 and 42°C. At different times during sporulation aliquots were collected and analyzed under the light microscope to assess the number of cells, sporangia (cells containing forespores) and free spores (Fig. 2B). For each time point cells, sporangia and spores of eight independent microscopy fields were counted and averaged (Fig. 2A). After 30 hours at 37 and 42°C about 80% of free spores were observed in the culture while a similar percentage of free spores was reached only after 72 hours at 25°C (Fig. 2A), consistently with the delay factor calculated in Table 1. Based on these, spores produced after 30 hours at 37°C and 42°C and after 72 hours at 25°C were considered of similar age and used for all further experiments. The efficiency of sporulation at the three temperature was calculated as the percentage of the mature spore produced after 30 h at 37 and 42°C and after 72 h at 25°C respect the number of viable cells at T0. As shown in figure 2C, the sporulation is less efficient both at 25 and at 42 than 37°C.

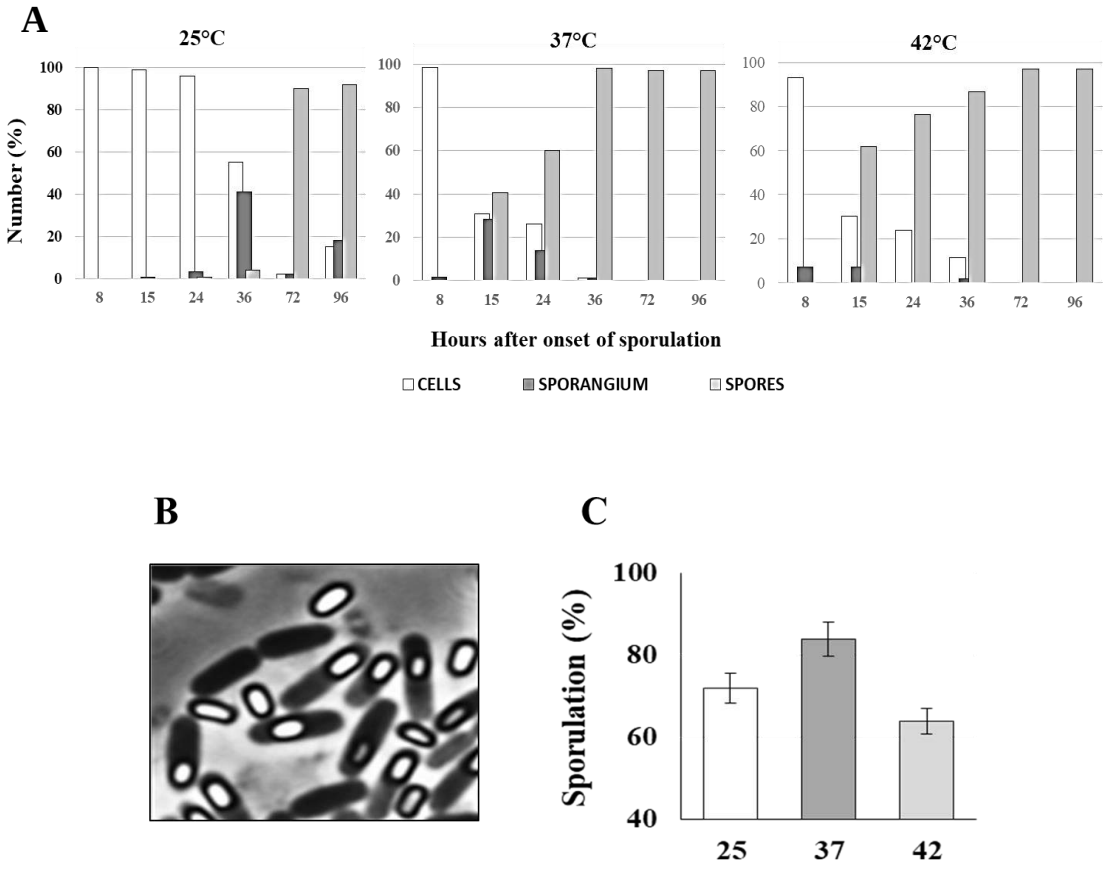

Figure 2: The course of morphogenesis during sporulation at different temperatures. Samples from sporulating cultures were collected at various times after the onset of sporulation and analyzed at light microscopy. Panel (**A**) reports the percentages of cells (white histograms), sporangia (dark-grey histograms) and free spores (light-grey histograms) during sporulation at the three temperatures. (**B**) Phase-contrast microscopy image illustrating cells, sporangia and free spores. (**C**) Estimation of sporulation efficiency of PY79 spores formed at 25, 37 and 42°C.

2.3.2 Physiological analysis of spores of similar age grown at 25, 37 and 42°C

Purified spores of similar age produced at the three different temperatures were analyzed for their resistance properties, efficiency of germination and hydrophobicity. As shown in Fig. 3, spores produced at lower temperature are slightly more sensitive to lysozyme digestion respect ones produced at 37°C, while spores produced at 42°C appeared as the ones more resistant. Even if the observed differences between the three strains are very small, they are statistically consistent (P value - 0.05).

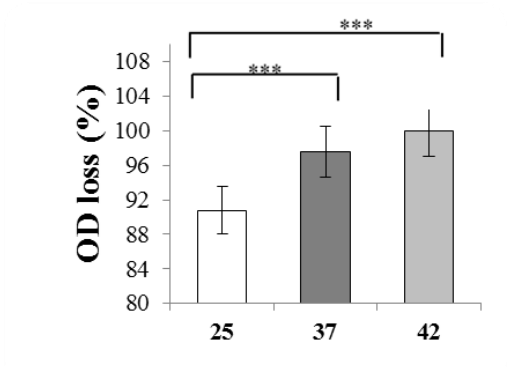

Figure 3: Sensitivity of spores to lysozyme digestion: spores formed at 25°C (white histogram), 37°C (dark-grey histogram) and 42°C (light-grey histogram) were incubated with 50 mg/ ml of lysozyme and the percentage of loss refraction calculated. The results are the mean from six replicate experiments, each performed with an independently prepared spore suspension. Bars represent standard deviations. *** at Pvalues of - 0.05 (Tukey's test).

The spores of three groups were not equally resistant to heat: spores formed at 42°C contained more DPA (Fig. 4A) and, probably for this reason, were more heat-resistant than those produced at 25 and 37°C (Fig. 4B). As previously observed, the spores produced at 25°C appeared the most sensitive ones.

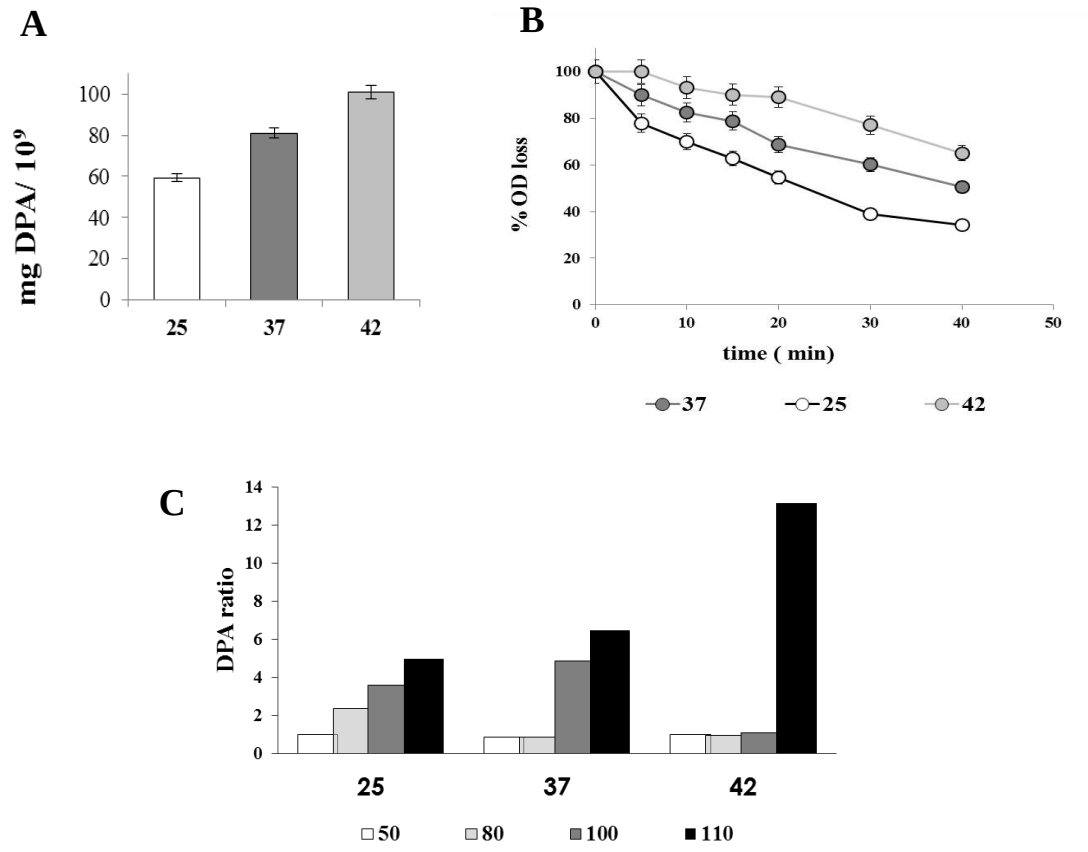

Figure 4: (**A**) DPA content of spores produced at 25°C (white histogram), 37°C (dark-grey histogram) and 42°C (light-grey histogram). (**B**) Sensitivity to wet heat at 100°C. (**C**) DPA release from spores incubated at 50, 80, 100 and 110°C (from white to black histograms).

The previous results were confirmed by measuring the release of DPA from the spores after 15 min of incubation at 50, 80, 100 and 110°C. As shown in Fig. 4C, 80°C treatment is sufficient for the DPA release from the 25°C-spores while a higher temperature (110°C) stress is necessary for the release of DPA from 42°C spores.

The germination efficiency was measured using asparagine as germinant (Fig.5A). 42°C spores (light-grey line in Fig. 5B) were about 15 min delayed with respect to 25 and 37°C spores (black and dark-grey lines respectively in Fig. 5B).

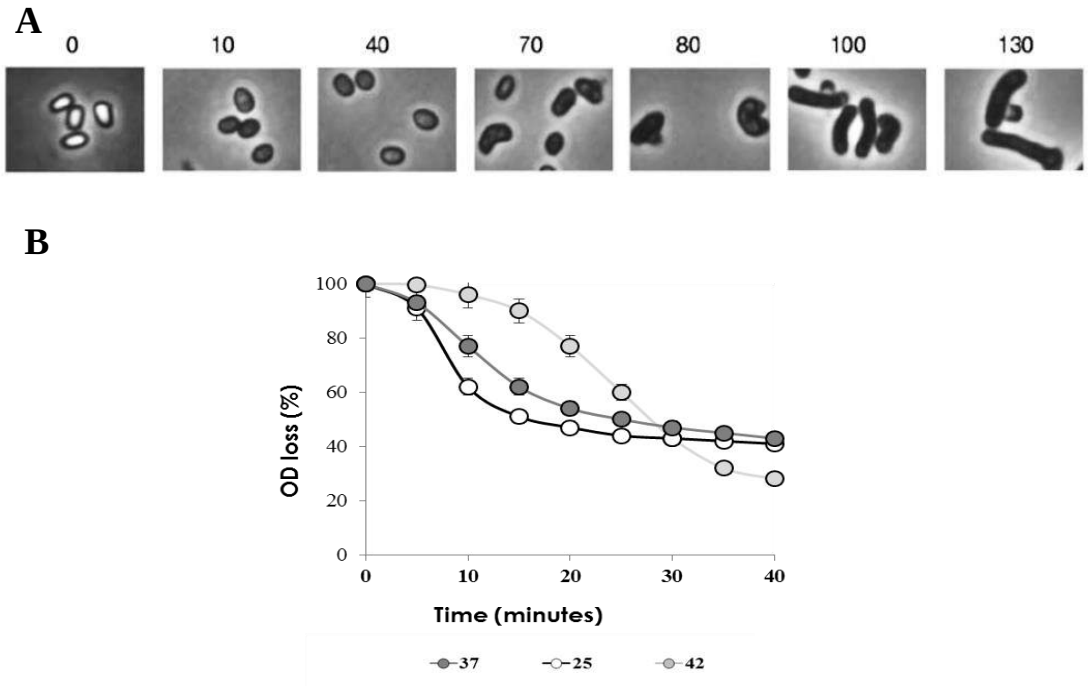

Figure 5: (**A**) Schematic representation of spore germination [Keijser *et al*., 2007].(**B**) Germination in response to asparagine. The percentage of germination was determined as OD_{580} loss. The numbers represent the means from three replicate experiments, each performed with an independently prepared spore suspension. Bars represent standard deviations.

Then, we checked if the sporulation temperature affects also the hydrophobicity of the spore surface. An assay based on the partitioning of spores purified through extensive water washing between aqueous and hexadecane phases was used. Spores produced at 42°C were significantly (P - 0.05) less hydrophobic than spores formed at lower temperature (Fig. 6).

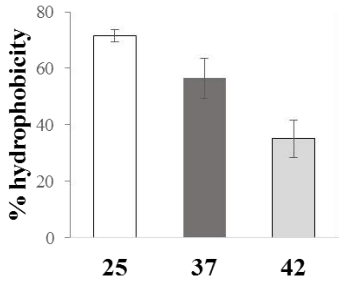

Figure 6: Hydrophobicity of spores prepared at 25, 37 and 42°C. The percentage of hydrophobicity represents the proportion (+ 100) of spores in n-hexadecane after a separation into solvent and water phases. Each hydrophobicity percentage is the mean from three replicate experiments, each performed with an independently prepared spore suspension. Bars represent standard deviations.

All together results (Fig. 3- 6) suggested that sporulation temperature is able to affect the composition and structure of the spore, above all the surface layers, directly involved in the lysozyme resistant, germination efficiency and in the hydrophobicity of the spore. We therefore tested whether the sporulation temperature could affect the coat and crust composition.

2.3.3 Ultra-structure of spores produced at 25, 37 and 42 °C

The different hydrophobicity of 25, 37 and 42°C spores suggested structural differences in the spore surface. Therefore, we analyzed the three spore suspensions by transmission electron microscopy (Fig. 7). As expected, the 37°C spore surface was composed of two layers, the lamellar inner coat and the thick electron-dense outer coat. In the spores produced at 25 ° C, the outercoat appeared more compact, lamellar and partially detached from the inner coat while at 42°C was more widespread and thick. These observations reflected a different organization of the proteins in the superficial layers of the spores as evidenced by physiological assays.

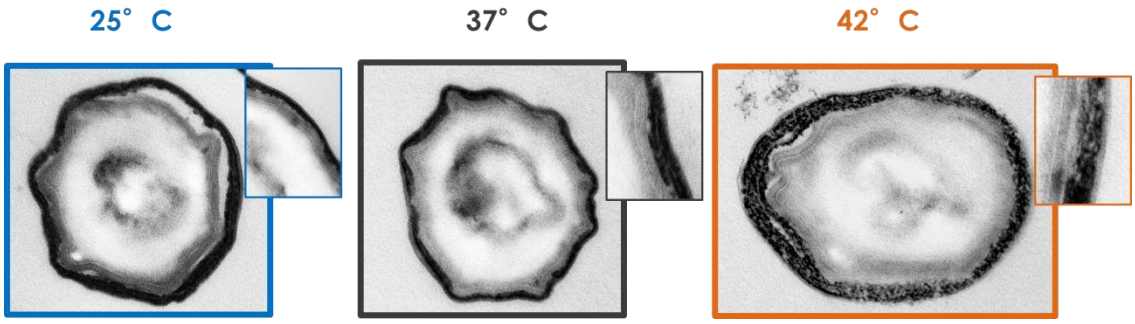

Figure 7: Transmission electron microscopy of thin section of spores produced at 25, 37 and 42°C.

2.3.4 CotH and some CotH-dependent coat proteins are more abundant at 25 °C than at 37°C

Previous results revealed a coat structure affected by the sporulation temperature. Therefore, we used purified spores of similar age to extract coat proteins by SDS-DTT procedure [Nicholson and Setlow,

1990]. The SDS-PAGE profiles of the extracted proteins did not differed drastically, however, some differences were observed and CotB (65 kDa), CotG (36 kDa), CotQ (48 kDa) and CotS (40 kDa) were all less represented in spores grown at 42 and 37 than at 25°C (Fig. 8A). CotQ and CotS were identified by determining the N-terminal amino acid sequence of the migrating bands as 40 and 48 kDa. CotB and CotG were identified by a western blot approach. As shown in Fig. 8B, both CotB and CotG are less abundant in the coat of 42 than that of 37 and 25°C spores. As a control, we used anti-CotA antibody that showed no differences in the amount of CotA present in the three samples (Fig. 8B).

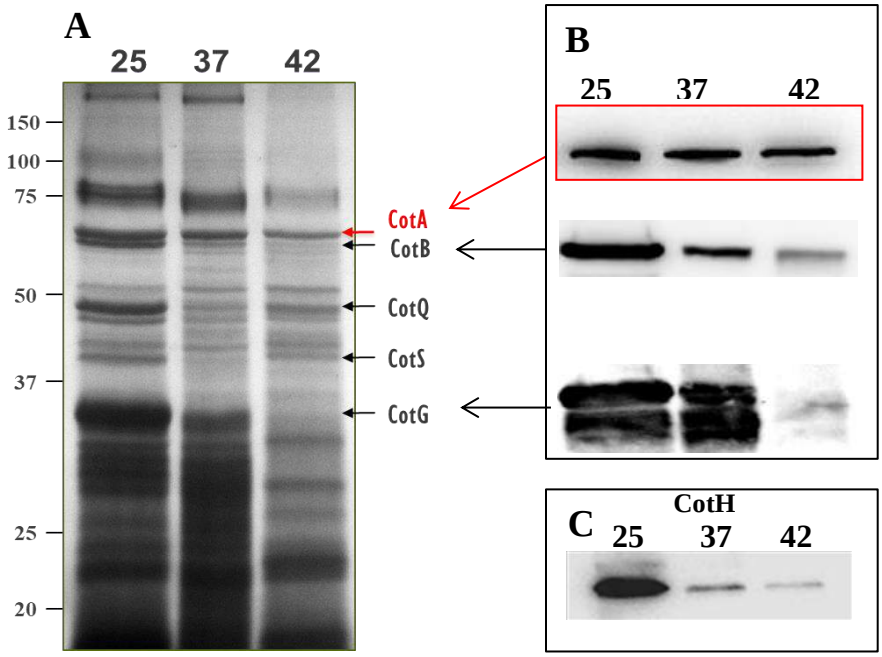

Figure 8: Effects of sporulation temperature on surface layers composition. **(A)** Pattern of spore surface proteins extracted from *B.subtilis* strain PY79 prepared at 25°C(lane 1), 37°C (lane 2) and 42°C (lane 3). The arrows indicate the bands corresponding to CotB (65kDa), CotQ (48 kDa), CotS (40 kDa) and CotG (36-33 kDa) proteins. **(B)**Western blot analysis of proteins extracted from mature spores prepared at the three temperatures with anti-CotB and CotG antibodies or anti-CotA (66 kDa (**C**) western blot analysis of the previous proteins with anti-CotH antibody.

Since the assembly of CotB, CotG, CotQ and CotS is dependent on the action of the morphogenetic protein CotH [Kim *et al*, 2006; Zilhao *et al*., 2004], we checked whether also the amount of CotH in the coat was dependent on the temperature of sporulation. The western blot of Fig. 8C clearly showed that CotH was more abundant in the coat of spores grown at 25 than at 37 and 42°C, suggesting that the observed different amounts of CotB, CotG, CotQ and CotS could be CotH dependent. This hypothesis had supported by the observation that the amount of CotA, whose assembly in the coat is independent on CotH, was not affected by the temperature (Fig. 8B). So, we verified whether the assembly of other CotH-dependent proteins was not affected by the sporulation temperature as CotC, CotU and CotZ. CotZ is a representative protein responsible for spore surface hydrophobicity and adhesion. CotZ was more abundant at 25 than at 37 and 42°C as well as CotB and CotG (Fig. 9A), explaining the higher hydrophobicity (Fig. 6) of spores produced at low temperature. CotC and CotU are two homologous

CotH-dependent proteins that recognized by both anti-CotC and CotU antibodies. CotC is one of the most abundant proteins of the outer coat and is present in this layer as a monomer (12 kDa), homodimer (21 kDa), and heterodimer with CotU (17kDa) of 23 kDa and as two additional forms of 12.5 and 30 kDa [Isticato *et al*., 2004; Isticato *et al*., 2008]. CotC and CotU are affected by the temperature but in the opposite way respect CotB and CotG: CotC and CotU were less representative at 25 and 37 than at 42°C in which the multimeric forms were more abundant (Fig. 9B).

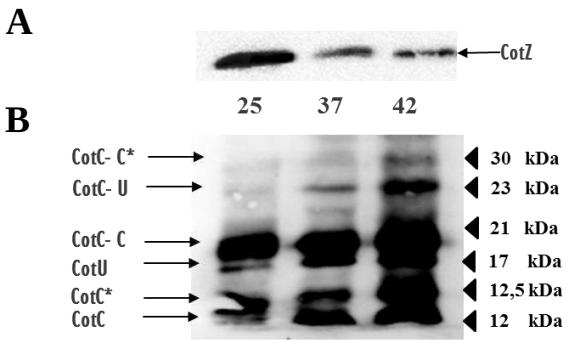

Figure 9: Effects of sporulation temperature on surface layers composition.Western blot with anti CotZ (**A**) and anti-CotC (**B**) antibodies of proteins extracted from mature spores of PY79 prepared at 25, 37 and 42°C. (**B)**The various forms of CotC and CotU are indicated. CotC* indicates a post-translationally modified form of CotC [Isticato *et al*., 2004].

Our results highlight that the sporulation temperature influences the coat and crust composition probably through the action of the morphogenetic protein CotH.

2.3.5 CotH is more stable at 25°C than at 37 and 42°C

Previous western blot analysis revealed a higher amount of CotH in the extract of spore formed at 25°C (Fig . 8C). We investigated if the different amount observed was due to a different expression level of *cotH* or to a different stability of the protein at the three temperatures. To this aim, we used a wild-type strain carrying a translational gene fusion between the *cotH* promoter region and the *lacZ* gene of *E. coli* and measured the activity of β-galactosidase at various times (ranging from T0 to T20) at the three temperatures after the onset of sporulation. The time-course experiment in Fig. 10 shows that *cotH*-directed β-galactosidase production begins at different times in function of sporulation temperature, as expected, and that the expression levels of the gene are comparable at the tested temperatures.

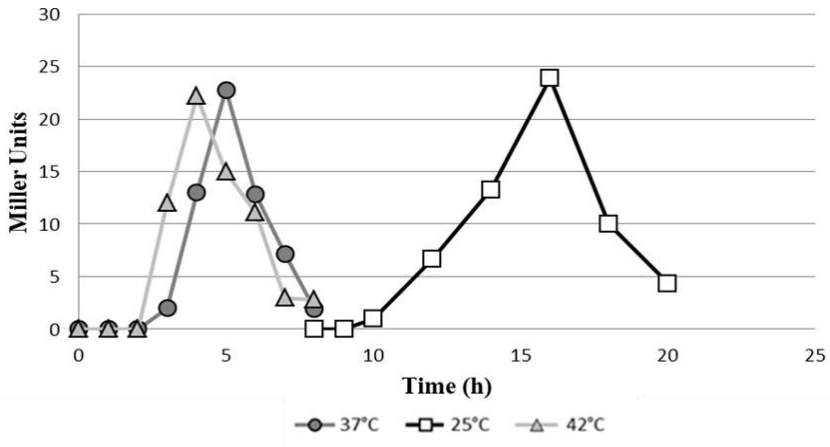

Figure 10: Expression of a *cotH::lacZ* translational fusion during sporulation in wild-type at 25°C (white squares), 37°C (dark-grey circles) and 42°C (light-grey triangles). Samples were collected at various times after the onset of sporulation. Enzyme activity is expressed in Miller units. The data are the means of three independent experiments.

Then we investigated the stability of CotH using the prediction program SCooP that provides the temperature-dependent stability curve of a monomer protein by the analysis of its 3D-structure. The graph in Fig. 11A shows that the free energy (ΔG) associated with the CotH folding is lower at temperatures between 10 to 30°C, suggesting a major stability of the protein in this temperature range.

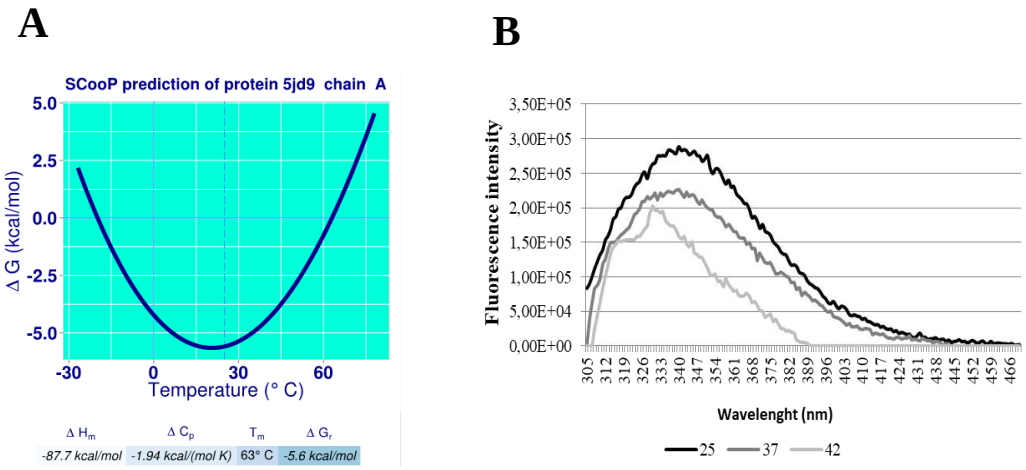

Figure 11: **(A)** Stability curve of CotH in function of temperature obtaining by SCooP program prediction. This automated tool uses the protein structure and the host organism as sole entries and predicts the full T-dependent stability curve of monomeric proteins assumed to follow a two-state folding transition. **(B)** CotH thermal stability monitored by Trp fluorescence. CotH emission scan after 30 min incubation at 25 (black line), 37 (dark-grey line) and 42°C (light-grey line). For each temperature, the fluorescence emission of Trp was measured and normalized with the native protein. CotH concentration 5mmol/L in PBS. Each spectrum was the average of three scans.

To confirm this result, we used a sensitive spectrofluorimetric method of measuring intrinsic fluorescence of Trp residues present in CotH sequence. Those residues can be used to follow protein folding because their fluorescence properties are sensitive to the environment which changes when protein folds/unfolds. In native condition, Trp residues are hidden in the hydrophobic core of the

protein with high fluorescence intensity. The loss of folding induces an exposition of Trp residues to a hydrophilic environment with a decrease of fluorescent emission. As shown in figure 11B, the higher fluorescent emission was observed after the incubation of CotH at 25°C (black line), with a decrease of the intensity emission at the increase of incubation temperature (dark and light-grey lines respectively 37 and 42°C). This analysis confirmed that CotH is more stable at low temperature and that the higher amount of CotH (Fig. 8C) was due to a major stability of the protein at 25°C than 37 or 42°C

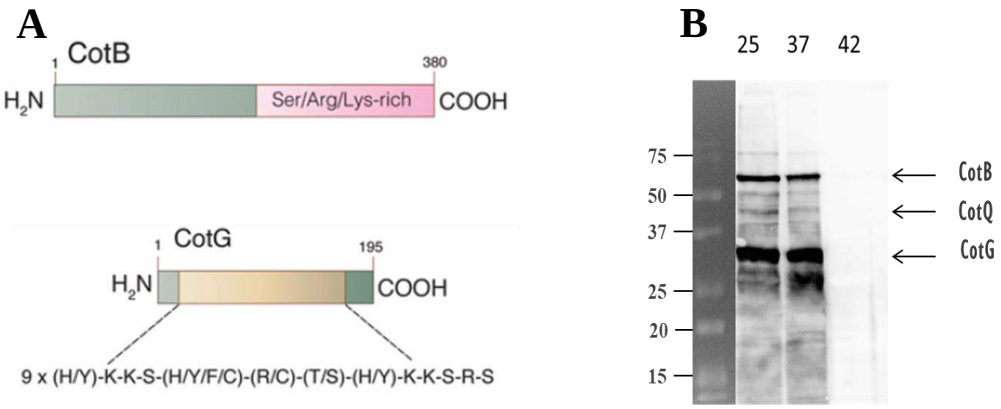

Figure 12: *B. subtilis* CotH phosphorylates the spore coat proteins CotB and CotG. (**A**) Schematic representation of *B. subtilis* CotB depicting the Ser/Arg/Lys-rich C-terminal region and CotG depicting the nine tandem repeats in the protein [Ngujen *et al*., 2016]. (**B**) Protein immunoblotting of PY79 spore coat extracts using a phosphospecific PKC substrate antibody depicting the phosphorylation of spore coat proteins in the spore produced at 25, 37 and 42°C. The arrows depict proteins that we infer are CotB(65kDa), CotQ (48kDa) and CotG (36 kDa) based on their molecular masses.

Recently, it has been demonstrated that CotH is an atypical protein kinase-like (PKL) and CotB and CotG are its substrates [Nguyen *et al*., 2016]. Both CotB and CotG are phosphorylated on Ser residues adjacent to basic amino acids. In fact, 37 of the 39 Ser residues in CotG and more than half of the 57 Ser residues within the C terminus of CotB contain a Lys or Arg at the n − 2 or n + 2 position (R/K-x-S-x or x-S-x-R/K) (Fig. 12A). This motif resembles the consensus recognition sequence for the eukaryotic protein kinase C (PKC)[Nguyen *et al*., 2016].

In order to understand whether the sporulation temperature affected kinase activity of CotH, we purified 25, 37 and 42 °C spores and analyzed spore coat extracts by immunoblotting with a PKC substrate-specific antibody (pPKC-Ab) that recognizes the PKC consensus phosphorylation motif. The western blot of Fig. 12B showed that CotH kinase activity was not altered when the sporulation was performed at 25 or 37 °C, while no enzyme activity was detected at 42°C. This result was probably due to either the instability of the enzyme or a decrease in its substrates at the higher temperature.

2.4 Conclusions

Our results show that the sporulation temperature affects the beginning and lasting of the process and its efficiency. We observed that the sporulation process is 1.3 folds faster but less efficient at 42 than 37°C and 2.5 folds slower and less efficient at 25 than at 37°C. Supporting these data, we compared *B. subtilis* spores produced at the three temperatures but of similar age for their resistance properties and germination efficiency. When formed at 42°C, the spores, containing more DPA, are more resistant to

wet-heat treatment than 37 and 25°C spores that appear the more sensitive. Furthermore, a weak treatment (50°C) is sufficient for the DPA release from the 25°C spores while a higher temperature (110°C) stress is necessary for the release of DPA from 42°C spores. In addition, 42°C spores are much more resistant than 25 and 37°C spores to lysozyme and they are also 15 min delayed with respect to 25 and 37°C spores in the germination process. The inaccessibility of both the germinant and the lysozyme in the spores at 42°C could be due to a different structural composition revealed by electronic microscopy. At 25°C the outercoat is more compact, lamellar and partially detached from the inner-coat while at 42°C is more widespread and thick. Conversely, spores formed at 25°C appear more hydrophobic that those at 37 and 42°C. Consistent with the ultrastructural analysis, the coat of spores produced at the three temperatures differs in the protein composition. This temperature-dependent effect is due to the kinase CotH, responsible for the assembly of more than 11 coat proteins. Our data show that the enzyme is more abundant in the spores formed at 25 than at 37 or 42°C.

The amount of CotH, in turn, influences the coat structure. The CotH-dependent coat proteins, CotB, CotG, CotS, CotZ, CotQ are more represented in extracts from spores produced at 25°C than in those produced at 37 and 42°C. CotC and CotU, other two CotH-dependent, are also affected by the temperature but in the opposite way. The higher amount of CotC and CotU in the 42°C produced spores could be due to the lower levels of CotG, allegedly involved in their degradation [Isticato *et al*., 2008]. Interestingly, we demonstrated that the CotH amount is due to the stability of the protein at low temperature and not to at a temperature-dependent expression level of the gene.

Preliminary data show that the kinase activity does not change at 25 and 37°C, while no phosphorylation CotH dependent was detected at 42°C. This could be due either to a less representation of CotH substrates or different protein stability at the three temperatures.

Our results suggest that the temperature of sporulation causes a switch in the spore coat structure with a different coat profile between 25, 37 and 42°C. Understanding the spore assembly mechanisms under different environmental conditions may help to assess the structure and properties of spores existing in the natural environment and the development of optimized industrial treatments, particularly in the food chain, to limit the survival and germination of contaminating spores.

2.5 Materials and Methods

2.5.1 Bacterial strains

B. subtilis strains are listed in the following Table:

Strain	Relevant genotype	Reference
PY79	wild type	[Youngman P. *et al*., 1984]
	cotH::6hys	[Isticato *et al*., 2015]
GC314	*cotH::lacZ*	[Lab Stock]
2466	*amyE:: PspoIIq-GFP*	[Lab stock]
2467	*amyE::PgerE-GFP*	[Lab stock]
RH283	*amyE::PcotC-GFP*	[Lab stock]

2.5.2 Physiological assays

Germination efficiency: Purified spores were heat activated as previously described [Cutting S, Vander Horn PB, 1990] and diluted in 10 mM Tris-HCl (pH 8.0) buffer containing 1 mM glucose, 1 mM fructose, and 10 mM KCl. The germination was induced by adding 10 mM asparagine and the optical density at 580 nm was measured in a microplates reader Biotek - Synergy H4, reading for an hour every 5 min [Cutting S, Vander Horn PB, 1990].

Lysozyme resistance: Sensitivity to lysozyme was measured as described by Zheng *et al*. Spores were prepared as previously described [Cutting S, Vander Horn PB, 1990], omitting the lysozyme step and eliminating vegetative cells by heat treatment (10 min at 80°C). Purified spores were then suspended in 10 mM Tris-HCl (pH 7.0) buffer containing lysozyme (50 mg/ml), and the decrease in optical density was monitored at 595 nm in a microplates reader Biotek - Synergy H4, reading for an hour every 5 min.

Heat resistance: Purified spores were incubated at 80°C for 20 min. The decrease in optical density was monitored at 580 nm in a microplates reader Biotek - Synergy H4, reading for an hour every 5 min.

Hydrophobicity assay: The BATH assay [Wiencek KM *et al*., 1990] was used to assess the relative hydrophobicity of bacterial spores. Briefly, wild-type spore suspensions ($1.5 \times 10^8 \pm 0.1 \times 10^8$ counted under an optical microscope with a Burker chamber) were incubated for 15 min at 25°C, and then 1.0 ml of hexadecane (Sigma-Aldrich) was added to 3.0 ml of each spore suspension. The mixture was vortexed for 1 min in glass test tubes (15 by 100 mm), and the hexadecane and aqueous phase were allowed to partition for 15 min. The aqueous phase was carefully removed with a Pasteur pipette, and the OD440 was measured. As previously reported [Wiencek KM *et al*., 1990], the decrease in OD_{440} of the aqueous suspension indicated the relative hydrophobicity, and this was calculated as 100 $(A_0 - A_f)/A_0$, where A_0 and A_f were the initial and final OD_{440}, respectively.

2.5.3 DPA content and its release from spores

$1x10^9$ spores were washed twice in 50 mM KCl to remove readily exchangeable calcium from them. Subsequently, the spores were autoclaved at 121°C for 30 min to completely release DPA from endospores. The samples were centrifuged for 10 min at 13,000 x g, to fractionate pellet and supernatant. Then, the supernatants were transferred to a multiwell plate, in presence of 50 µM $TbCl_3$. The DPA content was measured following the formation of Tb^{3+} - DPA complex in a microplates reader Biotek - Synergy H4, reading for an hour every 5 min (λex=270 nm, λem=545 nm). Standard curves of calcium DPA (from 100 ng/l to 10 mg/l) were constructed to determine mg of DPA/ 10^9 spores. In the case of DPA release, a suspension of ~$1x10^9$ spores was added to 150 µl of 10 mM pH8 TRIS- HCl. The samples were incubated at different temperatures 50, 80, 100 and 110°C for 15 min and then centrifuged for 2 min at 13,000 x g, to fractionate pellet and supernatant. The DPA concentration was measured as described above.

2.5.4 Spore purification, extraction of spore coat proteins and western blot analysis

Sporulation was induced by exhaustion by growing cells in DSM (Difco Sporulation Medium) as described elsewhere [Cutting S, Vander Horn PB, 1990]. After 30 h of incubation at 37°C, spores were collected, washed four times, and purified as described by Nicholson and Setlow [29] using overnight incubation in H_2O at 4°C to lyse residual sporangial cells. Spore coat proteins were extracted from a suspension of spores by SDS-dithiothreitol (DTT) [Cutting S, Vander Horn PB, 1990], or NaOH [29] treatment. The concentration of extracted proteins was determined by using Bio-Rad DC protein assay kit (Bio-Rad), and 20 µg of total spore coat proteins were fractionated on 12,5% SDS polyacrylamide gels and electro-transferred to nitrocellulose filters (Bio-Rad) for Western blot analysis following standard procedures. CotH-, CotA-, CotC-, CotB- CotG- and PKC specific antibodies were used at working dilutions of 1:150 for CotH detection, 1:7000 for CotA, CotC, CotB and CotG detection and 1:10000 for PKC. Then an horseradish peroxidase (HRP)-conjugated anti-rabbit secondary antibody was used (Santa Cruz). Western blot filters were visualized by the ECL method as specified by the manufacturer.

2.5.5 β-galactosidase assay

Samples (1.0 ml each) of *cotH-lacZ*-bearing cells to be analysed for β- galactosidase activity were collected at the indicated times (T0-T20) during sporulation by centrifugation, and the cell pellets were stored at -70°C until the time of assay [Ricca *et al*., 1992]. The specific activity of β-galactosidase was determined as described by Miller [Miller, J. H. 1972] with the substrate o-nitrophenol-p-D-galactosidase (ONPG). Briefly, 0.3 ml of a Z-Buffer solution (60mM Na_2HPO_4 x $7H_2O$, 40mM NaH_2PO_4, 10mM KCl, 1mM $MgSO_4$ x $7H_2O$, 50 mM β-mercaptoethanol) and 10µl of toluene, to permeabilize the cells, were added to the thawed pellets. After pre-incubation at 30 ° C for 15 min, 0, 15 ml of each sample was transferred in a 96 multiwell. The reaction starts adding 30 µL of 4mg/ml ONPG. The optical density was monitored at 420 and 595 nm in a microplates reader Biotek - Synergy H4, reading for the first 10 min every 2 min and then for 20 min every 5 min. The specific β-galactosidase activity was expressed in Miller units, calculated as follows:

$$Miller\ unit = \frac{A420}{reaction\ time\ \ x\ OD590}\ x\ 1000$$

2.5.6 Expression and purification of CotH

For CotH production, cells of *Escherichia coli* strain CotH-Hys, bearing pBAD-B expression vector (*Life Technologies*) carrying an in-frame fusion of the 5′ end of the *cotH* coding region to six histidine codons under the transcriptional control of a T7 promoter, were grown for 18 h at 37°C in 100 ml of autoinduction medium to express the heterologous protein [Isticato *et al*., 2015]. The His_6-

tagged CotH protein was purified under native conditions using a His-Trap column as recommended by the manufacturer (GE Healthcare Life Science). Purified protein was desalted using a PD10 column (GE Healthcare Life Science) to remove high NaCl and imidazole concentrations.

2.5.7 Spectrofluorometric method to monitor changes in protein structure

The purified CotH protein was dissolved in phosphate buffer saline (PBS: 150 mmol/l NaCl, 1,9 mmol/l NaH_2PO_4, 8,1 mmol/l Na_2HPO_4 pH 7,4) at a concentration of 5 µmol/l. Fluorescence spectra were acquired at time 0 and after 30 min of incubation at three different temperatures, (25, 37 and 42 °C) using a Fluoromax-4 fluorometer (Horiba, Edison, NJ, USA) using a 1 cm path length quartz cuvette. Samples were continuously stirred and allowed to equilibrate to each temperature before fluorescence readings were taken. Excitation wavelength of 295 nm was used to avoid the contribution from tyrosine residues. The excitation and emission band widths were set to 5 and 2,5 nm, respectively. The emission spectra were recorded from 305 to 470. Each spectrum was the average of three scans [Jokiel *et al*., 2006]. The percentage of denatured protein is given by the equation:

$$P = \frac{F(T) - FN}{FD - FN} x\ 100\%$$

Where FN and FD are fluorescence intensities for a native and denatured protein, respectively. F(T) is the fluorescence intensity that corresponds to temperature T[Jokiel *et al*., 2006].

2.6 References

Ball DA, Taylor R, Todd SJ, Redmond C, Couture-Tosi E, Sylvestre P, Moir A, Bullough PA. 2008. Structure of the exosporium and sublayers of spores of the *Bacillus cereus* family revealed by electron crystallography. Mol Microbiol 68:947–958.

Bressuire-Isoard C, Bornard I, Henriques AO, Carlin F, Broussolle V. Sporulation Temperature Reveals a Requirement for CotE in the Assembly of both the Coat and Exosporium Layers of *Bacillus cereus* Spores. Appl Environ Microbiol. 2015 Oct 23;82(1):232-43.

Boydston JA, Chen P, Steichen CT, Turnbough CL. 2005. Orientation within the exosporium and structural stability of the collagen-like glycoprotein BclA of *Bacillus anthracis*. J Bacteriol 187:5310 –5317.

Carlin F. 2011. Origin of bacterial spores contaminating foods. Food Microbiol 28:177–182.

Cutting, S., and P. B. Vander Horn. 1990. Genetic analysis, p. 27–74. In C. Harwood and S. Cutting (ed.), Molecular biological methods for Bacillus. John Wiley & Sons, Chichester, United Kingdom.

Daubenspeck JM, Zeng HD, Chen P, Dong SL, Steichen CT, Krishna NR, Pritchard DG, Turnbough CL. 2004. Novel oligosaccharide side chains of the collagen-like region of BclA, the major glycoprotein of the *Bacillus anthracis* exosporium. J Biol Chem 279:30945–30953

Donadio G, Lanzilli M, Sirec T, Ricca E, Isticato R. Localization of a red fluorescence protein adsorbed on wild type and mutant spores of *Bacillus subtilis*. Microb Cell Fact. 2016 Sep 8;15(1):153.

El-Bisi HM, Ordal ZJ. The effect of sporulation temperature on the thermal resistance of *Bacillus coagulans var. thermoacidurans*.J Bacteriol. 1956 Jan;71(1):10-6.

Fujita M1, Losick R. The master regulator for entry into sporulation in Bacillus subtilis becomes a cell-specific transcription factor after asymmetric division. Genes Dev. 2003 May 1;17(9):1166-74.

Henriques AO, Moran CP, Jr. 2007. Structure, assembly, and function of the spore surface layers. Annu Rev Microbiol 61:555–588.

Isticato R, Esposito G, Zilhão R, Nolasco S, Cangiano G, De Felice M, et al. Assembly of Multiple CotC Forms into the *Bacillus subtilis* Spore Coat. J. Bacteriol. 2004; 186:1129–1135.

Isticato R, Pelosi A, Zilhão R, Baccigalupi L, Henriques AO, De Felice M, et al. CotC-CotU heterodimerization during assembly of the *Bacillus subtilis* spore coat. J. Bacteriol. 2008; 190:1267–1275.

Isticato R, Sirec T, Vecchione S, Crispino A, Saggese A, Baccigalupi L, Notomista E, Driks A, Ricca E. The Direct Interaction between Two Morphogenetic Proteins Is Essential for Spore Coat Formation in *Bacillus subtilis*. PLoS One. 2015 Oct 20;10(10):e0141040.

Jokiel M, Klajnert B, Bryszewska M. Use of a spectrofluorimetric method to monitor changes of human serum albumin thermal stability in the presence of polyamidoamine dendrimers. J Fluoresc. 2006 Mar;16(2):149-52.

Kailas L, Terry C, Abbott N, Taylor R, Mullin N, Tzokov SB, Todd SJ, Wallace BA, Hobbs JK, Moir A, Bullough PA. 2011. Surface architecture of endospores of the *Bacillus cereus/anthracis/thuringiensis* family at the subnanometer scale. Proc Natl Acad SciUSA108:16014 –16019.

Keijser BJ1, Ter Beek A, Rauwerda H, Schuren F, Montijn R, van der Spek H, Brul S. Analysis of temporal gene expression during *Bacillus subtilis* spore germination and outgrowth. J Bacteriol. 2007 May;189(9):3624-34.

Kim H, Hahn M, Grabowski P, McPherson DC, Otte MM, Wang R, Ferguson CC, Eichenberger P, Driks A. The *Bacillus subtilis* spore coat protein interaction network. Mol Microbiol. 2006 Jan;59(2):487-502.

Lequette Y, Garenaux E, Combrouse T, Thays Del Lima D, Ronse A, Slomianny C, Trivelli X, Guerardel Y, Faille C. 2011. Domains of BclA, the major surface glycoprotein of the *B. cereus* exosporium: glycosylation patterns and role in spore surface properties. Biofouling 27:751–761.

Lequette Y, Garenaux E, Tauveron G, Dumez S, Perchat S, Slomianny C, Lereclus D, Guerardel Y, Faille C. 2011. Role played by exosporium glycoproteins in the surface properties of *Bacillus cereus* spores and in their adhesion to stainless steel. Appl Environ Microbiol 77:4905–4911.

McKenney PT, Driks A, Eichenberger P. 2013. The Bacillus subtilis endospore: assembly and functions of the multilayered coat. Nat Rev Microbiol 11:33–44. 11.

Melly E, Genest PC, Gilmore ME, Little S, Popham DL, Driks A, Setlow P. 2002. Analysis of the properties of spores of *Bacillus subtilis* prepared at different temperatures. J Appl Microbiol 92:1105–1115.

Miller, J. H. 1972. Experiments in molecular genetics, p.352-355. Cold Spring Harbor Laboratory, Cold Spring Harbor,N.Y.

Naclerio G, Baccigalupi L, Zilhao R, De Felice M, Ricca E (1996) *Bacillus subtilis* spore coat assembly requires cotH gene expression. J Bacteriol 178(15):4375–4380.

Nguyen KB, Sreelatha A, Durrant ES, Lopez-Garrido J, Muszewska A, Dudkiewicz M, Grynberg M, Yee S, Pogliano K, Tomchick DR, Pawłowski K, Dixon JE, Tagliabracci VS. Phosphorylation of spore coat proteins by a family of atypical protein kinases. Proc Natl Acad Sci U S A. 2016 Jun 21;113(25):E3482-91.

Nicholson WL, Setlow P (1990) Sporulation, germination and outgrowth. In C. Harwood and S. Cutting (Eds.), Molecular Biological Methods for Bacillus. John Wiley and Sons, Chichester, UK. pp. 391-450.

Nicholson WL, Munakata N, Horneck G, Melosh HJ, Setlow P. 2000. Resistance of Bacillus endospores to extreme terrestrial and extraterrestrial environments. Microbiol Mol Biol Rev 64:548 –572.

Nicolas P1, Mäder U, Dervyn E, Rochat T, Leduc A, Pigeonneau N, Bidnenko E, Marchadier E, Hoebeke M, Aymerich S, Becher D, Bisicchia P, Botella E, Delumeau O, Doherty G, Denham EL, Fogg MJ, Fromion V, Goelzer A, Hansen A, Härtig E, Harwood CR, Homuth G, Jarmer H, Jules M, Klipp E, Le Chat L, Lecointe F, Lewis P, Liebermeister W, March A, Mars RA,

Nannapaneni P, Noone D, Pohl S, Rinn B, Rügheimer F, Sappa PK, Samson F, Schaffer M, Schwikowski B, Steil L, Stülke J, Wiegert T, Devine KM, Wilkinson AJ, van Dijl JM, Hecker M, Völker U, Bessières P, Noirot P. Condition-dependent transcriptome reveals high-level regulatory architecture in *Bacillus subtilis*. Science. 2012 Mar 2;335(6072):1103-6.

Ricca E, Cutting S, Losick R. 1992. Characterization of bofA, a gene involved in intercompartmental regulation of Pro-σK processing during sporulation in *Bacillus subtilis*. J. Bacteriol. 174:3177–3184.

Saggese A, Scamardella V, Sirec T, Cangiano G, Isticato R, Pane F, Amoresano A, Ricca E, Baccigalupi L. Antagonistic role of CotG and CotH on spore germination and coat formation in *Bacillus subtilis.* PLoS One. 2014 Aug12;9(8):e104900.

Sanchez-Salas JL, Setlow B, Zhang P, Li YQ, Setlow P. Maturation of released spores is necessary for acquisition of full spore heat resistance during *Bacillus subtilis* sporulation. Appl Environ Microbiol. 2011 Oct;77(19):6746-54.

Segev E, Smith Y, Ben-Yehuda S. RNA dynamics in aging bacterial spores. Cell. 2012 Jan 20;148(1-2):139-49.

Setlow P. 2006. Spores of *Bacillus subtilis*: their resistance to and killing by radiation, heat and chemicals. J Appl Microbiol 101:514 –525.

Sylvestre P, Couture-Tosi E, Mock M. 2002. A collagen-like surface glycoprotein is a structural component of the *Bacillus anthracis* exosporium. Mol Microbiol 45:169 –178.

Terry C, Shepherd A, Radford DS, Moir A, Bullough PA. 2011. YwdL in *Bacillus cereus*: its role in germination and exosporium structure. PLoS One 6(8):e23801.

Warth AD. Relationship between the heat resistance of spores and the optimum and maximum growth temperatures of Bacillus species. J Bacteriol. 1978 Jun;134(3):699-705.

Wiencek KM, Klapes NA, Foegeding PM. 1990. Hydrophobicity of Bacillus and Clostridium spores. Appl. Environ. Microbiol. 56:2600–2605.

Youngman P, Perkins JB, Losick R (1984) A novel method for the rapid cloning in Escherichia coli of *Bacillus subtilis* chromosomal DNA adjacent to Tn917 insertion. Mol. Gen. Genet. 195:424-433.

Zheng L, Donovan WP, Fitz-James PC, Losick R (1988) Gene encoding a morphogenic protein required in the assembly of the outer coat of the *Bacillus subtilis* endospore. Genes Develop. 2:1047-1054.

Zilhão R, Serrano M, Isticato R, Ricca E, Moran CP Jr., and Henriques AO. Interactions among CotB, CotG, and CotH during assembly of the *Bacillus subtilis* Spore Coat.J Bacteriol. 2004 Feb; 186(4): 1110–1119.

Part 2:

Biotechnology Applications of Bacterial spores

Chapter 3

Localization of a red fluorescence protein adsorbed on wild type and mutant spores of *Bacillus subtilis*

Giuliana Donadio,[#1] ***Mariamichela Lanzilli,***[#1] *Teja Sirec,*[1,2] *Ezio Ricca,*[1]

and Rachele Isticato[1]

[1]*Department of Biology, University of Naples Federico II-MSA-Via Cinthia 26-80126 Naples, Italy*

[#1]*Equally contributed to work*

Published in 2016 September 8 on *Microb Cell Fact* 15(1): 153

3.1 Abstract

Background: Bacterial spores have been proposed as vehicles to display heterologous proteins for the development of mucosal vaccines, biocatalysts, bioremediation and diagnostic tools. Two approaches have been developed to display proteins on the spore surface: a recombinant approach, based on the construction of gene fusions between DNA molecules coding for a spore surface protein (carrier) and for the heterologous protein to be displayed (passenger); and a non-recombinant approach based on spore adsorption, a spontaneous interaction between negatively charged, hydrophobic spores and purified proteins. The molecular details of spore adsorption have not been fully clarified yet.

Results: We used the monomeric Red Fluorescent Protein (mRFP) of the coral *Discosoma* sp. and *Bacillus subtilis* spores of a wild type and an isogenic mutant strain lacking the CotH protein to clarify the adsorption process. Mutant spores, characterized by a strongly altered coat, were more efficient than wild type spores in adsorbing mRFP but the interaction was less stable and mRFP could be in part released by raising the pH of the spore suspension. A collection of isogenic strains carrying GFP fused to proteins restricted in different compartments of the *B. subtilis* spore was used to localize adsorbed mRFP molecules. In wild type spores mRFP infiltrated through crust and outer coat, localized in the inner coat and was not surface exposed. In mutant spores mRFP was present in all surface layers, inner, outer coat and crust and was exposed on the spore surface.

Conclusions: Our results indicate that different spores can be selected for different applications. Wild type spores are preferable when a very tight protein-spore interaction is needed, for example to develop reusable biocatalysts or bioremediation systems for field applications. *cotH* mutant spores are instead preferable when the heterologous protein has to be displayed on the spore surface or has to be released, as could be the case in mucosal delivery systems for antigens and drugs, respectively.

3.2 Introduction

Bacterial endospores (spores) are quiescent cells produced in response to harsh environments by Gram-positive bacteria mainly belonging to the *Bacillus* and *Clostridium* genera [1]. Spores can survive in their dormant state for long periods, resisting to a vast range of stresses such as high temperature, dehydration, absence of nutrients and presence of toxic chemicals. When the environmental conditions ameliorate, the spore germinates originating a vegetative cell able to grow and sporulate [2]. The ability of the spore to survive non-physiological conditions is, in part, due to its surface structures. In *Bacillus subtilis*, the model system for spore formers, the spore surface is organized in a multilayered coat and in a crust. The latter has been recently discovered and described as the outermost layer of the spore [2]. When observed by thin-section electron microscopy the spore coat appears formed by a lamellar inner coat and a more coarsely layered outer coat. The crust is only visible after a ruthenium red staining and appears as an amorphous layer surrounding the outer coat [2]. Coat and crust together are formed by at least 70 different proteins (Cot proteins) that spontaneously assemble into the multilayered structures, as recently reviewed [2]. *B. subtilis* spores are negatively charged [3, 4] and have a relative hydrophobicity, due in part to the glycosylation of some spore surface proteins [5].

The bacterial spore has been proposed as a platform to display heterologous proteins, with potential applications ranging from the development of mucosal vaccine to re-usable biocatalysts, diagnostic tools and bioremediation devices for field use [1, 6–8]. Various reasons support the use of the spore as a display system: (i) the remarkable and well documented resistance of the spore [2] that ensures high stability of the display system; (ii) the availability of genetic tools [9] that allows an easy manipulation; (iii) the safety record of several endospore-forming species [10, 11], that makes spores of those species ideal candidates also to deliver displayed molecules to mucosal surfaces [1, 8].

Two strategies have been so far developed to display heterologous proteins on the spore surface. A recombinant strategy based on the construction of gene fusions between the gene coding for a selected spore surface protein (carrier) and the heterologous DNA coding for the protein to be displayed was first developed to display an antigen, the C fragment of the tetanus toxin [12]. By this recombinant approach a variety of heterologous proteins have been displayed and recombinant spores proposed for several potential applications, as extensively reviewed [8]. More recently, a non-recombinant approach based on the spontaneous adsorption between purified spores and purified proteins has been also proposed [3]. Enzymes [13–15] and antigens [3, 16] have been efficiently displayed also by this approach and the system has been recently reviewed [17].

Spore adsorption is more efficient when the pH of the binding buffer is acidic (pH 4) and less efficient or totally inhibited at pH values of 7 or 10 [3, 15, 16]. A combination of electrostatic and hydrophobic interactions between spores and antigens has been suggested to drive the adsorption, which is not dependent on specific spore coat components [3, 17]. However, some mutant spores with severely altered spore surface were shown to interact more efficiently than isogenic wild type spores with the model enzyme beta-galactosidase [15]. In addition, heat-inactivated spores have been also shown to be able to efficiently display heterologous proteins [18, 19].

We used a fluorescent protein, the monomeric form of the Red Fluorescent Protein (mRFP) of the coral *Discosoma* sp. [20] and *B. subtilis* spores of a wild type and an isogenic mutant lacking the CotH protein [21] to analyze in more details the spore adsorption process. Spores lacking CotH have been previously shown to be more efficient than wild type spores in adsorbing the model enzyme beta-galactosidase [15] and to have a strongly altered coat: the inner coat is thinner than in wild type spores, the outer coat is much less electron-dense, and the two coat layers do not tightly adhere to each other [22]. These strong structural effects do not cause a strong phenotype in laboratory conditions and only a minor germination defect could be associated to the mutant spore [21]. CotH is a coat component with a regulatory role on other coat components [21], therefore spores lacking CotH also lack at least nine other proteins in the outer coat and crust [23]. Recently, it has been observed that the assembly of some CotH-dependent proteins, such as CotC, CotU, CotS and CotZ, is restored in spores lacking both CotH and CotG, another outer coat protein, and therefore that CotH counteracts CotG negative effects on spore coat assembly [24].

3.3 Results and Discussion

3.3.1 mRFP of *Discosoma* sp. adsorbs to *B. subtilis* spores

In an initial experiment 5 μg of mRFP of the coral *Discosoma* sp., over-expressed in *E. coli* and purified by affinity chromatography with Ni–Nta columns ("Methods" section), was incubated with 2.0×10^9 purified spores of the *B. subtilis* strain PY79 [25] or of the isogenic strain ER209, lacking CotH [21]. The adsorption reactions were performed at pH 4.0, as previously described [15]. After the adsorption reaction spores were extensively washed, spore surface proteins were extracted as previously described [26] and analyzed by western blot with monoclonal anti-polyHistidine–peroxidase antibody (*Sigma*), able to recognize the his tagged N terminus of mRFP. As shown in Fig. 1a, mRFP was extracted from both wild type and *cotH* mutant spores, indicating that it was absorbed by both types of spores, retained during the washing steps and released by the extraction treatment. mRFP adsorption was extremely stable over time and the protein was still extracted by SDS–DTT treatment after 2 weeks of storage at room temperature of the adsorbed spores (Additional file 1: Fig. S1).

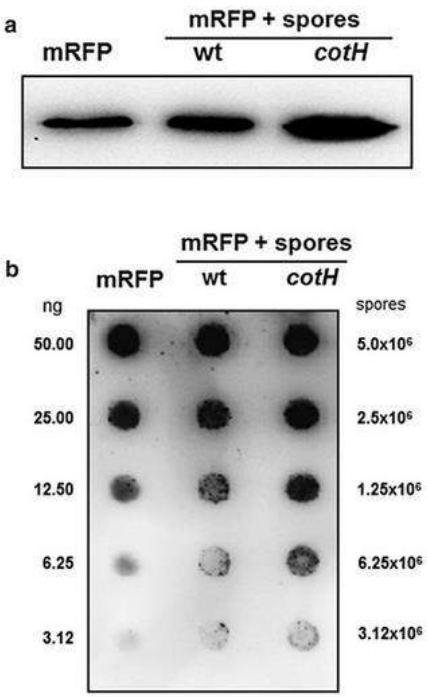

Figure 1: Western (**a**) and dot (**b**) blot of proteins extracted from wild type and *cotH* mutant spores after mRFP-spore adsorption. Purified recombinant mRFP is used as marker. In *panel b* the amount of purified recombinant mRFP (ng) and the number of spores present in each dilution are indicated. Immuno reactions were performed with anti-His primary antibody conjugated with horseradish peroxidase ("Methods" section).

Although the western blot of Fig. 1a is not quantitative, it suggested that *cotH* mutant spores released more mRFP than wild type spores. To confirm this suggestion by a quantitative approach we performed a dot blot experiment using purified mRFP as a standard. After the adsorption reaction spores were collected by centrifugation, serially diluted and analyzed by dot blotting (Fig. 1b). A

densitometric analysis of the dot blot (Additional file 2: Table S1) showed that when 5 µg of mRFP were used in the adsorption reaction, wild type and mutant spores were able to adsorb, respectively, 3.40 µg (68 %) and 4.43 µg (88 %) of the total protein. (P = 0.00132). Therefore, indicating that mutant spores lacking CotH are more efficient than isogenic wild type spores in adsorbing mRFP.

To analyze in more details the efficiency of adsorption, increasing amounts of mRFP (2, 5, 10 and 20 µg) were used in the reaction with the same amount of wild type or *cotH* mutant spores. In all cases the supernatant fraction of the adsorption reaction was serially diluted and analyzed by dot blotting with mRFP-recognizing anti-His antibody (Fig. 2a). Results of the densitometric analysis of the dot blots (Additional file 3: Table S2) are reported in Fig. 2b and indicate that with all amounts of mRFP tested, *cotH* mutant spores were more efficient than wild type spores in adsorbing the fluorescent protein.

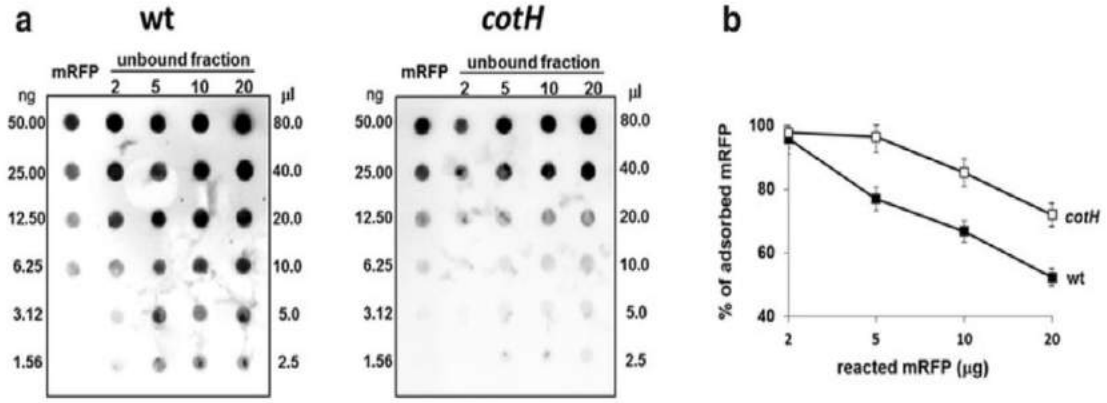

Figure 2: (**a**) Dot blot of serial dilutions of unbound mRFP after adsorption reactions with wild type and *cotH* mutant spores. The amount of purified recombinant mRFP (ng) and the volume of supernatant loaded are indicated. Immuno reactions were performed with anti-His primary antibody conjugated with the horseradish peroxidase ("Methods" section). (**b**) Efficiency of adsorption (%) of wild type and mutant spores (*black and white squares*, respectively) with various amounts of mRFP. The graph is designed on the base of the averages from densitometric analysis of three independent dot blots, reported in Additional file 2: Table S1. *Error bars* show the standard errors of the mean from the three experiments (P = 0.0025).

3.3.2 Adsorbed mRFP is tightly bound to spores

Upon adsorption to spores, mRFP is not easily released even after multiple washes. Spores adsorbed with mRFP were washed three times with 100 µl PBS buffer at pH 3.0 or pH 7.0 or extracted with 1 M NaCl, 0.1 % Triton X-100 [3]. With wild type spores no mRFP was released by any of these treatments, while with cotH mutant spores some mRFP was released by the washes at pH 7.0 and by the NaCl−Triton extraction (Fig. 3a). To evaluate the kinetic of mRFP-release adsorbed mutant spores were washed two times, resuspended in PBS pH 7.0 or 1 M NaCl, 0.1 % Triton X-100 for 5, 10, 15 or 30 min and the supernatant fractions analyzed by dot blot (not shown). A densitometric analysis of the dot blot (Additional file 4: Table S3) was performed and Fig. 3b reports the percentage of mRFP released by the two treatments at the different time points. The pH 7.0 buffer extracted about 5 % of the adsorbed mRFP within the first 5 min of incubation and did not extract more protein over time. The NaCl–Triton solution extracted about 3 % of mRFP in the first 5 min and the amount of extracted

mRFP increased over time in an almost linear way reaching over 9 % of mRFP released after 30 min of treatment (Fig. 3b).

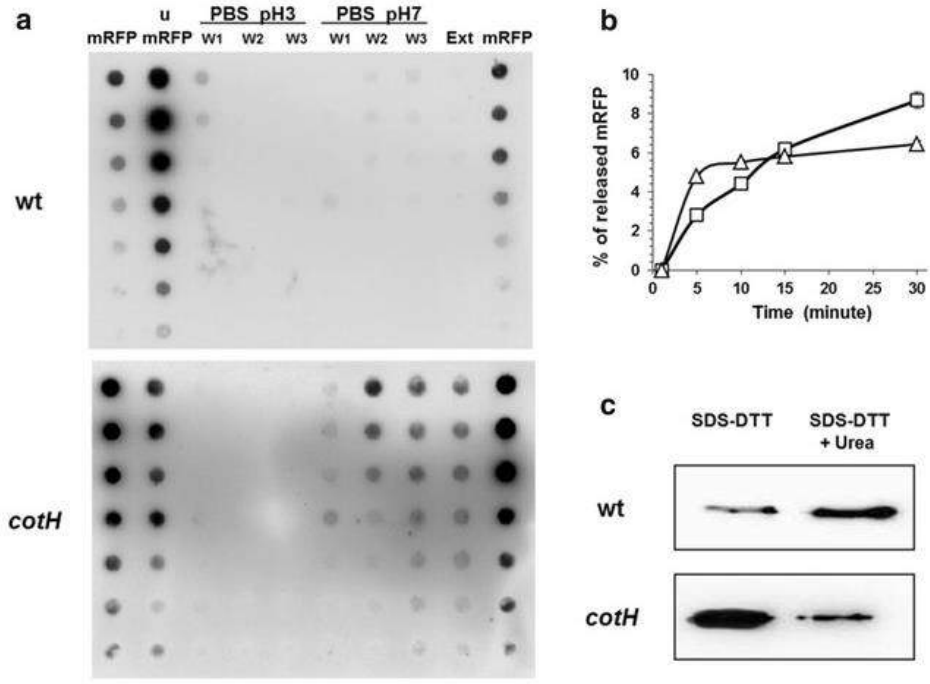

Figure 3: (**a**) *Dot blot* of released mRFP after three washes (W1, W2 and W3) with PBS buffer at pH 3 or pH 7 or after extraction with 1 M NaCl, 0.1 % Triton X-100 (Ext) ("Methods" section). Purified recombinant mRFP (mRFP) and unbound mRFP (u-mRFP) after the adsorption reaction were used as markers. (**b**) Kinetic of mRFP release based on the densitometric analysis (Additional file 4: Table S3) of mRFP released upon incubation either in PBS buffer pH 7.0 (*triangles*) or 1 M NaCl, 0.1 % Triton X-100 (*squares*). (**c**) Western blot of mRFP extracted by a SDS–DTT or after consecutive SDS–DTT and urea treatments of wild type and cotH mutant spores. Immuno reactions were performed with anti-His primary antibody anti-His primary antibody conjugated with the horseradish peroxidase ("Methods" section).

When spores were extracted with an SDS–DDT treatment, the standard protocol for extract spore coat proteins [26], mRFP was released by both wild type and mutant spores (Fig. 3c). The release of some mRFP after washes at pH 7.0 or 1 M NaCl, 0.1 % Triton X-100 treatment (Fig. 3a) and the high amount of mRFP released after SDS–DTT extraction by mutant spores may reflect the higher amount of mRFP adsorbed by mutant than wild type spores (Fig. 2). However, if spores previously extracted with SDS–DTT were re-extracted with Urea, a procedure used to completely remove the spore coat [27], additional mRFP molecules were released but, in this case, in higher amount from wild type than from mutant spores (Fig. 3c). Taken together the experiments of Figs. 2 and 3 suggest that wild type spores adsorb mRFP less efficiently but more tightly than *cotH* mutant spores.

3.3.3 Localization of adsorbed mRFP on wild type and mutant spores

To assess whether spore-adsorbed mRFP molecules retained their fluorescence properties and investigate their distribution around the spore we performed a fluorescence microscopy analysis. With

both wild type and mutant spores red fluorescent signals were observed all around the spore (Fig. 4), and in agreement with results of Figs. 2 and 3, the fluorescence signal appeared stronger with mutant than with wild type spores (Fig. 4). In all cases the fluorescent signal was stronger at the spore poles, indicating that adsorbed mRFP molecules were not evenly distributed around the spore and accumulated at the poles (Fig. 4).We used Image J software (v1.48, NIH) to perform a quantitative fluorescence image analysis and the corrected spore fluorescence was calculated as described in the "Methods" section. The analysis of 80 spores of each strain indicated an average fluorescence intensity, in arbitrary units, of 7816 ± 2712 and of 11541 ± 2573 for wild type spores and mutant spores, respectively (Fig. 5, $P < 0.0001$), confirming that *cotH* mutant spores adsorb more mRFP than wild type spores.

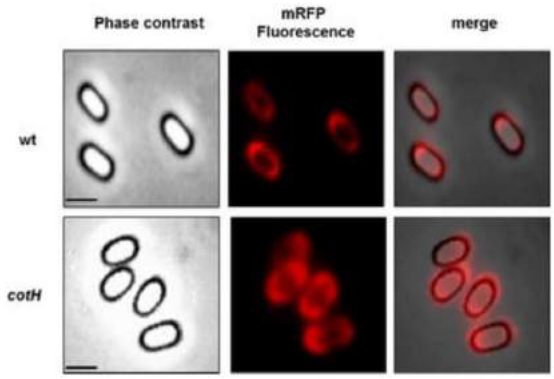

Figure 4: Fluorescence of mRFP upon adsorption to wild type and mutant spores. For each strain the same microscopy field was observed by phase contrast and fluorescence microscopy. Merge panels are reported. The exposure time was of 500 ms for both strains. *Scale bar* 1 μm.

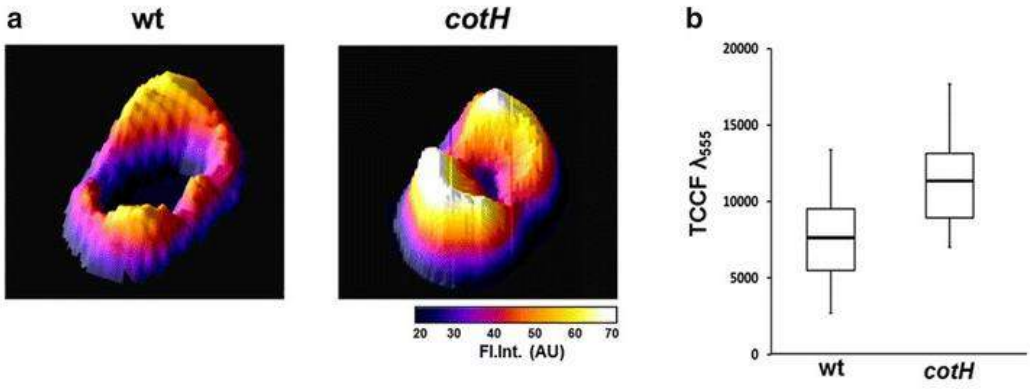

Figure 5: Fluorescence intensity profiles (Fl. Int.; scale in arbitrary units) of wild type and mutant spores adsorbed with mRFP. The profiles were generated from fluorescence microscopy images using the 3D Surface plotter function of Image J (http://imagej.nih.gov/ij/). **(a)** Representative fluorescence intensity profiles of a wild type (*left*) and *cotH* mutant spore (*right*). The fluorescence intensity is reported in arbitrary units. **(b)** Box plots displaying the total corrected cellular fluorescence (TCCF) for 80 different spores of each strain. Limits of each box represent the first and the third quartile (25 and 75 %) and the values outside the boxes represent the maximum and the minimum values. The line dividing the box indicates the median value for each strain. *P value* is less than 0.0001.

3.3.4 Adsorbed mRFP is not exposed on the surface of wild type spores

To assess whether adsorbed mRFP molecules were exposed on the spore surface we followed an immuno-fluorescence microscopy approach. Wild type and mutant spores adsorbed with mRFP were reacted with monoclonal mRFP-recognizing anti-His antibody, then with fluorescent anti-mouse secondary antibody (Santa Cruz Biotechnology, Inc.) and observed under the fluorescence microscope. While mRFP molecules adsorbed to mutant spores were accessible to the specific antibody all around the spore surface, mRFP molecules adsorbed to wild type spores were only poorly accessible to the antibody and only in specific spots mainly at the spore poles (Fig. 6). A fluorescent signal was observed with wild type spores only with an exposure time fivefold longer that used with mutant spores (Fig. 6). Results of Fig. 6, then indicate that mRFP molecules are mostly not accessible to the antibody upon adsorption on wild type spores. Since mRFP is abundantly present at the poles of wild type spores (Fig. 4) but it is only accessible to anti-mRFP antibody in few specific spots at the spore poles (Fig. 6) we hypothesize that either mRFP molecules bind wild type spores in an orientation that precludes the interaction with the antibody or that mRFP molecules infiltrate inside the spore coat layers of wild type spores.

While Ser15 is in the N-terminal part of CotG, Ser39, Thr147 and all the other possible sites of phosphorylation are located in the repeated central region (Fig. 6 and Table S2). This region is composed by random coiled repeats [11], each containing serine residues surrounded by positively charged amino acids (Fig. 6). In a bioinformatic analyses of known phosphorylated proteins [22] all these features have been indicated as typical of intrinsically disordered structures and have been identified as predictor of phosphorylation substrates.

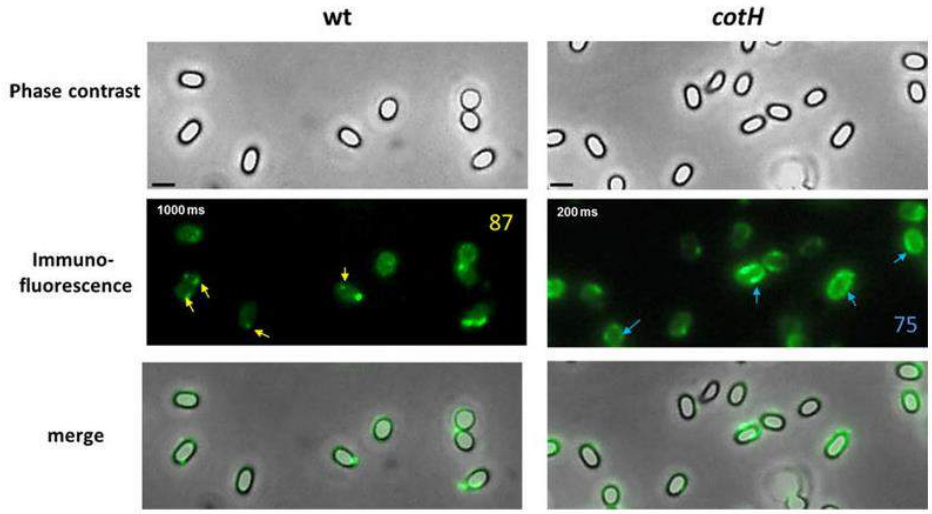

Figure 6: Immuno-fluorescence microscopy of wild type and mutant spores adsorbed with mRFP. Immuno reactions were performed with anti-His primary antibody and fluorescent anti-mouse secondary antibody conjugated with FITC ("Methods" section). For each strain, the same microscopy field was observed by phase contrast and fluorescence microscopy. Merge panels are reported. The exposure time is indicated as ms.The *numbers in the panels* are the percentage of spores found with a similar mRFP-localization pattern in three different microscopy fields. *Scale bar* 1 μm.

3.3.5 Adsorbed mRFP infiltrates in the inner coat of wild type spores

In order to verify whether mRFP molecules infiltrate inside the spore we used a fluorescence microscopy approach ("Methods" section). In particular we followed the red fluorescence of mRFP and the green fluorescence of GFP fused to *B. subtilis* proteins known to localize in the spore core (SpoIIQ [28]), cortex (YhcN [29, 30]), inner coat (CotS [31]), outer coat (CotC [30, 32]) or crust (CotZ [30]). Spores purified from isogenic strains carrying the *spoIIG::gfp, yhcN::gfp, cotS::gfp, cotC::gfp* or *cotZ::gfp* gene fusion were used to adsorb mRFP and observed by fluorescence microscopy (Fig. 7A). In order to determine the relative position of red and green signals quantitatively, more than 20 free spores for each strain were used to measure the intensity of GFP and RFP fluorescence along the spore axis by using image J software ("Methods" section). Averages of red and green fluorescence intensities of the various strains were plotted in Fig. 7B. With spores carrying the SpoIIQ–GFP (core) or the YhcN–GFP (cortex) fusion the green signal was internal with respect to the red one indicating that mRFP molecules were localized outside of the spore core (SpoIIQ) and of the cortex (YhcN). With spores carrying the CotS–GFP (inner coat) fusion the intensity peaks of green and red signals were coincident, indicating a co-localization of the two fluorescence signals. With spores carrying the CotC–GFP (outer coat) or the CotZ–GFP (crust) fusion, the intensity peaks of the green signals were slightly external to the red ones, indicating that in both cases mRFP molecules were inside the outer coat (CotC) and of the crust (CotZ) (Fig. 7). These results then indicate that mRFP molecules cross crust and outer coat layers and localize at the level of the inner coat of wild type spores, explaining why mRFP is not exposed on the surface of the spore (Fig. 6).

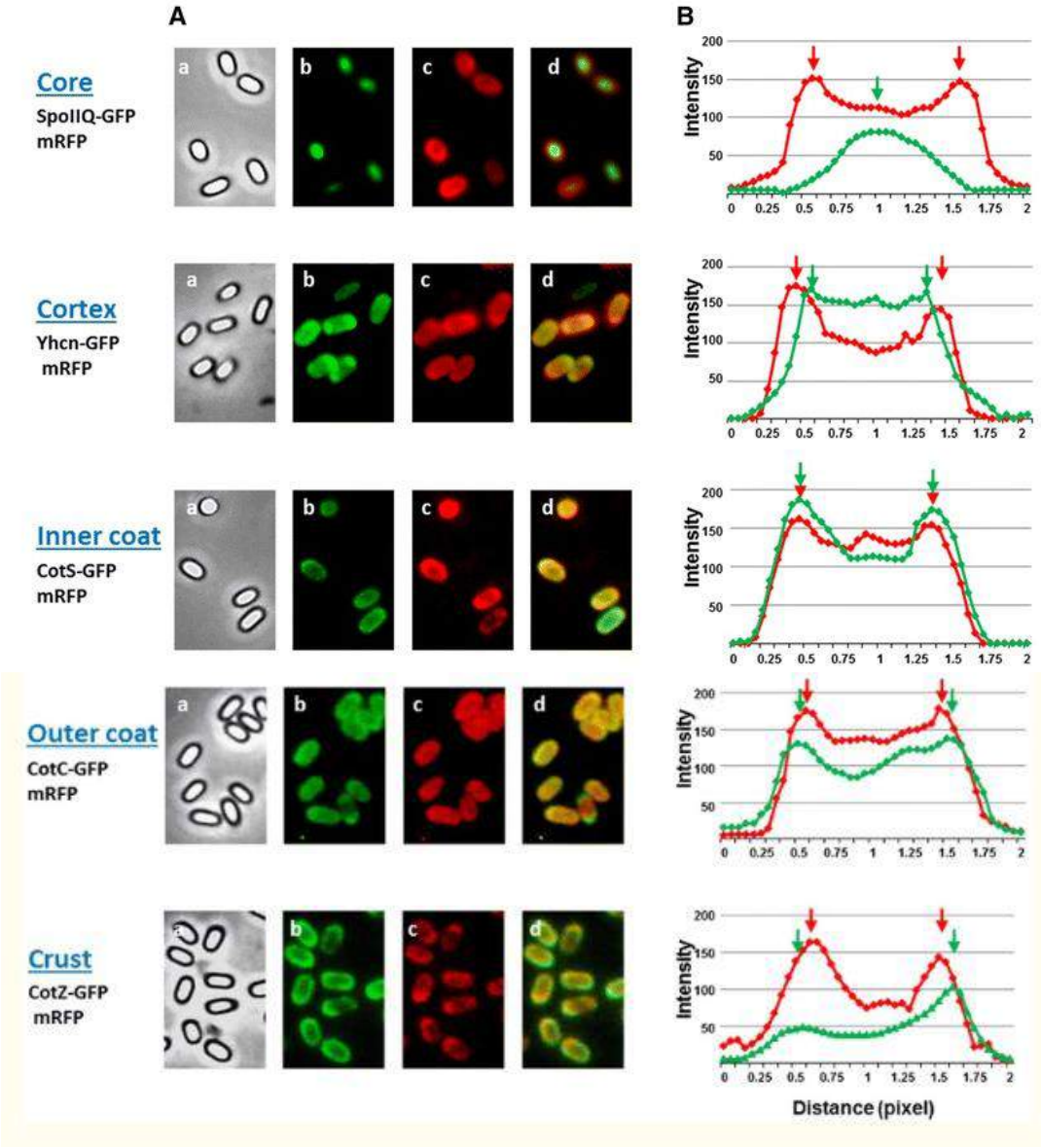

Figure 7: Fluorescence localization of coat protein-GFP fusions and adsorbed-mRFP (**A**) and plots of fluorescence intensities along the long axis of the spore (**B**). Spores of otherwise wild type *B. subtilis*strains carrying GFP fused to core, cortex, inner coat, outer coat or crust proteins were adsorbed with mRFP and observed by fluorescence microscopy. Phase-contrast images (***a***), GFP fluorescence images (***b***), mRFP fluorescence images (***c***) merged images (***d***) are shown.

3.3.6 Adsorbed mRFP localizes in all surface layers of *cotH* mutant spores

The same approach was used to localize mRFP molecules inside mutant spores. Spores purified from isogenic strains carrying the *cotH* mutation and the *spoIIG::gfp, yhcN::gfp, cotS::gfp, cotC::gfp* or *cotZ::gfp* gene fusion were used to adsorb mRFP and observed by fluorescence microscopy (Fig. 8A). Since CotS (inner coat marker) and CotC (outer coat marker) fail to assemble within the coat of a *cotH*mutant [23, 33] but assemble normally in a strain lacking both CotH and CotG [24], we used a double mutant strain carrying null mutations in *cotH* and *cotG* genes for those two GFP fusions. As above, more than 20 free spores for each strain were used to measure the intensity of GFP and RFP fluorescence signals along the spore axis by using image J software ("Methods" section).

Averages of red and green fluorescence intensities of the various strains were plotted in Fig. 8B. With spores carrying the SpoIIQ–GFP (core) or the YhcN–GFP (cortex) fusion the green signal was internal with respect to the red one indicating that mRFP molecules were localized outside of the spore core (SpoIIQ) and of the cortex (YhcN). With spores carrying the CotS–GFP (inner coat) and CotC–GFP (outer coat) fusion the red peaks were slightly outside the green ones and with the CotZ–GFP (crust) fusion the intensity peaks of green and red signals were coincident (Fig. 8). However, with mutant spores the red peaks did not appear sharp but rather broad suggesting that the red fluorescent molecules were not concentrated in a specific point but were diffused in a large space. Taken together these observations suggest a localization of mRFP molecules in all surface layers of *cotH* mutant spores that explains why mRFP is exposed on the surface of the spore (Fig. 6).

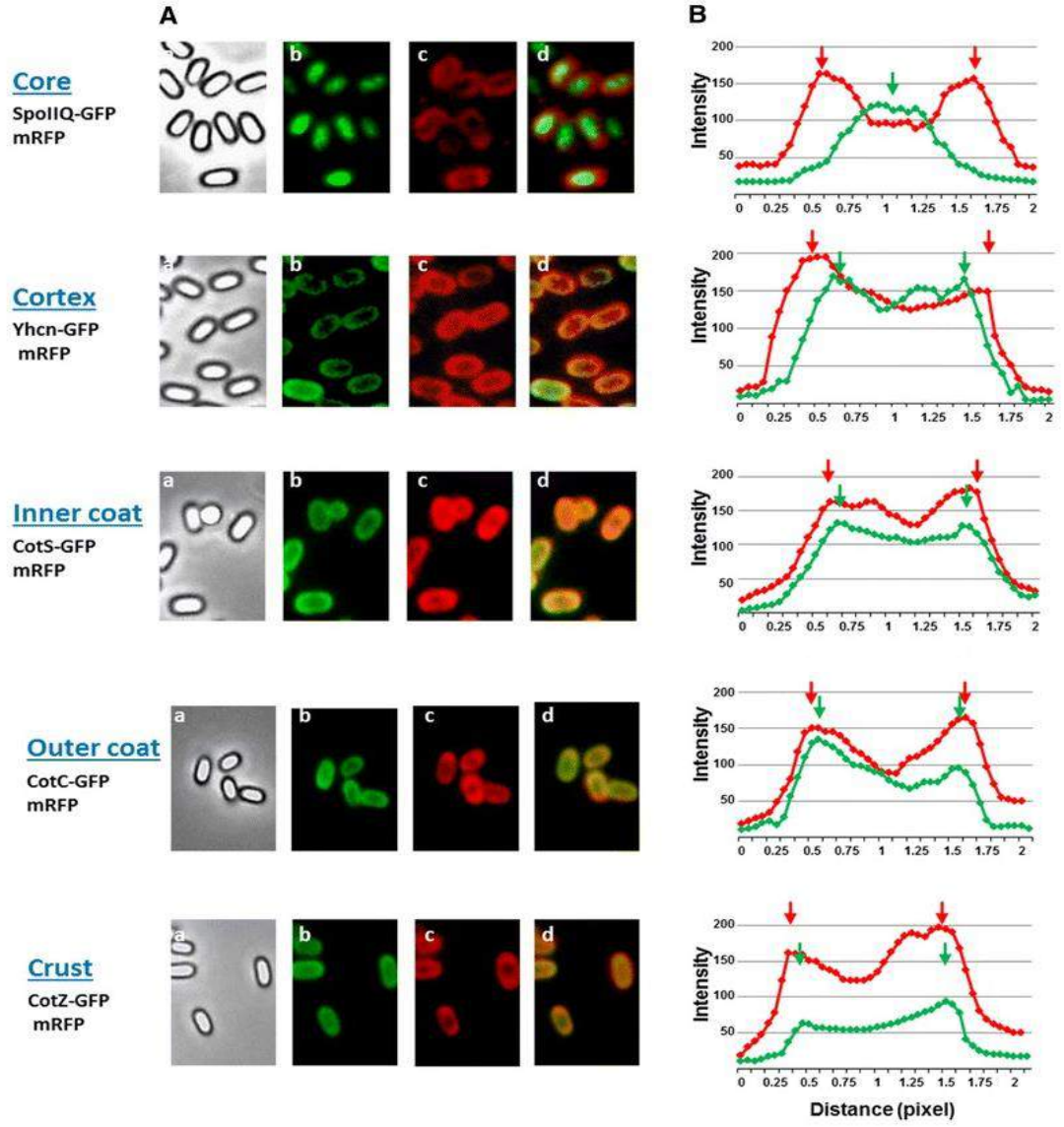

Figure 8: Fluorescence localization of coat protein-GFP fusions and adsorbed-RFP (A) and plots of fluorescence intensities along the long axis of the spore (B). Spores of *cotH* mutant strains carrying GFP fused to core, cortex or crust proteins and of *cotH cotG* mutant strains carrying GFP fused to inner and outer coat were adsorbed with mRFP and analyzed by fluorescence microscopy. Phase-contrast images (***a***), GFP fluorescence images (***b***), RFP fluorescence images (***c***) and merged images (***d***) are shown.

The experiments of Figs. 7 and and 8 were performed using standard adsorption conditions: 5 μg of purified mRFP were incubated with 2.0×10^9 purified spores for 1 h. To evaluate whether the amount of mRFP and/or the incubation time had an effect on mRFP localization we incubated 2.0×10^9 wild type spores either with 50 μg of purified mRFP for 1 h or with 5 μg of mRFP for 4 h. In both cases mRFP localized in the inner coat of wild type spores as under standard conditions (Additional file 5: Figure S2), indicating that neither the amount of mRFP nor the incubation time affected mRFP localization.

3.4 Conclusions

Wild type spores of *B. subtilis* adsorb and tightly bind mRFP that is not displayed on the spore surface. We propose that it infiltrates through crust and outer coat layers, localizes in the inner coat and appears more abundantly concentrated at the spore poles (Fig. 9a). The observation that mRFP crosses crust and outer coat indicates these structures as permeable to a 27 kDa protein. Permeability of the spore surface is not totally surprising since germinants (small molecules with molecular masses typically <200 Da) present in the environment have to cross the external layers of the spore to reach their receptors. In addition, studies conducted on *B. megaterium* suggested that the spore surface is permeable to the passage of molecules with masses somewhere between 2 and 40 kDa [34, 35].

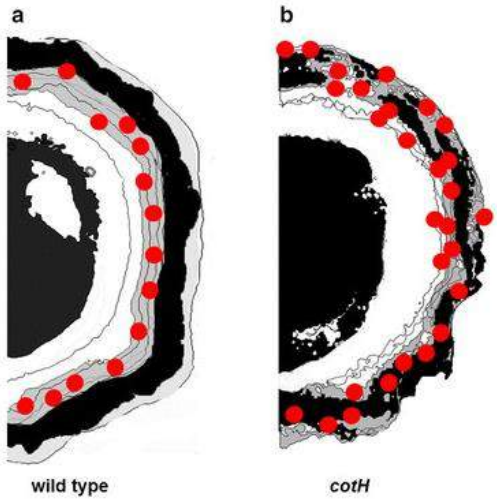

Figure 9: Cartoon model of mRFP localization in wild type (**a**) and *cotH* mutant (**b**) spores. Wild type and mutant spores are over imposed with *red dots* representing mRFP molecules

Mutant spores lacking CotH are strongly defective: (i) their outer coat is diffuse, lacks the characteristic multilayered pattern, electron density, and a defined outer edge; (ii) the typical lamellar structure of the inner coat, in which three to five lamellae can usually be recognized, is reduced to one or two lamellae; (iii) the inner and outer coats are not tightly associated [22]; at least nine spore coat proteins are not present [23]. These mutant spores are more efficient than wild type spores in adsorbing mRFP that, although more abundant at the spore poles is present all around the spore and exposed on

its surface. However, the interaction between mRFP and *cotH* spores is less stable than with wild type spores and mRFP is partially released by washes at pH 7.0 (Fig. 3). We propose that mRFP molecules adsorb better to *cotH* mutant than to wild type spores because they not only localize in the inner coat but also in the outer coat and in the crust (Fig. 9b).

The observation that neither the amount of heterologous protein or the time of incubation affect mRFP localization in wild type spores (Additional file 1: Figure S1) argue that in those spores crust and outer coat are compact structures that allow mRFP transit but not accumulation. In *cotH* spores the outer coat is rather diffuse [22] and allows mRFP to localize and accumulate.

These findings shed light on the mechanism of spore adsorption and indicate that different spores, wild type or mutant, can potentially have different applications. As a carrier of enzymes to be re-used several times a surface display of the enzyme may be not strictly required while a tight adhesion to the carrier could desirable making wild type spores preferable over the mutant spores. On the contrary, as a drug/vaccine delivery vehicle a surface display could be essential and the release of the drug/antigen in some cases an useful property, making mutant spores preferable over the wild type.

3.5 Methods

3.5.1 Bacterial strains and transformation

Bacillus subtilis strain PY79 strain [25] was used as a wild type. Strain ER220 (*cotH* null mutant [21] and all other mutant strains of *B. subtilis* used in this study were isogenic derivatives of PY79. *B. subtilis* strains used in this study are listed in Additional file 6: Table S4. Isolation of plasmid DNA, restriction digestion, ligation of DNA and transformation of *E. coli* competent cells were carried out by standard methods [36].

3.5.2 Construction of *gfp* fusions

The coding sequence of *yhcN* (564 bp) and the promotor region of *spoIIQ* (500 bp) were PCR amplified using *B. subtilis* chromosomal DNA as a template and synthetic oligonucleotide pairs spoIIQ-F/spoIIQ-R and yhcN-F/yhcN-R (Additional file 7: Table S5) respectively to prime the reactions. Purified DNA fragments were cloned in frame to the 5′ end of the *gfp* gene [37]. Plasmids were used to transform competent cells of strain PY79 yielding strain RH2466 (P_{spoIIQ}*::gfp*) and RH282 (*yhcN::gfp*). Chromosomal DNA of the two strains and of AZ573 (*cotZ::gfp*) was used to transform competent cells of isogenic strains RH220 (*cotH::spc*) (Additional file 6: Table S4), yielding strains RH285 (P_{spoIIQ}*::gfp cotH::spc*) and RH284 (*yhcN::gfp cotH::spc*) and RH278 (*cotZ::gfp cotH::spc*). Chromosomal DNA of strains DS127 (*cotC::gfp*) was used to transform competent cells of isogenic strains AZ603 (*ΔcotG ΔcotH::neo*), yielding strains AZ636 (*cotC::gfp ΔcotG ΔcotH::neo*).

3.5.3 Purification of spores and RFP

Sporulation of wild type and recombinant strains was induced by the exhaustion method. After 30 h of growth in Difco Sporulation medium at 37 °C with vigorous shaking [36] spores were collected, washed three times with distilled water and purified on a step gradient of 20–50 % of Gastrografin

(Bayer) as described before [38, 39]. The number of purified spores obtained was measured by direct counting with a Bürker chamber under an optical microscope (Olympus BH-2 with 40× lens).
Competent cells of *E. coli* strain BL21(DE3) (Invitrogen) was transformed with the expression vector pRSET-A carrying an in-frame fusion of the 5′ end of the *rfp* coding region to six histidine codons under the transcriptional control of a T7 promoter (generous gift of Dr. A. Storlazzi). The new strain RH161 was grown for 18 h at 37 °C in 100 ml of autoinduction medium to express the heterologous protein [40]. The six-His-tagged RFP protein was purified under native conditions using a His-Trap column as recommended by the manufacturer (GE Healthcare Life Science). Purified protein was desalted using a PD10 column (GE Healthcare Life Science) to remove high NaCl and imidazole concentrations and mRFP purity analyzed by SDS-PAGE.

3.5.4 Adsorption reaction

Unless otherwise specified 5 μg of purified recombinant mRFP were added to a suspension 2×10^9 spores in 0.15 M PBS pH 4.0 at 25 °C in a final volume of 200 μl. After 1 h of incubation, the binding mixture was centrifuged (10 min at 13,000*g*) to fractionate pellet and supernatant. The pellet was resuspended in 0.15 M PBS at pH 4.0 to a final concentration of 2×10^5 spores/μl and stored at 4 °C. The supernatant was stored at −20 °C.

3.5.5 Western and dot-blot analysis

2×10^8 mRFP-adsorbed spores were resuspended in 20 μl of spore coat extraction buffer [26], incubated at 68 °C for 1 h to solubilize spore coat proteins and loaded onto a 12 % SDS-PAGE gel. The proteins were then electro transferred to nitrocellulose filters (Amersham Pharmacia Biotech) and used for Western blot analysis as previously reported [39] using monoclonal mRFP-recognizing anti-His antibody (*Sigma*). A quantitative determination of the amount of mRFP was obtained by dot blot experiments analyzing serial dilutions of purified RFP, binding assay supernatant and RFP-adsorbed spores. Filters were then visualized by the ECL-prime (Amersham Pharmacia Biotech) method and subjected to densitometric analysis by Quantity One 1-D Analysis Software (Bio-Rad).

3.5.6 Fluorescence and immunofluorescence microscopy

Post adsorption spores were resuspended in 50 μl of 1× PBS and 5 μl of the suspension placed on microscope slides and covered with a coverslip previously treated for 30 s with poly-l-lysine (*Sigma*). Immunofluorescence was performed as described by Isticato et al. [16], with the following modifications: 2.0×10^6 RFP-adsorbed spores of wild type and *cotH* mutant spores were pretreated with 1 % bovine serum albumin (BSA)—1× PBS, pH 4.0 for 30 min prior to 2 h-incubation a 4 °C with the monoclonal anti-polyHistidine antibodies (mouse) (*Sigma*) diluted 1:20 in 1× PBS−1 % BSA. As a control of the specificity of this technique, non-adsorbed spores were directly treated with anti-His antibodies. After three washes, the samples were incubated with a 64-fold diluted anti-mouse secondary antibody conjugated with Fluorescein isothiocyanate, FITC (Santa Cruz Biotechnology, Inc.) and washed four times with PBS. Washed samples were resuspended in 20 μl of 1× PBS and

10 µl were analyzed. All samples were observed with an Olympus BX51 fluorescence microscope fitted with a 100× objective UPlanF1; U-MNG or U-MWIBBP cube-filters were used to detect the red and green fluorescence emission respectively. Images were captured using an Olympus DP70 digital camera equipped with Olympus U-CA Magnification Changer and processed with Image Analysis Software (Olympus) for minor adjustments of brightness, contrast and color balance and for creation of merged images of GFP and RFP [41]. Exposure times were in the range between 200 and 2000 ms for image capture of GFP fusions and for adsorbed RFP. Fluorescence intensities and the distance between two fluorescent peaks were measured using unadjusted merged images with Image J processing software (version 1.48, NIH) as previously describe by Imamura and collaborators [42]. One pixel corresponds to 1.18 nm in our detection system. Image J was also used to draw an outline around 80 spores for each strain, prior to area, integrated density and the mean fluorescence measurements being recorded, together with several adjacent background readings. The total corrected cellular fluorescence (TCCF) was calculated by subtracting (area of selected cell × mean fluorescence of background readings) from integrated density values. Minimum, maximum and mean value of TCCF were displayed as box-plots with 5–95 % confidence intervals [42]. Fluorescence intensity profiles were generated from the microscopy images using the 3D Surface plotter function of Image J as reported by Serrano and collaborators [43].

3.5.7 Statistical analysis

Results from dot blot and fluorescence microscopy analysis are the averages from three independent experiments. Statistical significance was determined by the Student *t* test, and the significance level was set at $P < 0.01$.

3.6 References

1. Cutting SM, Hong HA, Baccigalupi L, Ricca E. Oral vaccine delivery by recombinant spore probiotics. Int Rev Immunol. 2009;28:487–505.
2. McKenney PT, Driks A, Eichemberger P. The *Bacillus subtilis* endospore: assembly and functions of the multilayered coat. Nat Rev Microbiol. 2012;11:33–44.
3. Huang JM, Hong HA, Van Tong H, Hoang TH, Brisson A, Cutting SM. Mucosal delivery of antigens using adsorption to bacterial spores. Vaccine. 2010;28:1021–1030.
4. Pesce G, Rusciano G, Sirec T, Isticato R, Sasso A, Ricca E. Surface charge and hydrodynamic coefficient measurements of *Bacillus subtilis* spore by optical tweezers. Colloids Surf B. 2014;116C:568–575.
5. Cangiano G, Sirec T, Panarella C, Isticato R, Baccigalupi L, De Felice M, Ricca E. The *sps* gene products affect germination, hydrophobicity and protein adsorption of *Bacillus subtilis* spores. Appl Environ Microbiol. 2014;80:7293–7302.
6. Knecht LD, Pasini P, Daunert S. Bacterial spores as platforms for bioanalytical and biomedical applications. Anal Bioanal Chem. 2011;400:977–989.
7. Hinc K, Ghandili S, Karbalaee G, Shali A, Noghabi K, Ricca E, Ahmadian G. Efficient binding of nickel ions to recombinant *Bacillus subtilis* spores. Res Microbiol. 2010;161:757–764.
8. Isticato R, Ricca E. Spore surface display. Microbiol Spectr. 2014
9. Harwood C, Cutting S. Molecular biological methods for *Bacillus*. Chichester: Wiley; 1990.
10. Cutting SM. *Bacillus* probiotics. Food Microbiol. 2011;28:214–220.

11. Baccigalupi L, Ricca E, Ghelardi E. Non-LAB probiotics: spore formers. In: Probiotics and prebiotics: current research and future trends, Norfolk: Caister Academic Press; 2015. p. 93–103.
12. Isticato R, Cangiano G, Tran HT, Ciabattini A, Medaglini D, Oggioni MR, De Felice M, Pozzi G, Ricca E. Surface display of recombinant proteins on *Bacillus subtilis* spores. J Bacteriol. 2001;183(21):6294–6301.
13. Yim S-K, Jung H-C, Yun C-H, Pan J-G. Functional expression in *Bacillus subtilis* of mammalian NADPH-cytochrome P450 oxidoreductase and its spore-display. Protein Expr Purif. 2009;63:5–11.
14. Cho EA, Kim EJ, Pan JG. Adsorption immobilization of *Escherichia coli* phytase on probiotic *Bacillus polyfermenticus* spores. Enzyme Microb Technol. 2011;49:66–71.
15. Sirec T, Strazzulli A, Isticato R, De Felice M, Moracci M, Ricca E. Adsorption of beta-galactosidase of *Alicyclobacillus acidocaldarius* on wild type and mutants spores of *Bacillus subtilis*. Microb Cell Fact. 2012;11:100.
16. Isticato R, Sirec T, Treppiccione L, Maurano F, De Felice M, Rossi M, Ricca E. Non-recombinant display of the B subunit of the heat labile toxin of *Escherichia coli* on wild type and mutant spores of *Bacillus subtilis*. Microb Cell Fact. 2013;12:98.
17. Ricca E, Baccigalupi L, Cangiano G, De Felice M, Isticato R. Mucosal vaccine delivery by non-recombinant spores of *Bacillus subtilis*. Microb Cell Fact. 2014;13:115.
18. Reljic R, Sibley L, Huang JM, Pepponi I, Hoppe A, Hong HA, Cutting SM. Mucosal vaccination against tuberculosis using inert bioparticles. Infect Immun. 2013;81:4071–4080.
19. Nguyen VA, Huynh HA, Hoang TY, Ninh NT, Pham AT, Nguyen HA, Phan TN, Cutting SM. Killed *Bacillus subtilis* spores expressing streptavidin: a novel carrier of drugs to target cancer cells. J Drug Targ. 2013;21:528–541.
20. Campbell RE, Tour O, Palmer AE, Steinbach PA, Baird GS, Zacharias DA, Tsien RY. A monomeric red fluorescent protein. Proc Natl Acad Sci. 2002;99:7877–7882.
21. Naclerio G, Baccigalupi L, Zilhao R, De Felice M, Ricca E. *Bacillus subtilis* spore coat assembly requires *cotH* gene expression. J Bacteriol. 1996;178:4375–4380.
22. Zilhao R, Naclerio G, Baccigalupi L, Henriques A, Moran C, Ricca E. Assembly requirements and role of CotH during spore coat formation in *Bacillus subtilis*. J Bacteriol. 1999;181:2631–2633
23. Kim H, Hahn M, Grabowski P, McPherson D, Otte MM, Wang R, Ferguson CC, Eichenberger P, Driks A. The *Bacillus subtilis* spore coat protein interaction network. Mol Microbiol. 2006;59:487–502.
24. Saggese A, Scamardella V, Sirec T, Cangiano G, Isticato R, Pane F, Amoresano A, Ricca E, Baccigalupi L. Antagonistic role of CotG and CotH on spore germination and coat formation in *Bacillus subtilis*. PLoS ONE. 2014;9(8):e104900.
25. Youngman P, Perkins JB, Losick R. A novel method for the rapid cloning in *Escherichia coli* of *Bacillus subtilis* chromosomal DNA adjacent to Tn917 insertion. Mol Gen Genet. 1984;195:424–433.
26. Cutting S, Vander Horn PB. Genetic analysis. In: Harwood C, Cutting S, editors. Molecular biological methods for *Bacillus*. Chichester: Wiley; 1990. pp. 27–74.
27. Tennen R, Setlow B, Davis KL, Loshon CA, Setlow P. Mechanisms of killing of spores of *Bacillus subtilis* by iodine, glutaraldehyde and nitrous acid. J Appl Microbiol. 2000;89:330–338.
28. Rubio A, Pogliano K. Septal localization of forespore membrane proteins during engulfment in *Bacillus subtilis*. EMBO J. 2004;23:1636–1646.
29. Bagyan I, Noback M, Bron S, Paidhungat M, Setlow P. Characterization of *yhcN*, a new fore spore-specific gene of *Bacillus subtilis*. Gene. 1998;212:179–188.
30. Imamura D, Kuwana R, Takamatsu H, Watabe K. Localization of proteins to different layers and regions of *Bacillus subtilis* spore coats. J Bacteriol. 2010;192:518–524.
31. Takamatsu H, Chikahiro Y, Kodama T, Koide H, Kozuka S, Tochikubo K, Watabe K. A spore coat protein, CotS, of *Bacillus subtilis* is synthesized under the regulation of *Sigma* K and GerE

during development and is located in the inner coat layer of spores. J Bacteriol. 1998;180:2968–2974
32. Isticato R, Pelosi A, De Felice M, Ricca E. CotE binds to CotC and CotU and mediates their interaction during spore coat formation in *Bacillus subtilis*. J Bacteriol. 2010;192:949–954.
33. Isticato R, Esposito G, Zilhão R, Nolasco S, Cangiano G, De Felice M, Henriques AO, Ricca E. Assembly of Multiple CotC Forms into the *Bacillus subtilis* Spore Coat. J Bacteriol. 2004;186:1129–1135.
34. Koshikawa T, Beaman TC, Pankratz HS, Nakashio S, Corner TR, Gerhardt P. Resistance germination and permeability correlates of *Bacillus megaterium* spores successively divested of integument layers. J Bacteriol. 1984;159:624–632.
35. Nishihara T, Takubo Y, Kawamata E, Koshikawa T, Ogaki J, Kondo M. Role of outer coat in resistance of *Bacillus megaterium* spore. J Biochem. 1989;106:270–273.
36. Sambrook J, Fritsch EF, Maniatis T. Molecular cloning, laboratory manual. 2. NY: Cold Spring Harbor Laboratory Press; 1989.
37. Isticato R, Mase DS, Mauriello EMF, De Felice M, Ricca E. Amino terminal fusion of heterologous proteins to CotC increases display efficiencies in the *Bacillus subtilis* spore system. BioTechniques. 2007;42:151–156.
38. Nicholson WL, Setlow P. Sporulation, germination and out-growth. In: Harwood C, Cutting S, editors. Molecular biological methods for *Bacillus*. Chichester: Wiley; 1990. pp. 391–450.
39. Rusciano G, Zito G, Isticato R, Sirec T, Ricca E, Bailo E, Sasso A. Nanoscale chemical imaging of *Bacillus subtilis* spores by combining tip-enhanced Raman scattering and advanced statistical tools. ACS Nano. 2014;8:12300–12309.
40. Isticato R, Pelosi A, Zilhão R, Baccigalupi L, Henriques AO, De Felice M, Ricca E. CotC–CotU heterodimerization during assembly of the *Bacillus subtilis* spore coat. J Bacteriol. 2008;190:1267–1275.
41. Manzo N, Di Luccia B, Isticato R, D'Apuzzo E, De Felice M, Ricca E. Pigmentation and sporulation are alternative cell fates in *Bacillus pumilus* SF214. PLoS ONE. 2013;8:e62093.
42. McCloy R, Rogers S, Caldon E, Lorca T, Castro A, Burgess A. Partial inhibition of Cdk1 in G2 phase overrides the SAC and decouples mitotic events. Cell Cycle. 2014;13:1400–1412.
43. Serrano M, Crawshaw AD, Dembek M, Monteiro JM, Pereira FC, Pinho MG, Fairweather NF, Salgado PS, Henriques AO. The SpoIIQ–SpoIIIAH complex of Clostridium difficile controls forespore engulfment and late stages of gene expression and spore morphogenesis. Mol Microbiol. 2016;100:204–228.

3.7 Additional Informations

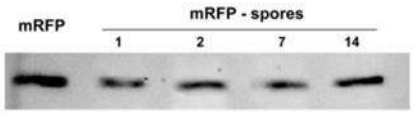

Figure S1: Stability of spore adsorption over time. Purified suspensions of wt spores were mixed with purified recombinant mRFP (5μg) for 1 h at RT. Spores were centrifuged, washed two times, resuspended in PBS, pH3 and stored at RT. After 1, 2, 7 and 14 days, the adsorption mixtures were fractionated by centrifugation and the pellet fractions used for protein extraction by SDS-DTT treatment. Extracted proteins were fractionated on SDS-PAGE and analyzed by western blot. Immuno-reactions were performed with anti-His antibody conjugated with horseradish peroxidase.

mRFP source	Amount of sample used	Density (OD/mm2) [a]	Amount of mRFP (ng) [b]	mRFP µg in 200 µl (% total) [b]
Purified	50.0 ng	74.35	NA	NA
mRFP	25.0 ng	42.31	NA	NA
	12.5 ng	17.80	NA	NA
	6.25 ng	6.89	NA	NA
wt	5.0 x10^6	59.14	39.28	3.4 (68%)
	2.5 x10^6	39.05	17.33	
	1.25x10^6	7.43	7.85	
cotH	5.0 x10^6	72.25	48.5	4.43 (92.6%)
	2.5 x10^6	58.75	26.1	
	1.25x10^6	115.52	10.9	

Table S1: Densitometric analysis of dot blot experiments reported in Fig 1 performed with the pellets of the adsorption reaction with wild type and cotH mutant spores.
[a] Density measured by optical density (OD) per square millimeter and obtained by ChemiDocXRS apparatus with Quantity-One software (Bio-Rad).
[b] Calculated from signals (density OD/mm2) obtained with purified mRFP. NA, not applicable.

mRFP source	Amount of sample used	Density (OD/mm2) [a]	Amount of mRFP (ng) [b]	mRFP µg in 200 µl (% total) [b]
Purified	100.0 ng	193.17	NA	NA
mRFP	50.0 ng	83.52	NA	NA
	25.0 ng	39.28	NA	NA
	12.5 ng	13.92	NA	NA
wt 2	80.0 µl	160.77	85.52	0.182 (9.12%)
	40.0 µl	60.83	35.33	
	20.0 µl	19.42	15.92	
cotH 2	80.0 µl	114.15	57.30	0.107 (5.35%)
	40.0 µl	40.8	27.25	
wt 5	20.0 µl	128.77	69.23	0.57 (11.4%)
	10.0 µl	56.83	33.33	
cotH 5	20.0 µl	42.35	26.30	0.32 (6,4%)
	10.0 µl	16.04	15.85	
wt 10	5.0 µl	157.99	83.52	2.96 (29.6%)
	2.5 µl	65.36	38.33	
	1.2 µl	43.01	27.12	
cotH 10	20.0 µl	193.61	101.30	1.29 (12.9%)
	10.0 µl	120.52	65.25	
	5.0 µl	66.32	39.11	
wt20	2.5 µl	166.25	88.25	7.43 (37.15%)
	1.2 µl	75.55	44.09	
*cotH*20	2.5 µl	60.78	35.78	2.96 (14.8%)
	1.25 µl	42.31	26.80	

Table S2: Densitometric analysis of dot blot experiments reported in Fig. 2 performed with the supernatants of the adsorption reaction performed with different amounts of mRFP and with wild type and cotH mutant spores.
[a] Density measured by optical density (OD) per square millimeter and obtained by ChemiDocXRS apparatus with Quantity-One software (Bio-Rad).
[b] Calculated from signals (density OD/mm2) obtained with purified mRFP. NA, not applicable.

mRFP source	Amount of sample used	Density (OD/mm2) [a]	Amount of mRFP (ng) [b]	mRFP µg in 200 µl (% total) [b]
Purified	25.0 ng	25.125	NA	NA
mRFP	12.50 ng	10.78.40	NA	NA
	6.25 ng	4.62	NA	NA
Unbound	40.0 µl	11.56	12.55	0.083 (4.3%)
mRFP	20.0 µl	6.89	7.78	
	10.0 µl	2.99	3.55	
1x PBS pH 7.0				
5 min	40.0 µl	20.75	19.23	0.092 (4.8%)
	20.0 µl	13.42	12.92	
10 min	20.0 µl	12.5	13.03	0.107 (5.6%)
	10.0 µl	7.2	7.25	
15 min	20.0 µl	11.77	12.83	0.111 (5.8%)
	10.0 µl	6.83	5.33	
30 min	20.0 µl	17.35	15.30	0.122 (6.4%)
	10.0 µl	6.04	5.85	
1M NaCl-0.1% Triton				
5 min	80.0 µl	18.5	20.03	0.053 (2.8%)
	40.0 µl	10.2	11.25	
10 min	40.0 µl	14.83	15.89	0.084 (4.4%)
	20.0 µl	8.02	8.78	
15 min	20.0 µl	12.25	13.01	0.115 (6.2%)
	10.0 µl	7.28	7.31	
30 min	20.0 µl	15.31	16.80	0.164 (8.6%)
	10.0 ul	6.59	7.58	

Table S3: Densitometric analysis of dot blot experiments with the supernatants of adsorption reaction and with washes after various time of incubation with 1× PBS pH7.0 or 1M NaCl–0.1% Triton 100.
[a] Density measured by optical density (OD) per square millimeter and obtained by ChemiDocXRS apparatus with Quantity-One software (Bio-Rad).
[b] Calculated from signals (density OD/mm2) obtained with purified mRFP. NA, not applicable.

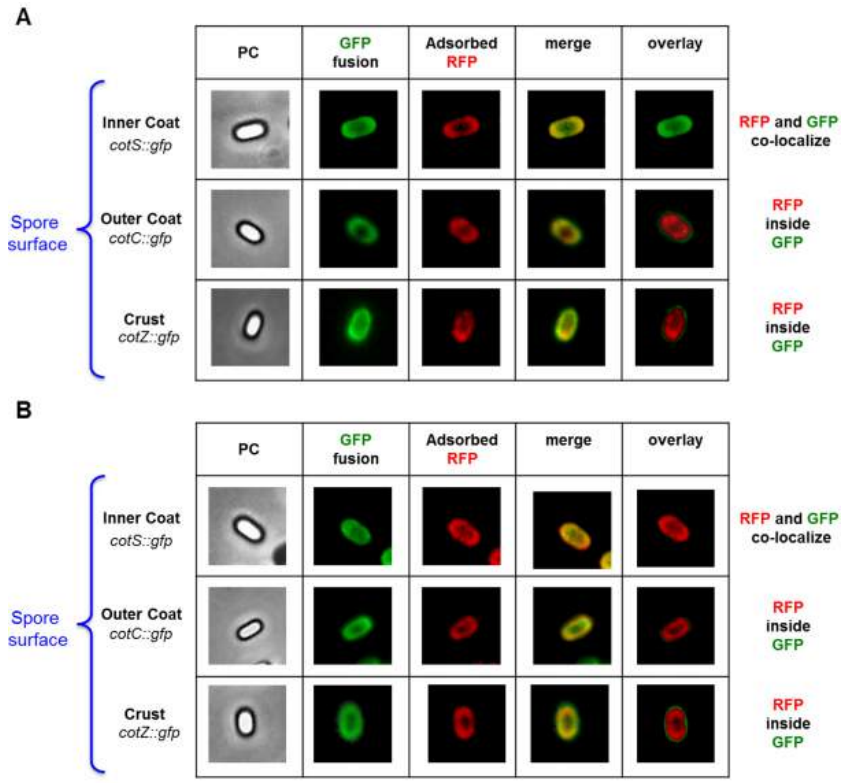

Figure S2: Fluorescence microscopy analysis of spores of otherwise wild type *B. subtilis* strains carrying GFP fused to inner coat, outer coat or crust proteins adsorbed with 50 µg of purified mRFP for 1 h (A) or with 5 µg of purified mRFP for 4 h (B). For each strain the same microscopy fields was observed by phase contrast and fluorescence microscopy (red and green). Merge and overlay (red on green or viceversa) are also shown.

Strain	Genotype	Source
PY79	*wild type*	[25]
ER220	*cotH::spc*	[21]
AZ573	*cotZ::gfp*	[5]
DS127	*cotC::gfp*	[35]
AZ644	*cotS::gfp*	[24]
AZ645	*cotS::gfp ΔcotG ΔcotH::neo*	[24]
RH2466	*pspoIIQ::gfp*	This study
RH285	*pSpoIIQ::gfp cotH::spc*	This study
RH282	*yhcN::gfp*	This study
RH284	*yhcN::gfp cotH::spc*	This study
AZ636	*cotC::gfp ΔcotG ΔcotH::neo*	This study
RH278	*cotZ::gfp cotH::spc*	This study

Table S4: *Bacillus subtilis* strains.

Primer	Sequence [a]	Restriction site
spoIIQ-F	ttcgaaATGAAGGCCATAAGTGAGCGGATGC	*Hin*dIII
spoIIQ-R	ctgcagTTCCTCTCTCATGTTTCATCACCTC	*Pst*I
yhcN-F	ttcgaaATGTTTGGAAAAAAAACAAGTCCTTGCG	*Hin*dIII
yhcN-R	ctgcagAGCGTTAGGGAATACACGCTG	*Pst*I

Table S5: List of oligonucleotides used to prime amplification reactions.

[a] Not capital letters indicate restriction recognition sites.

Chapter 4

The exosporium of *Bacillus megaterium* QM B1551 is permeable to the red fluorescence protein of the coral *Discosoma sp.*

Mariamichela Lanzilli[1], *Giuliana Donadio*[1], *Roberta Addevico*[1], *Anella Saggese*[1], *Giuseppina Cangiano*[1], *Loredana Baccigalupi*[1], *Graham Christie*[2], *Ezio Ricca*[1], *Rachele Isticato*[1].

[1]*Department of Biology, University of Naples Federico II-MSA-Via Cinthia 26-80126 Naples, Italy*

[2]*Department of Chemical Engineering and Biotechnology, University of Cambridge Cambridge, UK.*

Front. Microbiol., 2016 Nov 4;7:1752

4.1 Abstract

Bacterial spores spontaneously interact and tightly bind heterologous proteins. A variety of antigens and enzymes have been efficiently displayed on spores of *Bacillus subtilis*, the model system for spore formers. Adsorption on *B. subtilis* spores has then been proposed as a non-recombinant approach for the development of mucosal vaccine/drug delivery vehicles, biocatalysts, bioremediation, and diagnostic tools. We used spores of *B. megaterium* QM B1551 to evaluate their efficiency as an adsorption platform. Spores of *B. megaterium* are significantly larger than those of *B.subtilis* and of other *Bacillus* species and are surrounded by the exosporium, an outermost surface layer present only in some *Bacillus* species and lacking in *B. subtilis.* Strain QM B1551 of *B. megaterium* and a derivative strain totally lacking the exosporium were used to localize the adsorbed monomeric Red Fluorescent Protein (mRFP) of the coral *Discosoma* sp., used as a model heterologous protein. Our results indicate that spores of *B. megaterium* adsorb mRFP more efficiently than *B. subtilis* spores, that the exosporium is essential for mRFP adsorption, and that most of the adsorbed mRFP molecules are not exposed on the spore surface but rather localized in the space between the outer coat and the exosporium.

4.2 Introduction

Gram-positive bacteria of the *Bacillus* and *Clostridium* genera can differentiate to form an endospore (spore), a metabolically quiescent cell produced in response to conditions that do not allow cell growth [McKenney *et al*., 2012]. Once released in the environment, the spore survives in its dormant state for extremely long periods, resisting to a vast range of stresses such as high temperatures, dehydration, absence of nutrients and the presence of toxic chemicals [McKenney *et al*., 2012]. However, the quiescent spore is able to continuously monitor the environment and respond to the presence of water and nutrients by germinating and originating a vegetative cell that is able to grow and sporulate [McKenney *et al*., 2012]. Resistance to non-physiological conditions is, in part, due to the spore surface structures. In *Bacillus subtilis*, the model system for spore formers, the spore surface is organized in a multilayered coat and in a crust, a recently discovered layer that surrounds the spore coat [McKenney *et al.*, 2012]. *B. subtilis* spores are negatively charged [Huang *et al.*, 2010; Pesce *et al.*, 2014] and have a relative hydrophobicity that is in part due to the glycosylation of some spore surface proteins [Cangiano *et al*., 2014; Rusciano *et al*., 2014]. In several *Bacillus* and *Clostridium* species, including *B. cereus, B. anthracis, B. megaterium*, and *C. difficile*, the outermost spore structure is the exosporium, a morphologically distinct layer composed of proteins and glycoproteins that surrounds the coat [Díaz-González *et al.*, 2015; Manetsberger *et al.*, 2015b; Stewart, 2015].

The bacterial spore has been proposed as a platform to display heterologous proteins, with potential applications ranging from the development of mucosal vaccines to re-usable biocatalysts, diagnostic tools, and bioremediation devices [Knecht *et al.*, 2011; Isticato and Ricca, 2014; Ricca *et al.*, 2014]. The remarkable and well documented resistance of the spore [McKenney *et al.*, 2012], the amenability of several spore-forming species to the genetic manipulation [Harwood and Cutting, 1990] and the safety record of several species [Cutting, 2011; Baccigalupi *et al.*, 2015] support the use of the spore as a display and delivery system. Two strategies have been developed to display heterologous proteins on

the spore surface. A recombinant strategy, based on the construction of gene fusions between DNA coding for a selected spore surface protein and DNA coding for the protein to be displayed, has been used over the years to display a variety of heterologous proteins [Isticato and Ricca, 2014]. A non-recombinant approach, based on the spontaneous adsorption between purified spores and purified proteins, has been also used to display various enzymes and antigens [Ricca *et al.*, 2014]. The molecular details controlling spore adsorption have not been fully elucidated. It is known that the adsorption is more efficient when the pH of the binding buffer is acidic (pH 4) [Huang *et al.*, 2010; Sirec *et al.*, 2012] and that a combination of electrostatic and hydrophobic interactions are likely involved in the interaction [Huang *et al.*, 2010; Sirec *et al.*, 2012]. It is also known that mutant spores with severely altered spore surfaces interact more efficiently than isogenic wild type spores with model proteins [Sirec *et al.*, 2012; Donadio *et al.*, 2016].

Here, we used a fluorescent protein, the monomeric form of the Red Fluorescent Protein (mRFP) of the coral *Discosoma* sp. [Campbell *et al*., 2002], to evaluate whether spores of *B. megaterium* are able to interact with and adsorb a model heterologous protein. *B. megaterium* comprises a number of morphologically distinct strains sharing the unusual large dimensions of both cells (length up to 4 μm and a diameter of 1.5 μm) and spores (length up to 3 μm and diameter of 1 μm) [Di Luccia *et al.*, 2016]. Spores of some strains of *B. megaterium* are surrounded by an exosporium, and since so far only spores of species that lack an exosporium have been considered as adsorption platforms, no data are available on the impact of the exosporium in the interaction with heterologous proteins.

The QM B1551 strain is the best-characterized strain of *B. megaterium*. This strain carries about 11% of its genome on seven indigenous plasmids [Rosso and Vary, 2005; Vary *et al.*, 2007; Eppinger *et al*., 2011], two of which – pBM500 and pBM600 – have been identified as carrying genes that are essential to the formation of this strain's distinctive "walnut-shaped" exosporium [Manetsberger *et al.*, 2015a]. The protein composition of the QM B1551 exosporium is as yet poorly characterized, with only a few genes encoding orthologs of recognized exosporium protein in spores of other species being identified by genomic analyses. These include genes encoding BclA nap proteins, which form a localized nap in *B. megaterium* QM B1551 spores, plus an ortholog of the BxpB protein that forms the basal layer of the exosporium in *B. cereus* family spores. The latter appears to fulfill a different role in *B. megaterium* QM B1551 spores, since a null mutant strain retained an apparently normal exosporium [Manetsberger *et al.*, 2015a].

In this paper, we present data that demonstrates that spores of *B. megaterium* QM B1551 can efficiently adsorb mRFP, and provide evidence that protein molecules are able to cross the permeability barrier presented by the exosporium to localize in the inter-coat space.

4.3 Materials and Methods

4.3.1 Bacterial Strains, Spore, and RFP Production

The *B. megaterium* strains employed in this study are QM B1551 and its plasmid-less derivative PV361 [Rosso and Vary, 2005]. The *B. subtilis* strain used in this study was PY79 [Youngman *et al*., 1984]. Sporulation of all *Bacillus* strains was induced by the exhaustion method [Cutting and Vander

Horn, 1990]. After 30 h of growth in Difco Sporulation (DS) medium at 37°C with vigorous shaking spores were collected and purified as described by Nicholson and Setlow (1990) using overnight incubation in H_2O at 4°C to lyse residual sporangial cells. The number of purified spores obtained was measured by direct counting with a Bürker chamber under an optical microscope (Olympus BH-2 with 40× lens).

For mRFP production, cells of *Escherichia coli* strain RH161 [Donadio et al., 2016], bearing the expression vector pRSET-A carrying an in-frame fusion of the 5′ end of the *rfp* coding region to six histidine codons under the transcriptional control of a T7 promoter, were grown for 18 h at 37°C in 100 ml of autoinduction medium to express the heterologous protein [Isticato *et al.*, 2010]. The His_6-tagged RFP protein was purified under native conditions using a His-Trap column as recommended by the manufacturer (GE Healthcare Life Science). Purified protein was desalted using a PD10 column (GE Healthcare Life Science) to remove high NaCl and imidazole concentrations.

4.3.2 Adsorption Reaction

Unless otherwise specified 5 μg of purified recombinant mRFP was added to a suspension of spores (5×10^8) in 50 mM Sodium Citrate pH 4.0 at 25°C in a final volume of 200 μl. After 1 h of incubation, the binding mixture was centrifuged (10 min at 13,000 g) to fractionate mRFP bound-spores in the pellet from free mRFP in the supernatant.

4.3.3 Western and Dot-Blot Analysis

Spore pellets from adsorption reactions were resuspended in 40 μl of spore coat extraction buffer [Nicholson and Setlow, 1990; Giglio et al., 2011], incubated at 68°C for 1 h to solubilize spore coat proteins and loaded onto a 12% SDS-PAGE gel. The proteins were then electro-transferred to nitrocellulose filters (Amersham Pharmacia Biotech) and used for Western blot analysis as previously reported [Isticato et al., 2008] using monoclonal mRFP-recognizing anti-His antibody (Sigma). A quantitative determination of the amount of mRFP was obtained by dot blot experiments comparing serial dilutions of purified mRFP and binding assay supernatant. Filters were then visualized by the ECL-prime method (Amersham Pharmacia Biotech) and subjected to densitometric analysis by Quantity One 1-D Analysis Software (Bio-Rad). Dot blot and relative densitometric analyses were performed three times to verify the significance of the results.

4.3.4 Fluorescence and Immunofluorescence Microscopy

Post-adsorption spores were resuspended in 50 μl of 1x PBS pH 4.0 and 5 μl of the suspension placed on microscope slides and covered with a coverslip previously treated for 30 s with poly-L-lysine (Sigma). Immunofluorescence was performed as described by Isticato et al. (2013), with the following modifications: 2.0×10^6 RFP-adsorbed spores of QM B1551 and PV361 *B. megaterium* strains were pretreated with 1% bovine serum albumin (BSA) – 1x PBS pH 4.0 for 30 min prior to 2 h-incubation at 4°C with the anti-polyHistidine antibodies (mouse; Sigma) diluted 1:20 in 1x PBS pH 4.0–1% BSA.

As a control of the specificity of this technique, non-adsorbed spores were directly treated with anti-His antibodies. After three washes, the samples were incubated with a 64-fold diluted anti-mouse secondary antibody conjugated with fluorescein isothiocyanate, FITC (Santa Cruz Biotechnology, Inc.) and washed four times with 1X PBS pH 4.0. Washed samples were resuspended in 20 µl of 1X PBS pH 4.0 and 10 µl were analyzed. All samples were observed with an Olympus BX51 fluorescence microscope fitted with a 100X UPlan F1 oil objective; U-MNG or U-MWIBBP cube-filters were used to detect the red fluorescence emission of mRFP or the green emission of FITC-conjugated antibodies, respectively. Exposure times were in the range between 200 and 3000 ms. Images were captured using an Olympus DP70 digital camera and processed with Image Analysis Software (Olympus) for minor adjustments of brightness, contrast and color balance [McCloy *et al.*, 2014]. ImageJ (v1.48, NIH) was used to draw an outline around 80 spores for each strain and minimum, maximum and mean fluorescence values per pixel were recorded for each spore. Values of fluorescence intensity were displayed subsequently as box-plots with 5–95% confidence intervals [McCloy *et al.*, 2014].

4.3.5 Statistical Analysis

Results from dot blot and fluorescence microscopy analysis are the averages from three independent experiments. Statistical significance was determined by the Student *t*-test, and the significance level was set at $P < 0.05$.

4.4 Results

4.4.1 mRFP of *Discosoma* sp. is Adsorbed by *B. megaterium* Spores

To verify whether spores of *B. megaterium* QM B1551 were able to adsorb mRFP, 5 µg of the purified protein (Materials and Methods) were incubated with 5.0×10^8 purified spores. The adsorption reaction was performed in 50 mM sodium citrate at pH 4.0, as previously described (Sirec *et al.*, 2012). After the reaction, spores were extensively washed with 1X PBS pH 4.0, spore surface proteins were extracted as described in Materials and Methods and analyzed by western blotting with anti-polyHistidine-Peroxidase antibody (Sigma), which recognizes the histidine-tagged N terminus of mRFP. As shown in Fig. 1A, mRFP was extracted from spores, indicating that it was absorbed during the reaction and then released by the extraction treatment. To evaluate the efficiency of adsorption, we analyzed the amount of mRFP left unbound, i.e., post-adsorbed spores were collected by centrifugation and the supernatant serially diluted and analyzed by dot blotting (Fig. 1B). A densitometric analysis of the dot blot (Additional File Table 1) showed that when 5 µg of mRFP was used in the adsorption reaction less than 1% was left unbound, indicating that about 99% of the heterologous protein was adsorbed to *B. megaterium* spores. To analyze whether adsorbed mRFP molecules were tightly bound to the spore surface, post-adsorption reaction spores were washed twice with PBS buffer at pH 3.0 or pH 7.0, or with a 1M NaCl, 0.1% Triton X-100 solution as previously described [Donadio *et al.*, 2016]. As shown in Fig. 1C, and supported by densitometric analysis of the dot blot (Additional File Table 2), the washes at pH 3.0 did not cause any release of the adsorbed mRFP, while the washes at pH 7.0 or

with 1M NaCl, 0.1% Triton X-100 caused a minimal, less than 1%, release of mRFP molecules. Therefore, results presented in Fig.1 suggest that mRFP was efficiently adsorbed and tightly bound to *B. megaterium* spores. To assess whether spore-adsorbed mRFP molecules retained their fluorescence properties, we performed a fluorescence microscopy analysis. As shown in Fig. 2, post-adsorption reaction spores were associated with a strong fluorescence signal visible around the entire spore surface.

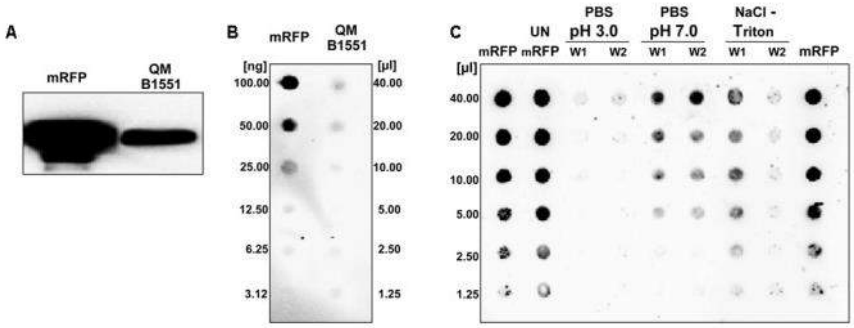

Figure 1: *Bacillus megaterium* QM B1551 spores adsorb mRFP. 5×10^8 spores were incubated with 5 µg of purified mRFP and then the samples subject to centrifugation. **(A)** Spore surface proteins were extracted from the pellet fraction by SDS-DTT treatment, fractionated on SDS-PAGE and analyzed by Western blot. Purified mRFP (20 µg) was used as a marker. **(B)** The supernatant, containing the unbound mRFP, was serially diluted and analyzed by dot blot (QM B1551). Serial dilutions of purified mRFP (mRFP) were used as a standard. **(C)** Spores adsorbed with mRFP were washed twice (W1 and W2) with PBS buffer at pH 3.0 or pH 7.0, or with a 1M NaCl, 0.1% Triton X-100 solution. Serial dilutions of purified mRFP and unbound mRFP (UN-mRFP) were used as standards. Immuno-reactions in all panels were performed with mRFP-recognizing anti-His antibody conjugated with horseradish peroxidase.

4.4.2 The Exosporium has an Essential Role in mRFP Adsorption

Strain QM B1551 of *B. megaterium* contains seven indigenous plasmids [Rosso and Vary, 2005; Eppinger *et al*., 2011] and plasmid-encoded genes are essential for exosporium formation [Manetsberger *et al.*, 2015a]. PV361 is a QM B1551-cured strain lacking all seven plasmids and, as a consequence, totally lacking the exosporium [Manetsberger *et al.*, 2015a]. We used spores of strain PV361 to analyze the role of the exosporium in mRFP adsorption. In parallel, we also used spores of *B. subtilis* PY79 that in a previous study have been shown to adsorb mRFP (Donadio *et al.*, 2016). To compare the adsorption efficiency of spores of the *B. subtilis* PY79 and *B. megaterium* QM B1551 and PV361 strains, we adsorbed 5 µg of purified mRFP with 5.0×10^8 spores of each of the three strains. After the adsorption reactions spores were collected by centrifugation, proteins extracted by SDS-DTT treatment and analyzed by western blotting with mRFP-recognizing anti-His antibody. As shown in Fig. 3A, mRFP was apparently extracted in larger amounts from spores of QM B1551 than from spores of the other two strains. In an attempt to quantify these apparent differences, unbound mRFP from the adsorption reactions was serially diluted and analyzed by dot blotting (Fig. 3B). A densitometric analysis of the dot blot of Fig- 3B (Additional File Table 3) indicated that PY79 and PV361 spores adsorbed about 90% of the total mRFP while QM B1551 spores adsorbed almost all (over 99%) purified mRFP.

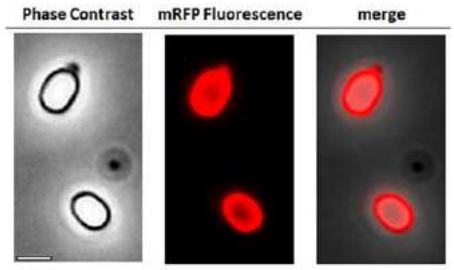

Figure 2: Fluorescence microscopy analysis of *B. megaterium* QM B1551-mRFP spores. QM B1551 spores incubated with mRFP (5 µg), and subsequently washed, were analyzed by fluorescence microscopy. The same microscopy field was observed by phase contrast and fluorescence microscopy. Scale bar 1 µm. The merge panel is reported. The exposure time was 200 ms.

Based on the results of Figs. 3 and **4**, we conclude that the exosporium, present in QM B1551 and lacking in PV361 has a relevant role in the adsorption of mRFP.

In addition, results of Fig. 4 indicated that *B. subtilis* PY79 spores are more efficient than *B. megaterium* PV361 spores in adsorbing mRFP, whereas dot blotting reported in Fig. 3B indicated similar adsorption efficiencies for the two strains. We believe that this discrepancy is due to a strong reduction of fluorescence when mRFP is bound to PV361 but not to PY79 or QM B1551 spores (see below).

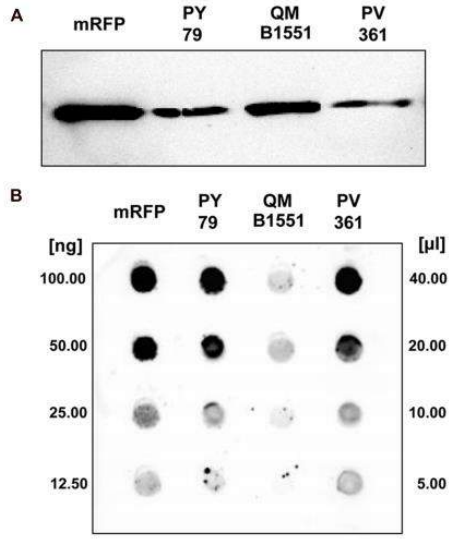

Figure 3: Monomeric Red Fluorescent Protein adsorption to spores of *B. megaterium* QM B1551 and PV361 and *B. subtilis* PY79. 5 × 108 spores of each strain were incubated with 5 µg of purified mRFP and then the samples subject to centrifugation. Spores in the pellet fractions were used to extract surface proteins that were subsequently analyzed by western blot (A), while the supernatants were serially diluted and analyzed by dot blot (B). Serial dilutions of purified mRFP were used as standards. Immuno-reactions in both panels were performed with anti-His antibody conjugated with horseradish peroxidase.

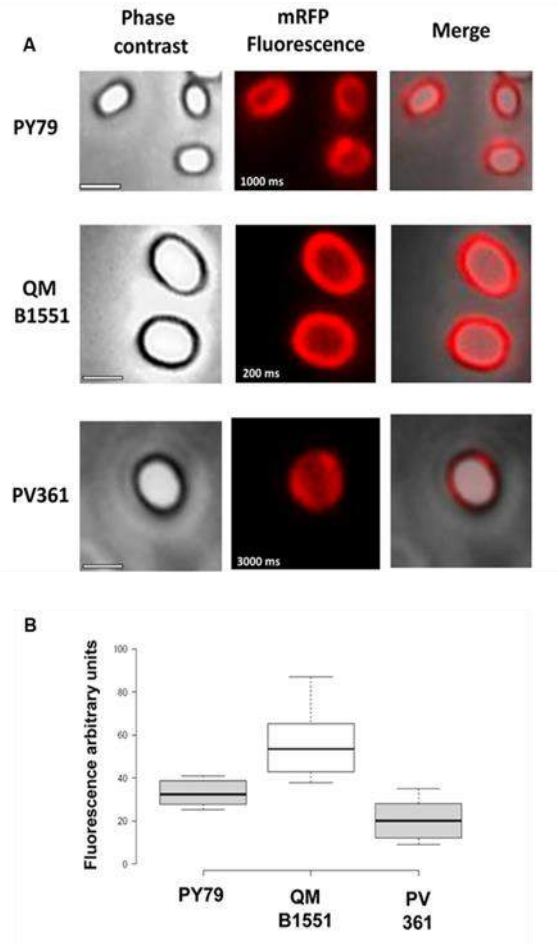

Figure 4: Efficiency of adsorption of mRFP to spores of *B. megaterium* QM B1551 and PV361 and *B. subtilis* PY79. (A) Fluorescence microscopy images of PY79, QM B1551, and PV361 spores following mRFP adsorption and washing. Exposure times are indicated. Phase contrast and red fluorescence overlays are shown (merge panel). Scale bars 1 µm. **(B)** Box plots displaying the fluorescence intensity of eighty different spores of each strain. Limits of each box represent the first and the third quartile (25 and 75%) and the values outside the boxes represent the maximum and the minimum values. The line dividing the box indicates the median value for each strain. *P* value is less than 0.0001.

4.4.3 Quantitative Assessment of mRFP Adsorption to QM B1551 Spores

Dot blot experiments (Fig. 3B) indicated that when 5 µg of purified mRFP was used in adsorption reactions with 5.0×10^8 spores of the QM B1551 strain almost all heterologous protein was bound to the spore. In order to define the maximal amount of mRFP that can be adsorbed to QM B1551 spores, we repeated the reactions with increasing concentrations of purified mRFP, i.e., 5.0×10^8 QM B1551 spores were reacted with 5, 10, 20, 40, 80, and 160 µg of purified mRFP. After the reactions spores were collected by centrifugation and the supernatants containing unbound mRFP were serially diluted and analyzed by dot blotting (Fig. 5A). Fig. 5B displays the results of densitometric analyses of the dot blot, which indicates that when 5–80 µg of mRFP was reacted with 5×10^8 spores, the percentage of protein bound to spores was over 90%. A decrease of bound mRFP was observed when 160 µg of purified protein were used in the reaction. However, even when 160 µg of purified mRFP was used over 60% of the protein was absorbed, indicating that 5.0×10^8 spores of QM B1551 can adsorb about 100 µg of mRFP.

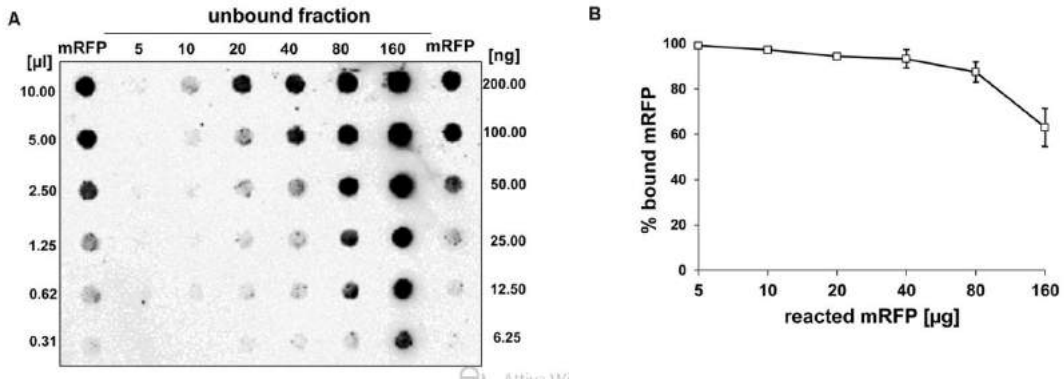

Figure 5: Quantitative assessment of mRFP adsorption to *B. megaterium* QM B1551 spores. 5×10^8 spores were incubated with 5, 10, 20, 40, 80, and 160 µg of purified mRFP. The reaction mixtures were subsequently subject to centrifugation and the supernatants serially diluted and analyzed by dot blot **(A)**. Serial dilutions of purified mRFP were used as standards. Immuno-reactions in both panels were performed with anti-His antibody conjugated with horseradish peroxidase. (**B**) Percentage of mRFP adsorbed to spores after reaction with defined amounts of endogenous mRFP. Error bars show the standard errors of the mean from three experiments and the *P* value never above 0.0025.

4.4.4 mRFP Localizes to the Inter-Coat Space in *B. megaterium* QM B1551 spores

An immuno-fluorescence microscopy approach was employed to assess whether adsorbed mRFP molecules were exposed on the surface of *B. megaterium* QM B1551 spores. QM B1551 spores adsorbed with various amounts of mRFP were reacted with monoclonal anti-His antibody recognizing the recombinant mRFP, then with fluorescent anti-mouse secondary antibody (Santa Cruz Biotechnology, Inc.) and observed under the fluorescence microscope (Fig. 6). With the lowest amount of mRFP used in this experiment (2 µg) the mRFP fluorescence signal (red) was observed all around the spore while the immunofluorescence signal (green) was weak and mainly concentrated at the spore poles, suggesting that only in those points mRFP was exposed on the spore surface. Increasing the amount of mRFP used in the reaction the number of green spots increased (5 and 10 µg) and with highest amount of mRFP used in the reaction (20 µg) an almost complete green ring was observed around the spores. Based on the results presented in Fig. 6, we hypothesized that mRFP molecules infiltrate through the exosporium and localizes in the inter-coat space between the outer coat and the exosporium, i.e., when a low amount of mRFP is used almost all protein molecules are internal to the exosporium and are available to the antibody at only a few locations. Increasing amounts of mRFP in adsorption reactions results in the inter-coat space "filling up," until ultimately more mRFP molecules are available to the antibody on the spore surface. This hypothesis implies that if the exosporium is lacking then all mRFP should be available to the antibody. To test this, we compared by immunofluorescence microscopy equal numbers of spores of QM B1551 (with exosporium) and of PV361 (without exosporium) incubated with the same amount of mRFP (5 µg). When the exosporium was present (QM B1551) mRFP was only partially available to the antibody and green spots were observed **(**Fig. 7 and Additional File Fig. S2). When the exosporium was not present (PV361) adsorbed

mRFP was available to the antibody all around the spore and a complete green ring was formed, supporting the hypothesis that mRFP is internal to the exosporium in QM B1551 spores.

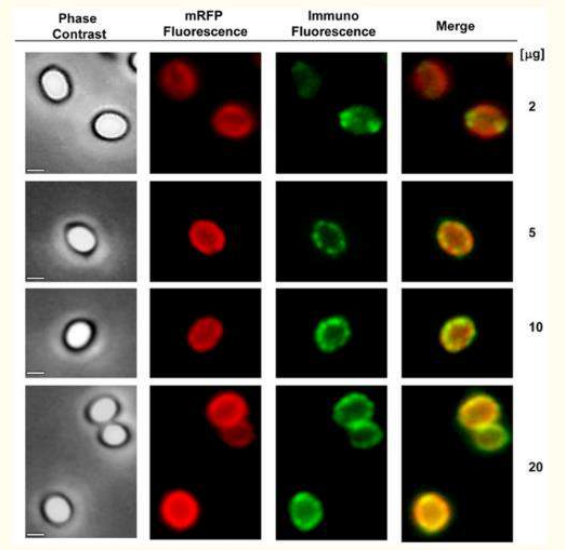

Figure 6: Immunofluorescence analysis of mRFP-adsorbed *B. megaterium* QM B1551 spores. Aliquots of 5×10^8 QM B1551 spores were incubated with variable concentrations of mRFP and were subsequently analyzed by phase contrast, fluorescence and immunofluorescence microscopy, as described in the Materials and Methods. The same microscopy field for each reaction is reported together with the merge panel. The exposure time was 200 ms for all images. Scale bar, 1 µm.

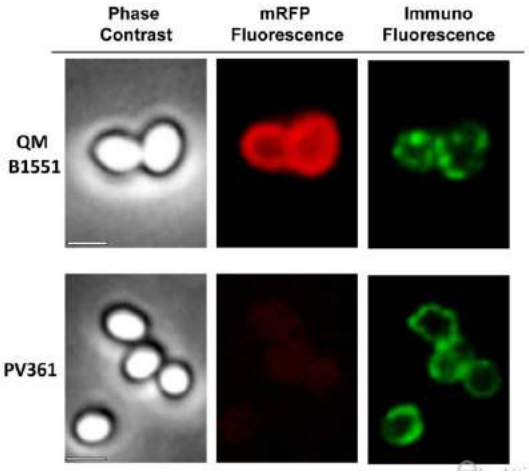

Figure 7: Immunofluorescence of mRFP adsorbed to *B. megaterium* QM B1551 and PV361 spores. 5×10^8 QM B1551 and PV361 spores were incubated with 5 µg mRFP and then analyzed by immunofluorescence microscopy, as described in the Materials and Methods. For each field phase contrast and immunofluorescence microscopy are shown. The exposure time was 200 ms for all images. Scale bar, 1 µm.

While QM B1551 spores used in the experiments of Fig. 7 showed a complete red fluorescent ring as in Fig. 2, PV361 spores showed a very weak red fluorescent signal. With PV361 spores a red signal was only observed using long exposure times at the fluorescence microscope (Fig. 4). Since mRFP is

present around PV361 spores (Fig. 3 and 7), we conclude that mRFP fluorescence is weakened when the protein is adsorbed to PV361 spores. Further experiments will be needed to fully address this point.

4.5 Discussion

The main findings of this report are that spores of *B. megaterium* are extremely efficient in adsorbing the heterologous model protein mRFP, that the exosporium has an important role in this process, and that mRFP molecules infiltrate through the exosporium localizing between the outer coat and the exosporium. These results expand previous work performed on spores of *B. subtilis* and demonstrate that spores of a different species may also be used to deliver heterologous proteins via the adsorption method. The high efficiency of adsorption observed with *B. megaterium* spores is in part due to the large size of its spore compared with that of *B. subtilis*. Indeed, the *B. megaterium* spore surface area is about 2.5-fold larger than the *B. subtilis* spore, with a surface of 5.33 μm^2 (h: 1.60 ± 0.16 w: 0.84 ± 0.07) vs. 1.98 μm^2 (h: 1.07 ± 0.09 w: 0.48 ± 0.03). The large dimensions allow the adsorption of up to 100 µg of mRFP when 160 µg of protein are reacted with spores.

The observation that mRFP crosses the exosporium indicates that it is permeable to mRFP, a 27 kDa protein. Permeability of the exosporium is not totally surprising since germinants present in the environment have to cross the external layers of the spore to reach their receptors, albeit germinants are typically small molecules with molecular masses typically <200 Da. Additionally, the mRFP data are broadly in agreement with the results of previous studies conducted with labeled dextrans and related molecules [Koshikawa *et al*., 1984; Nishihara *et al.*, 1989]. In those studies, the *B. megaterium* QM B1551 exosporium was suggested to represent a permeability barrier to molecules with molecular weights greater than 100 KDa, while influencing the passage of molecules with masses somewhere between 2 and 40 kDa [Koshikawa *et al*., 1984; Nishihara *et al.*, 1989].

An interesting challenge for future work will be to establish the mechanism or route of infiltration that mRFP, and by inference other heterologous proteins of interest, takes to enter the inter-coat space. Examination by transmission electron microscopy of sectioned *B. megaterium* QM B1551 spores indicates that the exosporium comprises two identical "shells" [Manetsberger *et al*., 2015a], and it may be that the interface between each of these structures (described as "apical openings" in early papers) permits ingress of relatively large molecules. Discerning the basis for the apparent loss of mRFP fluorescence upon adsorption to PV361 spores, and whether mRFP molecules are able to infiltrate the outer coat layers, as observed for *B. subtilis* spores [Donadio *et al.*, 2016], will also be of interest.

In the current study, we hypothesize that mRFP molecules preferentially cross the exosporium and accumulate in the inter-coat space between the outer coat and the exosporium. In this model, mRFP molecules are only adsorbed and displayed on the spore surface once adsorption sites (or volumetric capacity?) in the inter-coat space are sufficiently occupied. This implies that the adsorption approach to surface display can be used with *B. megaterium* QM B1551 spores, although the system is dependent on the spore to protein ratio used in adsorption reactions. Since various strains of *B. megaterium* have long been used industrially for the production of enzymes such as amylases and dehydrogenases, vitamins and antimicrobial molecules [Vary *et al.*, 2007], our data suggest a new biotechnological application for the *B. megaterium* spore as a vehicle to bind and deliver heterologous proteins.

4.6 References

1. Baccigalupi L., Ricca E., Ghelardi E. (2015). "*Non-LAB probiotics: spore Formers,"* in Probiotics and Prebiotics: Current Research and Future Trends eds Venema K., do Carmo A. P., editors. (Norfolk, VA: Caister Academic Press;) 93–103. 10.21775/9781910190098.06
2. Campbell R. E., Tour O., Palmer A. E., Steinbach P. A., Baird G. S., Zacharias D. A., et al. (2002). *A monomeric red fluorescent protein.* Proc. Natl. Acad. Sci. U.S.A. 99 7877–7882. 10.1073/pnas.082243699
3. Cangiano G., Sirec T., Panarella C., Isticato R., Baccigalupi L., De Felice M., et al. (2014). *The sps gene products affect germination, hydrophobicity and protein adsorption of Bacillus subtilis spores.* Appl. Environ. Microbiol. 80 7293–7302. 10.1128/AEM.02893-14
4. Cutting S. M. (2011). *Bacillus* probiotics. Food Microbiol. 28 214–220. 10.1016/j.fm.2010.03.007
5. Cutting S., Vander Horn P. B. (1990). "*Genetic analysis*" in Molecular Biological Methods for *Bacillus* eds Harwood C., Cutting S., editors. (Chichester: John Wiley and Sons;) 27–74.
6. Díaz-González F., Milano M., Olguin-Araneda V., Pizarro-Cerda J., Castro-Córdova P., Tzeng S. C., et al. (2015). *Protein composition of the outermost exosporium-like layer of Clostridium difficile 630 spores.* J. Proteom. 123 1–13. 10.1016/j.jprot.2015.03.035
7. Di Luccia B., D'Apuzzo E., Varriale F., Baccigalupi L., Ricca E., Pollice A. (2016). *Bacillus megaterium SF185 induces stress pathways and affects the cell cycle distribution of human intestinal epithelial cells.* Benef. Microb. 7 609–620. 10.3920/BM2016.0020
8. Donadio G., Lanzilli M., Sirec T., Ricca E., Isticato R. (2016) *Protein adsorption and localization on wild type and mutant spores of Bacillus subtilis* Microb. Cell Fact. 15:153 10.1186/s12934-016-0551-2
9. Eppinger M., Bunk B., Johns M. A., Edirisinghe J. N., Kutumbaka K. K., Koenig S. S., et al. (2011). *Genome sequences of the biotechnologically important Bacillus megaterium strains QM B1551 and DSM319*. J. Bacteriol. 193 4199–4213. 10.1128/JB.00449-11
10. Giglio R., Fani R., Isticato R., De Felice M., Ricca E., Baccigalupi L. (2011). *Organization and evolution of the cotG and cotH genes of Bacillus subtilis*. J. Bacteriol. 193 6664–6673. 10.1128/jb.06121-11
11. Harwood C. R., Cutting S. M. (1990). *Molecular Biological Methods for Bacillus.* Chichester: John Wiley and Sons.
12. Huang J. M., Hong H. A., Van Tong H., Hoang T. H., Brisson A., Cutting S. M. (2010). *Mucosal delivery of antigens using adsorption to bacterial spores.* Vaccine 28 1021–1030. 10.1016/j.vaccine.2009.10.127
13. Isticato R., Pelosi A., De Felice M., Ricca E. (2010). *CotE binds to CotC and CotU and mediates their interaction during spore coat formation in Bacillus subtilis.* J. Bacteriol. 192 949–954. 10.1128/JB.01408-09
14. Isticato R., Pelosi A., Zilhão R., Baccigalupi L., Henriques A. O., De Felice M., et al. (2008). *CotC-CotU heterodimerization during assembly of the Bacillus subtilis spore coat.* J. Bacteriol. 190 1267–1275. 10.1128/JB.01425-07
15. Isticato R., Ricca E. (2014). *Spore surface display*. Microbiol. Spectr. 2 351–366. 10.1128/microbiolspec.TBS-0011-2012
16. Isticato R., Sirec T., Treppiccione L., Maurano F., De Felice M., Rossi M., et al. (2013). *Nonrecombinant display of the B subunit of the heat labile toxin of Escherichia coli on wild type and mutant spores of Bacillus subtilis.* Microb. Cell Fact. 12:98 10.1186/1475-2859-12-98
17. Knecht L. D., Pasini P., Daunert S. (2011). *Bacterial spores as platforms for bioanalytical and biomedical applications.* Anal. Bioanal. Chem. 400 977–989. 10.1007/s00216-011-4835-4
18. Koshikawa T., Beaman T. C., Pankratz H. S., Nakashio S., Corner T. R., Gerhardt P. (1984). *Resistance, germination, and permeability correlates of Bacillus megaterium spores successively divested of integument layers.* J. Bacteriol. 159 624–632

19. Manetsberger J., Hall E. A. H., Christie G. (2015a). *Plasmid-encoded genes influence exosporium assembly and morphology in Bacillus megaterium QM B1551 spores.* FEMS Microbiol. Lett. 362:fnv147 10.1093/femsle/fnv147
20. Manetsberger J., Manton J. D., Erdelyi M. J., Lin H., Rees D., Christie G., et al. (2015b). *Ellipsoid localization microscopy infers the size and order of protein layers in Bacillus spore coats.* Biophys. J. 109 2058–2066. 10.1016/j.bpj.2015.09.023
21. McCloy R., Rogers S., Caldon E., Lorca T., Castro A., Burgess A. (2014). *Partial inhibition of Cdk1 in G2 phase overrides the SAC and decouples mitotic events.* Cell Cycle 13 1400–1412. 10.4161/cc.28401
22. McKenney P. T., Driks A., Eichemberger P. (2012). T*he Bacillus subtilis endospore: assembly and functions of the multilayered coat.* Nat. Rev. Microbiol. 11 33–44. 10.1038/nrmicro2921
23. Nicholson W. L., Setlow P. (1990). "*Sporulation, germination and out-growth,"* in Molecular biological methods for Bacillus eds Harwood C., Cutting S., editors. (Chichester: John Wiley and Sons) 391–450.
24. Nishihara T., Takubo Y., Kawamata E., Koshikawa T., Ogaki J., Kondo M. (1989). *Role of outer coat in resistance of Bacillus megaterium spore.* J. Biochem. 106 270–273.
25. Pesce G., Rusciano G., Sirec T., Isticato R., Sasso A., Ricca E. (2014). *Surface charge and hydrodynamic coefficient measurements of Bacillus subtilis spore by optical tweezers.* Colloids Surf. B Biointerfaces 116C 568–575. 10.1016/j.colsurfb.2014.01.039
26. Ricca E., Baccigalupi L., Cangiano G., De Felice M., Isticato R. (2014). *Mucosal vaccine delivery by non-recombinant spores of B.subtilis*. Microb. Cell Fact. 13 115 10.1186/s12934-014-0115-2
27. Rosso M. L., Vary P. S. (2005). *Distribution of Bacillus megaterium QM B1551 plasmids among other B. megaterium strains and Bacillus species.* Plasmid 53 205–217. 10. 1016 / j. Plasmid .2004 .10.005
28. Rusciano G., Zito G., Isticato R., Sirec T., Ricca E., Bailo E., Sasso A. (2014). *Nanoscale chemical imaging of Bacillus subtilis spores by combining tip-enhanced Raman scattering and advanced statistical tools.* ACS Nano 8 12300–12309. 10.1021/nn504595k
29. Sirec T., Strazzulli A., Isticato R., De Felice M., Moracci M., Ricca E. (2012). *Adsorption of beta-galactosidase of Alicyclobacillus acidocaldarius on wild type and mutants spores of Bacillus subtilis.* Microb. Cell Fact. 11:100 10.1186/1475-2859-11-100
30. Stewart G. C. (2015). *The* Exosporium *layer of bacterial spores: a connection to the environment and the infected host.* Microbiol. Mol. Biol. Rev. 79 437–457. 10.1128/MMBR.00050-15
31. Vary P. S., Biedendieck R., Fuerch T., Meinhardt F., Rohde M., Deckwer W. -D., et al. (2007). *Bacillus megaterium—from simple soil bacterium to industrial protein production host.* Appl. Microbiol. Biotechnol. 76 957–967 10.1007/s00253-007-1089-3
32. Youngman P., Perkins J. B., Losick R. (1984). *A novel method for the rapid cloning in Escherichia coli of Bacillus subtilis chromosomal DNA adjacent to Tn917 insertion.* Mol. Gen. Genet. 195 424–433. 10.1007/BF00341443

4.7 Additional Informations

mRFP source	Amount of sample used	Density (OD/mm2) [a]	Amount of mRFP (ng) [b]	mRFP µg (% total)
Purified	100.00 ng	565.31	NA	NA
mRFP	50.00 ng	279.67	NA	NA
	25.00 ng	139.18	NA	NA
	12.50 ng	56.84	NA	NA
	6.25 ng	38.73	NA	NA
unbound	40.0 µl	89.00	16.69	0.50 (0.55%)
mRFP	20.0 µl	77.31	11.05	
	10.0 µl	47.30	6.95	

TABLE S1: Densitometric analysis of dot blot experiments with the supernatants of the adsorption reaction with QM B1551 spores (Fig. 1B).

[a] Density measured by optical density (OD) per square millimeter and obtained by ChemiDocXRS apparatus with Quantity-One software (Bio-Rad).
[b]Calculated from signals (density OD/mm2) obtained with purified mRFP. NA, not applicable.

mRFP source	Amount of sample used	Density (OD/mm2) [a]	Amount of mRFP (ng) [b]	mRFP µg (% total)
Purified	50.0 ng	989205.3	NA	NA
mRFP	25.0 ng	487172.1	NA	NA
	12.5 ng	281015.5	NA	NA
	6.25 ng	170208.0	NA	NA
unbound	10.0 µl	1083584.0	55.17	1.125 (11%)
mRFP	5.0 µl	639823.0	31.83	
	2.5 µl	263354.4	12.40	
Wash 1	10.0 µl	14893.5	NA	NA
PBS pH3	5.0 µl	7695.1	NA	NA
Wash 2	40.0 µl	20188.1	NA	NA
PBS pH3	20.0 µl	9235.0	NA	NA
Wash 1	20.0 µl	252555.0	11.50	0.059 (0.59%)
PBS ph7	10.0 µl	147062.6	6.00	
	5 µl	68093.6	2.12	
Wash 2	10.0 µl	154130.0	6.53	0.055 (0.55%)
PBS pH7	5 µl	68093.6	2.45	
Wash 1	40.0 µl	374963.4	18.00	0.046 (0.46%)
0.1% Triton	20.0 µl	212687.3	9.30	
0.1M NaCl				
Wash 2	40 µl	65720.4	1.70	0.0037 (0.37%)
0.1% Triton	20 µl	46127.0	0.62	
0.1M NaCl				

TABLE S2: Densitometric analysis of dot blot experiments with the supernatants of various washes after the adsorption reaction (Fig. 1C).

[a] Density measured by optical density (OD) per square millimeter and obtained by ChemiDocXRS apparatus with Quantity-One software (Bio-Rad).
[b]Calculated from signals (density OD/mm2) obtained with purified mRFP. NA, not applicable.

mRFP source	Amount of sample used	Density (OD/mm2) [a]	Amount of mRFP (ng) [b]	mRFP µg 200 µl (% total)
Purified	100.0 ng	344.07	NA	NA
mRFP	50.0 ng	167.22	NA	NA
	25.0 ng	86.72	NA	NA
	12.5 ng	42.70	NA	NA
PY79	40.0 µl	642.27	189.5	4.81 (9.62%)
	20.0 µl	322.82	97.02	
	10.0 µl	180.45	55.83	
QMB155	40.0 µl	32.17	10.92	0.27 (0.55%)
	20.0 µl	14.80	5.64	
PV361	20.0 µl	344.95	96.15	5.23 (10.46%)
	10.0 µl	192.56	52.32	
	5.0	89.75	30.52	

TABLE S3: Densitometric analysis of dot blot experiments with the supernatants of the adsorption reaction performed with spores of strains PY79, QM B1551, and PV361 (Fig.3B).

[a] Density measured by optical density (OD) per square millimeter and obtained by ChemiDocXRS apparatus with Quantity-One software (Bio-Rad).
[b]Calculated from signals (density OD/mm2) obtained with purified mRFP. NA, not applicable.

mRFP source	Amount of sample used	Density (OD/mm2) [a]	Amount of mRFP (ng) [b]	mRFP µg (% total)
Purified	200.0 ng	497377.00	NA	NA
mRFP	100.0 ng	234815.52	NA	NA
	50 ng	130591.46	NA	NA
	25 ng	39776.74	NA	NA
	12.5 ng	21699.47	NA	NA
	6.25 ng	12754.88	NA	NA
	3.12 ng	7494.43	NA	NA
5 µg	10.0 µl	3336.70	NA	NA
	5.0 µl	1942.96	NA	
10 µg	10.0 µl	15553.08	12.76	0.28 (2.8%)
	5.0 µl	8226.25	7.66	
20 µg	10.0 µl	98835.80	58.70	1.14 (5.7%)
	5.0 µl	34504.54	23.28	
	2.5 µl	17289.19	13.80	
40 µg	1.25 µl	16725.41	13.35	2.72 (6.8%)
	0.625 µl	12065.26	10.34	
80 µg	2.5 µl	223133.86	127.45	10.88 (13.6%)
	1.25 µl	122514.80	72.36	
160 µg	2.5 µl	903113.64	502.31	58.8 (37%)
	1.25 µl	422611.05	238.22	
	0.625 µl	220020.65	123.15	

TABLE S4: Densitometric analysis of dot blot experiments with the supernatants of the adsorption reaction performed with different amounts of mRFP.

[a] Density measured by optical density (OD) per square millimeter and obtained by ChemiDocXRS apparatus with Quantity-One software (Bio-Rad).
[b]Calculated from signals (density OD/mm2) obtained with purified mRFP. NA, not applicable.

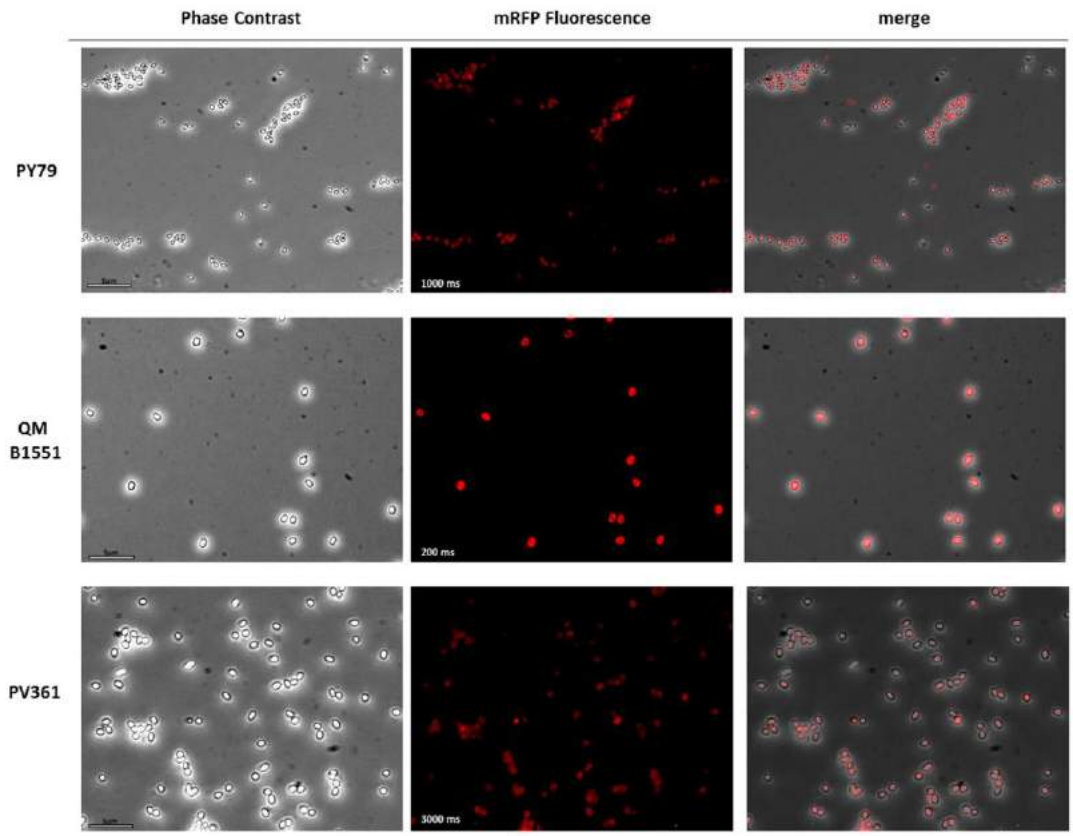

Figure S1: Whole field images of fluorescence microscopy analysis reported in Fig. 4. The same microscopy field was observed by phase contrast and fluorescence microscopy. Scale bar 5 µm. The merge panel is reported. The exposure time is indicated.

Chapter 5

Display of the peroxiredoxin Bcp1 of *Sulfolobus solfataricus* on probiotic spores of *Bacillus megaterium*

Mariamichela Lanzilli, [1] *Giuliana Donadio,*[1] *Francesca Anna Fusco,* [1]

Carmen Sarcinelli , [1] *Danila Limauro,*[1] *Ezio Ricca,*[1] *Rachele Isticato.*[1]

[1]*Department of Biology, University of Naples Federico II, Complesso Universitario Monte Sant'Angelo, via Cinthia 4, 80126 Naples, Italy*

N Biotechnol. 2018 June 27;46:38-44.

5.1 Abstract

Bacterial spores displaying heterologous proteins have been proposed as a safe and effi cient method for delivery of antigens and enzymes to animal mucosal surfaces. Initial studies have been performed using *Bacillus subtilis* spores, but other spore forming organisms have also been considered. *B. megaterium* spores have been shown capable of displaying large amounts of a model heterologous protein (*Discosoma* red fluorescent protein mRFP) that in part crossed the exosporium to localize in the space between the outer coat layer and the exosporium. Here, *B. megaterium* spores have been used to adsorb Bcp1 (bacterioferritin comigratory protein 1), a peroxiredoxin of the archaeon *Sulfolobus solfataricus*, known to have an antioxidant activity. The spores were highly effi cient in adsorbing the heterologous enzyme, which, once adsorbed, retained its activity. The adsorbed Bcp1 localized beneath the exosporium, filling the space between the outer coat and the exosporium. This unusual localization contributed to the stability of the enzyme-spore interaction and to the protection of the adsorbed enzyme in simulated intestinal or gastric conditions.

5.2 Introduction

The delivery of drugs and antigens by the oral or nasal routes off ers several advantages over parenteral administration and is gaining in- creasing relevance for the treatment of human and animal diseases. Mucosal routes are promising alternatives to delivery by injection, be- cause the high vascularization of the mucosal surfaces allows the direct transfer of molecules into the systemic circulation [1]. However, the number of drugs and antigens that can be eff ectively administered by the oral or nasal route is severely limited by the rapid loss of activity encountered by many of these molecules at mucosal sites. Therefore, the successful development of mucosal therapeutic molecules relies on efficient delivery systems, able to stabilize and protect the molecules from degradation and to reduce or avoid completely the loss of biolo- gical activity [2]. A variety of drug delivery systems has been proposed, including live microorganisms, virus particles, synthetic nanoparticles, liposomes, microspheres, gels and cyclodextrins [2,3]. Bacterial spores displaying heterologous proteins have also been proposed as a tool for the delivery of molecules to mucosal surfaces [4,5]. Spores are extremely stable and are potentially able to combine some advantages of live microrganisms with those of synthetic nanoparticles [4,5].

Bacterial spores are mainly formed by Gram-positive organisms of diff erent genera and including more than 1000 species [6] in response to harsh environments. Spores can survive in a dormant state for long periods, resisting stresses such as high temperature, dehydration, ab- sence of nutrients, and presence of toxic chemicals. Their use as a drug/ antigen delivery system has been fostered by their high stability [7] and by the safety record of several species of spore formers [8]. Initially, spores of the model organism *Bacillus subtilis* were used [9], but other Bacillus species have also been tested for the display and mucosal de- livery of antigens and enzymes [4,10].

Here, the use of spores of *B. megaterium* for the delivery of ther- apeutic molecules to the gastrointestinal mucosa is proposed. The *B. megaterium* spore is particularly promising as a delivery vehicle due to its large

dimensions (length up to 3 μm and diameter of 1 μm, with a spore surface area about 2.5-fold larger than that of *B. subtilis*) [11] and the presence of an exosporium, a protective layer surrounding the spore found only in some spore-forming species [12,13]. The exosporium of spores of QM B1551, the best-characterized strain of *B. megaterium*, have recently been shown to be essential for the adsorption of the red fluorescent protein of the coral Discosoma sp (mRFP) [14]. mRFP was shown to cross the exosporium and localize in the inter-coat space [14]. We used a well-characterized archaeal enzyme, the bacterioferritin comigratory protein 1 (Bcp1) of *Sulfolobus solfataricus*, belonging to peroxiredoxin family [15–19], as a model to study the spore-based delivery of therapeutic agents to mucosal surfaces. Peroxiredoxins are thiol peroxidases commonly found in archaea and eukaryotes, including humans, and known to contribute to cell protection against inorganic and organic peroxides [18]. Recently, the highly thermostable Bcp1 of *S. solfataricus* has been found to protect cardiomyoblasts from oxidative stress in vitro and was proposed as potentially a health beneficial molecule with anti-oxidant activity [20]. The delivery of enzymes with antioxidant activity, such as Bcp1, may be a new strategy to address inflammation caused by oxidative stress [21,22].

5.3 Materials and Methods

5.3.1 Materials and suppliers

Difco Sporulation medium (DSM) - Oxoid, UK, 234000; BRAND®counting chamber BLAUBRAND® Bürker-Türk-Sigma, USA, BR719505; Isopropyl-β-D-thiogalactoside (IPTG) - Sigma, USA,6758; Ethylenediaminetetraacetic acid (EDTA) - Sigma, USA, E9884; Protran 0.45 NC nitrocellulose Western blotting membranes – Amersham Pharmacia Biotech, 10600002; His Trap HP – GE Healthcare, USA, 11-0012-38 AH; DL-Dithiothreitol (DTT) - Sigma, USA, D0632; Anti-polyhistidine-horseradish peroxidase coupled antibody - Sigma, USA, A7058; Bovine serum albumin (BSA) - Sigma, USA, A2153

5.3.2 Bacterial strains and spore purification

B. megaterium strains QM B1551 and PV361 [13] and *B. subtilis* strain PY79 [23] were used. Sporulation was induced by the exhaustion method [8]. After 30 h growth in Difco Sporulation medium (DSM) at 37 °C with vigorous shaking, spores were collected, washed 3 times with distilled water and incubated overnight in distilled water at 4 °C to lyse residual sporangial cells as previously described [14]. Spore counts were determined by direct counting with a Bürker chamber [Sigma, USA (BR719505)] under an optical microscope (Olympus BH-2 with 40X lens).

5.3.3 Expression and purification of Bcp1

BL21 *Escherichia coli* strain expressing Bcp1 protein [16] was grown to 0.8 OD600nm in Luria-Bertani (LB) medium supplemented with kanamycin (10 μg ml-1) and chloramphenicol (34 μg ml-1) at 37 °C. Expression was induced by 1mM isopropyl-β-D-thiogalactoside (IPTG) [Sigma, USA (6758)] for 6 h at 37 °C as previously described [16,24]. The cells were harvested by centrifugation, resuspended in 20mM Tris-HCl pH 8.0 containing a complete EDTA [Sigma, USA (E9884)] free

protease inhibitors cocktail and disrupted by ultrasonication with 20 min pulses at 20 Hz (Sonicator Ultrasonic liquid processor; Heat System Ultrasonics Inc.). Protein purification was carried out in two steps: heat treatment of the cell extract at 80 °C for 15 min and affinity chromatography by His Trap HP [19]. The suspension was clarified by ultracentrifugation at 160,000 x g for 30 min. The crude extract obtained was heated at 80 °C for 15 min, and then centrifugated at 15,000 x g at 4 °C for 30 min removing almost 70% of the mesophilic host proteins. The extract was concentrated (Amicon, Millipore Corp.; Bedford, MA, USA) and applied to a HisTrap HP [GE Healthcare, USA (1-0012-38 AH)] equilibrated with 50mM Tris/HCl, pH 8.0, 0.3M NaCl (buffer A). The column was washed with buffer A with 20mM imidazole, and proteins were eluted with buffer A supplemented with 250mM imidazole. The active fractions were pooled and dialyzed against 20mM Tris/HCl, pH 8.0. [16].

5.3.4 Adsorption reaction

Different amounts of purified Bcp1 were incubated with 5×108 spores in 200 µl of 50mM sodium citrate pH 4.0 at 25 °C [25,26]. After 1 h incubation, the binding mixture was centrifuged (10 min at 13,000xg at room temperature) to separate Bcp1-adsorbed- spores in the pellet from free Bcp1 in the supernatant [25,26].

5.3.5 Western blot and dot-blot analysis

Extraction of proteins from spores and Bcp1-adsorbed spores was performed by treatment at 65 °C in 40 µl of sodium dodecyl sulfate (SDS) dithiothreitol (DTT) extraction buffer [10mM tris pH 8.0, 1% SDS, 50mM DTT, 10mM EDTA, 50mM Tris−HCl, pH 8.0]. 20 µl of extracted proteins were separated on 12.5% denaturing poly- acrylamide gels, electrotransferred to nitrocellulose membranes [Amersham Pharmacia Biotech, (10600002)] and analysed by western blot using a monoclonal anti-polyhistidine-horseradish peroxidase coupled antibody (1:7000) [Sigma, USA (A7058)], as previously reported [26]. A quantitative determination of the amount of Bcp1 was obtained by dot blot experiments comparing serial dilutions of purified Bcp1 and binding assay supernatant. Filters were then visualized by the ECLsubstrates method (Clarity, Bio-rad) and subjected to densitometric analysis by Quantity One 1-D Analysis Software (Bio-Rad) [26]. Dot blot and relative densitometric analyses were performed 3 times.

5.3.6 Fluorescence and immunofluorescence microscopy

Immunofluorescence experiments were performed as described [14]. 2.0×10^6 Bcp1-adsorbed spores of QM B1551 and PV361 were incubated with 1% bovine serum albumin (BSA) ([Sigma, USA (A7058)] for 30 min and then for 2 h with mouse monoclonal antipolyhistidine antibodies (1:200) in 1xPBS-1% BSA. Samples were washed and treated with a 1:64 goat anti-mouse IgG secondary antibody conjugated with fluorescein isothiocyanate, FITC [Thermo Fisher Scientific, USA (62-6511)] (1 h at 4 °C, in the dark). After 4 washes, the samples were resuspended in 20 µl of 1xPBS and 10 µl were analyzed. For the analysis of mRFP-adsorbed spores, following the adsorption reaction the spores were resuspended in 50 µl of 1xPBS pH 4.0 and 5 µl of the suspension observed by fluorescence microscopy

[27]. All samples were observed with an Olympus BX51- DP70 fluorescence microscope fitted with a 100x UPlan F1 oil objective; U-MNG or U-MWIBBP cube-filters were used to detect the red fluorescence emission of mRFP or the green emission of FITC-conjugated antibodies respectively. ImageJ (v1.48, NIH) was used to draw an outline around 50 spores for each strain and mean fluorescence values per pixel were recorded for each spore [14,27].

5.3.7 Peroxidase activity

The peroxidase activity of free or spore-adsorbed Bcp1 was tested as previously reported [28]. 100 µl of reaction mixture (50 mM HEPES pH 7.0, 10mM DTT 0.2 mM H_2O_2) containing different concentrations of Bcp1, spores or Bcp1-adsorbed spores were incubated at 37 °C for 5 min. 900 µl of trichloroacetic acid (10%, w/v) were added to stop the reactions and the mixture was combined with 200 µl of 10mM ferrous ammonium sulfate $Fe(NH_4)_2(SO_4)_2$ and 100 µl of 2.5M potassium thiocyanate KSCN, which led to the formation of a red colored iron complex. The peroxide concentration is proportional to the color intensity measured at λ=492 nm [28]. The percentage of peroxide removed was calculated on the basis of the change in A492nm obtained with Bcp1 relative to that obtained without Bcp1 [28].

5.3.8 Treatments with simulated gastric and intestinal fluids

Free Bcp1, spores and Bcp1-adsorbed spores were incubated for 1 h at 37° in 100 µl of simulated gastric juice (SGF) [1 mg of pepsin (porcine stomach mucosa; Sigma) per ml of 10mM HCl; pH 2.0] or small intestine fluid (SIF) [1 mg of pancreatin (porcine pancreas; Sigma) per ml and 0.2% bile salts (50% sodium cholate-50% sodium deoxycholate; Sigma); pH 6.8]. To remove the proteases contained in SIF and SGF, after incubation, the samples containing free Bcp1 were treated at 90 °C for 15 min while samples containing spores were centrifuged for 10 min at 13000xg [29]. For the pH-stability assay, free Bcp1, spores and Bcp1-adsorbed spores were incubated at 37 °C for 1 h in following buffers: 0.1 M glycine- HCl pH 2.0; 0.1M citrate-phosphate pH 4.0 and pH 6.0, or 0.1 M HEPES pH 7.0. After incubation, the peroxidase activity of the samples was measured following the protocol described above [16].

5.3.9 Statistical analysis

Results of peroxidase activity analysis are the means of 3 independent experiments. The error bars reported in the figures show the standard errors of the mean from the 3 experiments. Statistical significance was determined by Student t-test, using Microsoft Office Excel, and the significance level was set at $P < 0.05$.

5.4 Results and discussion

5.4.1 Display of active Bcp1 of *S. solfataricus* on *B. megaterium* spores

To verify whether *B. megaterium* spores were able to adsorb Bcp1 onto their surface, 20, 50 or 70 μg of the purified enzyme was incubated with 5.0×10^8 purified spores of QM B1551 or PV361. The reactions were performed in 50mM sodium citrate at pH 4.0 [25]. After the reaction, spores were extensively washed with PBS pH 4.0, collected by centrifugation, surface proteins extracted and analyzed by western blotting. As shown in Fig. 1A, specific signals were observed with extracts of spores reacted with the different amounts of purified Bcp1, indicating that Bcp1 was absorbed during the reaction by spores of both strains and released by the extraction treatment. Bcp1 was apparently extracted in comparable amounts from spores of QM B1551 previously adsorbed with 50 and 70 μg of the enzyme. To confirm this observation, a well-established procedure [9,14,26,27] was followed and the amount of Bcp1 remaining unbound was quantified, i.e., post-adsorption spores were collected by centrifugation and the supernatant serially diluted and analyzed by dot blotting (Supplementary material, Additional Figs. 1 and 2). The results of the densitometric analysis (Supplementary material, Additional Tables 1 and 2) are shown in Fig. 1B and indicated that with QMB 1551 spores, almost all the Bcp1 was adsorbed when using 20 or 50 μg in the reaction (100 and 95% respectively). The efficiency of adsorption decreased by about 40% when 70 μg of enzyme was used, suggesting saturation of the adsorption with 50 μg (Fig. 1B). With PV361 spores, the efficiency of adsorption was lower than with QMB 1551 at all concentrations of Bcp1. With the lowest Bcp1 concentration analyzed (20 μg), only 60% of the enzyme was adsorbed and a maximum of about 30 μg of adsorbed Bcp1 was observed when 50 or 70 μg was used in the reaction (Fig. 1B). Based on these results, it was concluded that 5.0×10^8 spores of QMB 1551 are able to adsorb about 50 μg and that the exosporium, present in QM B1551 and absent in PV361, is essential for an efficient adsorption of Bcp1.

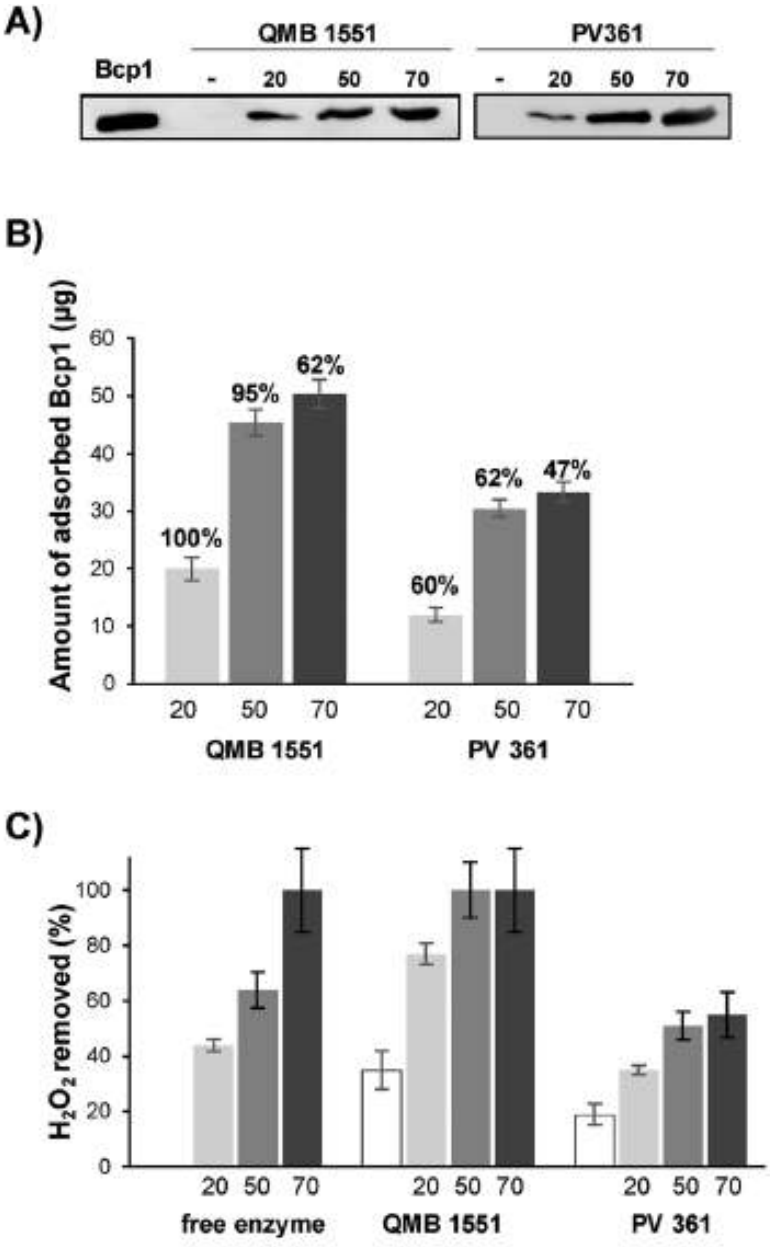

Figure 1: Adsorption of Bcp1 to *B. megaterium* spores.
5×10^8 spores of QM B1551 and PV361 strains were incubated with 20, 50 or 70 µg of Bcp1 and then the samples subject to centrifugation. (**A**) Spore surface proteins were extracted from the pellet fractions by SDS-DTT treatment, separated by SDS-PAGE and analyzed by western blot with an anti-polyhistidine antibody conjugated to horseradish peroxidase. Free Bcp1 (Bcp1) was used as a marker and free spore protein extracts as control (-). Whole images of western blots are reported in the Supplementary material. (**B**) The percentage of spore-adsorbed Bcp1 was calculated from dot blotting (Figs. 1 and 2) of the supernatants fractions containing unbound Bcp1, and relative densitometric analysis (Supplementary material, Additional Table 1–2). (**C**) Peroxidase activity of QM B1551 spores (grey bars), of 20 and 50 µg of free Bcp1 (white bars) or of the same amounts of enzyme adsorbed to spores (black bars). Error bars show the standard errors of the mean from the three different experiments. P value<0.05.

To assess whether spore-adsorbed Bcp1 retained its enzymatic activity the efficiency of H_2O_2 removal by the free and spore-bound enzyme was assayed. As a control, *B. megaterium* QM B1551 and PV361 spores alone were assayed and showed an antioxidant activity (white bars in Fig. 1C). Interestingly, PV361 spores were less efficient than QMB 1551 in removing H_20_2, suggesting that antioxidant activity was localized in the exosporium. Although we cannot distinguish between the enzymatic activity due to the adsorbed Bcp1 or to the spore itself, QMB 1551 spores adsorbed with Bcp1 had an antioxidant activity higher than similar amounts of free Bcp1 and also than spores alone, indicating that the adsorbed enzyme was active (grey bars in Fig. 1C). With Bcp1- adsorbed PV361 spores, the antioxidant activity was lower than the free enzyme but higher than that of spores alone, suggesting that the small amount of enzyme adsorbed to spores (Fig. 1B) was active (Fig. 1C). Thus, the activity observed with Bcp1 adsorbed to spores is most likely due to the combination of the activities of the adsorbed enzyme and of the spores, with QM B1551 spores being more efficient that PV361 in adsorbing active Bcp1.

5.4.2 Bcp1 localizes in the inter-coat space

Immunofluorescence was used to localize the adsorbed Bcp1 on the spore surface. 5.0×10^8 spores of strains QMB 1551 or PV361 after adsorption of various amounts of Bcp1, were reacted with Bcp1-recognizing anti-polyhistidine antibody and a fluorescent secondary antimouse IgG. As shown in Fig. 2A, with QMB 1551 spores almost no fluorescence was observed when 10 μg of Bcp1 was used and only a weak fluorescence signal, localized in spots, was observed with 20 μg of enzyme. Stronger signals were observed by increasing the amount of Bcp1 to 30 and 50 μg; however, with 30 μg the signal appeared non uniform but rather comprised of spots interrupted by non-fluorescent regions (Fig. 2A). With PV361 spores, the fluorescent signal was almost absent with 10 μg of enzyme but present and evenly distributed around the spores with all other concentration of Bcp1 (Fig. 2A).

The fluorescent signal intensity was quantified using ImageJ software [11]. The mean value determined was higher with PV361 than with QMB 1551 spores when 10 or 20 μg Bcp1 were used (Fig. 2B). The signals were of similar intensity when spores of the two strains were reacted with 30 μg and became stronger with QMB 1551 than PV361 when 50 μg of enzyme were used (Fig. 2B). These results are not consistent with the previous results (Fig. 1) showing that QMB 1551 were more efficient than PV361 spores in absorbing Bcp1. To explain this apparent inconsistency, we hypothesized that, with QMB 1551 spores, the enzyme was unavailable to the Bcp1-detecting antibody because the Bcp1 had crossed the exosporium and localized in the inter-coat space, as previously reported for the mRFP protein [11]. According to this, when 10 or 20 μg of Bcp1 were used for the adsorption reaction all Bcp1 crossed the exosporium of QMB 1551 spores, localizing in the inter-coat space and becoming mostly unavailable to antibody. By increasing the amount of Bcp1 in the adsorption reaction, the inter-coat space was gradually filled up and with 30 and 50 μg of enzyme strong but still irregular signals were observed (Fig. 2A). With spores lacking the exosporium (PV361) all Bcp1 adsorbed to spores was recognized by antibody, producing a strong and uniformly distributed signal.

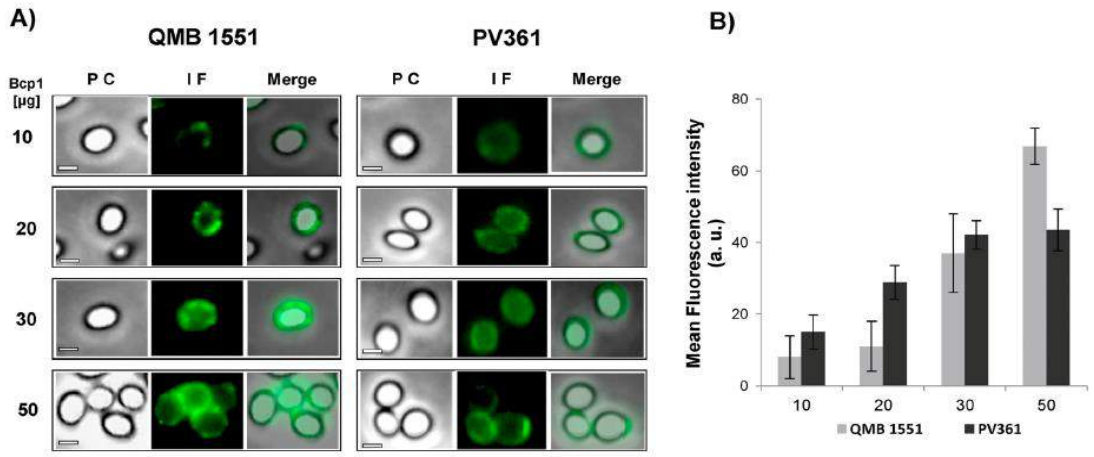

Figure 2: Immunofluorescence microscopy of *B. megaterium* spores adsorbed with increasing amounts of purified Bcp1. (A) After adsorption reaction with different amount of Bcp1 (10, 20, 30, or 50 µg) of Bcp1, QMB 1551 and PV361 spores were reacted with mouse anti-polyhistidine primary antibody and fluorescein isothiocyanate-conjugated secondary anti-mouse IgG. The same microscopy field for phase contrast (PC) and immunofluorescence (IF) is shown together with the merge panel. The exposure time was 500 ms for all images. Scalebar,1 µm. (B) Data are expressed as fluorescence intensity in arbitrary unit (a.u.) and represent the mean of fifty spores in each group. P value<0.01.

5.4.3 Bcp1 is stably and tightly adsorbed to QMB 1551 spores

To test the stability of Bcp1 adsorption, adsorbed spores were incubated at 37 °C under various conditions of pH. After 30 and 60 min, spores were collected by centrifugation and the amount of Bcp1 present in the supernatant measured by dot-blotting (Additional File Fig. 3). Fig. 3 shows the results of the densitometric analysis of the dot-blot (Additional File Table 3) and indicated that at pH 4.0 no Bcp1 was found in the supernatants, while at pH 6 and 7 some of the adsorbed enzyme was released. The release of a maximum of 20% of Bcp1 after 1 h at pH 7.0 was unsurprising, as it was already known that the adsorption of several other proteins to spores of *B. subtilis* or *B. megaterium* preferentially occurred at pH 4.0 and was less efficient at other pHs [13,26,27]. To further analyze the stability of the interaction between Bcp1 and QMB 1551 spores a displacement assay was performed using Discosoma red fluorescent protein mRFP, already shown to efficiently adsorb onto QMB 1551 spores [14]. 5×10^8 spores were reacted with 50 µg of Bcp1, washed and then incubated with 50 µg of mRFP. After 1, 1.5 and 2 h incubation, the antioxidant activity of spores was measured. As shown in Fig. 4A, antioxidant activity measured in the absence of mRFP (dark grey bar) was only slightly reduced by incubation with the competing protein (black bars), suggesting that the adsorbed Bcp1 was not displaced by mRFP. Spores adsorbed with Bcp1 and then with mRFP were also analyzed by fluorescence microscopy. As shown in Fig. 4B, the red fluorescence signal was weak compared to spores adsorbed only with mRFP and did not increase over time, confirming that mRFP was not able to replace the previously adsorbed Bcp1. In a parallel experiment, spores were reacted with mRFP and then with Bcp1. Consistently, the antioxidant activity of spores was only minimally increased by the adsorption of Bcp1 (Fig. 4C, black bars), indicating that Bcp1 was also unable to displace mRFP. The

results indicate that the adsorption of heterologous proteins to spores is tight and cannot be displaced by a second heterologous protein present in high concentration outside the spore.

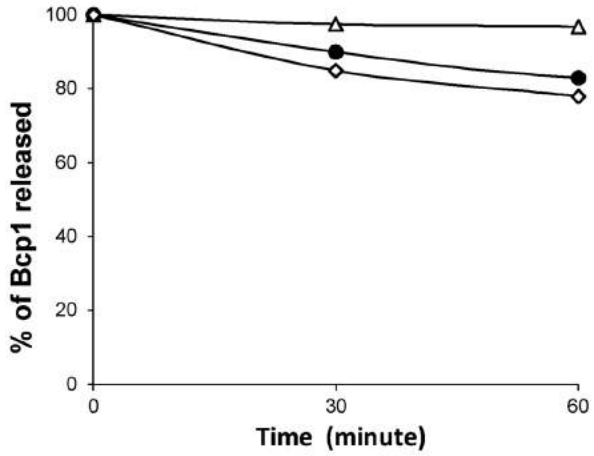

Figure 3: Kinetics of Bcp1 release. Bcp1-adsorbed spores were incubated either in 0.1M glycine−HCl, pH 2.0 (triangles), 0.1M citrate-phosphate pH 6.0 (circle) or 0.1M HEPES pH 7.0 (diamonds) and the amount of released Bcp1 estimated by dot blot assay and its relative densitometric analysis (Supplementary material, Additional Fig. 3).

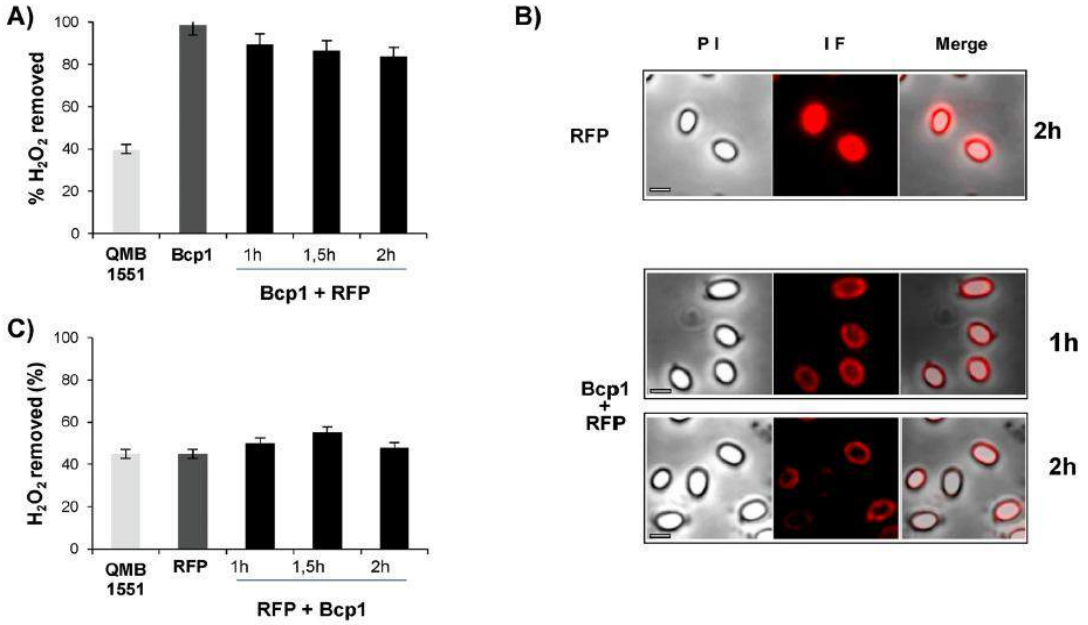

Figure 4: Displacement assays. (A) Peroxidase activity of 5.0×10^8 spores of QMB 1551 alone (light grey bar) or adsorbed with 50 µg of Bcp1 (Bcp1 - dark grey bar) and then with mRFP (Bcp1+RFP - black bars). The assay was performed after 1, 1.5 and 2 h from the addition of mRFP. **(B)** QMB 1551 spores were adsorbed with 5 µg of mRFP (RFP) or with 50 µg of Bcp1 and then with 50 µg of mRFP (RFP+Bcp1), washed and analyzed by fluorescence microscopy after 1 or 2 h of incubation. The livery of enzymes with antioxidant activity, such as Bcp1, may be a same field was observed by phase contrast and fluorescence microscopy. The merge panel is shown. The exposure time was 200 ms. Scalebar,1 µm. **(C)** Peroxidase activity of QMB 1551 spores (light grey bar) or adsorbed with 50 g of mRFP (RFP - dark grey bar) and then with 50 g of Bcp1 (RFP+Bcp1 - black bars); the experiment was performed as described in **(A).**

5.4.4 Effects of simulated gastric or intestinal conditions on Bcp1-adsorbed spores

To analyze the effects of simulated intestinal conditions on Bcp1 adsorbed onto spores, Bcp1-adsorbed spores of the QMB 1551 and PV361 strains were treated with simulated gastric fluid (SGF) or simulated intestinal fluid (SIF). Since spores of the two strains adsorb Bcp1 with different efficiencies (Fig. 1), in order to have similar amounts of enzyme adsorbed to spores of the two strains, 5.0×10^8 spores of the QMB 1551 and PV361 strains were adsorbed with 30 μg and 50 μg respectively. After the adsorption reaction, spores were treated with SGF or SIF, washed, and used to extract surface proteins which were analyzed by western blotting as above. In parallel, the same amount of free Bcp1 was also treated with SGF or SIF and analyzed by western blot. As shown in Fig. 5A, free Bcp1 was totally degraded by SGF treatment and only a minimal amount of the enzyme was still detected after the SIF treatment. Bcp1 adsorbed to PV361 spores, lacking the exosporium, was totally degraded by both SGF and SIF treatments. Bcp1 molecules were, in contrast, still extractable and detected after either treatment when adsorbed on QMB 1551 spores, indicating that they were only partially affected by SGF or SIF (Fig. 5A). To verify whether the enzyme activity was still present on QMB 1551 spores after the SIF or SGF treatment, their antioxidant activity was analyzed. As shown in Fig. 5B, the antioxidant activity of the spores alone was not affected by either treatment (white bars), while the activity of the free enzyme (50 μg) was strongly affected by both (black bars). The activity of 5.0×10^8 spores adsorbed with 50 μg of Bcp1 was also affected, but the reduction was about 20% and 30% with SIF and SGF respectively (Fig. 5B). Both SGF and SIF affected free and sporebound Bcp1, but the antioxidant activity of spore-bound Bcp1 was slightly higher than the sum of the activities of spores and free enzyme (Fig. 5B), suggesting that at least part of the adsorbed enzyme was still active after the treatments. Partial protection from degradation of the adsorbed Bcp1 is not surprising, since it has been previously reported that the β-galactosidase of Alicyclobacillus acidocaldarius was protected against heat and acidic conditions when adsorbed on *B. subtilis* spores [25]. For Bcp1, protection was only observed with QMB 1551 spores and not with PV361 (Fig. 5A), indicating that the exosporium is essential for this effect. A possible explanation for the partial protection of Bcp1 on QMB 1551 is that the enzyme, localized in the inter-coat space (Fig. 2), was protected by the exosporium and was not accessible to degradative enzymes. We hypothesized that these proteases were not able to cross the exosporium and degrade Bcp1 because, as shown for mRFP (Fig. 4), the inter-coat space was already fully occupied by Bcp1. For verification, the experiment of Fig. 5B was repeated, adsorbing QMB 1551 spores with a reduced amount of enzyme (20 μg), insufficient to completely fill the inter-coat space. As shown in Fig. 5C, the activity of spores adsorbed with 20 μg of Bcp1 was strongly reduced by SIF and almost completely eliminated by the SGF. The antioxidant activity of spore-bound Bcp1 was slightly higher than or identical to that of spores alone after the SIF or SGF treatment, respectively (Fig. 5C), indicating that the enzyme was almost completely degraded. Thus, under these conditions, some of the protease contained in SGF and SIF apparently crossed the exosporium and degraded Bcp1, supporting the hypothesis that the protection of Bcp1 observed in Fig. 5A, B was due to the inability of the degradative molecules to enter the pre-filled inter-coat space.

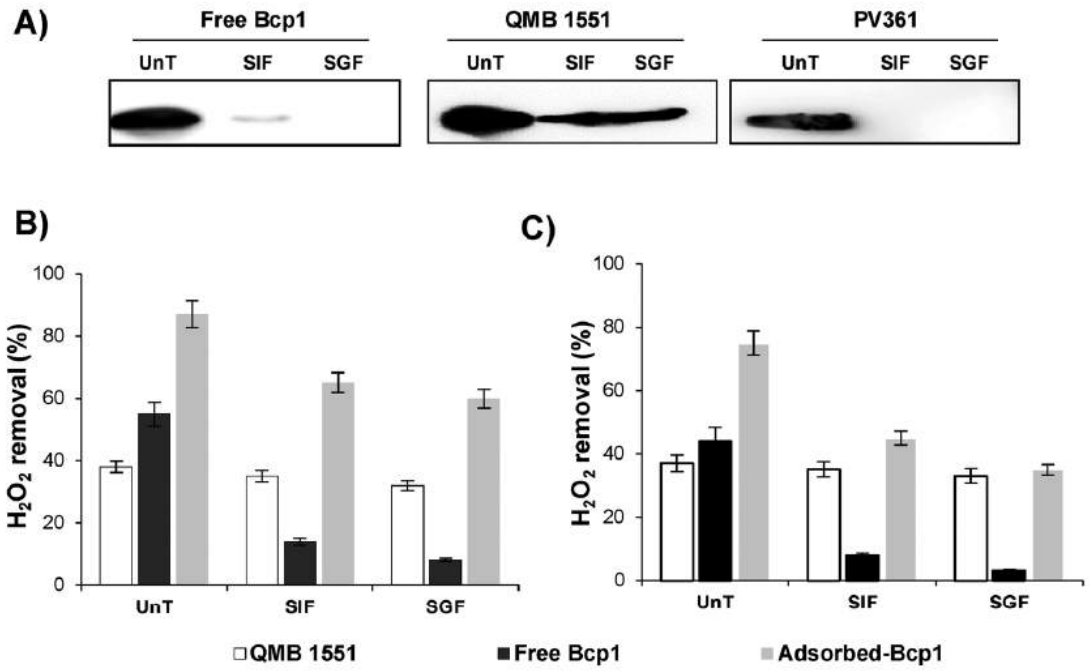

Figure 5: Effect of SIF and SGF on spore adsorption. (A) Western blotting, performed with Bcp1-recognizing anti-polyhistidine antibody, of free Bcp1 and of proteins extracted from spores of *B. megaterium* QMB 1551 and PV361 adsorbed with 30 µg and 50 µg of Bcp1 respectively. Free and spore-adsorbed enzyme was not treated (UnT) or treated with SIF or SGF (see Methods). Whole images of western blots are reported in the Supplementary material. **(B)** Peroxidase activity of 5.0×10^8 spores of QMB 1551 (white bars), of 50 µg of free Bcp1 (black bars) or the same amount of enzyme adsorbed to spores (grey bars) without (UnT) or with SIF or SGF treatment. **(C)** The experiment was performed as described in **(B)**, but using 20 µg of enzyme. Error bars show the standard errors of the mean of three independent experiments ($P < 0.05$).

5.5 Conclusions

The main conclusion of this report is that the thermoacidophilic enzyme Bcp1 of *S. solfataricus* can be efficiently adsorbed nto spores of *B. megaterium*, with about 50 µg adsorbed by 5.0×10^8 spores. Based on the deduced molecular mass of 17.46 kDa for Bcp1, we estimated that about 9.5×10^9 molecules of Bcp1 can be displayed on each spore. The adsorption is in part due to the presence of the exosporium. Adsorbed Bcp1 localized in the space between the outer coat and the exosporium and this unusual localization contributed to the protection of the enzyme from degradation by treatment with SIF or SGF. The Bcp1-spore interaction is highly stable. The enzyme was not spontaneously released under the reaction conditions and the presence of high concentrations of other molecules outside the spore did not displace the adsorbed molecules. However, a partial release of the adsorbed Bcp1 was observed when the pH conditions shifted from acidic to neutral. All these properties are particularly desirable for an oral delivery system aimed at crossing the stomach and delivering the transported molecules at the level of the intestinal mucosal surfaces. An additional interesting observation highlighted by this report is that *B. megaterium* spores have an endogenous antioxidant activity. This is in part associated with the exosporium and represents a potentially useful property for a display platform to be used for the delivery of molecules to animal mucosal surfaces.

5.6 References

1. Zhang H, Zhang J, Streisand JB. Oral mucosal drug delivery: clinical pharmacoki-netics and therapeutic applications. Clin Pharmacokinet 2002;41:661–80.
2. Tiwari G, Tiwari R, Sriwastawa B, Bhati L, Pandey S, Pandey PB, et al. Drug delivery systems: an updated review. Int J Pharm Investig 2012;2:2–11.
3. Wells J. Mucosal vaccination and therapy with genetically modified lactic acid bacteria. Annu Rev Food Sci Technol 2011;2:423–45.
4. Isticato R, Ricca E. Spore surface display. Microbiol Spectr 2014;2:351–66.
5.Ricca E, Baccigalupi L, Cangiano G, De Felice M, Isticato R. Mucosal vaccine de-livery by non-recombinant spores of *Bacillus subtilis*. Microb Cell Fact 2014;13:115.
6. Cutting SM, Hong HA, Baccigalupi L, Ricca E. Oral vaccine delivery by recombinant spore probiotics. Intern Rev Immunol 2009;28:487–505.
7. McKenney PT, Driks A, Eskandarian HA, Grabowski P, Guberman J, Wang KH, et al. A distance-weighted interaction map reveals a previously uncharacterized layer of the *Bacillus subtilis* spore coat. Curr Biol 2010;20:934–8.
8. Cutting SM. Bacillus probiotics. Food Microbiol 2011;28:214–20.
9. Isticato R, Cangiano G, Tran HT, Ciabattini A, Medaglini D, Oggioni MR, et al. Surface display of recombinant proteins on *Bacillus subtilis* spores. J Bacteriol 2001;183:6294–301.
10. Knecht LD, Pasini P, Daunert S. Bacterial spores as platforms for bioanalytical and biomedical applications. Anal Bioanal Chem 2011;400:977–89.
11. Di Luccia B, D'Apuzzo E, Varriale F, Baccigalupi L, Ricca E, Pollice A. Bacillus megaterium SF185 induces stress pathways and affects the cell cycle distribution of human intestinal epithelial cells. Benef Microb 2016;7:609–20.
12. Koshikawa T, Beaman TC, Pankratz HS, Nakashio S, Corner TR, Gerhardt P. Resistance, germination, and permeability correlates of *Bacillus megaterium* spores successively divested of in tegument layers. J Bacteriol 1984;159:624–32.
13. Manetsberger J, Hall EAH, Christie G. Plasmid-encoded genes influence exosporium assembly and morphology in *Bacillus megaterium* QM B1551 spores. FEMS Microbiol Lett 2015;362:fnv210.
14. Lanzilli M, Donadio G, Addevico R, Saggese A, Cangiano A, Baccigalupi L, et al. The exosporium of *Bacillus megaterium* QM B1551 is permeable to the red fluorescence protein of the coral Discosoma sp. Front Microbiol 2016;7(1752).
15. Limauro D, Pedone E, Pirone L, Bartolucci S. Identification and characterization of 1-Cys peroxiredoxin from *Sulfolobus solfataricus* and its involvement in the response to oxidative stress. FEBS J 2006;273:721–31.
16. Limauro D, Pedone E, Galdi I, Bartolucci S. Peroxiredoxins as cellular guardians in *Sulfolobus solfataricus*: characterization of Bcp1, Bcp3 and Bcp4. FEBS Journal 2008;275:2067–77.
17. Pedone E, Limauro D, Bartolucci S. The machinery for oxidative protein folding in thermophiles antioxidants and redox signaling. Antioxid Redox Signal 2008;10:157–69.
18. Limauro D, Saviano M, Galdi I, Rossi M, Bartolucci S, Pedone E. Sulfolobus solfa-taricus protein disulphide oxidoreductase: insight into the roles of its redox sites. Protein Eng Des Sel 2009;22:19–26.
19. Limauro D, De Simone G, Pirone L, Bartolucci S, D'Ambrosio K, Pedone E. *Sulfolobus solfataricus* thiol redox puzzle: characterization of an atypical protein disulfide oxidoreductase extremophiles. Extremophilesextremophiles 2014;18:219–28.
20. Sarcinelli C, Fiorentino G, Pizzo E, Bartolucci S, Limauro D. Discovering antioxidant molecules in the archaea domain: peroxiredoxin Bcp1 from *Sulfolobus solfataricus* protects H9c2 cardiomyoblasts from oxidative stress. Archea 2016.
21. LeBlanc JG, Laiño JE, del Valle MJ, Vannini V, van Sinderen D, Taranto MP, et al. B-group vitamin production by lactic acid bacteria–current knowledge and potential applications. J Appl Microbiol 2011;111:1297–309.

22. Arulselvan P, Fard MT, Tan WS, Gothai S, Fakurazi S, Norhaizan ME, et al. Role of antioxidants and natural products in inflammation. Oxid Med Cell Longev 2016:5276130.
23. Youngman P, Perkins JB, Losick R. A novel method for the rapid cloning in *Escherichia coli* of *Bacillus subtilis* chromosomal DNA adjacent to Tn917. Mol Gen Genet 1984;195:424–33.
24. Del Giudice I, Limauro D, Pedone E, Bartolucci S, Fiorentino G. A novel arsenate reductase from the bacterium Thermus thermophilus HB27: its role in arsenic de-toxification. Biochim Biophys Acta 2013;1834:2071–9.
25. Sirec T, Strazzulli A, Isticato R, De Felice M, Moracci M, Ricca E. Adsorption of beta-galactosidase of Alicyclobacillus acidocaldarius on wild type and mutants spores of *Bacillus subtilis*. Microb Cell Fact 2012;11(100).
26. Isticato R, Sirec T, Treppiccione L, Maurano F, De Felice M, Rossi M, et al. Non-recombinant display of the B subunit of the heat labile toxin of *Escherichia coli* on wild type and mutant spores of *Bacillus subtilis*. Microb Cell Fact 2013;12(98).
27. Donadio G, Lanzilli M, Sirec T, Ricca E, Isticato R. Localization of a red fluorescence protein adsorbed on wild type and mutant spores of *Bacillus subtilis*. Microb Cell Fact 2016;15:153.
28. Limauro D, D'Ambrosio K, Langella E, De Simone G, Galdi I, Pedone C, et al. Exploring the catalytic mechanism of the first dimeric Bcp: functional, structural and docking analyses of Bcp4 from *Sulfolobus solfataricus*. Biochimie 2010;92:1435–44.
29. Fakhry S, Sorrentini I, Ricca E, De Felice M, Baccigalupi L. Characterization of spore forming Bacilli isolated from the human gastrointestinal tract. J Appl Microbiol 2008;105:2178–86.

5.7 Additional Informations

Additional Figure 1: Dot blot of serial dilutionsof unbound Bcp1after adsorption reactions with 5.0 x 10^8 *B.megaterium* QMB 1551spores and different amountsof Bcp1 (20, 50 or 70µg). The amount of purified Bcp1 (µg) and the volume of supernatant (µl) loaded are indicated. Immunoreactions were performed with Bcp1-recognizing antibody conjugated with the horseradish peroxidase ("Methods" section).

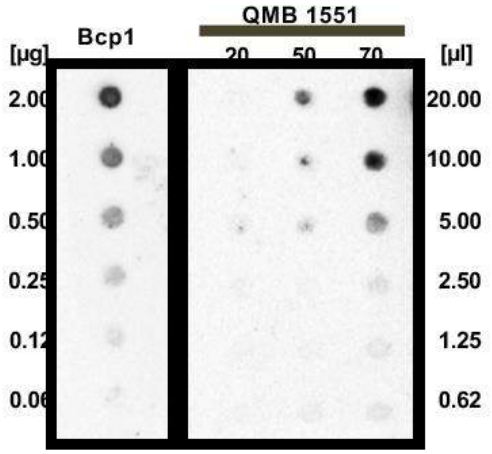

Additional Table 1: Densitometric analysis of dot blot experiments reported in Add. Fig 1.

Bcp1 source	Amount of sample used	Density (OD/mm2) [a]	Amount of Bcp1 (µg) [b]	Average Bcp1 µg (% total)
Purified	2.00 µg	1543.80	N/A	N/A
	1.00 µg	683.31	N/A	N/A
	0.50 µg	292.54	N/A	N/A
	0.25 µg	155.80		
Unbound				
20 µg		N/A	N/A	N/A
50 µg	20µl	223.55	0.30	2.6 (5.2%)
	10µl	88.01	0.11	
70 µg	10µl	767.33	1.19	28.2 (38%)
	5µl	310.69	0.57	
	2.5µl	112.51	0.19	

[a] Density measured by optical density (OD) per square millimeter and obtained by ChemiDocXRS apparatus with Quantity-One software (Bio-Rad).
[b] Calculated from signals (density OD/mm2) obtained with purified mRFP. NA, not applicable.

Additional Figure 2: Dot blot analysis of serial dilutions of unbound Bcp1 after adsorption reactions with 5.0 x10^8 *B. megaterium* PV361 spores and different amounts of Bcp1(20, 50 or 70 µg). The amount of purified Bcp1 (µg) and the volume of supernatant (µl) loaded are indicated. Immuno reactions were performed with with Bcp1-recognizing antibody conjugated with the horseradish peroxidase ("Methods" section).

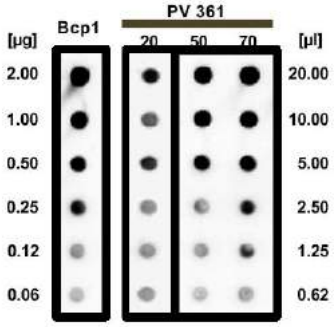

Additional Table 2: Densitometric analysis of dot blot experiments reported in Add. Fig 2.

Bcp1 source	Amount of sample used	Density (OD/mm2) [a]	Amount of Bcp1 (µg) [b]	Bcp1 µg (% total)
Purified Bcp1	1.00 µg	2641.90	N/A	N/A
	0.50 µg	1352.54	N/A	N/A
	0.25 µg	568.23	N/A	N/A
	0.12µg	218.69	N/A	N/A
Unbound				
20 µg	20µl	2577.55	0.89	7.83 (39.1%)
	10µl	625.25	0.29	
	5µl	521.89	0.21	
50 µg	5 µl	1513.84	0.59	19.5 (39%)
	2.5µl	508.01	0.20	
	1.25µl	223.13	0.12	
70 µg	5 µl	2425.55	0.98	37.2 (53%)
	2.5µl	1199.17	0.41	
	1.25µl	498.23	0.24	

[a]Density measured by optical density (OD) per square millimeter and obtained by ChemiDocXRS apparatus with Quantity-One software (Bio-Rad).
[b] Calculated from signals (density OD/mm2) obtained with purified mRFP. NA, not applicable.

Additional Figure 3: Dot blot analysisof serial dilutionsof released Bcp1after 0,30 and 60min. at pH 4.0, 6.0 and 7.0 ("Methods" section). The amount of purified Bcp1 (µg) and the volume of supernatant (µl) loaded are indicated. Immunoreactionswere performed with with Bcp1-recognizing antibody conjugated with the horseradish peroxidase("Methods" section).

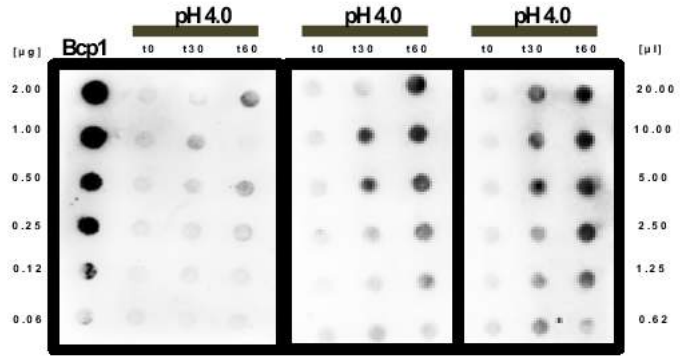

Additional Table 3: Densitometric analysis of dot blot experiments reported in Add. Fig 3.

Bcp1 source		Amount of sample used	Density (OD/mm2) [a]	Amount of Bcp1 (µg) [b]	Bcp1 µg (% total)
Purified Bcp1		0.50 µg	3467.88	N/A	N/A
		0.25 µg	2045.56	N/A	N/A
		0.12µg	1257.43	N/A	N/A
		0.06µg	657.11	N/A	N/A
Released					
pH 4.0	t0	20µl	N/A	N/A	N/A
	t30	10µl	677.39	0.072	1.25
		5.0µl	255.53	0.029	(2.5%)
	t60	20µl	1556.23	0.16	1.67
		5.0µl	635.53	0.04	(3.2%)
pH 6.0	t0	20µl	N/A	N/A	N/A
	t30	10µl	1883.19	0.20	5.04
		5.0µl	1293.67	0.14	(10%)
	t60	10µl	3009.27	0.47	8.53
		5µl	1965.43	0.21	(17%)
pH 7.0	t0	20µl	N/A	N/A	N/A
	t30	5.0µl	1756.88	0.19	7.50
		2.5µl	839.47	0.08	(15%)
	t60	5.0µl	2396.15	0.31	11.3
		2.5µl	1478.26	0.14	(22%)

[a]Density measured by optical density (OD) per square millimeter and obtained by ChemiDocXRS apparatus with Quantity-One software (Bio-Rad).
[b] Calculated from signals (density OD/mm2) obtained with purified mRFP. NA, not applicable.

Additional Figure 4: whole image of western blots offigure 1A.

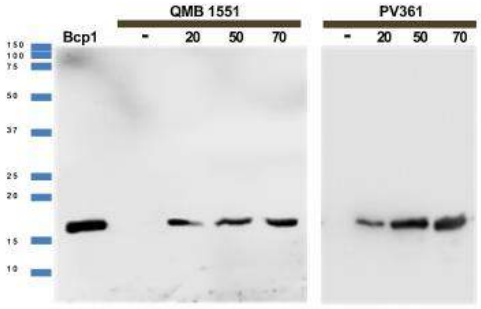

Additional Figure 5: whole image of western blots offigure 5A.

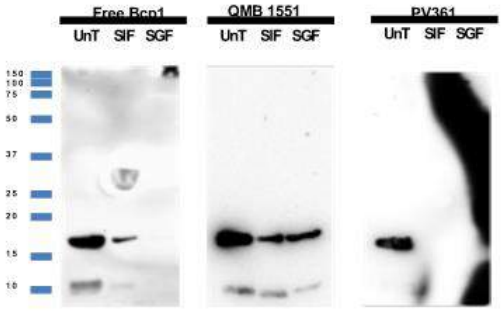

Part 3:

Bacterial Spores as Probiotics

Chapter 6

Alternative use of *Bacillus subtilis* spores: protection against environmental oxidative stress in human normal keratinocytes

*Ganna Petruk,[1] Giuliana Donadio,[2] **Mariamichela Lanzilli,**[2] Rachele Isticato,[2] and Daria Maria Monti[1,3]*

[1]*Department of Chemical Sciences, University of Naples FedericoII, Complesso Universitario Monte Sant'Angelo, via Cinthia 4, 80126 Naples, Italy*

[2]*Department of Biology, University of Naples Federico II, Complesso Universitario Monte Sant'Angelo, via Cinthia 4, 80126 Naples, Italy*

[3]*Istituto Nazionale di Biostrutture e Biosistemi (INBB), Rome, Italy*

Sci Rep. 2018 Jan 29; 8: 1745.

6.1 Abstract

Inorganic trivalent arsenic is a major environmental pollutant and exposure to human results in many pathologies, including keratosis and carcinoma. Here, we analyzed the effects of *B. subtilis* spores on human normal keratinocytes in the presence of sodium arsenite oxidative stress. Pre-treatment of cells with spores before inducing oxidative stress was able to keep normal levels of intracellular ROS, GSH and lipid peroxidation, as well as to inhibit the activation of the MAPK cascade. Moreover, spores showed a positive effect on cell proliferation, probably due to their binding on the cell surface and the activation of intracellular catalases. We found that spores exert their protective effect by the nuclear translocation of Nrf-2, involved in the activation of stress response genes. This, in turn, resulted in a protective effect against sodium arsenite stress injury, as oxidative stress markers were reported to physiological levels when cells were stressed before incubating them with spores. Therefore, *B. subtilis* spores can be considered as a new agent to counteract oxidative stress on normal human keratinocytes.

6.2 Introduction

Arsenic is a natural element widely present in food, water, air and soil[1]. The inorganic form exists predominantly in trivalent (As^{3+}, such as sodium arsenite and arsenic trioxide) or pentavalent (As^{5+}) form[2]and is generally considered more harmful than organic forms[3]. Epidemiological studies have shown that chronic exposure to trivalent arsenite is associated with dermal toxicity, neurodegenerative disorders, cardiovascular diseases and the increased incidence of cancer in lung, skin, bladder, and liver[4–6]. The major form of trivalent arsenite is sodium arsenite (herein denoted as SA), a water contaminant, known to induce several human diseases[5,7]. Indeed, SA carcinogenicity has been evaluated by International Agency for Research on Cancer (IARC) for the first time in 1973[3]. Moreover, it has been reported that the exposure of human cell lines to SA increases the production of reactive oxygen species (ROS)[8–10], which induce intracellular oxidative stress and result in oxidative DNA damage and end into apoptosis[11,12].

Cells are equipped with an array of antioxidant systems, as the superoxide dismutases (SODs), which catalyze the dismutation of superoxide anions into H_2O_2 and oxygen, maintaining a low intracellular ROS level. H_2O_2 is reduced by various systems, mainly by catalases and peroxidases. However, these endogenous systems are often insufficient for complete scavenging of ROS. Thus, endogenous or exogenous antioxidants have been proposed to be potentially beneficial in reducing SA-induced toxicity. Nowadays, a continuous search for new products able to prevent or retard stress-induced damages is still needed. Here, we propose the use of bacterial spores of *Bacillus subtilis* to counteract SA-induced damage.

Bacteria spores are metabolically dormant. They are produced by members of various *Bacillus* species in response to harsh environments[13]. The spore can survive in this state for long time, resisting to a vast range of stresses, such as high temperature, dehydration, absence of nutrients and presence of toxic chemicals[14]. When the environmental conditions ameliorate, spores germinate, thus giving rise to vegetative cells able to grow and to sporulate again in case conditions should require it.

Some *Bacillus* species are on the Food and Drug Administration's GRAS (generally regarded as safe) list and several spore-based products are widely commercialized as probiotics for human and animal use[15],[16]. It has been shown that the ingestion of spores produced by *B. subtilis*, the model organism for spore formers, restores the normal microbial flora following extensive antibiotic use or illness[17]. *B. subtilis* is a ubiquitous bacterium found on skin, in the digestive tract, in epithelial wounds, on extremities of the human body, in livestock and in soil[18],[19]. Thus, it has developed adaptive strategies to subsist in different environments *via*the production and secretion of a large number of molecules that could exert a probiotic activity in the host[20],[21]. In this article, the bacterial spores are used in a different field, i.e. that of exploiting their formidable resistance properties to prevent sodium arsenite oxidative stress in epithelial cells. Human keratinocytes have been selected as model epithelial cells since these cells are normally present in the outermost layer of the skin and more exposed to environmental stress.

6.3 Results

6.3.1 Effects of *B. subtilis* spores on human normal keratinocytes

Human keratinocytes (HaCaT cells) were chosen because normally exposed to different environmental stress, so they can be considered as guard cells of the body. The biocompatibility of wild type spores of *B. subtilis* (PY79) on HaCaT cells was tested by a time-course and dose-response test, using a ratio from 1:1 to 1:50 (cells:spore). As shown in Fig. 1, spores had a positive effect on cell viability, as an increase of about 60% and 30% was observed after 24 and 48 h, respectively, at the highest ratio used. No significant increase in cell viability was observed after 72 h, as normal cells are sensitive to the contact inhibition phenomenon, stopping their growth when they become confluent. On the basis of these results, subsequent experiments were carried out at a ratio 1:50 (cells: spores).

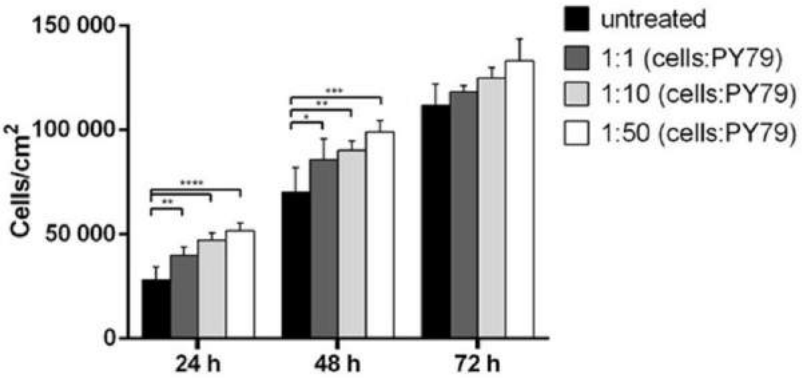

Figure 1: Effects of PY79 spores on human normal keratinocytes. Dose-response bar blot of HaCaT cells after 24, 48 and 72 h incubation in the presence of different concentrations of PY79 spores, in a ration from 1:1 to 1:50 (cells:spores). Cell survival percentage was defined as reported in Methods section. Values are given as means ± S.D. ($n \geq 3$). *Indicates $p < 0.05$; **Indicates $p < 0.005$, ***Indicates $p < 0.001$, ****Indicates $p < 0.0001$, with respect to untreated cells of each time point.

It has been reported that *B. subtilis* spores are not able to properly germinate and outgrowth in cell culture medium for at least 5 hours[22]. In our experimental conditions, a partial loss of spore-refraction was observed after 24 h incubation, in the presence of 5% CO_2, in complete medium, in absence or

presence of HaCaT cells. After 72 h incubation, the number of black spores represented the 90% of the total spores and no vegetative cells were observed. These data suggest that spores are able to start the germination process, but not the outgrowth, according to previously published data[22].

6.3.2 Pretreatment with *B. subtilis* spores inhibits SA-induced damage in eukaryotic cells

Trivalent inorganic arsenic (iAs^{3+}) is a toxic and carcinogenic environmental contaminant that humans are inadvertently exposed to every day through water, food and air. Epidemiological investigations demonstrate that long-term exposure to SA leads not only to different types of cancer in skin, but also in lung, liver, kidney and bladder[5]. SA exerts its toxic effect through ROS generation that, produced in the mitochondria, cause loss of GSH homeostasis and oxidations of molecules (such as formation or lipid peroxides)[23]. To analyze the effects of *Bacillus* spores on cells subjected to oxidative stress, HaCaT cells were pretreated with PY79 spores for 30 min and then stressed by using 300 µM SA. Immediately after oxidative stress induction, ROS production was determined by using H_2DCFDA (2,7-dichlorofluorescin diacetate) (Fig. 2A). As expected, 45 min treatment with SA induced a 90% increase in ROS intracellular levels compared to control cells (Fig. 2A). Interestingly, when cells were incubated with spores before SA treatment, no increase in ROS level was observed ($p < 0.001$). This finding suggests that mitochondrial dysfunction, induced by SA treatment, may be prevented by PY79 through a ROS-mediated signaling pathway. It is known that GSH is the most abundant low molecular weight thiol that plays important roles in redox, nutrient metabolism, and regulation of cellular events[24], and is oxidized during oxidative stress. Thus, we analyzed intracellular GSH content in cells incubated in the presence of spores. Following SA-oxidative stress induction, we found a 30% decrease ($p < 0.001$) in intracellular GSH levels with respect to control cells, whereas GSH levels were unaltered in cells incubated with spores and then stressed (Fig. 2B). The anti-stress activity of spores was further confirmed by TBARS assay, in which the peroxidation level of lipids was analyzed. The result of the experiment is reported in Fig. 2C and it clearly shows that administration of spores was able to keep unaltered lipid peroxidation levels. In fact, cells pre-treated with spores and then exposed to SA stress showed significantly lower intracellular levels of lipid peroxidation (100%, $p < 0.01$) if compared to untreated cells exposed to SA.

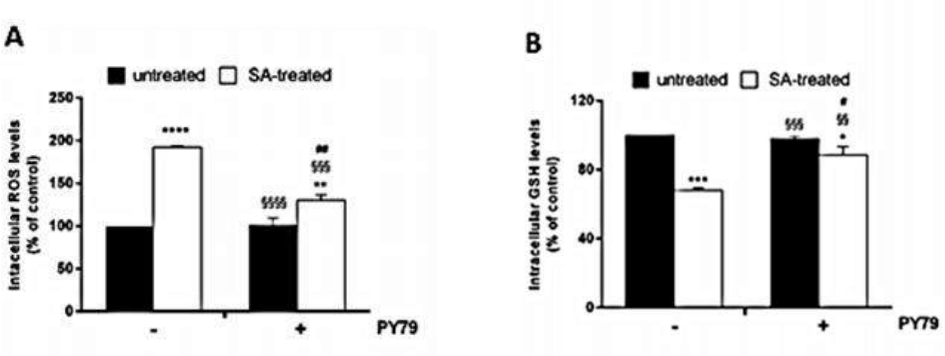

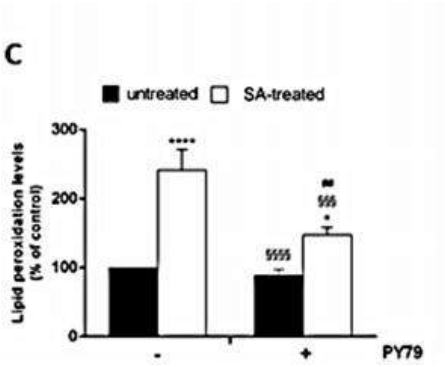

Figure 2: Analysis of the oxidative stress markers in HaCaT cells exposed to SA treatment in the presence of PY79 spores. Cells were pre-incubated in the presence of PY79 (1:50, cells:spores) for 30 min and then 300 μM SA was added to the culture medium for 45 min. (A) intracellular ROS levels were determined by DCFDA assay; (B) intracellular GSH levels determined by DTNB assay; (C) lipid peroxidation levels determined by TBARS assay. Values are expressed as fold increase with respect to control cells. Data shown are the means ± S.D. of three independent experiments. *Indicates $p < 0.05$, **Indicates $p < 0.005$, ****Indicates $p < 0.0001$, with respect to control cells; §§Indicates $p < 0.005$, §§§Indicates $p < 0.001$, §§§§Indicates $p < 0.0001$, with respect to SA-treated cells; #Indicates $p < 0.05$; ##Indicates $p < 0.005$ with respect to PY79-treated cells.

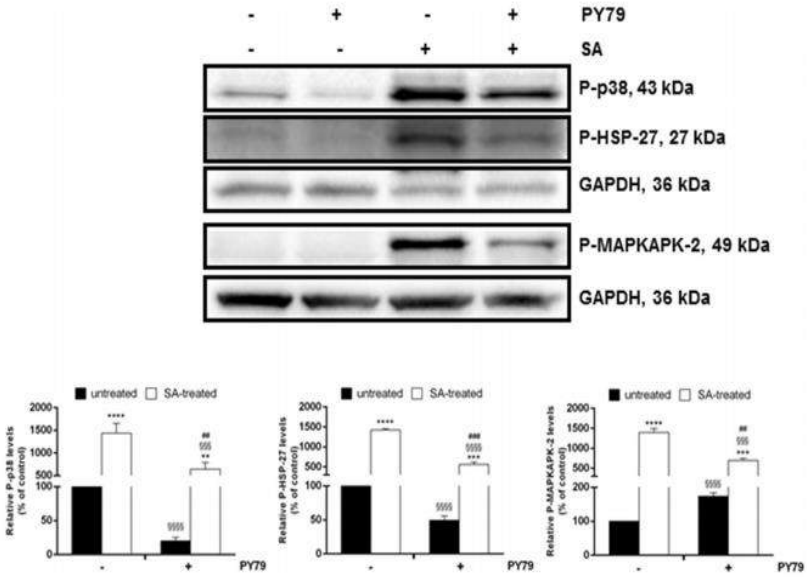

Figure 3: Effect of spores on SA-induced oxidative stress markers in HaCaT cells. Western blots show the phosphorylation levels of p38 (upper panel), HSP-27–2 (middle panel) and MAPKAPK (lower panel), with the relative densitometric analysis in the absence (black bars) or in the presence (white bars) of SA. GAPDH was used as internal standard. Full-length blots are presented in Supplementary Figure S2. **Indicates $p < 0.005$, ***Indicates $p < 0.001$, ****Indicates $p < 0.0001$, with respect to control cells; §§§Indicates $p < 0.001$, §§§§Indicates $p < 0.0001$, with respect to SA-treated cells; ##Indicates $p < 0.005$, ###Indicates $p < 0.001$, with respect to PY79-treated cells.

The protective effect of *B. subtilis* spores was finally confirmed by Western blot experiments. In particular, we analyzed the phosphorylation levels of p38, its direct target, MAPKAPK-2 and HSP-27 (Fig. 3). These proteins are important members of the mitogen-activated protein kinase (MAPK) family, and are directly involved in oxidative signaling stress pathways[25]. Under stress conditions, we

observed a significant increase in the phosphorylation levels of these three proteins, as expected (Fig. 3, third lanes). On the other hand, co-treatment of cells with PY79 spores and SA resulted in the inhibition of the phosphorylation of the analyzed markers (Fig. 3, fourth lanes). No oxidative stress was observed when cells were incubated with spores. Even though we cannot exclude that the levels of the proteins studied, rather than their phosphorylated forms, might vary, we believe that the alteration in the phosphorylation level of the three markers is due to SA treatment, as SA is known to induce phosphorylation of p38 and its targets[26,27]. Therefore, the present study suggests that skin toxicity induced by exposure to arsenic can be easily counteracted by adding *B. subtilis* spores. This new use of spores would be a novel strategy to protect derma cells from SA toxicity.

To verify whether the observed protective effect of the spores was not specific for the cell line or the induced stress type, we repeated the experiments using a different cell line, i.e. human colon cancer (LoVo) cells, stressed by SA, a well-known water contaminant[5]. Alternatively, HaCaT cells were exposed to a different oxidative stress inducer, i.e. UVA radiation, which normally reaches the outermost layer of the skin[25].

HaCaT cells were incubated with increasing number of spores (from ratio 1:1 to 1:50) for 30 min and then stressed by UVA irradiation (20 J/cm^2). After 90 min, cell lysates were analyzed by Western blotting. UVA induced a significant increase in the phosphorylation level of p38, whereas incubation of cells with spores prior to UVA irradiation, resulted in a dose-dependent decrease of p38 phosphorylation level. In particular, in the ratio 1:50, this level was similar to that observed in non-irradiated cells (Fig. S1A, $p < 0.0001$).

As for LoVo cells, cells were co-treated with 300 μM SA and spores and then intracellular ROS, GSH levels and lipid peroxidation were analyzed. As shown in Fig. S1(B–D), no alteration of these markers was observed during co-exposure of cells to SA spores, suggesting a general efficacy of spores in counteracting oxidative stress (Fig. S1).

6.3.3. *B. subtilis* spores are able to heal keratinocytes after SA injury

In the search of a general anti-stress application of spores, we evaluated if PY79 spores could restore cells after SA injury. To this purpose, cells were first stressed by SA for 45 min and then incubated for 30 min with spores. ROS production, GSH oxidation, activation of MAPK cascade and lipid peroxidation were evaluated at the end of incubation (Fig. 4). Interestingly, SA-induced alteration in ROS and GSH levels was suppressed by the presence of spores, as ROS and GSH levels were similar to those obtained for untreated and for spore-treated cells (Fig. 4A,B). Accordingly, a decrease in the phosphorylation level of p38 and in lipid peroxidation levels was detected after SA injury and spore-treatment (Fig. 4C,D).

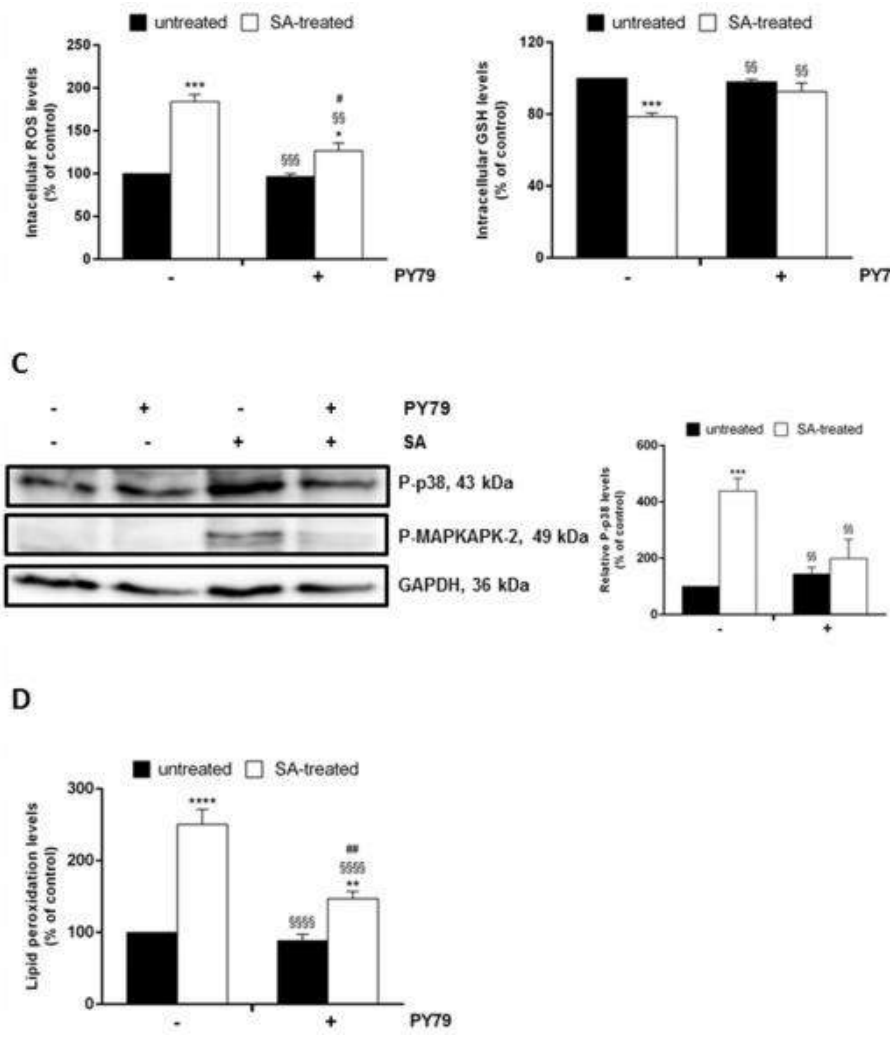

Figure 4: Ability of spores to heal SA-induced oxidative stress in HaCaT cells exposed to SA treatment. Cells were stressed by 300 μM SA for 45 min and then incubated in the presence of PY79 (1:50, cells:spores) for 30 min. (**A**) intracellular ROS levels were determined by DCFDA assay; (**B**) intracellular GSH levels determined by DTNB assay; (**C**) Western blots show the phosphorylation levels of p38 (upper panel), MAPKAPK-2 (middle panel), with the relative densitometric analysis in the absence (black bars) or in the presence (white bars) of SA. GAPDH was used as internal standard. Full-length blots are presented in Supplementary Figure [S2]; (**D**) lipid peroxidation levels determined by TBARS assay. Values are expressed as fold increase with respect to control cells. Data shown are the means ± S.D. of three independent experiments. *Indicates $p < 0.05$, **Indicates $p < 0.01$, ***Indicates $p < 0.001$, ****Indicates $p < 0.0001$, with respect to control cells; §§Indicates $p < 0.005$, §§§Indicates $p < 0.001$, §§§§Indicates $p < 0.0001$, with respect to SA-treated cells; #Indicates $p < 0.05$, ##Indicates $p < 0.005$, with respect to PY79-treated cells.

6.3.4 The spore-induced antioxidant activity is regulated by Nrf-2 nuclear translocation

In order to get insights into the molecular mechanism of *B. subtilis* spores-protective effect, we analyzed the involvement of the transcription factor Nrf-2. Under normal physiological conditions, Nrf-2 is associated to Keap-1, which keeps Nrf-2 in the cytosol and directs it to proteasomal degradation. Upon either oxidative stress induction and/or in the presence of antioxidants, Keap-1 dissociates from Nrf-2. Nrf-2 is thus translocated to the nucleus, binds to antioxidant responsive

element (ARE) sequences and activates the transcription of several antioxidant enzymes[28]. It has been recently reported that lactobacilli, well-known probiotics, can elicit their beneficial effect, in intestinal epithelium cells, upon NOX binding[29],[30]. This binding induces the generation of near threshold levels of ROS, sufficient to induce Nrf-2 nuclear translocation[29],[30]. Therefore, we incubated HaCaT cells in the presence of PY79 spores for different length of time (from 5 min to 30 min) and lysates were analyzed by Western blotting using a Nrf-2 antibody. As shown in Fig. 5A, an increase in both cytosolic and nuclear Nrf-2 levels was observed after 5 min incubation, and then the nuclear signal decreased over time. Nrf-2 activation was confirmed by measuring heme oxygenase 1 (HO-1) level. This protein was chosen as it has been reported that the Nrf-2/ARE mediate the expression of many detoxification enzymes, such as HO-1 and SOD[31]. We found that a significant increase in HO-1 level was observed after 30 min incubation of cells in the presence of spores (Fig. 5B). In order to confirm the specificity of HO-1 activation, 25 μM quercetin was used as a positive control. This antioxidant molecule is known to activate Nrf-2 pathway and to induce an increase in HO-1 level[32],[33]. Nrf-2 activation was further confirmed by measuring the H_2O_2 consumption, directly related to the catalase activity. As reported in Fig. 5C, the catalase activity detected in keratinocyte lysates after incubation with spores was higher than in untreated cells ($p < 0.0001$). One should consider that no catalase activity was detected in *B. subtilis* spores when 1×10^9 spores were tested (Fig. 5C). Moreover, the antioxidant activity observed is not related to spores' intracellular enzymes, as spores are resistant to the lysis procedure followed for eukaryotic cells[34]. Spores ability to bind specifically to the cells was analyzed by using spores bound to fluorescent proteins[35]. Cells were incubated as described above, in the presence or absence of 0.6 M NaCl. High salt treatment was used to remove specifically bound spores, as this is a well-established procedure to remove surface bound ligands[36]. The results shown in Fig. 5D indicated that about 5% of the total amount of fluorescently labeled spores were specifically bound to the cell surface, and that, after incubation with NaCl, a significant decrease in fluorescence intensity was observed ($p < 0.001$).

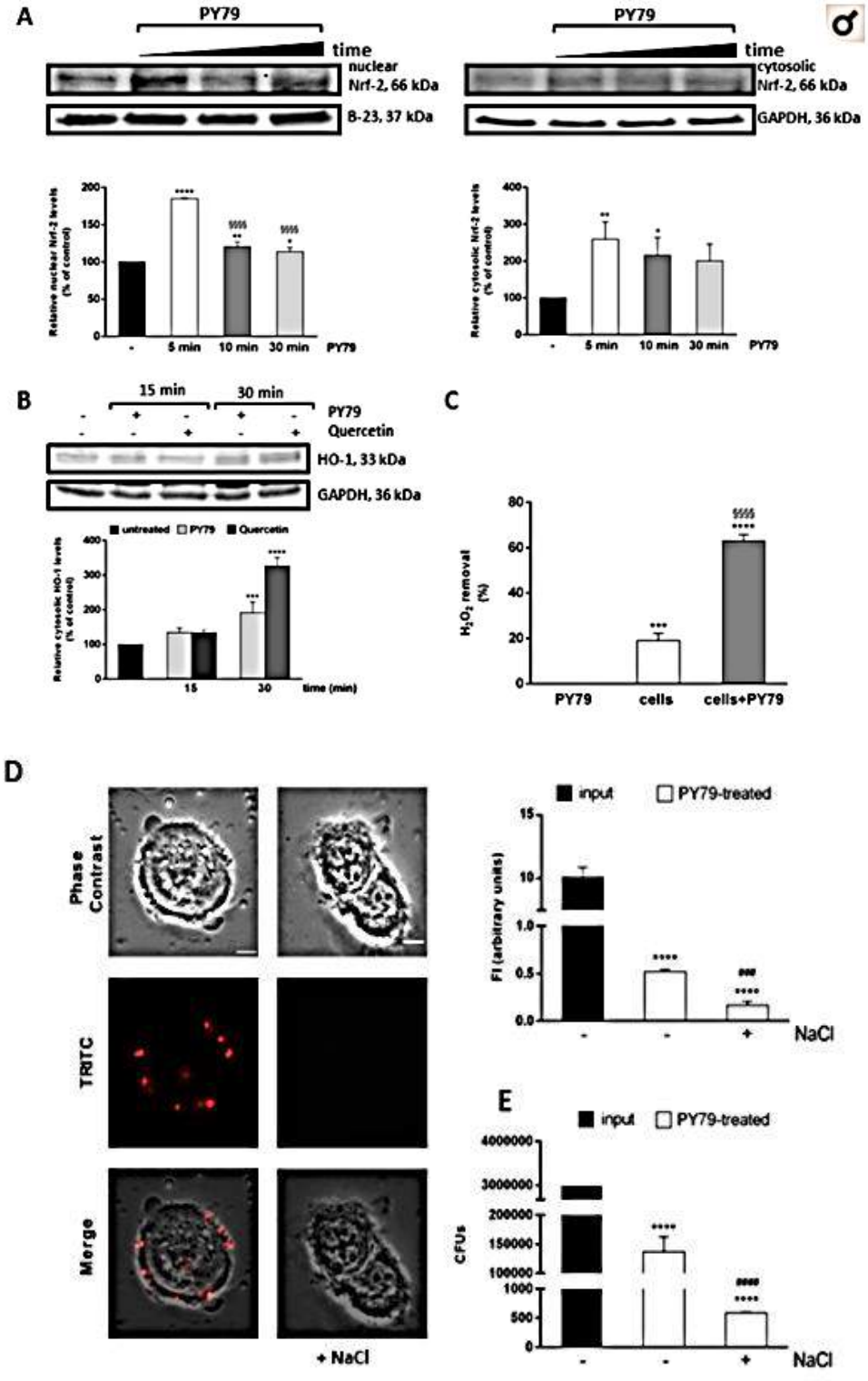

Figure 5: PY79 spores effects on HaCaT cells. (A) Western blot analysis for Nrf-2 was performed on cytosolic and nuclear proteins obtained from HaCaT cells after incubation with spores (ratio 1:50) for 5 min (white bars), 15 min (dark grey bars) and 30 min (light grey bars). Nrf-2 was quantified by densitometric analysis and normalized to GAPDH (cytosol) or B-23 (nucleus). (B) Western blot analysis for HO-1 was performed on total proteins obtained from HaCaT cells after incubation with spores (ratio 1:50, light grey bars) or quercetin (25 µM, dark grey bars) for 15 min and 30 min. HO-1 was quantified by densitometric analysis and normalized to GAPDH. Full-length blots are presented in Supplementary Figure [S2]. Data shown are the means ± S.D. of three independent experiments.

*Indicates $p < 0.05$, **Indicates $p < 0.005$, ***Indicates $p < 0.001$ ****Indicates $p < 0.0001$, with respect to control cells; §§§§Indicates $p < 0.0001$, with respect to PY79-treated cells for 5 min. (C) Catalase assay on HaCaT cells in the presence of PY79 spores. Cells were exposed to spores (1:50) for 30 min and then 50 µg of cell lysates were incubated with 0.036% (w/w) H_2O_2. Then, H_2O_2 concentration in solution was determined by measuring the absorbance at 240 nm. The experiments were performed in triplicate and the data were expressed as the mean of three independent experiments. ***Indicates $p < 0.001$, ****Indicates $p < 0.0001$, with respect to spores; §§§§Indicates $p < 0.0001$, with respect to control cells. (D), Adhesion of spores to HaCaT cells. Cells were incubated with PY79 fluorescent spores (1:50, cells:spores) for 30 min, treated in the presence or absence of 0.6 M NaCl in PBS, washed, fixed and observed by fluorescence microscopy, as described in Methods section. A representative image is reported for both the experimental conditions tested. The same field has been observed by phase contrast and fluorescence microscopy. Merged panels are reported. The exposure time was of 200 ms. Scale bar 1 mm. Histograms on the right represent quantitative data obtained by spectrofluorimetric analysis. Values are expressed as fluorescence intensity. Data shown are the means ± S.D. of three independent experiments. (E) Determination of the number of spores bound to HaCaT cells. Input, total number of PY79 spores used. In (D and E), ****Indicates $p < 0.0001$, with respect to control cells; ###Indicates $p < 0.001$, ####Indicates $p < 0.0001$ with respect to PY79-treated cells without NaCl treatment.

Finally, the number of spores bound to the surface of HaCaT cells was measured by performing another experiment. Cells were treated as described above, but at the end of incubation, cells were detached by trypsin. The pellet, containing cells and the spore bound to the cells, was plated on LB-agar plates. Then, colonies were counted and the total colony forming units (CFUs) were reported in the histograms of Fig. 5E. Results clearly indicated that about 5% of initial spores remained bound to the cells, and after NaCl treatment, a significant decrease in CFUs was observed. These results were perfectly in agreement with those obtained in Fig. 5D.

6.4 Conclusions

Trivalent arsenite is a severe environmental injury to which humans are normally exposed. It has been associated with many disorders, from cardiovascular to cancer[4–6]. Human population is mostly exposed to SA through inhalation, ingestion and dermal contact[37]. Several lines of evidence demonstrated that exposure of human cell lines to SA induces an increase in ROS levels, DNA damage and leads to apoptosis[8–12]. In this context, we investigated the possibility of an alternative and innovative use of *B. subtilis* spores. In particular, using an array of biochemical methodologies, we analyzed the protective effect of spores in counteracting the SA-induced oxidative stress on human normal keratinocytes. Spores clearly induced a positive effect both in the prevention of stress as well as when used to heal cells after stress injury. This applicability was found to be independent of the cell type used and the source of stress, as the same protective effect was observed when colon cells were stressed by SA and when UVA was used on HaCaT cells (see Fig. S1). It is worth to notice that the protective effect exerted by spores is not only due to the antioxidant activity of the spore, but to the activation of Nrf-2, a nuclear transcription factor, actively involved in oxidative stress response[28]. As already reported, gut bacteria (as *B. subtilis* and *L. plantarum*) stimulate ROS production in epithelial cells by an enzymatic mechanism analogous to the pathogen-induced respiratory burst in phagocytes[29,38]. Interestingly, enzymatically generated ROS in the epithelia are stimulated not only by potential pathogens, but also by symbiotic bacteria, especially members of the *Lactobacilli* taxon. Bacteria promote cell proliferation

and migration[39],[40], accelerate restitution post injury[41] and modify epithelial NF-kB signaling[42]. Recently, Jones and co-workers demonstrated that the presence of *L. plantarum* was able to slightly increase ROS production, just enough to promote the dissociation between Keap-1 and Nrf-2[30]. The increase in ROS levels is mediated by the catalytic action of NADPH oxidases, such as Nox-1, present on the cell membrane. The expression of Nox enzymes has been found in barrier cells, including phagocytes, colon, lung and kidney epithelium, as well as in keratinocytes, and it seems to have a role in the defense of the organism, since it is activated by microorganisms or inflammatory mediators[43]. The finding that spores are able to bind to HaCaT cells suggests an activation of Nox, which will result in an increase of ROS levels and consequently in the nuclear translocation of Nrf-2. Accordingly, in our experimental system, no difference in p38 phosphorylation level was observed between control cells and cells incubated with spores after 75 min incubation (Fig. 3), whereas a small, although significant, increase was observed after 30 min incubation (Fig. 4). This result is in line with the hypothesis that the interaction between spores and cells gives rise to a transient, not toxic, activation of the oxidative stress pathway. The activation of the antioxidant system, through the up-regulation of Nrf-2, is critical for the protection of skin cells from oxidative stress-induced damage. Thus, our findings suggest that spores can be an effective component in the treatment of skin damage, photo-aging, and skin cancers.

6.5 Methods

6.5.1 *Bacillus subtilis* strains used and preparation of spores

B. subtilis wild type strain PY79 was used[44]. Sporulation was induced by exhaustion by growing cells in DSM (Difco Sporulation Medium) as described by Nicholson and Setlow[34]. After 30 h incubation at 37 °C, spores were collected, washed four times, incubated overnight in water at 4 °C to lyse residual sporangial cells and purified on a step gradient of 20% to 50% of Gastrografin[45].

6.5.2 Cell culture and cell survival assay

Human normal keratinocytes (HaCaT) and epithelial colorectal adenocarcinoma cells (LoVo) were obtained from ATCC. Both cell lines were cultured in Dulbecco's Modified Eagle's Medium (Sigma-Aldrich), supplemented with 10% fetal bovine serum (HyClone), 2 mM L-glutamine and antibiotics, all from Sigma-Aldrich, in a 5% CO_2 humidified atmosphere at 37 °C. For sub-culturing cells, the culture medium was removed and cells were rinsed with PBS, detached with trypsinEDTA and diluted in fresh complete growth medium.

Cells were seeded in 96-well plates (100 µl/well) at a density of 2×10^3/well (HaCaT cells). For dose-dependent survival assays, 24 h after seeding, increasing amount of spore (from 1:1 to 1:50) were added to the cells for 24–72 h. At the end of incubation, cells were detached by trypsin, centrifuged at 1000 g for 5 min at r.t. and the cell pellet was resuspended in 0.4% trypan blue buffer (Sigma-Aldrich) and counted in the hemocytometric chamber (Burker chamber, Sigma-Aldrich).

6.5.3 Oxidative stress

To analyze oxidative stress, cells were plated at a density of 4×10^4 cells/cm^2 (LoVo cells) and 2×10^4cells/cm^2 (HaCaT cells). 24 h after seeding, cells were incubated for 30 min in the presence or absence of PY79 spores (1:50, cells:spore), and then incubated in the presence of 300 μM SA for 45 min at 37 °C (treatment before injury). In a second group of experiments, cells were stressed with 300 μM SA for 45 min at 37 °C and then cell medium was changed to remove SA and cells were incubated for 30 min in the presence or absence of spores (treatment after injury). In case of UVA treatment, 24 h after seeding, cells were incubated for 30 min in the presence or absence of spores and then the medium was removed and cells were washed twice with PBS. After washing, cells were covered with a thin layer of PBS and irradiated for 2 min with UVA light (20 J/cm^2). Subsequently to oxidative stress, cells were washed again with PBS and re-incubated with spores at 37 °C for 90 min.

6.5.4 Measurement of intracellular ROS levels

To estimate ROS production, the protocol described in[46] was followed. Briefly, at the end of incubation cells were incubated with a cells permeable probe, 2′,7′-dichlorodihydrofluorescein diacetate (H_2-DCFDA, Sigma-Aldrich). The non fluorescent H_2DCFDA becomes fluorescent product, 2′,7′-dichlorofluorescein (DCF), in the presence of different species of ROS. Fluorescence intensity was measured by a Perkin-Elmer LS50 spectrofluorimeter (525 nm emission wavelength, 488 nm excitation wavelength, 300 nm/min scanning speed, 5 slit width for both excitation and emission). ROS production was expressed as percentage of DCF fluorescence intensity of the sample under test, with respect to the untreated sample.

6.5.5 Measurement of intracellular total GSH levels

Total activation of the GSH synthetic pathway was monitored by measuring GSH concentrations in the cells. Intracellular GSH levels were estimated as procedure previously was described[25]. Briefly, at the end of incubation, cells were detached by trypsin, lysed and protein concentration was determined by the Bradford assay. Then, 50 μg of proteins were incubated with 3 mM EDTA, 144 μM 5,5′-dithiobis-2-nitrobenzoic acid (DTNB) in 30 mM TrisHCl pH 8.2, centrifuged at 14,000 *g* for 5 min at 4 °C and the absorbance of the supernatant was measured at 412 nm by using a multiplate reader (Biorad). GSH levels were expressed as the percentage of TNB absorbance in the sample under test with respect to the untreated sample.

6.5.6 Measurement of lipid peroxidation

The thiobarbituric acid reactive substances (TBARS) assay quantifies a by-product of lipid peroxidation, the malondialdehyde, that reacts with thiobarbituric acid (TBA) forming an abduct (MDA-TBA).

We used the protocol described by Del Giudice *et al.*[47]. Briefly, at the end of incubation, cells were kept for 90 min at 37 °C, then detached and suspended (5×10^4 cells) in 0.67% thiobarbituric acid

(TBA) and 20% trichloroacetic acid (1:1 v/v). After heating and centrifugation at 3000 g for 5 min at 4 °C, samples were read at 532 nm. Lipid peroxidation levels were expressed as the percentage of the absorbance at 532 nm of the sample under test, with respect to untreated cells (100%).

6.5.7 Western blot analyses

HaCaT cells were plated at a density of 2×10^4 cells/cm^2 in complete medium for 24 h and then treated as described above (paragraph 4.3); 25 µM quercetin (Sigma-Aldrich) was used on HaCaT cells for 15 or 30 min. After treatment, total cell lysate was obtained by resuspend each cell pellet in 50 µL of lysis buffer (100 mM Tris-HCl, 300 mM NaCl and 0.5% NP40 at pH 7.4, with addiction of inhibitors of proteases and phosphatases). Nuclear pellet was obtained after extracting cytosolic proteins with PBS buffer containing 0.1% triton and proteases inhibitors. Nuclear lysate was obtained by resuspending the pellet in RIPA buffer (150 mM NaCl, 1% NP-40, 0.1% SDS, proteases inhibitors in 50 mM Tris-HCl pH8.0). Lysates (100 µg of proteins) were then analyzed by Western blotting performed as previously described[48]. Phosphorylation levels of p38, MAPKAPK-2, HSP-27 or total Nrf-2 were detected by using specific antibodies purchased from Cell Signal Technology (Danvers, MA, USA). HO-1 antibody was from Bethyl (Montgomery, TX, USA). To normalize protein intensity levels, a specific antibody against anti-GAPDH or anti B-23 (ThermoFisher, Rockford, IL, USA) were used for cytosolic and nuclear extracts, respectively. The chemiluminescence detection system (SuperSignal® West Pico) was from Thermo Fisher.

6.5.8 Catalase assay

Quantitative determination of catalase activity of spores and of cells after spore incubation was measured by the loss of absorbance at 240 nm as previously described by Beers and Sizer[49]. Briefly, spores (5×10^8or 1×10^9) or cell lysate (50 µg) were incubated for 30 min at room temperature in 1 ml of hydrogen peroxide solution [50 mM Potassium Phosphate Buffer, pH 7.0, 0.036% (w/w) H_2O_2]. Then, samples were centrifuged for 1 min at 13000 g to remove the spores and the hydrogen peroxide concentration in solution was determined by measuring the absorbance at 240 nm. The percentage of peroxide removed was calculated as following:

$$\% H_2O_{2rem} = 1 - OD_{240nm}\text{sample}/OD_{240nm}\text{standard}.$$

Standard is referred to 1 ml of hydrogen peroxide solution.

6.5.9 Spore adhesion assays

For adhesion assays, HaCaT cells were plated at a density of 3×10^4 cells/cm^2 in complete medium in a 24-well with cover glass for 24 h and then treated with spores previously bound with a red fluorescent protein[35] for 30 min (1:50, cells:spores). At the end of incubation, cells were washed 3 times with 500 µL PBS to remove non-adherent bacteria and then fixed in 4% paraformaldehyde in PBS for 15 min. To verify the specificity of the binding between cells and spores, in a parallel experiment cells were incubated with 0.6 M NaCl in PBS for 10 min[50] and then washed and fixed as described above.

After fixing, cells were washed 3 times with 500 µL PBS and then observed with an Olympus BX51 fluorescence microscope. Images were captured using an Olympus DP70 digital camera equipped with Olympus U-CA Magnification Changer (100×) and processed with Image Analysis Software (Olympus) for minor adjustments of brightness, contrast and color balance and for creation of merged images. To estimate the percentage of spores bound to cells, the same experiment described above was performed, but instead of fixing cells, cells were detached in trypsin and resuspended in PBS (2×10^4 cells/ml). Fluorescence intensity of the cell suspension was measured by a Perkin-Elmer LS50 spectrofluorimeter (540 nm excitation wavelength, 625 nm emission wavelength, 300 nm/min scanning speed, 5 slit width for both excitation and emission). Rhodamine fluorescence was expressed as fluorescence intensity of the sample under test, and the fluorescence of untreated cells was subtracted from PY79- and PY79 + NaCl- treated cells. Alternatively, to determine the amount of spores bound to the cells, the procedure described by Batista and colleagues was followed[51]. Briefly, at the end of the experiment, cells were detached by trypsin, lysed and heated at 65 °C for 30 min and then plated on LB-agar plates. After incubation at 37 °C over-night, CFUs were counted.

6.5.10 Statistical analyses

In all the experiments samples were analyzed in triplicate. The results are presented as mean of results obtained after at least three independent experiments (mean ± SD) and compared by one-way ANOVA following Tukey's multiple comparison test using Graphpad Prism for windows, Version 6.01.

6.6 References

1. Chen C, Jiang X, Zhao W, Zhang ZZ. Dual role of resveratrol in modulation of genotoxicity induced by sodium arsenite via oxidative stress and apoptosis. Food Chem. Toxicol. 2013;59:8–17.
2. Rossman TG. Mechanism of arsenic carcinogenesis: An integrated approach. Mutat. Res. - Fundam. Mol. Mech. Mutagen. 2003;533:37–65.
3. Hughes MF, Beck BD, Chen Y, Lewis AS, Thomas DJ. Arsenic exposure and toxicology: A historical perspective. Toxicol. Sci. 2011;123:305–332.
4. Cui X, Kobayashi Y, Akashi M, Okayasu R. Metabolism and the Paradoxical Effects of Arsenic: Carcinogenesis and Anticancer. Curr. Med. Chem. 2008;15:2293–2304.
5. Smith AH, et al. Cancer risks from arsenic in drinking water. Environ. Health Perspect. 1992;97:259–267
6. Rahman MM, Ng JC, Naidu R. Chronic exposure of arsenic via drinking water and its adverse health impacts on humans. Environ. Geochem. Health. 2009;31:189–200.
7. Brown KG, Ross GL. Arsenic, Drinking Water, and Health: A Position Paper of the American Council on Science and Health. Regul. Toxicol. Pharmacol. 2002;36:162–174.
8. Ruiz-Ramos R, Lopez-Carrillo L, Rios-Perez AD, De Vizcaya-Ruíz A, Cebrian ME. Sodium arsenite induces ROS generation, DNA oxidative damage, HO-1 and c-Myc proteins, NF-κB activation and cell proliferation in human breast cancer MCF-7 cells. Mutat. Res. - Genet. Toxicol. Environ. Mutagen. 2009;674:109–115.
9. Zhang Z, et al. Reactive oxygen species mediate arsenic induced cell transformation and tumorigenesis through Wnt/β-catenin pathway in human colorectal adenocarcinoma DLD1 cells. Toxicol. Appl. Pharmacol. 2011;256:114–121.
10. Imlay JA. Pathways of oxidative damage. Annu. Rev. Microbiol. 2003;57:395–418.
11. Hei TK, Filipic M. Role of oxidative damage in the genotoxicity of arsenic. Free Radic. Biol. Med. 2004;37:574–581.

12. Wang TS, Kuo CF, Jan KY, Huang H. Arsenite induces apoptosis in Chinese hamster ovary cells by generation of reactive oxygen species. J. Cell. Physiol. 1996;169:256–268.
13. Cutting SM, Hong Ha, Baccigalupi L, Ricca E. 18. Oral vaccine delivery by recombinant spore probiotics. Int. Rev. Immunol. 2009;28:487–505.
14. Isticato R, et al. Non-recombinant display of the B subunit of the heat labile toxin of Escherichia coli on wild type and mutant spores of Bacillus subtilis. Microb. Cell Fact. 2013;12:98.
15. Green, D. H. et al. Characterization of Two Bacillus Probiotics Characterization of Two Bacillus Probiotics. 65, 8–12 (1999).
16. Rhee K-J, Sethupathi P, Driks A, Lanning DK, Knight KL. Role of commensal bacteria in development of gut-associated lymphoid tissues and preimmune antibody repertoire. J. Immunol. 2004;172:1118–24.
17. Mazza P. The use of Bacillus subtilis as an antidiarrhoeal microorganism. Boll. Chim. Farm. 1994;133:3–18. [PubMed]
18. Ara K, et al. Foot odor due to microbial metabolism and its control. Can. J. Microbiol. 2006;52:357–364.
19. Earl AM, Losick R, Kolter R. Ecology and genomics of Bacillus subtilis. Trends Microbiol. 2008;16:269–275.
20. Stein T. Bacillus subtilis antibiotics: structures, syntheses and specific functions. Mol. Microbiol. 2005;56:845–857. doi: 10.1111/j.1365-2958.2005.04587.x. [PubMed] [Cross Ref]
21. Liu W-T, et al. Imaging mass spectrometry of intraspecies metabolic exchange revealed the cannibalistic factors of Bacillus subtilis. Proc. Natl. Acad. Sci. USA. 2010;107:16286–16290.
22. Alebouyeh M, et al. Characterization of the interaction of undomesticatedBacillus subtilis spores with Caco-2 cell line. Ann. Microbiol. 2009;59:273–277. doi: 10.1007/BF03178328. [Cross Ref]
23. Simon H-U, Haj-Yehia A, Levi-Schaffer F. Role of reactive oxygen species (ROS) in apoptosis induction. Apoptosis. 2000;5:415–418.
24. Anderson ME. Glutathione: An overview of biosynthesis and modulation. Chem. Biol. Interact. 1998;111–112:1–14.
25. Petruk G, et al. An ascorbic acid-enriched tomato genotype to fight UVA-induced oxidative stress in normal human keratinocytes. J. Photochem. Photobiol. B Biol. 2016;163:284–289.
26. Liu X, et al. p38 and Extracellular Signal-Regulated Kinases Activations have Opposite Effects on Primary-Cultured Rat Cerebellar Granule Neurons Exposed to Sodium Arsenite. J. Biochem. Mol. Toxicol. 2014;28:143–148.
27. Duyndam MCA, Hulscher STM, van der Wall E, Pinedo HM, Boven E. Evidence for a role of p38 kinase in hypoxia-inducible factor 1-independent induction of vascular endothelial growth factor expression by sodium arsenite. J. Biol. Chem. 2003;278:6885–95.
28. Ma Q. Role of nrf2 in oxidative stress and toxicity. Annu. Rev. Pharmacol. Toxicol. 2013;53:401.
29. Jones RM, et al. Symbiotic lactobacilli stimulate gut epithelial proliferation via Nox-mediated generation of reactive oxygen species. EMBO J. 2013;32:3017–3028.
30. Jones RM, et al. Lactobacilli Modulate Epithelial Cytoprotection through the Nrf2 Pathway. Cell Rep. 2015;12:1217–1225.
31. Hseu YC, et al. Ellagic acid protects human keratinocyte (HaCaT) cells against UVA-induced oxidative stress and apoptosis through the upregulation of the HO-1 and Nrf-2 antioxidant genes. Food Chem. Toxicol. 2012;50:1245–1255.
32. Chow J-M, Shen S-C, Huan SK, Lin H-Y, Chen Y-C. Quercetin, but not rutin and quercitrin, prevention of H2O2-induced apoptosis via anti-oxidant activity and heme oxygenase 1 gene expression in macrophages. Biochem. Pharmacol. 2005;69:1839–1851.
33. Kang C-H, Choi YH, Moon S-K, Kim W-J, Kim G-Y. Quercetin inhibits lipopolysaccharide-induced nitric oxide production in BV2 microglial cells by suppressing the NF-κB pathway and activating the Nrf2-dependent HO-1 pathway. Int. Immunopharmacol. 2013;17:808–813.
34. Colin, R. Harwood, S. M. C. Molecular biological methods for Bacillus. (1990).

35. Donadio G, Lanzilli M, Sirec T, Ricca E, Isticato R. Localization of a red fluorescence protein adsorbed on wild type and mutant spores of Bacillus subtilis. Microb. Cell Fact. 2016;15:153.
36. Faussner A, et al. Binding characteristics of [3H]-JSM10292: a new cell membrane-permeant non-peptide bradykinin B2 receptor antagonist. Br. J. Pharmacol. 2012;167:839–53.
37. Singh N, Kumar D, Sahu AP. Arsenic in the environment: effects on human health and possible prevention. J. Environ. Biol. 2007;28:359–65. [PubMed]
38. Alam A, et al. Redox signaling regulates commensal-mediated mucosal homeostasis and restitution and requires formyl peptide receptor 1. Mucosal Immunol. 2014;7:645–655.
39. Wentworth CC, Jones RM, Kwon YM, Nusrat A, Neish AS. Commensal-Epithelial Signaling Mediated via Formyl Peptide Receptors. Am. J. Pathol. 2010;177:2782–2790.
40. Wentworth CC, Alam A, Jones RM, Nusrat A, Neish AS. Enteric commensal bacteria induce extracellular signal-regulated kinase pathway signaling via formyl peptide receptor-dependent redox modulation of dual specific phosphatase 3. J. Biol. Chem. 2011;286:38448–38455.
41. Swanson PA, et al. Enteric commensal bacteria potentiate epithelial restitution via reactive oxygen species-mediated inactivation of focal adhesion kinase phosphatases. Proc. Natl. Acad. Sci. USA. 2011;108:8803–8808.
42. Kumar A, et al. Commensal bacteria modulate cullin-dependent signaling via generation of reactive oxygen species. EMBO J. 2007;26:4457–4466.
43. Lambeth JD. NOX enzymes and the biology of reactive oxygen. Nat. Rev. Immunol. 2004;4:181–9.
44. Youngman P, Perkins JB, Losick R. A novel method for the rapid cloning in Escherichia coli of Bacillus subtilis chromosomal DNA adjacent to Tn917 insertions. Mol. Gen. Genet. 1984;195:424–33.
45. Henriques AO, Melsen LR, Moran CP. Involvement of superoxide dismutase in spore coat assembly in Bacillus subtilis. J. Bacteriol. 1998;180:2285–2291. [PMC free article] [PubMed]
46. Del Giudice R, et al. Carotenoids in fresh and processed tomato (Solanum lycopersicum) fruits protect cells from oxidative stress injury. J. Sci. Food Agric. 2017;97:1616–1623.
47. Del Giudice R, et al. Antioxidant bioactive compounds in tomato fruits at different ripening stages and their effects on normal and cancer cells. J. Funct. Foods. 2015;18:83–94.
48. Guglielmi, F. et al. Enzymatically active fibrils generated by the self-assembly of the ApoA-I fibrillogenic domain functionalized with a catalytic moiety. Biomaterials30 (2009). [PubMed]
49. Beers R, Sizer I. A spectrophotometric method for measuring the breakdown of hydrogen peroxide by catalase. J. Biol. Chem. 1952;195:133–140. [PubMed]
50. Arciello A, et al. Insights into the fate of the N-terminal amyloidogenic polypeptide of ApoA-I in cultured target cells. J. Cell. Mol. Med. 2011;15:2652–2663.
51. Tavares Batista M, et al. Gut adhesive Bacillus subtilis spores as a platform for mucosal delivery of antigens. Infect. Immun. 2014;82:1414–23.

6.7 Additional Informations

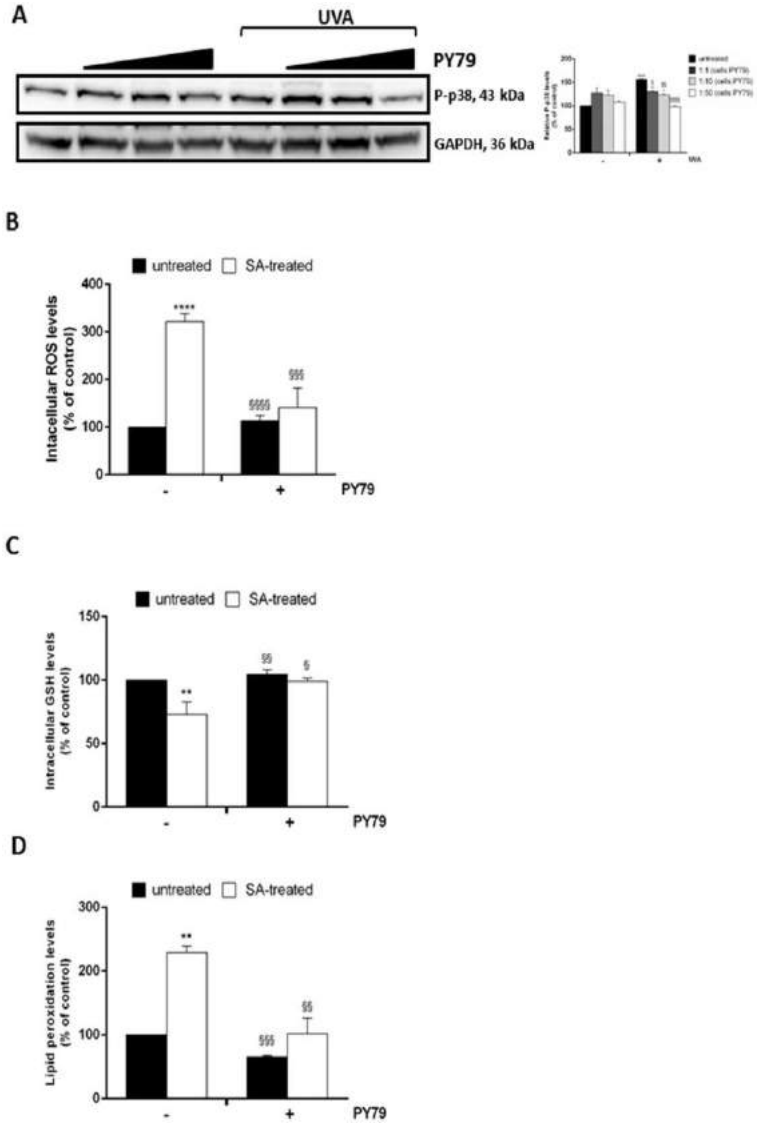

Figure S1: Analysis of oxidative stress in HaCaT cells exposed to UVA treatment and LoVo cells stressed by SA in the presence of PY79 spores. A, HaCaT cells were pre-incubated in the presence of increasing amount of PY79 (from 1:1 to 1:50, cells:spores) for 30 min and then irradiated by UVA (20 J/cm2). Western blots show the phosphorylation level of p38, with the relative densitometric analysis in the absence (-) or in the presence (+) of UVA stress. GAPDH was used as internal standard. * indicates $p<0.05$, ** indicates $p<0.01$, **** indicates $p<0.0001$, with respect to control cells; § indicates $p<0.05$,§§ indicates $p<0.01$, §§§§ indicates $p<0.0001$, with respect to UVA-treated cells. **B-D**, LoVo cells incubated with PY79 (1:50, cells:spores) for 30 min before treatment with 300 µM SA for 45 min. **B**, DCFDA assay; **C**, DTNB assay; **D**, TBARS assay. Values are expressed as fold increase with respect to control cells. Data shown are the means ± S.D. of three independent experiments. ** indicates $p<0.005$, **** indicates $p<0.0001$, with respect to control cells; § indicates $p<0.05$, §§ indicates $p<0.01$, §§§ indicates $p<0.001$, §§§§ indicates $p<0.0001$, with respect to SA-treated cells.

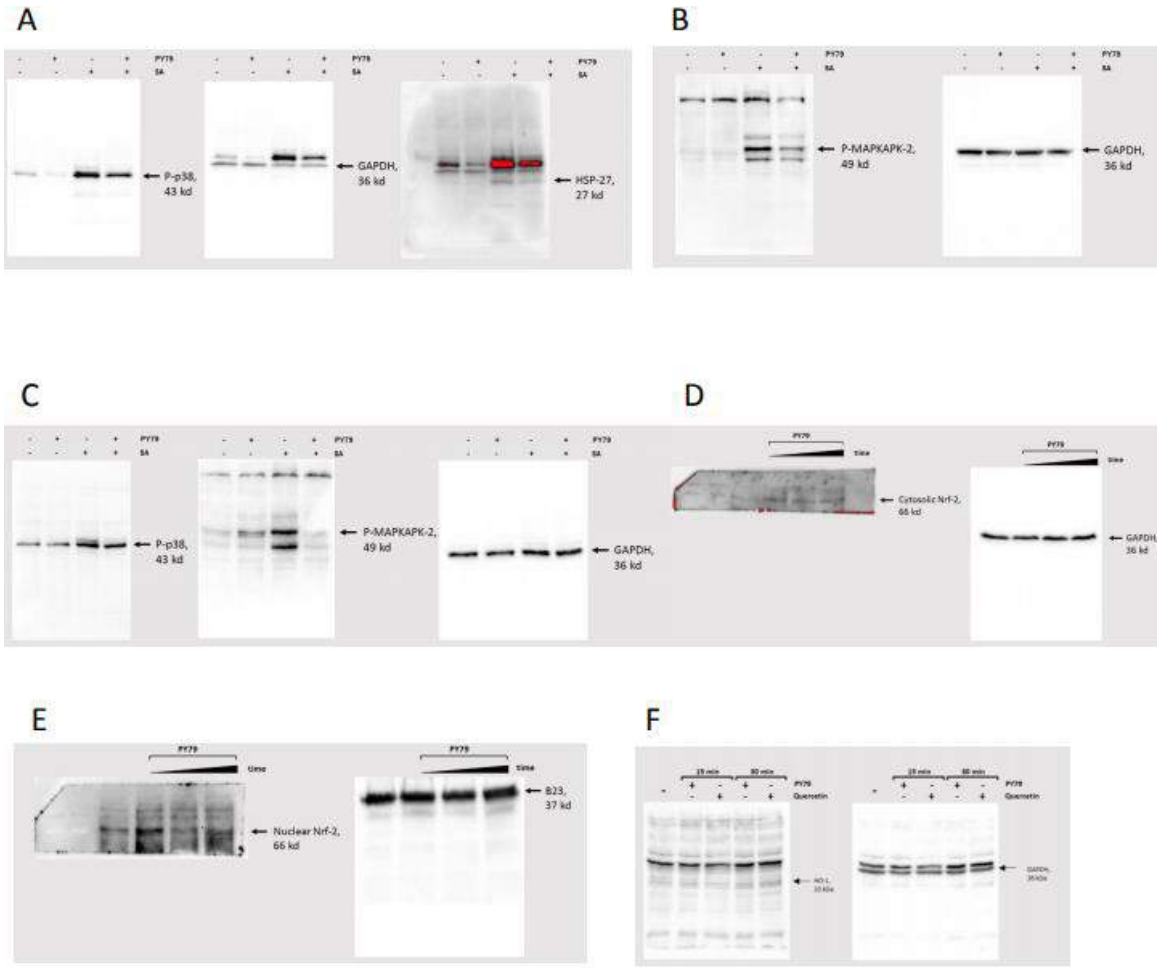

Figure S2: Uncropped blots corresponding to main Figures 3-5. All SDS- PAGE were run under the same experimental conditions. Following transfer, membranes were either subsequently incubated with antibodies or cut into strips to minimize the required amount of antibody. Arrows indicate were blots were cropped.
(A-B) Uncropped blots for images shown in Fig. 3.
(C) Uncropped blots for images shown in Fig. 4.
(D-F) Uncropped blots for images shown in Fig. 5.

Chapter 7

Protective and therapeutic effects of *Bacillus megaterium* spores on gut oxidative stress

Giuliana Donadio, Arianna Mazzoli , **Mariamichela Lanzilli**, Andrea Maria Guarino, Miriam Rivetti, Raffaella Crescenzo, Ezio Ricca, Susanna Iossa, Alessandra Pollice and Rachele Isticat1[*]

[a] *Department of Biology University of Naples Federico II, Via Cintia, 80126, Naples, Italy.*

[b] *Wallenberg Laboratory, Department of Molecular and Clinical Medicine, University of Gothenburg, Göteborg, Sweden*

Manuscript in preparation

7.1 Abstract

Background. Endogenous reactive oxygen species (ROS) are by-products of the aerobic metabolism of cells and have an important signalling role as secondary messengers in various physiological processes, including cell growth and development. However, the excessive production of ROS as well as the exposure to exogenous ROS, originated, for example, from xenobiotics or foods, can cause protein oxidation, lipid peroxidation and DNA damages leading to cell damages and a number of health disorders. ROS accumulation has been associated, for example, to neurodegenerative diseases, progression of arteriosclerosis and inflammatory bowel diseases. Varieties of molecules and live bacteria with antioxidant activity have been proposed as food additives to avoid ROS accumulation.

Objective. Here we demonstrate that spores of SF185, a human isolate of *Bacillus megaterium*, have intrinsic antioxidant activity and we analyse their effect *in vitro* and *in vitro*.

Methods. The antioxidant effects of SF185 spores were tested *in vitro* on Caco-2 cells measuring the ability of spores to reduce the toxicity of hydrogen peroxide and *in vivo* in a murine model of dextran sodium sulfate (DSS) -induced oxidative stress.

Results. *In vitro,* spores have a scavenging action reducing the amount of intracellular ROS and so inducing a protected state in cells. Pre-dosing mice with spores before the treatment with DSS protects the animals from the chemically-induced damages.

Conclusions. The consumption of spores-based products could prevent or reduce the damages caused by oxidative stress. The human origin of SF185, its strong antioxidant activity, and its protective effects both *in vitro* and *in vivo* led to propose the spore of this strain as a new probiotic for gut health.

7.2 Introduction

Reactive Oxygen Species (ROS), including hydrogen peroxide, superoxide and hydroxyl radicals, are common by-products of the aerobic metabolism of all cells [1]. While at low intracellular concentrations ROS are critical signalling molecules with a role in cell proliferation and survival [2], their accumulation severely damages DNA, proteins and lipids leading to a variety of chronic diseases, including atherosclerosis, arthritis, diabetes, neurodegenerative, cardiovascular problems and inflammatory bowel diseases [3-7]. All aerobic organisms avoid ROS accumulation with a variety of enzymes (catalase, superoxide dismutase, glutathione peroxidase, and glutathione reductase) and with non-enzymatic molecules with antioxidant activity (glutathione, thioredoxin, Vitamin C, Vitamin E). The production of an excess of ROS induces the development of a state of oxidative stress that has a crucial role in the development and perpetuation of an inflammatory status, thus contributing to the pathophysiology of several diseases [8]. In particular, intestinal epithelial cells are continuously exposed to ROS derived by their own metabolism, by the metabolism of the huge number of microbes normally living in the animal gut and by ingested foods [9]. Antioxidant additives contribute to avoid the accumulation of ROS and thus have a protective role against oxidative damages [10]. During years many natural antioxidant additives have been proposed and tested. Examples include polyphenols (green tea), flavones, ginsenosides and more recently carotenoids [11-12].

Intestinal bacteria have a clear role in protecting the animal body against oxidative damages. A study performed with a rat model of diet-induced oxidative stress has shown that an antibiotic treatment, as well as the replacement of the gut microbiota, was able to prevent the oxidative damages in liver and skeletal muscle [13]. Therefore, it is not surprising that beneficial bacteria (probiotics) with strong antioxidant properties have been proposed to prevent oxidation of cellular substrates [10]. Examples are species of the *Bifidobacterium* and *Lactobacillus* genera, shown able to scavenge hydroxyl radicals and superoxide anions *in vitro* and to enhance the action of antioxidant enzymes *in vivo* [14-16], or cells of a carotenoid-producing strain of *Bacillus indicus*, shown to reduce oxidative markers in plasma and liver *in vivo* [17].

In addition to vegetative cells also bacterial spores have been shown to have antioxidant properties. Spores are quiescent cell forms produced by over 1,000 bacterial species, mainly belonging to the *Clostridium* or *Bacillus* genera [18]. These microorganisms respond to adverse environmental conditions by producing a highly resistant spore that can survive indefinitely in the absence of water and nutrient [19]. The dormant spore can, however, germinate originating a vegetative cell able to grow when appropriate conditions are encountered [19]. Spores of several *Bacillus* species are commonly used as probiotics and are known to have beneficial properties [20, 21]. An *in vitro* study has recently shown that a pre-treatment with *Bacillus subtilis* spores before a sodium arsenite-induced oxidative stress allows human keratinocytes to keep normal levels of intracellular ROS, GSH and lipid peroxidation [22]. Spores have been proposed to contribute to cell protection by inducing the expression of antioxidant enzymes by activating the nuclear translocation of the E2-related factor 2 (Nrf2). In the nucleus, Nrf2 binds to *cis*-acting Antioxidant Response Elements (sequence ARE), present in the promoter region of genes coding for antioxidant/detoxifying enzymes, activating transcription initiation [3, 22].

Here, we report that spores of a human isolate of *Bacillus megaterium* have a strong antioxidant activity and a treatment with these spores protects Caco-2 cells from oxidative damages and reduces the DSS-induced gut damages in mice.

7.3 Methods

7.3.1 Bacterial strains

Sporulation of *Bacillus megaterium* SF185 and QM B1551 strains was induced by the exhaustion method [23]. After 30 hours of growth in Difco Sporulation medium (DSM) at 37°C with vigorous shaking, spores were collected, washed three times with distilled water and purified by gastrografin gradient as described before [23]. Spore counts were determined by serial dilution and plate-counting.

7.3.2 Cell culture conditions and MTT assay

Human colon adenocarcinoma Caco-2 cells (ATCC HTB-37) were routinely cultured at 37°C in a humidified 5% CO2 incubator in Dulbecco's Modified Eagle Medium (DMEM, Gibco) supplemented with 10% (v/v) FBS (Gibco), 1% penicillin-streptomycin (Gibco), 1% L-glutamine (Gibco) [24]. Cell viability was assessed using the MTT assay (Sigma-Aldrich). It is based on the reduction of the

tetrazolium ring of 3-(4,5-dimethylthiazol-2-yl)-2,5-diphenyltetrazolium bromide (MTT) by mitochondrial dehydrogenases, yielding a purple dye (formazan), which can be measured spectrophotometrically; the amount of formazan produced is proportional to the number of viable cells. Cells were incubated for 3 h at 37°C with a 1X MTT solution diluted in DMEM without Phenol Red, supernatant was removed, and acidic isopropanol 0.01 N was added to each well to dissolve insoluble formazan crystals formed. The absorbance of the samples was measured at a 570 nm using a microplate reader (Multiskan spectrum, Thermo) [25].

7.3.3 Catalase Assay

Quantitative determination of catalase activity of spores was measured by the loss of absorbance at 240 nm as previously described by Beers and Sizer [27]. Briefly, spores ($5x10^8$ or $1x10^9$) were incubated for 30 min at room temperature in 1ml of hydrogen peroxide solution [50mM Potassium Phosphate Buffer, pH 7.0; 0.036% (w/w) H_2O_2]. Then, samples were centrifuged for 1 min at 13000 g to remove the spores and the hydrogen peroxide concentration in solution was determined by measuring the absorbance at 240 nm. The percentage of peroxide removed was calculated as follows:

$$\mathrm{H_2O_2\ removed\ (\%)} = \left(1 - \frac{A_{samples}}{A_{control}}\right) \times\ 100$$

Where $A_{control}$ is the absorbance of 1 ml of hydrogen peroxide solution.

7.3.4 pH-stability assay

Spores were incubated at 37°C for 1 hour in following buffers: 0.1 M Glycine-HCl pH 2.0; 0.1 M citrate-phosphate pH 4.0 and pH 6.0, or 0.1 M HEPES pH 7.0. After incubation, the samples were centrifuged for 5 min. at 13000 rpm. The catalase activity of the samples was measured following the protocol described above.

7.3.5 The intestinal-stability assay

Spores were incubated for 1 hour at 37°C in 100 µl of simulated gastric juice (SGF) [1 mg of pepsin (porcine stomach mucosa; Sigma) for ml of 10 mM HCl; pH 2.0] or small intestine fluid (SIF) [1 mg of pancreatin (porcine pancreas; Sigma) for ml and 0.2% bile salts (50% sodium cholate-50% sodium deoxycholate; Sigma); pH 6.8]. To remove the proteases contained in SIF and SGF, after incubation, spores were washed, collected by centrifugation (10 min at 13000xg) and then assayed for the catalase activity.

7.3.6 Intracellular ROS evaluation

Intracellular ROS levels were quantified by a DCFDA assay (Abcam), based on the cell permeant reagent 2',7'- dichlorofluorescin diacetate (DCFDA), a fluorogenic dye that measures reactive oxygen species activity within the cell. After diffusion into the cell, DCFDA is deacetylated by cellular esterase to a non-fluorescent compound, which is later oxidized by ROS into 2', 7'-dichlorofluorescein (DCF). DCF is a highly fluorescent compound which can be detected by fluorescence spectroscopy,

and the fluorescence intensity is proportional to intracellular ROS produced. DCFDA (25 μM) was added to cells that were then incubated for 45 min in the dark at 37°C. Fluorescence intensity was measured at λexcitation and λemission of 485 nm and 535 nm, respectively, in a plate reader (Synergy 4, BioTek).

7.3.7 Lipid peroxidation in Caco-2 cells

Lipid peroxidation products [thiobarbituric acid reactive substances (TBARS) also known as malondialdehyde-equivalents (MDA-equivalents)] from Caco-2 cells were measured by the thiobarbituric acid colorimetric assay, according to Fernandes et al. [28]. Briefly, Caco-2 cells were preincubated for 24 hours with spores at 1:1 ratio cells/spores and then subjected to oxidative stress with 100μM H_2O_2 for 2 hours. Then, the medium was removed, and cells were washed with PBS, counted and centrifuged at 500 g for 5 min at 25 °C. After removal of supernatant, 0.5 ml of ice-cold 40% trichloroacetic acid and 0.5 ml of 0.67% of aqueous thiobarbituric acid were added to the pellet. The mixtures were heated at 90 °C for 15 min, then cooled in ice for 10 min, and centrifuged at 800 g for 10 min. The supernatant fractions were collected, and lipid peroxidation estimated spectrophotometrically at 530 nm. The amount of TBARS formed was calculated using a molar extinction coefficient of 1.56×10^5/mol/cm and expressed as nmol TBARS/10^6 cells.

7.3.8 Mouse model and experimental design

Eight-week-old C57BL-6 mice were housed in standard animal cages under specific pathogen-free conditions. The mice were maintained in an environment of constant temperature and humidity with a 12-hours light-dark cycle and were given free access to food and water. Treatment, housing, and euthanasia of the animals met the guidelines set by the Italian Health Ministry. All experimental procedures involving animals were approved by "Comitato Etico-Scientifico per la Sperimentazione Animale" of the University "Federico II" of Naples. Experimental colitis was induced in the C57BL-6 mice by added DSS (2%, wt:vol) in drinking water ad libitum from day 2 to day 6, followed by DSS-free water for 2 days. Mice were randomly allocated into the three following groups (n = 6 per group): 1) untreated mice receiving placebo (Control group); 2) mice receiving DSS in water (DSS group) for 5 days; 3) mice receiving DSS in water for 5 days and spores by gavage, starting from two days before the DSS treatment, until two days after DSS treatment (DSS spores group). During the treatments, body weight, food and water intake were monitored daily.

7.3.9 Evaluation of experimental colitis

After mice euthanasia, the macroscopic score was evaluated according to the scheme of Table 1.
The macroscopic score was determined by combining the scores from these 4 categories and dividing the resulting number by 4.

Score	Bleeding	Prolapse	Stool consistency	Blood
0	negative	negative	normal	normal
1	red	signs of prolapse	soft	red
2	dark red	visible prolapse	soft	dark red
3	gross bleeding	extended prolapse	diarrhea	black

Table 1: Scoring criteria applied to the macroscopic injuries in the mice colon

7.3.10 Lipid peroxidation in colon samples

Protein extracts from distal colon were assayed for lipid peroxidation as described above. The amount of TBARS formed was calculated using a molar extinction coefficient of 1.56×10^5/mol/cm and expressed as nmol TBARS/mg tissue.

7.3.11 Determination of TNF-α, IL-12 and IL-10 in proximal colon samples

TNF-α and IL-12/IL-10 concentrations in protein extracts from colon were determined using a rat specific enzyme linked immunosorbent assay (R&D Systems, MN, USA and ThermoFisher Scientific, lL USA, respectively) according to manufacturer instructions. Briefly, for TNF-**α** the wells of a microtitre plate were coated with 100 µl of mouse anti-rat TNF-**α** (4 µg/ml) in PBS (137 mM NaCl; 2.7 mM KCl; 8.1 mM Na_2HPO_4;1.5 mM KH_2PO_4, pH 7.4), and incubated overnight at room temperature. The antibody excess was then removed by washing with Wash Buffer (containing 0.05% (v/v) Tween 20 in PBS, pH 7.4), and the remaining sites on the plate were blocked with reagent diluent (PBS containing 1% BSA) (1 h, room temperature). After extensive washing, 100 µl of samples (1:2-1:10 dilution in reagent diluent) were added to the wells and incubated for 2 hours at room temperature. After further washing, the wells were incubated with biotinylated goat anti-rat TNF-**α** (225 ng/ml in reagent diluent) followed by treatment with Streptavidin-HRP (1:200 dilution; 1h, room temperature). For IL-12/IL-10 determination, 50 µl of samples (1:2 dilution in reagent diluent for IL-12, undiluted for IL-10) were added in the wells of a microtiter plate and incubated for 1 h at 20-25°C for IL-12 and for 3 h at 20-25° for IL-10. After 3 washing with Wash Buffer (provided by the kit), the wells were incubated with 100 ml for IL-12 and 50 ml for IL-10 of Biotinylated Antibody Reagent (BAR) for 1 hours at 20-25°C. After 3 washing with wash buffer, the wells were treated with Streptavidin-HRP (1:400 dilution; 30 min., 20-25°C). For both TNF-α and IL-12/IL-10 determination, peroxidase-catalyzed color development from tetramethylbenzidine was measured at 450 nm.

7.3.12 Myeloperoxidase (MPO) activity in distal colon

MPO activity was assessed in colon samples as previously described [29]. Briefly, tissue samples (100 mg) were homogenized in 1 ml of hexadecyltrimethylammonium bromide (HTAB) buffer (0.5% HTAB in 50 mM phosphate buffer, pH 6.0) and centrifuged at 13400 x g for 6 min. at 4°C. MPO activity was measured spectrophotometrically: 10 µl of supernatant were combined with 200 µl of 50

mM phosphate buffer, pH 6.0, containing 0.167 mg/ml 0-dianisidine hydrochloride and 1.25% hydrogen peroxide. The change in absorbance at 450 nm was measured and one unit of MPO activity was defined as that degrading 1 μmol of peroxide per minute at 25°C.

7.3.13 Statistical analysis

All data are expressed as means of independent experiments ± standard errors (SE). The analysis of variance was carried out by using One-way ANOVA or by two-tail unpaired t-test. The statistical analysis of *in vitro* and *in vivo* experiments was performed with the use of Graph-Pad Prism (Graph-Pad Software).

7.4 Results

7.4.1 Spores of *B. megaterium* have antioxidant activity

Spores of *B. subtilis* have been recently shown to have antioxidant activity [22]. To assess whether other spore-forming species have a similar activity we analysed spores of *B. megaterium*, a species characterized by the large dimensions of its cells and spores [30]. Antioxidant activity of the spores was assayed catalase assay. Different number of purified spores of the *B. megaterium* strains QM B1551 (reference strain) or SF185 (isolated from human ileal biopsies [31, 32]), were added to 1 ml of solution containing 0, 0036% hydrogen peroxide solution (see methods section). Spores of both strains showed the ability to scavenge H_2O_2 (Fig. 1A) and the activity increased by increasing the number of spores used in the assay. Results of Fig. 1A indicated that spores of the two strains were characterized by similar antioxidant activity. Based on this and on the origin of the strain, we decided to perform all further experiments using only spores of the human-isolated strain SF185.

While it is well established that ingested spores transit safely through the stomach [33], it is not known whether enzymes present on the spore surface remain active after the exposure to the low pH conditions typical of the stomach. Therefore, in order to evaluate SF185 spores as potential oral antioxidant additive, we analysed the stability of the spore-associated catalase at various pH conditions and after treatment with either simulated gastric or intestinal conditions. To this aim, 1.0 $x10^{10}$ spores of SF185 were incubated for 1 hour either at various acidic conditions or at simulated gastric or simulated intestinal fluid (SGF or SIF, respectively) and the catalase activity was assayed as reported in the Methods section. As shown in Fig. 1B, spores were able to remove hydrogen peroxide at all the pH conditions tested. At pH 2.0 the spore-associated catalase was still active and able to remove almost 80% of H_2O_2 (Fig. 1B). Incubation of spores in either SGF or SIF only slightly affected the catalase activity (Fig. 1C), suggesting that SF185 spores could be able to remove H_2O_2 and act as antioxidants at the intestinal level upon the ingestion and transit through the gut.

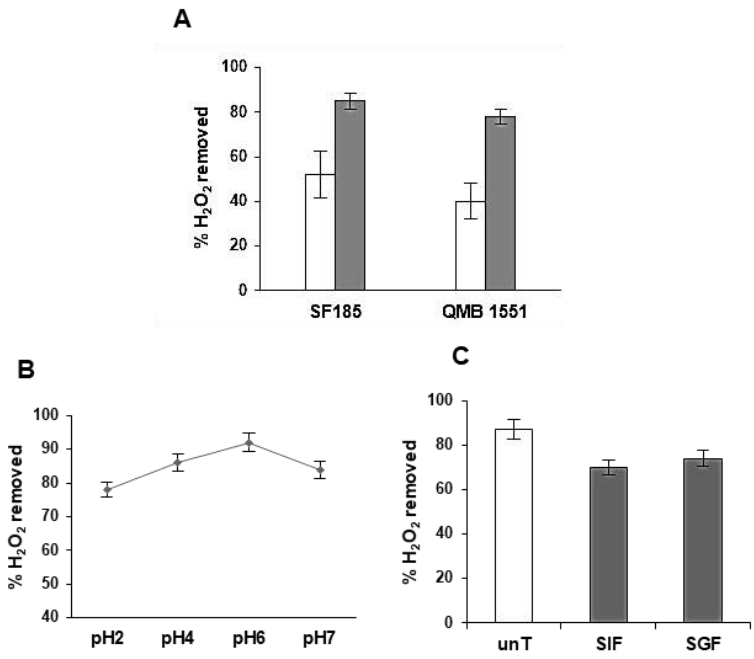

Figure 1: Antioxidant activity of *B. megaterium* spores. (**A**) Catalase activity of $5.0x10^8$ (white bars) or $1.0\ x10^{10}$ (grey bars) spores of SF185 and QMB 1551 strains. (**B**) Effect of low pH conditions and (**C**) of SIF or SGF treatments on the catalase activity of SF185 spores. Data are mean of a three independent experiments ± SE (n=5).

7.4.2 SF185 spores exert anti-oxidant activity and stimulate Caco-2 cell viability

Direct evaluation of ROS is a good indicator of the oxidative damage to living cells. Measurement of the intracellular ROS levels was carried out on Caco-2 cells by using a well-established method based on the compound DCFDA that, when administered to cells, becomes deacetylated by cellular esterase and then oxidized by intracellular ROS into DCF, whose level of fluorescence can be used as an indirect measurement of intracellular ROS production. We first verified that spores did not germinate when incubated in standard culture conditions (DMEM +10%FBS) used to cultivate Caco-2 cells in the following experiments. In agreement with what previously reported for B. subtilis spores [22], we observed that SF185 spores did not germinate after 24 hours of incubation in DMEM at 37°C under CO2 pressure (data not shown). Next, we analysed the oxidative status of Caco-2 cells grown under physiological conditions, in the presence or absence of B. megaterium spores at a 1:1 ratio spores/cells. As Fig. 2A shows, while 2 hours of incubation with spores caused only a slight reduction in ROS production (light grey bar), an overnight (ON) incubation induced a drastic effect (dark grey bar), with over 10-fold reduction in ROS production (Fig. 2A). The protective effect exerted by spores was also observed when cells were subjected to oxidative stress by H2O2: treatment of cells with 100 mM H_2O_2 for 2 hours in the presence of 1:1 ratio spores/cells, induced a less pronounced oxidative stress in terms of ROS production (Fig. 2B). Interestingly, the effect was more pronounced when Caco-2 cells were pre-incubated ON with spores, washed to eliminate the spores and then challenged with H_2O_2 for 2 hours (Fig. 2C, dark grey bars), indicating that SF185 spores were not only able to contrast the

oxidative stress by scavenging H2O2 but also to exert a preventive effect. Indeed, when cells were challenged with hydrogen peroxide, spores were no longer present. Accordingly, if spores where re-added during the H_2O_2 treatment following the ON pre-incubation with spores, there is only a slight reduction of ROS, further indicating the preventive, protective effect of spores (Fig. 2C light grey bar). Overall, these experiments suggest that SF185 spores are able to contrast but also prevent the H_2O_2-induced intracellular increase of ROS in Caco-2 cells.

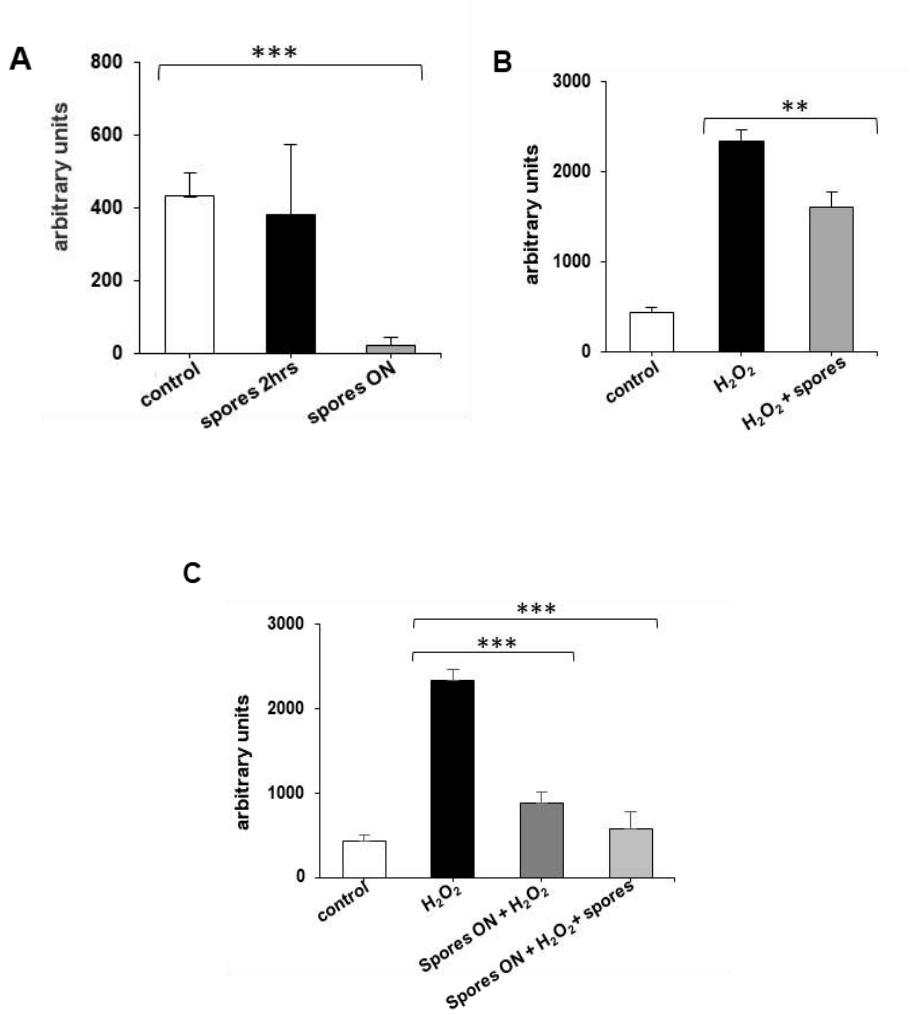

Figure 2: Intracellular ROS analysis (**A**) Caco-2 cells were grown for 2 or 18 hours in presence (grey bars, spores 2 hrs and spores ON respectively) or not (white bar, control) of spores at 1:1 ratio with cells. Cells were then washed from spores and Intracellular ROS measured by DCFDA assay. (**B**) Caco-2 cells were treated (black and grey bars) or not (white bar, control) for 2 hours with 100 µM H_2O_2 in presence (grey bar) or absence (black bar) of spores at 1:1 ratio with cells. (**C**) Caco-2 cells were grown for 18 hours in presence (grey bars) or not of spores at 1:1 ratio with cells. Cells were then washed from spores and cultured for additional 2 hours with 100 µM H_2O_2 (black and grey bars) or 100 µM H_2O_2 and spores (light grey bar). Data are expressed as means ± SE (n=3). Analysis of variance has been performed by One-way ANOVA (Asterisks indicates statistical significance with *P<0.05; **P<0.01; ***P<0.001; ****P<0.0001)

Further, we analyzed ROS-induced oxidative damages through evaluation of lipid peroxidation of the Caco-2 cell membranes. To this purpose, cells were pre-incubated for 24 hours with a 1:1 ratio spores/cells, washed and challenged with 100 µM H_2O_2 for 2 hours. The lipid peroxidation level was

measured as described in methods section. Briefly, the end products of lipid peroxidation are reactive aldehydes, such as Malondialdheyde, whose levels can be quantified through a reaction with a chromogenic reagent, TBA (2-thiobarbituric acid), which yield a chromophore with absorbance maximum at 532 nm. As shown in Fig. 3, the TBARS levels, an indirect measurement of lipid peroxidation, was markedly reduced in samples pretreated with spores with respect to not only H_2O_2-treated cells but also to control cells, confirming that spores have an antioxidant activity against both exogenous and endogenous ROS.

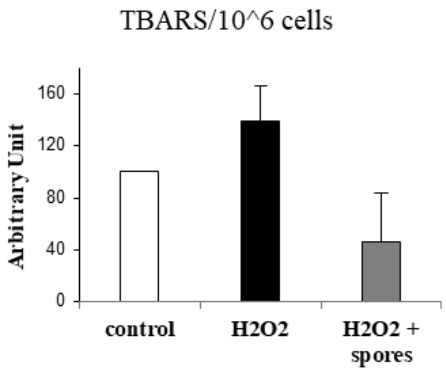

Figure 3: Effects of spores on lipid peroxidation in Caco-2 cells Caco-2 cells were serum-starved for 2 hours and then treated with 100 µM H_2O_2 (black bar) or 100 µM H_2O_2 and spores at 1:1 ratio (cells/spores) (grey bar) for an additional 2 hours. Data are expressed as percentage of untreated cells (white bar, control) set at 100 and presented as mean ± SE (n=4). Analysis of variance has been performed by One-way ANOVA (Asterisks indicates statistical significance with *P<0.05; **P<0.01; ***P<0.001; ****P<0.0001)

To further analyze the effects of spores on Caco-2 cells, we asked whether they can affect cell viability. Therefore, an MTT assay was conducted following a 24 hours incubation of Caco-2 cell with B. megaterium SF185 spores at 1:1 ratio. Interestingly, cell viability increased about 1.5 folds with respect to the control when cells were incubated with spores (Fig. 4), confirming that spores are not only non-toxic for Caco-2 cells but, instead, exert a beneficial effect.

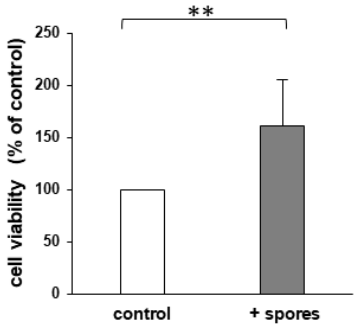

Figure 4: Effects of spores on Caco-2 cell viability Caco-2 cells were incubated for 24 hours with spores at 1:1 ratio. Data are expressed as percentage of control (no spores) (white bar) set at 100 and presented as mean ± SE of three independent experiments. Analysis of variance has been performed by two-tail unpaired t-test (Asterisk ** indicates statistical significance with p =0.0045).

7.4.3 *In vivo* antioxidant activity of SF185 spores

The antioxidant activity of SF185 spores was also tested *in vivo*, using a mouse model, in which colitis was induced by DSS administration in drinking water [34]. While the DSS addition to drinking water did not influence food or water intake (Fig. 5A-B), we observed a reduction in the body weight gain in the mice of the DSS group but not in those of control and DSS + spore ones, (Fig. 5C), showing that spore treatments protected mice from DSS-induced body weight loss.The induction of colitis by DSS treatment and the protective effect of SF185 spores were also confirmed by the determination of macroscopic score (Fig. 5D), that revealed a strong disease activity index in DSS-challenged mice but not in those pre- and post-treated with the spores.

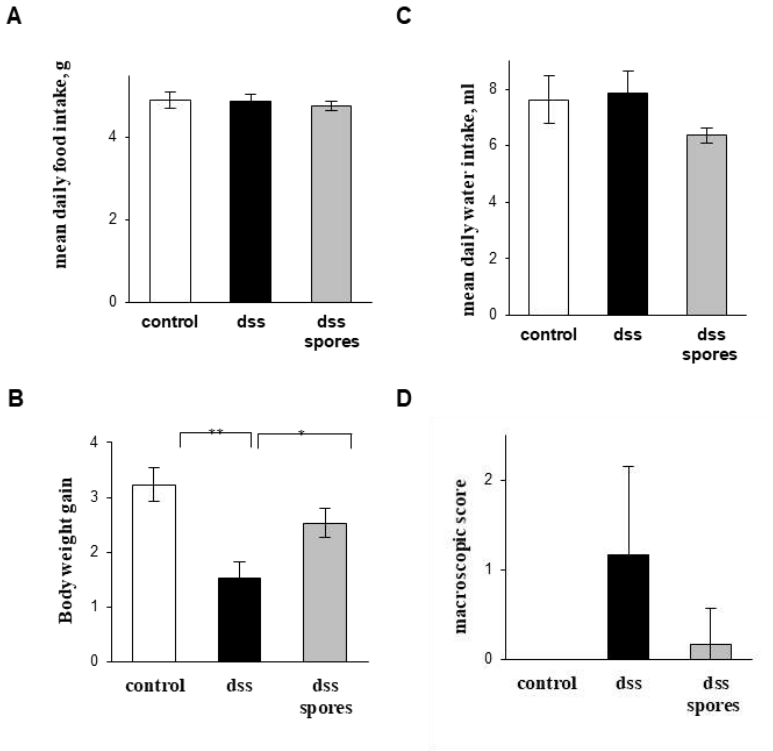

Figure 5: Macroscopic effects of DSS *in vivo* (**A - B**) Food and water intake and (**C**) body weight were monitored daily while (**D**) macroscopic damage scores were assessed on the day of euthanasia. In all panels, untreated mice (control, white bars), mice treated with DSS without (black bars) or with spores (grey bars). Values are reported as means with their SE (n=6). Analysis of variance has been performed by One-way ANOVA (Asterisks indicates statistical significance with *P<0.05; **P<0.01; ***P<0.001; ****P<0.0001).

The antioxidant protective effect of SF185 spores was also confirmed *in vivo* in colon samples of DSS-treated mice by evaluating lipid peroxidation, MPO activity, the concentration of the inflammatory cytokine TNFα and the IL12/IL10 cytokines ratio (Fig. 6). As Fig. 6A shows, lipid peroxidation increased in colon samples of mice treated with DSS and was restored to levels similar to the control, in mice also treated with spores. The determination of MPO activity can be used as a surrogate of marker of inflammation, since it has been shown that the activity of MPO solubilized from the inflamed tissue is directly proportional to the number of neutrophils seen in histologic sections

investigating intestinal inflammation in DSS-induced model of IBD [27]. As shown in Figure 6b, the strong increase of MPO activity observed in animals treated with DSS was totally abolished by the pre-treatment with SF185 spores. Also, colonic TNFa and IL12/IL10 ratio (two cytokines with inflammatory and anti-inflammatory activities, respectively), common markers of inflammation [35, 36], are restored in spore treated mice (Fig. 6 C, D, E). Overall, these *in vivo* experiments indicate that DSS treatment significantly increases all markers of inflammation in the colon, while treatment with SF185 spores is able to exert a strong protective effect.

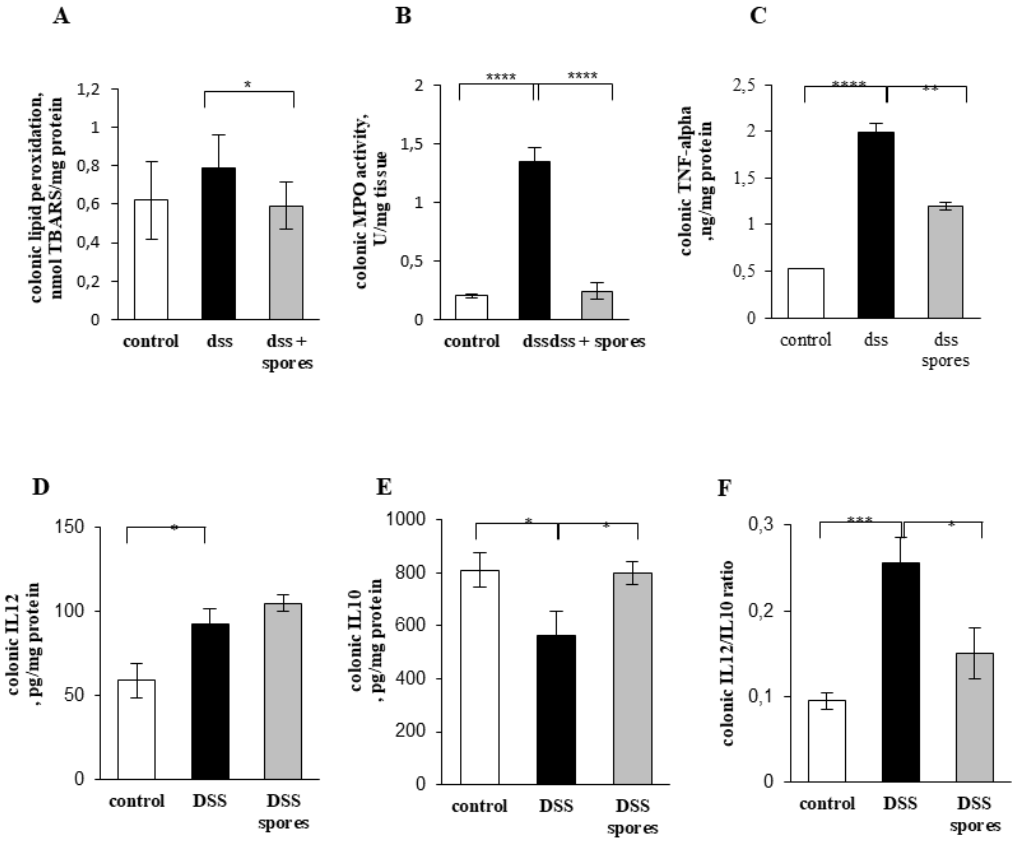

Figure 6: Effects of spores on oxidation, inflammation and cytokines levels (**A**) Lipid peroxidation, (**B**) MPO activity, (**C**) TNF-alpha levels, (**D**) IL-12 levels and (**E**) IL-10 levels (B) were evaluated on colonic tissue samples collected after euthanasia. (**F**) The IL-12/IL-10 ratio is a marker of disease severity. Values are reported as means with their SE (n=6). Analysis of variance has been performed by One-way ANOVA (Asterisks indicates statistical significance with *P<0.05; **P<0.01; ***P<0.001; ****P<0.0001).

7.5 Discussion

Main conclusions of this work are that spores of *B. megaterium* have an intrinsic antioxidant activity and that have protective effects *in vitro* on Caco-2 cells against exogenous ROS and *in vivo* on murine intestinal cells against DSS-induced oxidative damages. The *in vitro* antioxidant activity of spores clearly suggests that spores act as ROS scavengers reducing free oxidants outside cells and tissues. Such scavenging effect was also exerted against oxidants produced by the physiological metabolic activity of Caco-2 cells, as shown by the increased viability of cells incubated with spore but not subjected to H_2O_2 insults.

Accordingly, a protective effect was also observed when spores were incubated with Caco2 cells for 18 hours and then removed before the treatment of cells with hydrogen peroxide. This indicates that a mechanism other than ROS scavenging is also played by spores. One explanation is that spores are able to reduce oxidants or catabolites produced by the cell's metabolism, thus conferring better conditions of growth as indicated by the observed reduction of intracellular ROS in physiological conditions. On the other hand, it has been recently reported that spores of a different *Bacillus* species, *B. subtilis*, induce the nuclear translocation of the Nrf-2 factor with the subsequent activation of stress response genes [22]. We have not investigated this aspect and can only hypothesize that *B. megaterium* spores are also able to induce the activation of genes coding for antioxidant/detoxifying enzymes, rendering the cells more resistant to a subsequent oxidative insult and allowing us to conclude that spores protect cells against ROS *in vitro*.

In *in vivo* assays, the pre and post-dosing treatments with SF185 spores showed marked protective effects against weight loss and colon damage, reducing inflammation and the oxidative stress damages. The exerted protection against the DSS-induced colitis symptoms can be due to the scavenging mechanism, to the activation of stress-response genes or to a combination of the two spore-mediated effects. While additional experiments are needed to clarify the mechanism of action of spores, the presented experiments strongly suggest that spores of *B. megaterium* SF185 represent a promising new probiotic with antioxidant activity and that administration of spore-based products may have therapeutic and possibly preventive efficacy in human colitis.

7.6 References

1. Ames BN, Shigenaga MK, Hagen TM (1993) Oxidants, antioxidants, and the degenerative diseases of aging. Proc Natl Acad Sci USA 90:7915–7922.
2. Ray PD, Huang BW, Tsuji Y (2012) Reactive oxygen species (ROS) homeostasis and redox regulation in cellular signalling. Cell Signal 24:981-990.
3. Eftekharzadeh B, Maghsoudi N, Khodagholi F (2010) Stabilization of transcription factor Nrf2 by tBHQ prevents oxidative stress-induced amyloid β formation in NT2N neurons. Biochimie 92:245–253.
4. Harrison D, Griendling KK, Landmesser U, Hornig B, Drexler H (2003) Role of oxidative stress in atherosclerosis. Am J Cardiol 91:7–11.
5. Ostrakhovitch EA, Afanas'ev IB (2001) Oxidative stress in rheumatoid arthritis leukocytes: Suppression by rutin and other antioxidants and chelators. Biochem Pharmacol 62:743–746.
6. Griendling KK, FitzGerald GA (2003) Oxidative stress and cardiovascular injury part I: Basic mechanisms and in vivo monitoring of ROS. Circulation 108:1912–1916.
7. Ceriello A, Motz E (2004). Is oxidative stress the pathogenic mechanism underlying insulin resistance, diabetes, and cardiovascular disease? The common soil hypothesis revisited. Arterioscler Thromb Vasc Biol 24:816–823.
8. Lugrin J, Rosenblatt-Velin N, Parapanov R, Liaudet L (2014). The role of oxidative stress during inflammatory processes Biol Chem 395(2): 203–230.
9. Engler JA, Gupta A, Li L, Rao R K (1999) Inhibition of DNA synthesis in Caco-2 cells by oxidative stress. Amelioration by epidermal growth factor. Dig Dis Sci 44:1902–1909.
10. Wang, Y, Wu Y, Wang Y, Xu H, Mei X, Yu D, Wang Y, Li W (2017) Antioxidant properties of probiotic bacteria. Nutrients 9, 521.
11. Lü JM, Lin PH, Yao Q, Chen C (2010) Chemical and molecular mechanisms of antioxidants: experimental approaches and model system. Cell Mol Med 14 (4): 840-860

12. Kaulmann A, Bohn T (2014) Carotenoids, inflammation, and oxidative stress--implications of cellular signaling pathways and relation to chronic disease prevention. Nutr Res. 34(11):907-929.
13. Di Luccia B, Crescenzo R, Mazzoli A, Cigliano L, Venditti P, Walser J-C, Widmer A, Baccigalupi L, Ricca E, Iossa S (2015) Rescue of Fructose-Induced Metabolic Syndrome by Antibiotics or Faecal Transplantation in a Rat Model of Obesity. PLoS ONE 10(8): e0134893.
14. Shen Q, Shang N, Li P (2011) In vitro and in vivo antioxidant activity of Bifidobacterium animalis isolated from centenarians. Curr Microbiol 62:1097–1103.
15. Bao Y, Wang Z, Zhang Y, Wang L, Dong X, Su F, Yao G, Wang S, Zhang H. Effect of Lactobacillus plantarum P-8 on lipid metabolism in hyperlipidemic rat model. Eur J Lipid Sci Technol 2012; 114:1230–1236.
16. Martarelli D, Verdenelli M.C, Scuri S, Cocchioni M, Silvi S, Cecchini C, Pompei P (2011) Effect of a probiotic intake on oxidant and antioxidant parameters in plasma of athletes during intense exercise training. Curr Microbiol 62:1689–1696.
17. Crescenzo R, Mazzoli A, Cancelliere R, Bucci A, Naclerio G, Baccigalupi L, Cutting S.M, Ricca E, Iossa S (2017) Beneficial effects of carotenoid-producing cells of Bacillus indicus HU16 in a rat model of diet-induced metabolic syndrome. Beneficial Microbes 8(5):823-831.
18. Fritze D. Taxonomy and systematics of the aerobic endospore forming bacteria: Bacillus and related genera (2004) In: E Ricca, AO Henriques, and SM Cutting (Eds.), Bacterial Spore Formers. Norfolk, UK: Horizon Biosience pp. 17–34.
19. Tan IS, Ramamurthi KS (2014) Spore formation in Bacillus subtilis. Environ Microbiol Rep 6(3):212-225.
20. Cutting SM. Bacillus probiotics. Food Microbiology 2011; 28: 214-220.
21. Cutting SM, Hong HA, Baccigalupi L, Ricca E (2009) Oral Vaccine Delivery by Recombinant Spore Probiotics. Inter Rev Immunol 28:6, 487—505.
22. Petruk G, Donadio G, Lanzilli M, Isticato R, Monti DM (2018) Alternative use of Bacillus subtilis spores: protection against environmental oxidative stress in human normal keratinocytes. Sci Rep 8(1):1745.
23. Nicholson WL, Setlow P. Sporulation, germination and out-growth(1990) In Molecular biological methods for Bacillus. Edited by Harwood C, Cutting S. Chichester, United Kingdom: John Wiley and Sons 391–450.
24. Troiano A, Lomoriello IS, di Martino O, Fusco S, Pollice A, Vivo M, La Mantia G, Calabrò V (2015) Y-box Binding Protein-1 Is Part of a Complex Molecular Network Linking ΔNp63α to the PI3K/akt Pathway in Cutaneous Squamous Cell Carcinoma. J Cell Physiol. 2015 Sep;230(9):2067-74.
25. Vivo M, Fontana R, Ranieri M, Capasso G, Angrisano T, Pollice A, Calabrò V, La Mantia G (2017) p14ARF interacts with the focal adhesion kinase and protects cells from anoikis. Oncogene. 26. Kedare SB, Singh RP (2011) Genesis and development of DPPH method of antioxidant assay. JFood Sci Technol 48: 412-422.
27. Beers R & Sizer I (1952) A spectrophotometric method for measuring the breakdown of hydrogen peroxide by catalase. J Biol Chem 195: 133-140.
28. Fernandez J (1997) Thiobarbituric acid test for monitoring lipid oxidation in meat. Food Chemistry 59 (3): 345-353.
29. Kim JJ, Shajib MS, Manocha MM, Khan WI (2012) Investigating intestinal inflammation in DSS-induced model of IBD. J Vis Exp 60. pii: 3678.
30. Vary PS (1994) Prime time for Bacillus megaterium. Microbiology 140:1001-1013
31. Di Luccia B, D'Apuzzo E, Varriale F, Baccigalupi L, Ricca E, Pollice, A (2016) Bacillus megaterium SF185 induces stress pathways and affects the cell cycle distribution of human intestinal epithelial cells. Benef Microbes 7(4):609-20.
32. Fakhry S, Sorrentini I, Ricca E, De Felice M, Baccigalupi L (2008) Characterisation of spore forming Bacilli isolated from the human gastrointestinal tract. J. Applied Microbiology 105:2178-2186.

33. Hoa TT, Duc LH, Isticato R, Baccigalupi L, Ricca E, Van PH, Cutting SM (2001). Fate and dissemination of Bacillus subtilis spores in a murine model. Appl Environ Microbiol 67: 3819-3823.
34. Di Luccia B, Mazzoli, Cancelliere R, Crescenzo R, Ferrandino I, Monaco A, Bucci A, Naclerio G, Iossa S, Ricca E, Baccigalupi L (2018) Lactobacillus gasseri A SF1183 protects the intestinal epithelium and prevents colitis symptoms in vivo. J Functional Food 42: 195-202
35. Foligne B, Dessein R, Marceau M, Poiret S, Chamaillard M, Pot B, Simonet M, Daniel C (2007) Prevention and treatment of colitis with Lactococcus lactis secreting the immunomodulatory Yersinia LcrV protein. Gastroenterology 133(3):862-74.
36. Sokol H, Pigneur B, Watterlot L, Lakhdari O, Bermúdez-Humarán LG, Gratadoux JJ, Blugeon S, Bridonneau C, Furet JP, Corthier G et al (2008) Faecalibacterium prausnitzii is an anti-inflammatory commensal bacterium identified by gut microbiota analysis of Crohn disease patients. Proc Natl Acad Sci U S A 105(43):16731-6.

Part 4:

Collaboration

Chapter 8

Fluorescent peptide dH3w: a sensor for environmental monitoring of mercury (II)

Siepi M.[a], Oliva R.[b]*, Petraccone L.[b], Del Vecchio P.[b], Ricca E[a],*

*Isticato R.[a], **Lanzilli M.**[a], Maglio O.[bc], Lombardi A.[b], Leone L.[b] ,*

Notomista E.[a§] and Donadio G.[a§] .

[a] *Department of Biology University of Naples Federico II, Via Cintia, 80126, Naples, Italy.*

[b] *Department of Chemical Sciences University of Naples Federico II, Via Cintia, 80126, Naples, Italy*

[c] *IBB, CNR, Via Mezzocannone 16, 80134 Naples (Italy)*

PLoS One. 2018 Oct 10

8.1 Abstract

Heavy metals are hazardous environmental contaminants, often highly toxic even at extremely low concentrations. Monitoring their presence in environmental samples is an important but complex task that has attracted the attention of many research groups. We have previously developed a fluorescent peptidyl sensor, dH3w, for monitoring Zn^{2+} in living cells. This probe, designed on the base on the internal repeats of the human histidine rich glycoprotein, shows a turn on response to Zn^{2+} and a turn off response to Cu^{2+}. Other heavy metals (Mn^{2+}, Fe^{2+}, Ni^{2+}, Co^{2+}, Pb^{2+} and Cd^{2+}) do not interfere with the detection of Zn^{2+} and Cu^{2+}. Here we report that dH3w has an affinity for Hg^{2+} considerably higher than that for Zn^{2+} or Cu^{2+}, therefore the strong fluorescence of the Zn^{2+}/dH3w complex is quenched when it is exposed to aqueous solutions of Hg^{2+}, allowing the detection of sub-micromolar levels of Hg^{2+}. Fluorescence of the Zn^{2+}/dH3w complex is also quenched by Cu^{2+} whereas other heavy metals (Mn^{2+}, Fe^{2+}, Ni^{2+}, Co^{2+}, Cd^{2+}, Pb^{2+}, Sn^{2+} and Cr^{3+}) have no effect. The high affinity and selectivity suggest that dH3w and the Zn^{2+}/dH3w complex are suited as fluorescent sensor for the detection of Hg^{2+} and Cu^{2+} in environmental as well as biological samples.

8.2 Introduction

Heavy metal ions when present in excess are toxic for all organisms [1]. They are difficult to remove from the environment and unlike many other pollutants cannot be chemically or biologically degraded, therefore, heavy metals constitute a global environmental hazard [2]. Mercury and its compounds, in particular, are regarded as “priority hazardous substances” by the Agency for Toxic Substances and Disease Registry (ATSDR) because of its toxicity, mobility, long residence time, and biomagnification in food chains [3]. For examples, Hg^{2+} is highly toxic even at low levels [4] and in humans it can affect liver, kidneys and the cardiovascular, gastro-intestinal and neurological systems [5]. Hg^{2+} detection is undoubtedly significant in environment and health monitoring. This has prompted the development of highly selective and sensitive, low cost chemosensors for the detection of Hg^{2+} in environmental and biological samples. Many of these Hg^{2+} sensors are based on colorimetric and/or fluorometric detection [6–13], but very sensitive sensors based on surface enhanced Raman spectroscopy (SERS) [14], chiroptical signal and electrical conductivity [15] have also been developed.

Fluorescent sensors usually have a metal binding module (often an organic ligand) linked to a fluorescent moiety [6–13]. The binding of a specific metal ion to the sensor, through mechanisms like photoinduced electron transfer (PET) and chelation enhanced fluorescence (CHEF), causes variation in the fluorescence thus allowing an easy and real-time detection of the metal/sensor interaction [7]. However, some colorimetric and fluorometric sensors exploit metal catalyzed reactions like spirocyclic ring opening in rhodamine derivatives [7] or deprotection of dithioacetals ([8] and references therein). Major drawbacks of these sensors can be difficult synthesis, limited solubility in water or the fact that they undergo an irreversible reaction with the analyte.

Metal binding proteins are intriguing alternatives to organic ligands. Protein-based Hg biosensor based on electrochemical [16,17] and optical [18] techniques has been already prepared. However, poor

stability of proteins at ambient conditions limit their applications. On the other hand, short metal binding peptides are particularly suited for the development of fluorescent probes. The structural complexity and the flexibility of peptides allow to exploit metal induced conformational changes as part of the sensing mechanism [19], moreover, peptidyl probes properties can be tuned by changing/mutating specific amino acids as well as changing the fluorescent moiety and the residue to which it is attached. In addition, short peptides can be easily synthesized via 9-fluorenyl-ethoxycarbonyl (Fmoc) solid-phase peptide synthesis (SPPS) [20], and can be generally employed in aqueous solutions. In previous work [19] we devoted our attention to histidine-rich glycoproteins (HRGs), complex multidomain proteins found in the serum of vertebrates, characterized by an impressive variety of functions in blood coagulation, fibrinolysis and in the innate immune systems [21]. We demonstrated that the designed peptide dH3w (dansyl-HPHGHW-NH_2), containing the repeated sequence of human HRG (HPHGH) plus a dansyl group and a tryptophan residue at the two ends, can be used as a turn-on fluorescent probe for Zn^{2+} and a turn-off probe for Cu^{2+} in biological systems [19]. Here we demonstrate that dH3w has an affinity for mercury (II) ions 1000 times higher than that for Zn^{2+}, thus being able to displace zinc from the dH3w/Zn^{2+}. With the exception of Cu^{2+} no other heavy metal is able to displace Zn^{2+},therefore, dH3w complex with Zn^{2+} could be used as selective probes for environmental monitoring of $Hg^{2+}$and Cu^{2+}.

8.3 Materials and methods

8.3.1 Chemicals

All chemicals were reagent grade unless noted, and deionized distilled water was used to prepare solutions. Peptide dH3w (dansyl-His-Pro-His-Gly-His-Trp-NH_2) was synthesized by Primm srl. with a purity grade of 98% (Figs. S1 and S2). Stock solutions of metal ions were prepared by dissolving the appropriate chloride salt in a 20 mM Mops [3-(N-morpholino) propanesulfonic acid] buffer, pH 7.0. All samples solutions were prepared by proper dilution of stock solutions.

8.3.2 Steady-state fluorescence measurements

Steady-state fluorescence spectra were recorded on a Fluoromax-4 fluorometer (Horiba, Edison, NJ, USA) using a 1 cm path length quartz cuvette. The temperature was set to 25 °C. The excitation wavelength was set to 340 nm and emission spectra were recorded in the range 400 nm – 660 nm. The slit widths for excitation and emission were set to 2 nm and 3 nm, respectively. Fluorescence emission spectra as a function of Hg^{2+} concentration were recorded by titrating a solution of dH3w (7 μM) with a solution of Hg^{2+}. All the experiments were carried out in 20 mM Mops buffer adjusted at the appropriate pH values with the addition of sulfuric acid or sodium hydroxide. For displacement experiments, a solution of dH3w (7 μM) saturated with Zn^{2+} (100 μM), was titrated with a solution of Hg^{2+} ranging from 0 up to ~ 100 μM. The fraction of bound peptide (α) at each point of titration was obtained by following the changes in the fluorescence intensity at the maximum emission wavelength by means of the equation:

$$\alpha = \frac{I_\lambda - I_\lambda^{free}}{I_\lambda^{bound} - I_\lambda^{free}}$$

where I_λ is the fluorescence intensity at each point of the titration, I_λ^{free} is the intensity of free peptide and I_λ^{bound} is the intensity of the peptide at saturation. The displacement binding curve was obtained by plotting the fraction of bound peptide (α) versus Hg^{2+} concentration and the experimental points were fitted using a two non-equivalent and independent binding sites model.

8.3.3 Metal selectivity studies

dH3w (10 µM) and Zn^{2+} (100 µM) were incubated in the presence of different concentrations (30, 60 and 90 µM) of metal ions (Cu^{2+}, Ni^{2+}, Co^{2+}, Mn^{2+}, Pb^{2+}, Cd^{2+}, Fe^{2+}, Sn^{2+} and Cr^{3+}) and the fluorescence intensity at 515 nm was recorded after excitation at 340 nm, using a plate reader (Synergy HTX Multi-Mode Reader-BIOTEK).

8.3.4 Job's plot

To check all the possible binding stoichiometries between dH3w and Hg^{2+} ions, the continuous variations method (Job's plot) was applied [22]. The mole fraction of dH3w ranged from 0.1 to 0.9 and the total molar concentration (dH3w+Hg^{2+}) was fixed at 40 µM.

8.3.5 Quantum yield determination

Fluorescence quantum yields in the presence of Hg^{2+} (100 µM) were determined as previously described [19] using fluorescein as a standard. Measurements were performed in 20 mM Mops buffer, pH 7.0. All emission spectra were recorded in the range 360–700 nm after excitation at 370 nm.

8.3.6 Determination of the detection limit

The detection limit (LOD) for Hg^{2+} was calculated by performing a fluorescence titration. The emission intensity of free dH3w was measured 10 times and the standard deviation determined. Then, calibration curves were obtained by recording the fluorescence at Hg^{2+} concentrations up to 1200 nM. Each calibration curve was obtained in triplicate. The detection limit was then calculated as LOD = 3σ/k, where σ is the standard deviation of the free peptide measurements and k is the slope of the line obtained by plotting fluorescence intensity versus the metal ion concentration [23]. The detection limit was calculated at pH 4.0 and 7.0.

8.3.7 NMR spectroscopy

All NMR spectra were acquired at 298 K on Bruker Avance 600 MHz spectrometer, equipped with triple resonance cryo-probe. NMR characterization was performed in H2O/D_2O (90/10 v/v).
NMR samples of dH3w were prepared by dissolving weighted amounts of the peptide in the solvent systems (V = 0.520 µl) for a final concentration of 0.5 mM. Metal/peptide complex was prepared using

the following conditions: to a 0.5 mM dH3w solution in 90% H_2O/10% D_2O (pH 3.8), small aliquots (2.6 □L) of a freshly prepared aqueous stock solution of $HgCl_2$ (25 mM) were added until a 1:1 peptide:metal ratio was reached. The pH was then adjusted to 4.5 with NaOH and the concentration of Hg^{2+} was gradually increased up to 10 mM.

Chemical shifts were referenced to internal sodium 3-(trimethylsilyl)[2,2,3,3-d_4] propionate (TSP). Two-dimensional (2D) experiments, such as total correlation spectroscopy (TOCSY)[24], nuclear Overhauser effect spectroscopy (NOESY) [25,26], rotating frame Overhauser effect spectroscopy (ROESY) [27], double quantum-filtered correlated spectroscopy (DQF-COSY) [28] and Heteronuclear single quantum coherence (1H, 13C HSQC) were carried out with standard pulse sequences. The data file generally consisted of 512 and 2048 (4096 for DQF-COSY) data points in the ω1 and ω2 dimensions, respectively, which was zero-filled to obtain 2048 x 4096 data points in the spectrum. In all homonuclear experiments the data matrix was resolution enhanced in both dimensions by a cosine-bell function before Fourier Transformation. Solvent suppression was achieved with excitation sculpting sequence [29].

TOCSY experiment was acquired with a 70 ms mixing time. NOESY experiment was acquired with a 300 ms mixing time, and ROESY experiments with a 180 and 250 ms mixing time, using a continuous spin-lock. Heteronuclear single quantum coherence (1H, 13C HSQC) was performed using sensitivity improvement [30] and in the phase-sensitive mode using Echo/Antiecho gradient selection, with multiplicity editing during selection step.

According to Wüthrich [31], identification of amino-acid spin systems was performed by comparison of TOCSY and DQF-COSY, while sequential assignment was obtained by the analysis of NOESY and ROESY spectra (see Table 1 Fig. S3).

Data acquisition and processng were performed with Topspin 2.1 software package (Bruker).

8.3.8 Fluorescence imaging of dH3w-treated cell cultures

Human normal keratinocytes (HaCaT), were cultured in Dulbecco's Modified Eagle's Medium (DMEM), supplemented with 10% foetal bovine serum, 2 mM L-glutamine and 1% penicillin–streptomycin in a 5% CO_2 humidified atmosphere at 37 ºC.

Cells were seeded in 24-well plates (500 µl/well) on sterile cover-slips at a density of 5 x 10^4/well and then grown at 37 °C for 48 hours. Cells were first treated with ZnCl (100 µM) for 3 hours. After incubation, three washes with PBS buffer were performed hence dH3w was added at the final concentration of 7 µM. After 2 hours, cells were incubated with $HgCl_2$ (10 µM). Cells were analyzed under an Olympus BX51 fluorescence microscope (magnification 100X) using a DAPI filter (excitation 358 nm and emission 470 nm). Typical acquisition time was 500 ms. The images were captured using an Olympus DP70 digital camera (Olympus, NY, USA) and processed by using the analysis software supplied by the manufacturer.

8.4. Results and Discussion

8.4.1. dH3w emission spectra in the presence of various concentrations of Hg^{2+}

The fluorescence emission spectra of dH3w at pH 7 and increasing Hg^{2+} concentrations (up to 100 μM) were recorded after excitation at 340 nm, the maximum absorption wavelength of the dansyl moiety. Unexpectedly two distinct behaviours were observed (Fig 1). At low Hg^{2+} concentrations (<10μM) dH3w showed a turn off response with a 60% reduction of the emission but no change in the spectrum features. At Hg^{2+} concentrations higher than 12 μM, dH3w showed a turn on response coupled with a noteworthy blue-shift of the λ_{max}, from 560 to 710 nm.

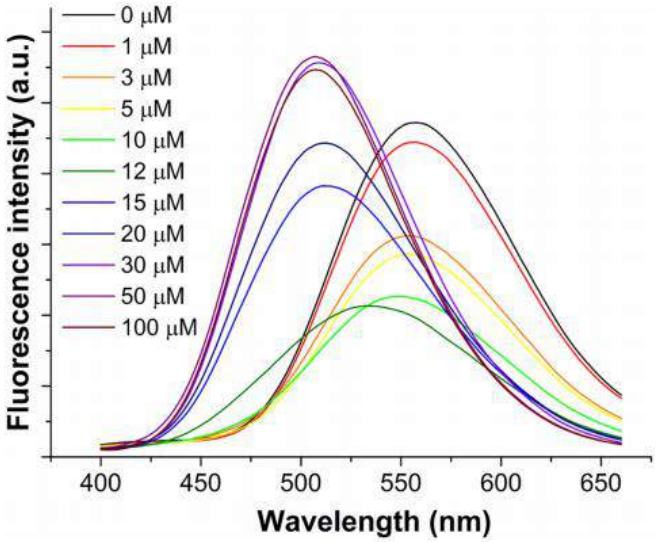

Figure 1: Fluorescence emission spectra of dH3w (7 μM) in the absence (black line) and in the presence of increasing concentrations of Hg^{2+} (1, 3, 5, 10, 12, 15, 20, 30, 50, 100 μM) at pH 7.0.

This bimodal spectral behaviour strongly suggests the presence of at least two different binding modes of Hg ion having very different affinity constants.

To get more information on the complex binding behaviour of Hg^{2+} to dH3w we employed the continuous variations method. The Job's plot (Fig. 2) showed two intersection points at dH3w mole fractions of about 0.52 and 0.34 corresponding to stoichiometric ratios (dH3w:Hg) of 1:1 and 1:2 thus confirming that dH3w has two non equivalent binding sites for Hg ions.

dH3w contains at least four potential ligands for transition metal cations, i.e. the three imidazole moieties of the histidine residues at positions 1, 3 and 5 and the sulphonamide of the dansyl-sulphonamide fluorophore (Fig. 3A). Other potential but lower affinity sites are the C-terminal amide and the internal peptide bonds. The significant blue-shift of the maximum emission observed at high Hg^{2+} concentrations can be likely attributed to the deprotonation of the dansyl-sulphonamide moiety upon binding to the strongly electrophilic Hg^{2+} ion. Direct binding of a dansyl-sulphonamide anion to Hg^{2+} has been previously suggested or demonstrated in several turn-on mercury sensors with different chemical structures [32]. In all these complexes, deprotonation and direct binding of the NH group of the sulphonamide to Hg^{2+} was always accompanied by a 40-50 nm blue shift in the emission due to the reduced conjugation between the deprotonated sulphonamide and the (dimethylamino)naphthalene moiety [32]. Moreover, it is well known that, in the presence of ligands with nitrogen as donor, Hg^{2+} prefers the (linear) 2-coordination and that a third ligand usually binds with a lower affinity [33–36].

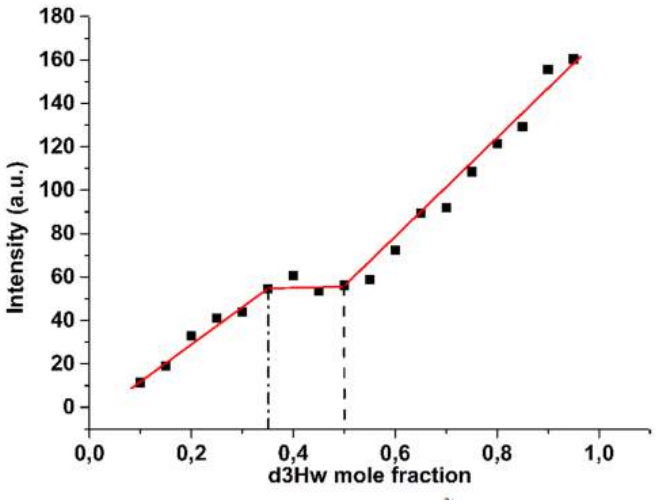

Figure 2: The Job's plot obtained from the titration of dH3w peptide with Hg^{2+} ions. The dashed lines highlighted the found binding stoichiometry at mole fraction of dH3w of 0.52 and 0.34 which correspond to 1:1 and 1:2 (dH3w:Hg^{2+}) complexes, respectively. The experiment was carried out in 20 mM Mops buffer, pH 7.0 at the temperature of 25 °C. Errors are not shown because they were always smaller than the symbols sizes.

Therefore, it is reasonable to hypothesize that, at low Hg^{2+} concentrations, a single Hg ion binds to the peptide through, likely, two or three histidine residues, whereas, at higher Hg^{2+} concentrations, a second ion binds through the sulphonamide (Fig. 3B) and, possibly, one of the histidine residues.

To complete the characterization of the fluorescence properties of dH3w, we determined the quantum yield of dH3w in the absence and presence of saturating concentrations of Hg^{2+} (100 µM). The obtained values 0.049 ± 0.002 and 0.047 ± 0.005, respectively – show that Hg^{2+} binding does not change the quantum yield in spite of the large variations in the emission spectrum.

8.4.2. pH-titration curves in the presence of mercury (II)

As the pK_a of the imidazole and sulphonamide moieties are very different, about 6 and 10 respectively, in order to confirm the involvement of these groups in the binding process we studied the behaviour of the dH3w/Hg^{2+} complex as function of pH. The response of free dH3w to pH has been previously described [19]. In the pH range 4-8 the fluorescence emission of dH3w was scarcely influenced by pH [19]. At pH <4 the fluorescence intensity of dH3w decreased and disappeared completely below pH 2 likely due to protonation of the dimethylamino group, which prevents the charge transfer between the amine and naphthyl ring thus leading to the quenching of fluorescence. On the contrary at pH >8 the fluorescence intensity of dH3w increased and shifted of 50 nm toward the blue region due to the above-mentioned deprotonation of the sulphonamide moiety whose pK_a is ~ 10.

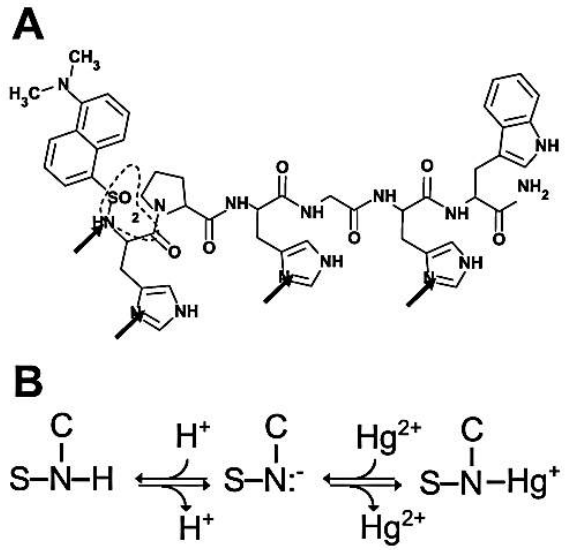

Figure 3: Structure of dH3w (A) and possible interaction mode of the sulphonamide moiety with Hg^{2+} (B). In panel A the arrows indicate the more likely Hg^{2+} ligands. Imidazole groups are arbitrarily shown with the proton at the Nε atom. The dashed line highlights the group shown in details in panel B.

Therefore, we studied the interaction dH3w/Hg^{2+} at pH 8.0, 6.0 and 4.0. At all the pH values dH3w showed two distinct behaviours but with significant differences respect to pH 7. In particular, at pH 8 (Fig. 4A) dH3w showed a turn off response only for Hg^{2+} concentrations lower than 8 µM and with a reduction of the emission of about 22%, i.e. much more modest with respect to that observed at pH 7. At higher concentrations, again a turn-on response and a blue-shift of the λ_{max}, from 560 to 710 nm, was observed. Intriguingly at acidic pH values, high Hg^{2+} concentrations only induced the blue-shift not accompanied by the turn-on response (Figs. 4B,C). Moreover, the blue-shift of the λ_{max} was observed at Hg^{2+} concentrations equal or higher than 40 µM at pH 6 (Fig. 4B) and at concentrations equal or higher than 200 µM at pH 4 (Fig. 4C). These findings are in agreement with the hypothesis that the second Hg^{2+} binding site includes a deprotonated dansyl-sulphonamide. At pH 7 the binding of the second Hg^{2+} can be described as a competition reaction between protons and Hg^{2+} (Fig. 3B). As the concentration of H^+ is held constant at 10^{-7} M by the buffer and the blue shift/turn-on response is observed at Hg^{2+} concentrations between 10^{-5} and 10^{-4} M it can be concluded that the affinity of Hg^{2+} for the sulphonamide group is 100-1000 times lower than that of the protons. At pH 8 the H^+ concentration is ten times lower, therefore lower concentrations of Hg ions are needed to displace the proton from the sulphonamide nitrogen atom. The opposite is true at acidic pH were even the highest concentrations of Hg^{2+} tested can only partially replace protons in the NH group as evidenced by the blue shift in the of the λ_{max} not accompanied by the turn-on response. Obviously, acidic pH values should also weaken the binding of Hg^{2+} to histidine imidazole groups thus reducing also the binding constant of the first Hg^{2+}. Unfortunately, the variations in the spectra as function of the Hg^{2+} concentration were too complex to perform a reliable fit allowing the direct determination of the two binding constants at the different pH values. The constants were instead determined at pH 7 by displacement of the Zn^{2+} ion from the dH3w/Zn^{2+} complex as described in the next section.

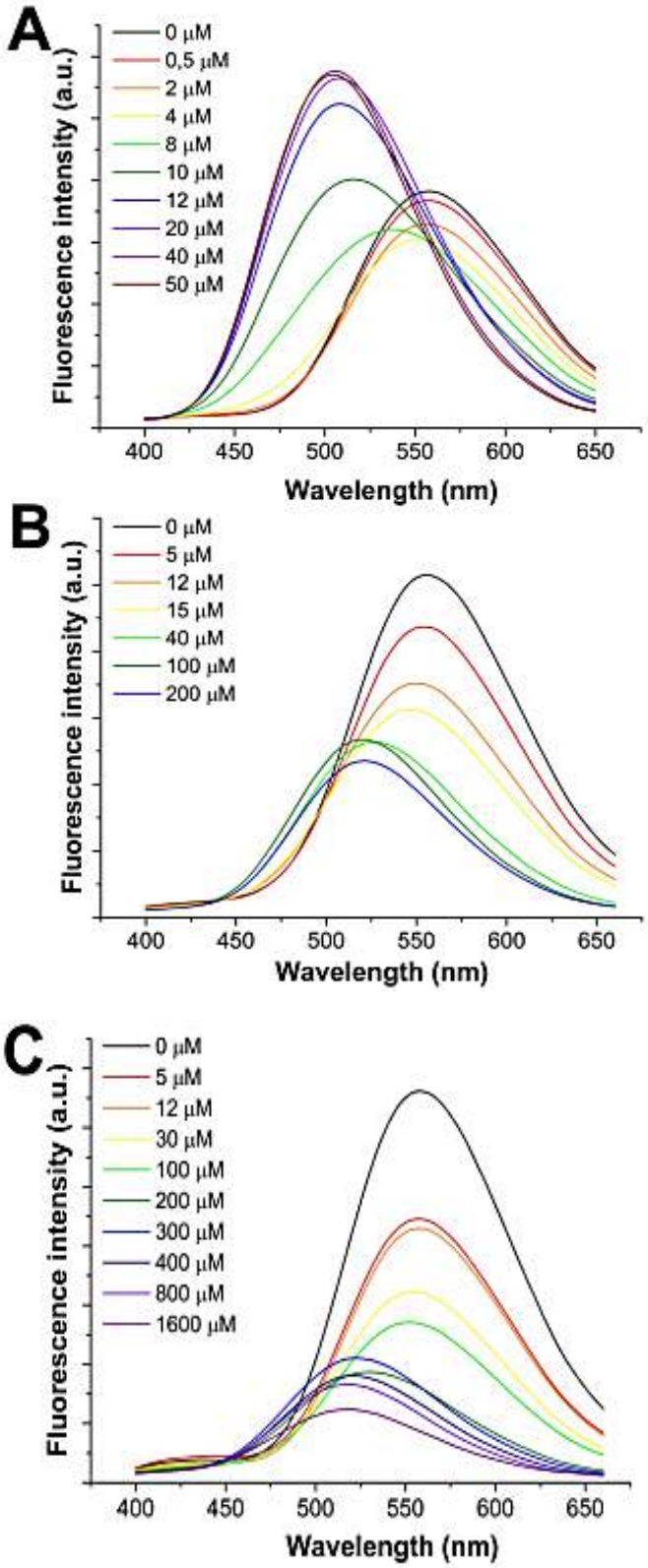
A
0 μM
0,5 μM
2 μM
4 μM
8 μM
10 μM
12 μM
20 μM
40 μM
50 μM
Fluorescence intensity (a.u.)
400
450
500
550
600
650
Wavelength (nm)
B
0 μM
5 μM
12 μM
15 μM
40 μM
100 μM
200 μM
Fluorescence intensity (a.u.)
400
450
500
550
600
650
Wavelength (nm)
C
0 μM
5 μM
12 μM
30 μM
100 μM
200 μM
300 μM
400 μM
800 μM
1600 μM
Fluorescence intensity (a.u.)
400
450
500
550
600
650
Wavelength (nm)

Figure 4: Fluorescence emission spectra recorded after excitation at 340 nm, of dH3w (7 μM) in the absence (black lines) and in the presence of increasing concentrations of Hg^{2+}, at pH 8.0 (**A**), 6.0 (**B**) and 4.0 (**C**).

8.4.3 Interaction of dH3w/Zn^{2+} with Hg^{2+}

We have previously shown that at pH 7 dH3w forms a stable complex with Zn^{2+} with a 2:1 stoichiometry and a binding constant of $(5.9\pm2.2)\cdot10^{7}$ M^{-1} [19]. It is worth noting that zinc ion binding causes a strong turn-on response and fluorescence intensity increases 8–9 fold in the presence of saturating amounts of Zn^{2+}. To evaluate whether Hg^{2+} is able to compete with Zn^{2+} for the binding to dH3w, we recorded the emission spectra of dH3w saturated with Zn^{2+} at increasing Hg^{2+} concentration in 20 mM Mops buffer, pH 7.0. Fig. 5A shows fluorescence emission spectra obtained from the titration with Hg^{2+} of a 7 μM solution of dH3w peptide saturated with 200 μM of Zn^{2+}. After the addition of Hg^{2+} to the Zn-complexed peptide, a decrease of fluorescence emission was observed together with a blue shift from ~525 nm (the λmax of the dH3w/Zn^{2+} complex) to ~509 nm suggesting that Hg^{2+} can bind dH3w displacing Zn^{2+}. The binding curve, obtained by plotting the fraction of bound peptide (α) as a function of Hg^{2+} molarity, is shown in Fig. 5B. Keeping in mind the results obtained for the titration in absence of Zn^{2+} (Figs. 1 and 2), we modeled the binding curve by considering the presence of two independent and non-equivalent sites. This model accurately reproduces the experimental data providing apparent binding constants of $3\cdot10^{7}$ M^{-1} and $6\cdot10^{5}$ M^{-1}. It should be highlighted that these constants are referred to the process in which an Hg^{2+} ion binds dH3w and simultaneously displaces a Zn^{2+}. Considering the higher Zn^{2+} concentration used in these experiments, our results are consistent with Hg^{2+} binding constants for dH3w up to 1000-fold higher than the binding constant of Zn^{2+}. Displacement of zinc ion was not studied at pH < 7 because at these pH values the interaction of dH3w with zinc is very weak or absent [19].

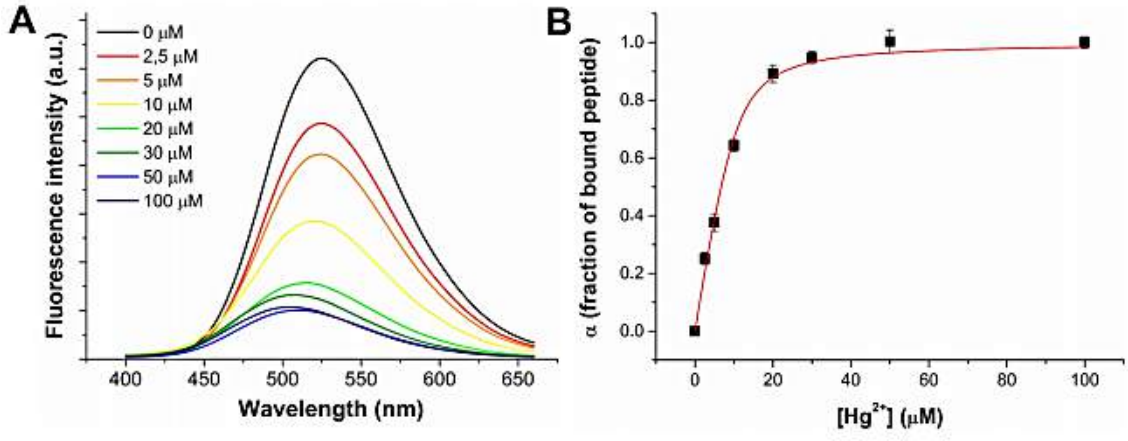

Figure 5: (**A**) Fluorescence emission spectra of Zn-complexed dH3w peptide (7 μM) in the presence of increasing concentration of Hg^{2+}. The black line represents the spectrum of free peptide. (**B**) Binding curve obtained by plotting the fraction of bound peptide (α) versus the Hg^{2+} concentration. The red line represents the best fit of experimental points obtained using a two non-equivalent binding sites model. The experiment was carried out in 20 mM Mops buffer, pH 7.0 at the temperature of 25 °C.

We have previously shown that Cu^{2+} is able to displace Zn^{2+} causing a turn off of the fluorescence of the dH3w/Zn^{2+} complex [19]. Therefore, in order to verify if other metal ions, in addition to Cu^{2+} and

Hg^{2+}, are able to displace Zn^{2+} from the dH3w/Zn^{2+}complex, dH3w and Zn^{2+} were incubated in the presence of different concentrations of several heavy metal ions (Cu^{2+}, Ni^{2+}, Co^{2+}, Mn^{2+}, Pb^{2+}, Cd^{2+}, Fe^{2+}, Sn^{2+} and Cr^{3+}) and the fluorescence intensity at 515 nm was recorded. As shown in Fig. S4, except Cu^{2+}, no other metal ion was able to quench the fluorescence of the dH3w/Zn^{2+} complex. It can be concluded that the dH3w/Zn^{2+}complex is a turn-off sensor highly specific for copper and mercury.

8.4.4 NMR

In order to investigate the interaction of dH3w with Hg^{2+}, NMR experiments were performed in H_2O (10% D_2O) by varying the metal-to-peptide ratio.

Upon addition of 1 equivalent of $HgCl_2$ at pH 3.8, we observed a broadening of His^1 imidazole protons and of Gly^2, His^3 and His^7 amide protons. By increasing the pH to 4.5 the amide protons underwent a further broadening and this effect was also observed for almost all the aliphatic protons (see Fig. S5). The non-selective broadening of the above-mentioned protons, including those of non-coordinating groups (amide and aliphatic protons) could be ascribed to the presence of several coordination modes, which are in relatively slow (intermediate) exchange with each other and with the unbound peptide. No significant changes were observed by increasing the concentration of Hg^{2+} up to 20 equivalents (see Fig. S6), thus indicating a stoichiometric ratio Hg/dH3w of 1:1 at pH values in the range 3.8-4.5. This finding is in agreement with the results obtained studying the fluorescence of the dH3w in the presence of Hg^{2+} at acidic pH values (see section 3.2). Keeping in mind the above mentioned preference of Hg^{2+} for 2-coordination, it is likely to hypothesize that the dH3w/Hg^{2+} complex in solution exists as a mixture of three forms each with only two histidine residues bound to the metal ion (His^1 + His^3, His^1 + His^5 and His^3 + $Hi5^7$). These three complexes could interconvert through a minor form with a tricoordinated Hg^{2+}. Similar equilibria have been studied in the case of the interaction between histidine-rich peptides and immobilized divalent metal ions [37].

NMR experiments were also performed at pH 7.0 (50 mM phosphate buffer), in absence and in presence of $HgCl_2$. During titration experiments with Hg^{2+} precipitate formation was observed and upon the addition of 1.0 equiv. of $HgCl_2$, no NMR signal was recorded. This finding supports the formation of a dH3w-Hg(II) complex, that is poorly water-soluble at the concentration used in the NMR experiments (0.5 mM).

8.4.5 Detection Limit

To assess the potential of dH3w as a probe for Hg^{2+}, we determined the detection limit (LOD) at pH 4 and 7 in the absence of Zn^{2+} and at pH 7 in the presence of 100 μM Zn^{2+}. To this aim we performed fluorescence titrations at low concentrations of Hg^{2+} (0-1200 nM). A good linear relationship between the fluorescence intensity at 740 nm and the metal ion concentration was obtained in all the conditions investigated (Fig. S7). The LOD values at pH 4 and 7 were 422±80 and 363±73 nM, respectively, whereas a LOD value of 76±12 nM was obtained at pH 7 in the presence 100 μM Zn^{2+}, thus indicating that the dH3w/Zn^{2+} complex is a very sensitive probe for the detection of Hg^{2+}.

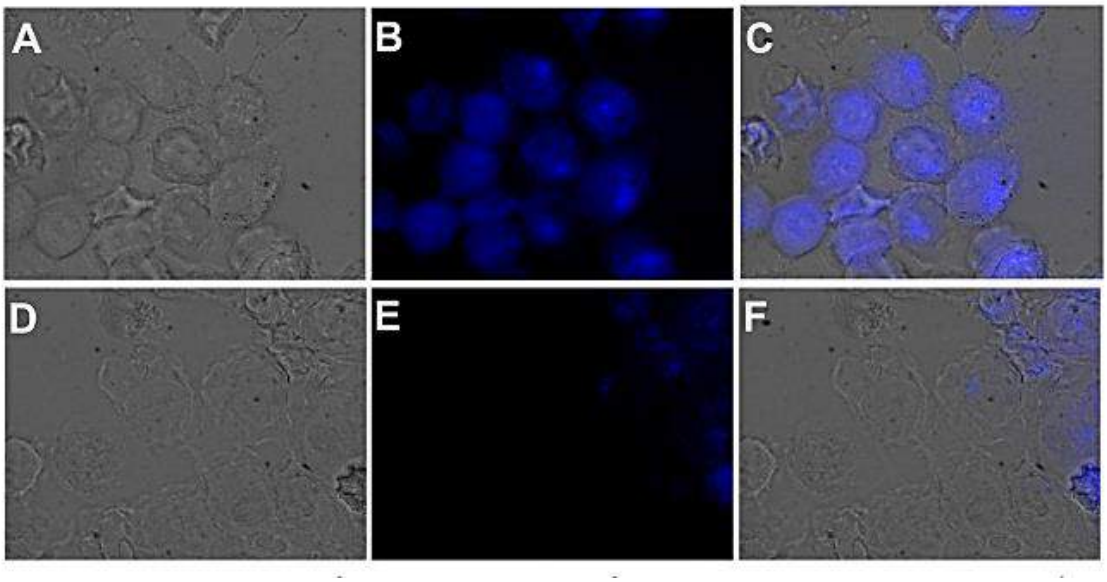

Figure 6: Fluorescent response of peptide to Zn^{2+} in the absence and presence of Hg^{2+} in HaCaT cells. **A-C**) Images of cells preincubated with Zn^{2+} for 3 h upon treatment with peptide. **D-F**) Images of cells after 2 h introduction of Hg^{2+}. Conditions: [Zn^{2+}] = 100 μM; [dH3w] = 10 μM; [Hg^{2+}] = 10 μM. HaCaT cells were analysed by phase contrast (**A,D**) and fluorescence microscopy (**B,E**). Panels **C** and **F** are merged images.

8.4.6 Staining of HaCaT cells with dH3w and dH3w/Zn^{2+} to detect Hg^{2+}

AS we previously showed that dH3w is cell permeable [19] we also investigated the possible application of dH3w as a sensor for the detection of Hg^{2+} levels in eukaryotic cells. Preliminarily we determined the toxicity of dH3w and Zn^{2+} for HaCaT cells, a keratinocyte cell line from adult human skin. To this aim HaCaT cells were cultured in the presence of increasing concentration of dH3w and Zn^{2+} for 24 hours. As shown in Fig. S7, neither dH3W nor Zn^{2+} affected cell viability at any of the concentrations tested. HaCaT cells, after incubation with dH3w and Zn^{2+} (100 μM), showed a strong fluorescence observable both by using a blue and a green filter as expected from the spectral properties of the dH3w/Zn^{2+} complex described in the previous sections (Figs. 6A-C). After further exposure even to low amounts of Hg^{2+} (10 μM) the fluorescence was almost completely lost (Figs. 6D-F). These findings suggest that the dH3w/Zn^{2+} complex could also be used as probe to measure Hg^{2+} levels in cell cultures even if the necessity to excite the dansyl fluorophore in the UV region could limit its usefulness to short observation times.

8.5 Conclusions

We have shown that the fluorescent peptide dH3w binds two Hg^{2+} ions with different affinities. The first binding event determines a strong turn-off response and is relatively independent from pH being observed also at acidic pH values (pH 4-6). The second binding event likely involves the direct participation of the sulphonamide moiety of the fluorophore and is accompanied by relevant changes in the emission spectrum i.e. a blue shift of the λ_{max} and an increase of the emission intensity. As the binding of the sulphonamide to Hg^{2+} likely requires the deprotonation of its NH group, the second binding event is strongly dependent on the pH value and, at acidic pH values is observed only at very

high concentrations of Hg^{2+}. In spite of this complex behavior, at pH values in the range 4-7, dH3w is a convenient turn-off fluorescent sensor for the detection of Hg^{2+} in a 100% aqueous environment with a LOD of about 400 nm.

Moreover, Hg^{2+}, like previously shown for Cu^{2+}, easily displaces the zinc ion from the dH3w/Zn^{2+} complex. No other heavy metal ion is able to compete effectively with Zn^{2+} inducing the strong turn off response observed upon the addition of Hg^{2+} and Cu^{2+}. Therefore, at neutral pH, the dH3w/Zn^{2+}complex can be used as a probe for the simultaneous selective detection of Hg^{2+} and Cu^{2+}. It is worth noting that using dH3w/Zn^{2+} complex as a sensor the LOD for Hg^{2+} decreases to about 60 nM. As regards specificity and sensitivity dH3w is comparable to several other peptidyl fluorescent sensors [38–43]. This suggests that dH3w is suited both for environmental monitoring purposes in a wide range of pH values and for the detection of Hg^{2+} levels in cell cultures.

8.6 References

1. DeSilva TM, Veglia G, Porcelli F, Prantner AM, Opella SJ. Selectivity in heavy metal- binding to peptides and proteins. Biopolymers. 2002;64: 189–197.
2. Tchounwou PB, Ayensu WK, Ninashvili N, Sutton D. Environmental exposure to mercury and its toxicopathologic implications for public health. Environ Toxicol. 2003;18: 149–175.
3. Singh AK, Bhattacharjee G, Singh R. Mercury(II)-selective membrane electrode using tetrathia-diazacyclotetradeca-2,9-diene as neutral carrier. Sens Actuators B Chem. 2004;99: 36–41.
4. Talanova GG, Elkarim NSA, Talanov VS, Bartsch RA. A Calixarene-Based Fluorogenic Reagent for Selective Mercury(II) Recognition. Anal Chem. 1999;71: 3106–3109.
5. Guo X, Qian X, Jia L. A Highly Selective and Sensitive Fluorescent Chemosensor for Hg $^{2+}$ in Neutral Buffer Aqueous Solution. J Am Chem Soc. 2004;126: 2272–2273.
6. Martínez R, Espinosa A, Tárraga A, Molina P. New Hg $^{2+}$ and Cu $^{2+}$ Selective Chromo- and Fluoroionophore Based on a Bichromophoric Azine. Org Lett. 2005;7: 5869–5872.
7. Rasheed T, Bilal M, Nabeel F, Iqbal HMN, Li C, Zhou Y. Fluorescent sensor based models for the detection of environmentally-related toxic heavy metals. Sci Total Environ. 2018;615: 476–485.
8. Ding J, Li H, Xie Y, Peng Q, Li Q, Li Z. Reaction-based conjugated polymer fluorescent probe for mercury(ii): good sensing performance with “turn-on” signal output. Polym Chem. 2017;8: 2221–2226.
9. Kim SH, Kim JS, Park SM, Chang S-K. Hg 2+ -Selective OFF−ON and Cu $^{2+}$ -Selective ON−OFF Type Fluoroionophore Based upon Cyclam. Org Lett. 2006;8: 371–374.
10. Shiraishi Y, Sumiya S, Kohno Y, Hirai T. A Rhodamine−Cyclen Conjugate as a Highly Sensitive and Selective Fluorescent Chemosensor for Hg(II). J Org Chem. 2008;73: 8571–8574.
11. Zhang H, Han L-F, Zachariasse KA, Jiang Y-B. 8-Hydroxyquinoline benzoates as highly sensitive fluorescent chemosensors for transition metal ions. Org Lett. 2007;7: 4217–4220.
12. Rasheed T, Li C, Zhang Y, Nabeel F, Peng J, Qi J, et al. Rhodamine-based multianalyte colorimetric probe with potentialities as on-site assay kit and in biological systems. Sens Actuators B Chem. 2018;258: 115–124.
13. Fang Y, Li X, Li J-Y, Wang G-Y, Zhou Y, Xu N-Z, et al. Thiooxo-Rhodamine B hydrazone derivatives bearing bithiophene group as fluorescent chemosensors for detecting mercury(II) in aqueous media and living HeLa cells. Sens Actuators B Chem. 2018;255: 1182–1190.
14. Makam P, Shilpa R, Kandjani AE, Periasamy SR, Sabri YM, Madhu C, et al. SERS and fluorescence-based ultrasensitive detection of mercury in water. Biosens Bioelectron. 2018;100: 556–564.
15. Pandeeswar M, Senanayak SP, Govindaraju T. Nanoarchitectonics of Small Molecule and DNA for Ultrasensitive Detection of Mercury. ACS Appl Mater Interfaces. 2016;8: 30362–30371.

16. Park SM, Kim MH, Choe J-I, No KT, Chang S-K. Cyclams Bearing Diametrically Disubstituted Pyrenes as Cu 2+ - and Hg 2+ -Selective Fluoroionophores. J Org Chem. 2007;72: 3550–3553.
17. Moon S-Y, Youn NJ, Park SM, Chang S-K. Diametrically Disubstituted Cyclam Derivative Having Hg 2+ -Selective Fluoroionophoric Behaviors. J Org Chem. 2007;70: 2394–2397.
18. Murphy K, Heery B, Sullivan T, Zhang D, Paludetti L, Lau KT, et al. A low-cost autonomous optical sensor for water quality monitoring. Talanta. 2015;132: 520–525.
19. Donadio G, Di Martino R, Oliva R, Petraccone L, Del Vecchio P, Di Luccia B, et al. A new peptide-based fluorescent probe selective for zinc(ii) and copper(ii). J Mater Chem B. 2016;4: 6979–6988.
20. Behrendt R, White P, Offer J. Advances in Fmoc solid-phase peptide synthesis: Advances in Fmoc Solid-Phase Peptide Synthesis. J Pept Sci. 2016;22: 4–27.
21. Wakabayashi S. New insights into the functions of histidine-rich glycoprotein. Int Rev Cell Mol Biol. 2013;304: 467–493.
22. Valeur B. Molecular fluorescence: principles and applications. Weinheim ; New York: Wiley-VCH; 2002.
23. Shrivastava A, Gupta V. Methods for the determination of limit of detection and limit of quantitation of the analytical methods. Chron Young Sci. 2011;2: 21.
24. Bax A, Davis DG. MLEV-17-based two-dimensional homonuclear magnetization transfer spectroscopy. J Magn Reson 1969. 1985;65: 355–360.
25. Jeener J, Meier BH, Bachmann P, Ernst RR. Investigation of exchange processes by two-dimensional NMR spectroscopy. J Chem Phys. 1979;71: 4546–4553.
26. Kumar A, Wagner G, Ernst RR, Wuethrich K. Buildup rates of the nuclear Overhauser effect measured by two-dimensional proton magnetic resonance spectroscopy: implications for studies of protein conformation. J Am Chem Soc. 1981;103: 3654–3658.
27. Griesinger C, Ernst R. Frequency offset effects and their elimination in NMR rotating-frame cross-relaxation spectroscopy. J Magn Reson 1969. 1987;75: 261–271.
28. Piantini U, Sorensen OW, Ernst RR. Multiple quantum filters for elucidating NMR coupling networks. J Am Chem Soc. 1982;104: 6800–6801.
29. Hwang TL, Shaka AJ. Water Suppression That Works. Excitation Sculpting Using Arbitrary Wave-Forms and Pulsed-Field Gradients. J Magn Reson A. 1995;112: 275–279.
30. Parella T, Sánchez-Ferrando F, Virgili A. Improved Sensitivity in Gradient-Based 1D and 2D Multiplicity-Edited HSQC Experiments. J Magn Reson. 1997;126: 274–277.
31. Wüthrich K. NMR of proteins and nucleic acids. New York: Wiley; 1986.
32. Joshi BP, Lohani CR, Lee K-H. A highly sensitive and selective detection of Hg(ii) in 100% aqueous solution with fluorescent labeled dimerized Cys residues. Org Biomol Chem. 2010;8: 3220.
33. Kaupp M, von Schnering HG. Dominance of Linear 2-Coordination in Mercury Chemistry: Quasirelativistic and Nonrelativistic ab Initio Pseudopotential Study of (HgX2)2 (X = F, Cl, Br, I, H). Inorg Chem. 1994;33: 2555–2564.
34. Brooks P, Davidson N. Mercury(II) Complexes of Imidazole and Histidine. J Am Chem Soc. 1960;82: 2118–2123.
35. Sjoberg S. Metal Complexes with Mixed Ligands. 12. A Potentiometrie Study of the Systems Hg2+—Imidazole, Hg2+—OH~—Imidazole and Hg2+—O—Imidazole in 3.0 M (Na)ClO4, Cl Media. Acta Chem Scand A. 1977;31: 718–728.
36. Sundeberg RJ, Martin B. Interactions of Histidine and Other Imidazole Derivatives with Transition Metal Ions in Chemical and Biological Systems. Chem Rev. 1974;74.
37. Knecht S, Ricklin D, Eberle AN, Ernst B. Oligohis-tags: mechanisms of binding to Ni2+-NTA surfaces. J Mol Recognit. 2009;22: 270–279.
38. White BR, Liljestrand HM, Holcombe JA. A ‘turn-on’ FRET peptide sensor based on the mercury bindingprotein MerP. The Analyst. 2008;133: 65–70.
39. Thirupathi P, Lee K-H. A new peptidyl fluorescent chemosensors for the selective detection of mercury ions based on tetrapeptide. Bioorg Med Chem. 2013;21: 7964–7970.

40. Gui S, Huang Y, Hu F, Jin Y, Zhang G, Zhang D, et al. Bio-inspired peptide for imaging Hg^{2+} distribution in living cells and zebrafish based on coordination-mediated supramolecular assembling. Anal Chem. 2018.
41. Wang P, Wu J, Zhou P, Liu W, Tang Y. A novel peptide-based fluorescent chemosensor for measuring zinc ions using different excitation wavelengths and application in live cell imaging. J Mater Chem B. 2015;3: 3617–3624.
42. Joshi BP, Park J, Lee WI, Lee K-H. Ratiometric and turn-on monitoring for heavy and transition metal ions in aqueous solution with a fluorescent peptide sensor. Talanta. 2009;78: 903–909.
43. Neupane LN, Oh E-T, Park HJ, Lee K-H. Selective and Sensitive Detection of Heavy Metal Ions in 100% Aqueous Solution and Cells with a Fluorescence Chemosensor Based on Peptide Using Aggregation-Induced Emission. Anal Chem. 2016;88: 3333–3340.

8.7 Additional Informations

HPLC Analysis

primm

Name	:Dansyl-HW6 Amide
Sequence	:Dansyl-HPHGHW-NH2
Lot. No	:PCM12195-2-0323
Pump A	:0.1% trifluoroacetic in 100% water
Pump B	:0.1% trifluoroacetic in 100% acetonrtrile
Total Flow	:1ml/min
Wavelength	:214nm
Analytical column type	:SHIMADZU Inertsil ODS-SP(4.6*250mm*5um)
Dissolution method	:15%ACN+85%H2O
Acquisition Time	:2017/4/7 11:26:45
Inj. Volume	:25ul

Time	Module	Action	Value
0.01	Pumps	B.Conc	2
30.00	Pumps	B.Conc	65
33.00	Pumps	B.Conc	100
38.00	Pumps	B.Conc	100
40.00	Pumps	B.Conc	2
50.00	Controller	Stop	

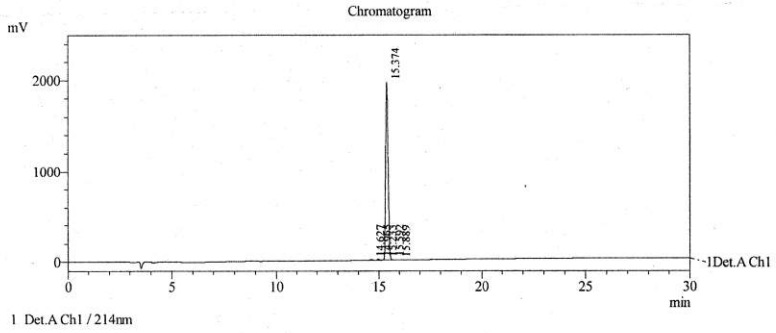

1 Det.A Ch1 / 214nm

PeakTable

Detector A Ch1 214nm

Peak#	Ret. Time	Area	Height	Area %
1	14.627	69536	8571	0.418
2	14.965	65905	10768	0.396
3	15.233	13833	5133	0.083
4	15.374	16458822	1955261	98.950
5	15.592	13501	8594	0.081
6	15.889	11798	2226	0.071
Total		16633395	1990552	100.000

Figure S1: dH3w HPLC analysis.

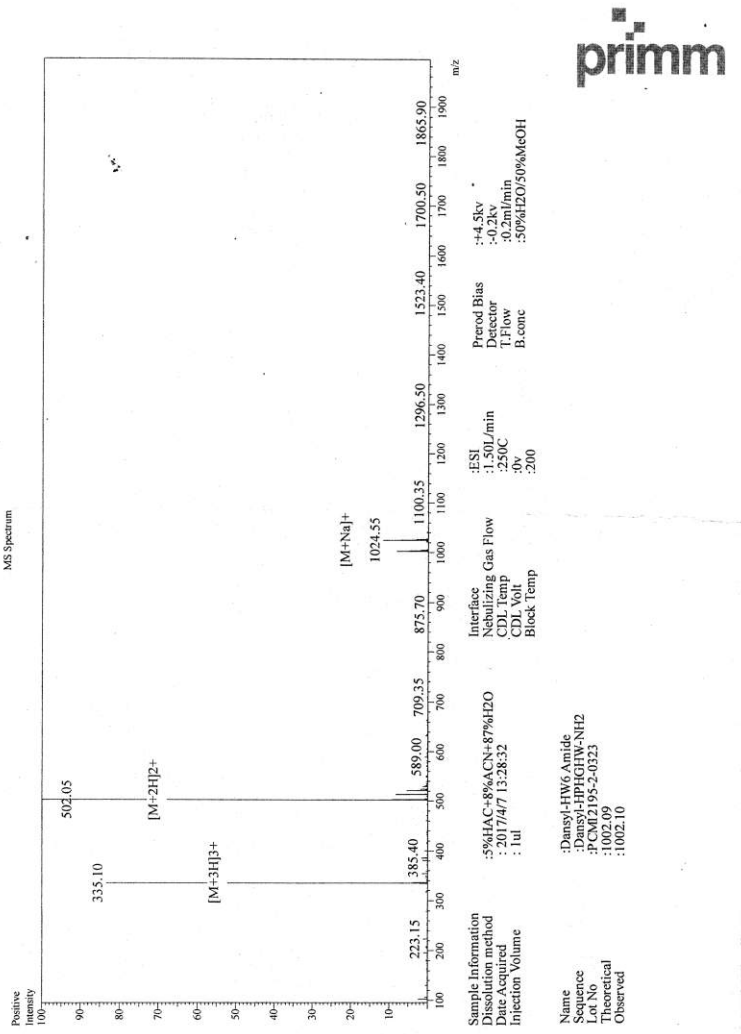

Figure S2: dH3w MS spectrum.

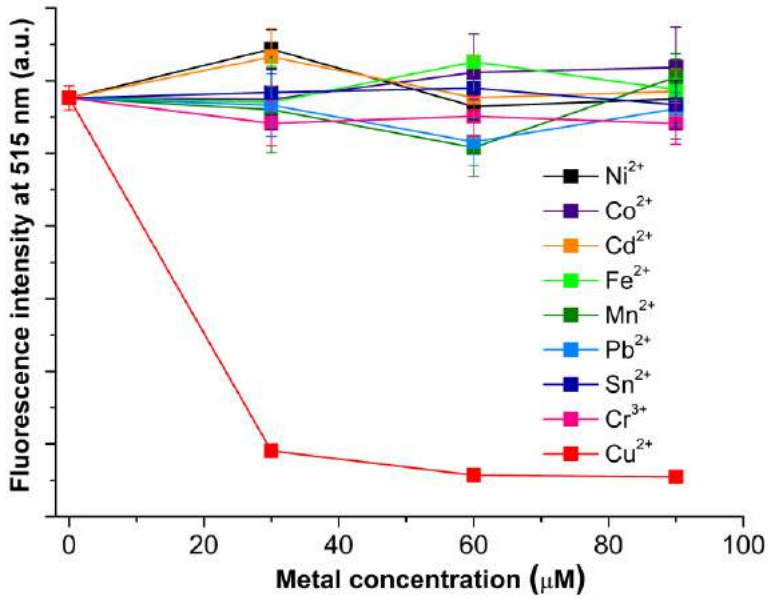

Figure S3: Fluorescence intensity changes of dH3W and Zn^{2+}, in the presence of increasing concentrations of heavy metals.

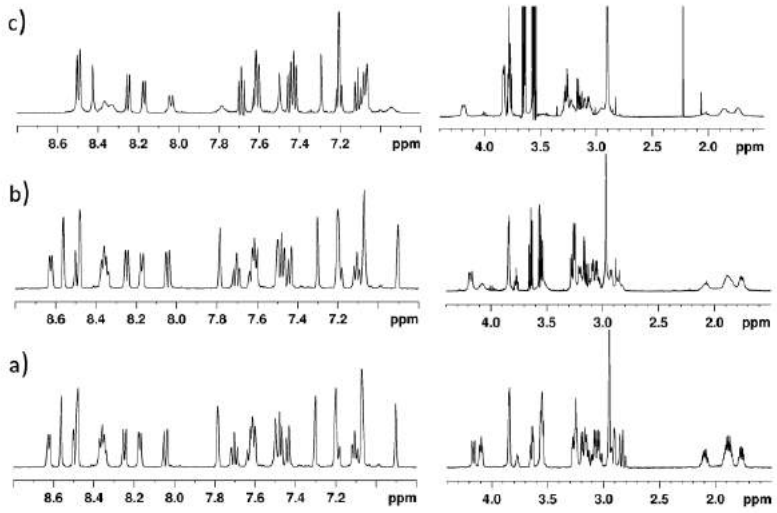

Figure S4: H NMR spectra in the amide and aliphatic regions of dH3w at pH 3.8 and 4.5.

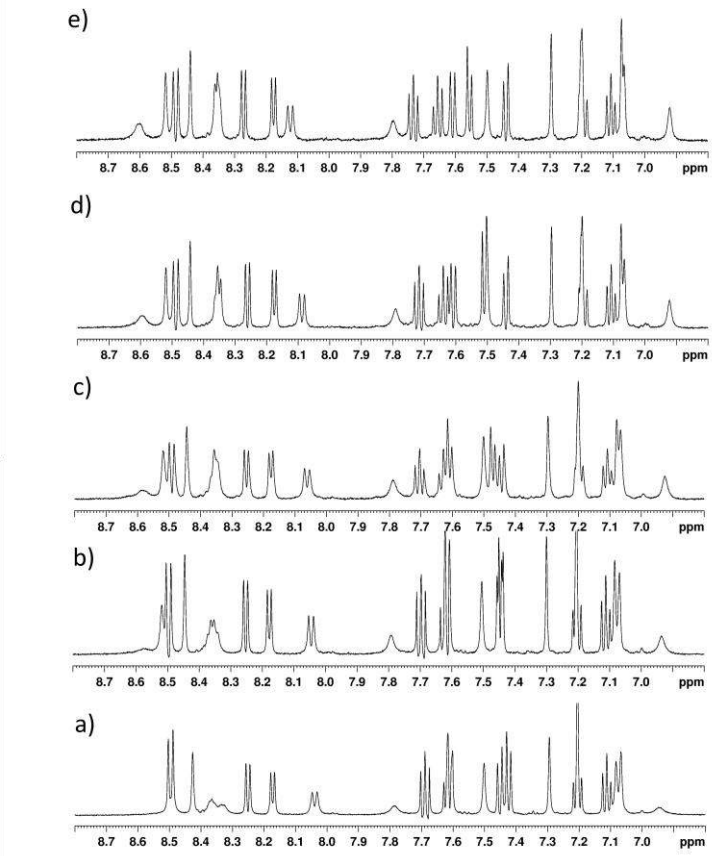

Figure S5: H NMR spectra in the amide region of dH3w at pH 4.5 in presence of different concentrations of Hg^{2}.

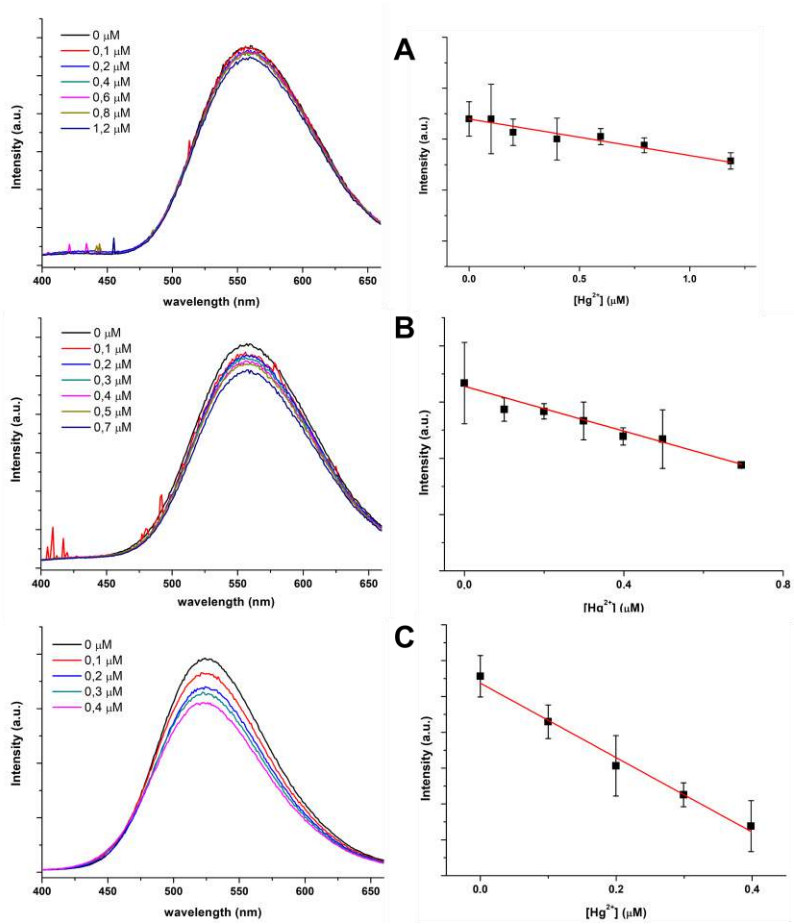

Figure S6: Detection limit (LOD) for Hg^{2+}.

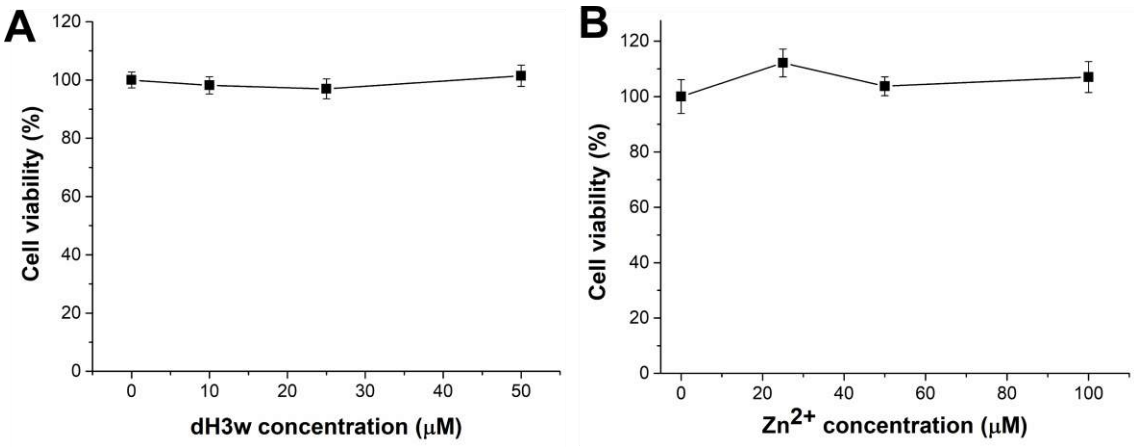

Figure S7: Biocompatibility of the increasing concentrations of dH3W and Zn^{2+} on HaCaT cells.

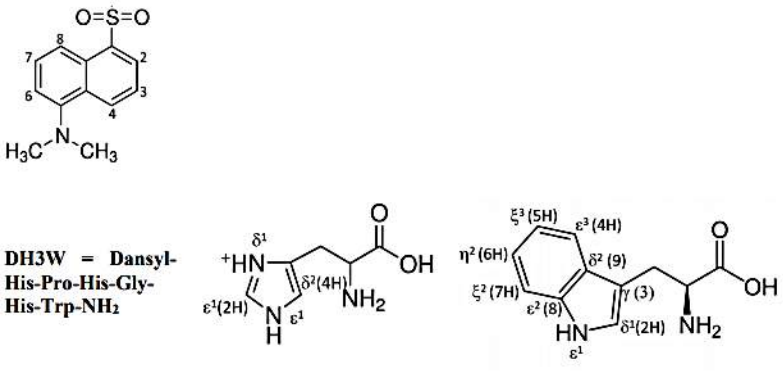

Figure S8: Proton chemical shifts (δ, in ppm) of DH3W (C = 0.5 mM H_2O/D_2O 90/10) in absence and in presence of Hg^{2+}.

	DH3W	DH3W - Hg(II) (1eq. pH 3.8)	DH3W- Hg(II) (1eq. pH 4.5)
Dansyl			
H2	8.25	8.25	8.25
H3	7.72	7.71	7.69
H4	8.49	8.49	8.49
H6	7.47)	7.50	7.41
H7	7.61	7.63	7.62
H8	8.04	8.04	8.04
CH_3	2.94	2.93	2.93
His^1			
NH	-		
αCH	4.16		
β,β'CH_2	2.92 -2.84	2.92	2.92
Hδ2 (4H)	6.90	6.92	6.94
Hε1 (2H)	7.78	7.78	7.78
Pro^2			
αCH	4.09	4.03	4.03
β,β' CH_2	2.10 - 1.77	2.04 - 1.73	2.04 - 1.73
γ,γ' CH_2	1.88	1.86	1.86
δ,δ' CH_2	3.56	3.46	3.46
His^3			
NH	8.63	8.61	-
αCH	4.65	-	
β,β' CH_2	3.23 - 3.17	3.25	3.25
Hδ2 (4H)	7.30	7.30	7.30
Hε1 (2H)	8.56	8.54	8.48
Gly^4			

NH	8.35	8.37	8.37
α,α' CH_2	3.84	3.83	3.83
His^5			
NH	8.37	8.35	8.35
αCH	4.59	4.58	4.58
β,β' CH_2	3.06	3.10	3.10
Hδ2 (4H)	7.07	7.08	7.08
Hε1 (2H)	8.47	8.46	8.43
Trp^6			
NH	8.17	8.17	8.17
αCH	4.60	4.62	4.62
β,β' CH_2	3.26 - 3.14	3.27 - 3.17	3.27 - 3.17
Hδ1 (2H)	7.18	7.21	7.21
Hε1 (NH)	10.09	10.09	10.09
Hε3 (4H)	7.60	7.60	7.60
Hζ3 (5H)	7.11	7.11	7.11
Hη2 (6H)	7.20	7.20	7.20
Hζ2 (7H)	7.44	7.44	7.44
NH_2			
H11	7.50	7.50	7.50
H12	7.07	7.07	7.07

S3 Table. Proton chemical shifts (δ, in ppm) of DH3W (C = 0.5 mM H2O/D2O 90/10) in absence (pH = 3.8) and in presence of Hg2+, (pH = 3.8 and pH = 4.5)

Chapter 9

Conclusions

9. Conclusions

My PhD work, summarized in this Thesis, allows me to draw several conclusions. In the **first part** of the Thesis (**Chapter 2**), I have investigated how the temperature of sporulation affects structure and function of the spore surface of *B. subtilis*. It shows that spores formed at 25, 37 and 42°C are affected by the sporulation temperature. The major changes were observed in spores produced at 25°C compared to 37 and 42°C. In fact, the former were the most sensitive to any type of physiological assay. Furthermore, the tested CotH-dependent proteins were more represented at 25°C than the other two temperatures. By exploring the role of CotH, I highlightited that the sporulation temperature influences CotH at the level of its stability (more stable at 25°C).The **second part** of the Thesis (**Chapters 3-5**) opens to a better understanding of the localization of heterologous proteins in a non-recombinant spore-based delivery system (Chapter 3). Moreover, I explored the possibility of using *B. megaterium* spores to display heterologous proteins (Chapter 4). This bacterium is a spore-forming far less studied than *B. subtilis*. Spores of this species are 2,5-fold larger than that *B. subtilis* and characterized by the presence of an exosporium, an additional protective layer lacking in *B. subtilis* spores. In my work, these spores were proved to be much more efficient than spores of *B. subtilis*, opening extremely interesting perspectives for the biotechnological use of this bacterial species. Keeping in mind these considerations, I used *B. megaterium* spores to display an antioxidant enzyme on their surface (Chapter 5) and studied the possilibity to deliver spores-bound enzyme to the gastro-intestinal mucosa. In more detail, I demonstrated the ability of the spores to adsorb the enzyme, stabilizing and protecting it from gastrointestal environment. Furthermore, the enzyme retained its activity and was not released. However , a partial release of the adsorbed enzyme was observed when the pH conditions shifted from acidic to neutral. All these properties are particularly desirable for an oral delivery system aimed at crossing the stomach and delivering the transported molecules at the intestinal mucosal surfaces. An additional interesting observation highlighted by this chapter is that *B. megaterium* spores have an endogenous antioxidant activity. This one has inspired the **third part** of my work (**Chapter 6-7**) in which I highlighted the purpose to use both spores as probiotics against oxidative stress. It is already known that *B. subtilis* spores represent good probiotics for human health but it is unknown the way in which they exert their beneficial effects. Therefore, I investigated how the spores act on stressed eukaryotic cells demonstrating that the protective effect is not only due to the antioxidant activity of the spore, but to the activation of Nrf-2, a nuclear transcription factor, actively involved in oxidative stress response (chapter 6). On the other hand, the work of chapter 7 reports the probiotic effects of *B.megaterium* spores on stressed eukaryotic cells and DSS murine model. A better understanding on the way through which the spores activate Nrf-2 pathway allowed to start a new research. The **final part** of this Thesis (**chapter 8**) deals with a different topic. I developed a new fluorescent peptide ,dH3w. The high affinity and selectivity suggest that dH3w and the $Zn^{2+/}$dH3w complex are suited as fluorescent sensor for the detection of Hg^{2+} and Cu^{2+} in environmental as well as biological samples.